

BIOETHANOL PRODUCTION FROM CO-
GASIFICATION OF LIGNOCELLULOSIC
BIOMASS AND CHARCOAL



MD. MINHAJ UDDIN MONIR

Doctor of Philosophy

UNIVERSITI MALAYSIA PAHANG

UNIVERSITI MALAYSIA PAHANG

DECLARATION OF THESIS AND COPYRIGHT

Author's Full Name : MD. MINHAJ UDDIN MONIR

Date of Birth : 5 SEPTEMBER 1979

Title : BIOETHANOL PRODUCTION FROM CO-GASIFICATION
OF LIGNOCELLULOSIC BIOMASS AND CHARCOAL

Academic Session : SEM 2 2018/2019

I declare that this thesis is classified as:

- CONFIDENTIAL (Contains confidential information under the Official Secret Act 1997)*
- RESTRICTED (Contains restricted information as specified by the organization where research was done)*
- OPEN ACCESS I agree that my thesis to be published as online open access (Full Text)

I acknowledge that Universiti Malaysia Pahang reserves the following rights:

1. The Thesis is the Property of Universiti Malaysia Pahang
2. The Library of Universiti Malaysia Pahang has the right to make copies of the thesis for the purpose of research only.
3. The Library has the right to make copies of the thesis for academic exchange.

Certified by:

(Student's Signature)

(Supervisor's Signature)

BQ0060886
New IC/Passport Number
Date:

DR. AZRINA BINTI ABD AZIZ
Name of Supervisor
Date:

NOTE : * If the thesis is CONFIDENTIAL or RESTRICTED, please attach a thesis declaration letter.

SUPERVISOR'S DECLARATION

I hereby declare that I have checked this thesis, and in my opinion, this thesis is adequate in terms of scope and quality for the award of the degree of Doctor of Philosophy.

(Supervisor's Signature)

Full Name : DR. AZRINA BINTI ABD AZIZ

Position : SENIOR LECTURER

Date :



UMP

STUDENT'S DECLARATION

I hereby declare that the work in this thesis is based on my original work except for quotations and citations which have been duly acknowledged. I also declare that it has not been previously or concurrently submitted for any other degree at Universiti Malaysia Pahang or any other institutions.

(Student's Signature)

Full Name : MD. MINHAJ UDDIN MONIR

ID Number : PKE16002

Date :



UMP

BIOETHANOL PRODUCTION FROM CO-GASIFICATION OF
LIGNOCELLULOSIC BIOMASS AND CHARCOAL



MD. MINHAJ UDDIN MONIR

Thesis submitted in fulfillment of the requirements
for the award of the degree of
Doctor of Philosophy

UMP

Faculty of Engineering Technology
UNIVERSITI MALAYSIA PAHANG

MAY 2019

ACKNOWLEDGEMENTS

Firstly, I would like to acknowledge my great debt of gratitude to all, who helped me over this research period. I would like to express my thanks to my main supervisor Dr. Azrina Binti Abd Aziz for all kind of mentoring, instructions and supported me enormously throughout my PhD studies. I would also like to thank my previous supervisors Dr. Abu Yousuf and Dr. Risky Ayu Kristanti for their cordial guidance. I wish to give a special thanks to the Prof. Madya Dr. Andri Kusbiantoro, Deputy Dean (Research & Postgraduates Studies), external examiners of Prof. Dr Suzana Binti Yusup and Prof. Dr. Hamidi Abdul Aziz, internal examiners of Prof. Madya Ts. Dr. Che Ku Mohammad Faizal Bin Che Ku Yahya, Dr. Samson Mekbib Atnaw and Dr. Nadzirah Mohd Mokhtar for their effective advice and comments during my PhD proposal defense, pre-viva and viva.

I would like to use this opportunity to express my sincere thanks to the Dean of Faculty of Engineering Technology (FTek), Prof. Dato' Ts. Dr. Zularisam Bin Ab Wahid for his cordial support throughout this work. I also extend my sincere thanks to the responsible persons in the Energy Management Laboratory, Toxicology Laboratory, Chemistry Laboratory and Cell Culture Laboratory for their kind cooperation with various instrumental facilities throughout my whole research. I would always appreciate the valuable support extended by all the academic and technical staff in the FTek. I would like to give cordial thanks to Prof. Dr. Md. Zahangir Alam, Faculty of Engineering, International Islamic University Malaysia (IIUM), Malaysia for providing me the microbial sample. I would also like to acknowledge the financial support of GRS Scholarship and PGRS (Internal Grant No. PGRS170370) received from University Malaysia Pahang, Malaysia.

I would like to acknowledge my university (Jashore University of Science and Technology, Jashore, Bangladesh) authority who provided me the permission for my study leave to start my PhD study at Universiti Malaysia Pahang (UMP). Afterward, I would like to convey my hearty thanks to the Dean of Institute of Postgraduate Studies, Prof. Dato' Dr. Hasnah Binti Haron, and all other IPS staffs for their help throughout my study. I also owe my sincere appreciation to all the staff in the International Office (IO) for their timely help and support. Finally, I would like to thanks to my wife who inspired me all the time for the successful completion of my PhD. I would also like to extend my special appreciation to my heartiest parents, sister, nieces, brother-in-law, relatives, friends and colleagues for their cordial support.

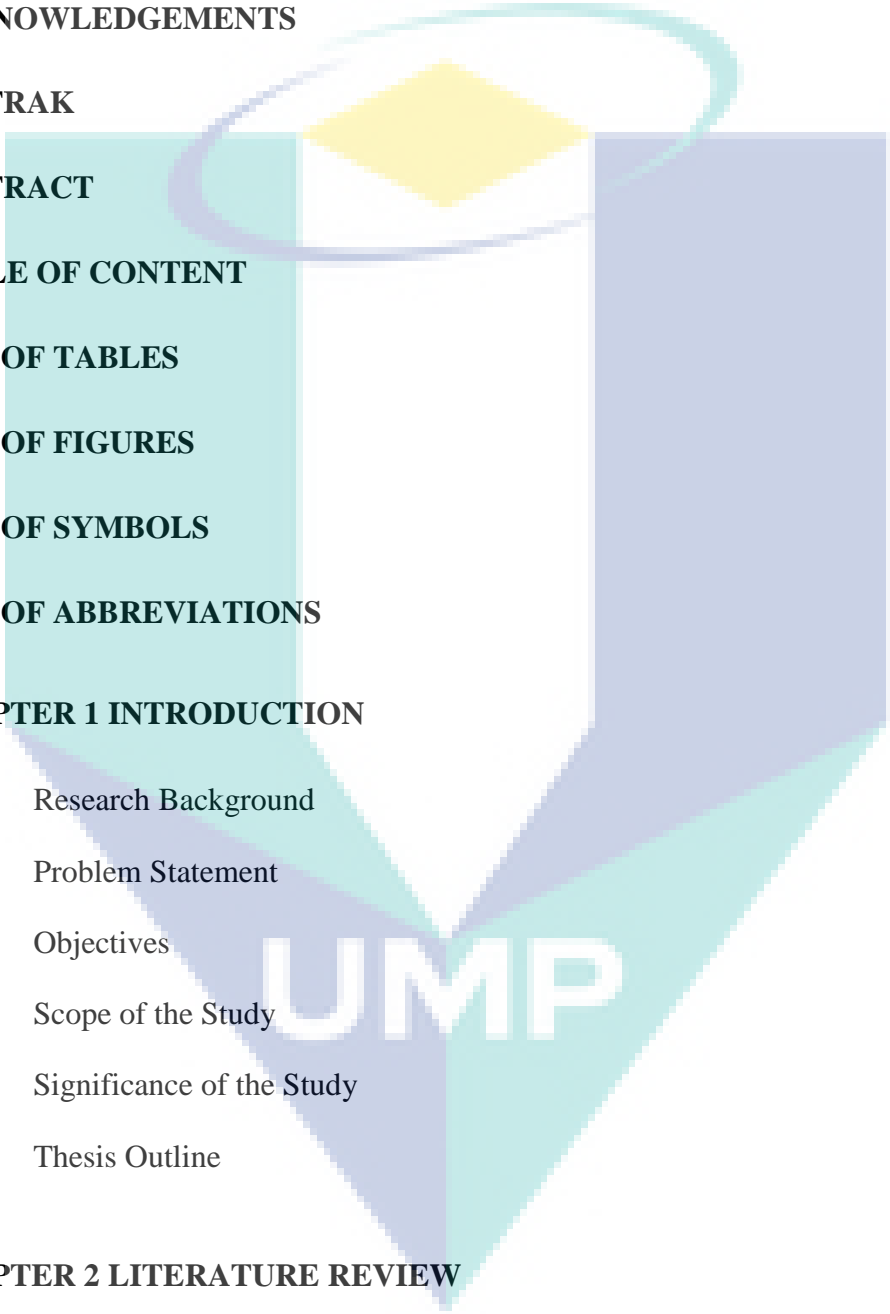
ABSTRAK

Permintaan tenaga global kian meningkat disebabkan perindustrian dan perbandaran yang pesat. Oleh itu, peningkatan penggunaan bahan api fosil menjadikan permintaan tenaga global adalah kritikal. Bagi memenuhi permintaan tenaga, pendekatan alternatif adalah wajib. Kajian ini memberi penekanan mengenai pemeliharaan sumber tenaga boleh diperbaharui melalui lignoselulosik biomas (buah kelapa sawit, sisa hutan dan tempurung kelapa kosong) dan keluarannya (arang) untuk pengeluaran syngas dan bioethanol melalui proses hibrid termokimia dan biokimia. Pencirian fizikokimia bahan bakar dilakukan untuk mengetahui potensi biotenaga mereka. Model simulasi dijalankan untuk mendapatkan keadaan optimum untuk penggabungan bersama berdasarkan beberapa tanggapan dengan menggunakan Aspen Plus® (V 8.6) di bawah keadaan operasi yang berubah (kadar aliran udara, kandungan lembapan dan komposisi bahan baku). Pelbagai campuran biomas dengan arang (0-40%) telah digabungkan bersama dalam gasifier downdraft (DG) untuk pengeluaran syngas. Faktor kawalan (iaitu, suhu, tekanan) reaktor dinilai pada pelbagai parameter iaitu nilai pemanasan, hasil syngas, kecekapan gas sejuk, kecekapan penukaran karbon, kecekapan exergy dan komposisi syngas untuk mengesahkan pengeluaran syngas semasa proses penggalian dengan udara ($\sim 35 \text{ m}^3\text{h}^{-1}$). Selepas itu, penapaian syngas dilakukan menggunakan bioreaktor TFB, dan pengeluaran bioethanol disiasat memandangkan pelbagai kesan (kekotoran syngas, suhu, pH, unit membentuk jajahan, jumlah karbon organik, komposisi syngas). Hasil awal syngas dicirikan oleh pengesanan kekonduksian kromatografi gas dan hasil akhir bioethanol telah dikenalpasti oleh spektrometri massa-kromatografi Gas dan resonans magnetik nuklear (^1H). Analisis morfologi kajian ini mendedahkan bahawa dari segi pengegasan, lebih tinggi selulosa dan hemiselulosa yang mengandungi biomas lebih baik daripada arang. Variasi kepekatan reaktor downdraft menunjukkan kepekatan CO dan H₂ meningkat dengan meningkatnya arang (hingga 40%) dan peningkatan suhu (800-1000 °C) serta tekanan (25-35bar). Sebaliknya, trend yang bertentangan untuk kepekatan CO₂ telah diperhatikan dengan meningkatkan arang dalam reaktor. Walau bagaimanapun, kepekatan CH₄ relatif tidak berubah sepanjang tindak balas beberapa nisbah koefisien. Hasilnya, nisbah syngas optimum (H₂: CO) untuk tiga pengegasan bersama yang berbeza didapati 1.10-1.55 selepas biomas: campuran arang 70:30 dan 60:40 w/w untuk memaksimumkan faedah pengegasan proses. Secara berterusan, kepekatan pengeluaran bioethanol menggunakan yis (*Saccharomyces cerevisiae*) dan bakteria (*Clostridium butyricum*) masing-masing adalah 15.28 mmol/L dan 14.97 mmol/L. Oleh itu, biomas lignoselulosa yang terdapat di EFB, FR dan CS dengan arang oleh-produk boleh digunakan untuk penggabungan untuk pengeluaran syngas, dan seterusnya, ia juga sesuai untuk penukaran bioethanol melalui penapaian syngas menggunakan *Saccharomyces cerevisiae* dan *Clostridium butyricum*. Penyelidikan ini boleh menyumbang kepada syngas yang berpatutan dan mesra alam dan tenaga berasaskan bioethanol dan untuk mengurangkan kebergantungan kepada bahan api berasaskan fosil yang terhad.

ABSTRACT

Global energy demand is increasing due to rapid industrialization and urbanization. Moreover, augmented consumptions of fossil fuels make the global energy demand critical. So, to meet up the future energy demand an alternative approach is mandatory. The present study emphasizes on the valorization of mostly available renewable energy resources of lignocellulosic biomass (empty fruit bunch of palm oil, forest residue and coconut shell) and its by-product (charcoal) for the production of syngas and bioethanol through the hybrid process of thermo-chemical (co-gasification of feedstocks to syngas) and biochemical (microbial fermentation of syngas), respectively. The physiochemical characterization of feedstocks was performed to find out their bioenergy potentiality. The simulation model was carried out to obtain an optimum condition for co-gasification based on some assumptions using Aspen Plus® (V 8.6) under variable operating conditions (air flow rate, moisture content and composition of the feedstock). Then various mixtures of biomass with charcoal (0-40%) were co-gasified in a downdraft gasifier (DG) for syngas production. The controlling factors (i.e., temperature, pressure) of the reactor were evaluated on various parameters namely heating value, syngas yield, cold gas efficiency, carbon conversion efficiency, exergy efficiency and syngas composition to verify the production of syngas during the co-gasification process with air ($\sim 35 \text{ m}^3\text{h}^{-1}$). Subsequently, syngas fermentation was performed using a TFB bioreactor, and bioethanol production was investigated considering various effects (syngas impurity, temperature, pH, colony forming unit, total organic carbon, syngas composition). The initial yield of syngas was characterized by Gas chromatography-thermal conductivity detector and the ultimate yield of bioethanol was identified by Gas chromatography-mass spectrometry and Nuclear magnetic resonance (^1H) analysis. Morphological analysis of this study reveals that in terms of gasification, higher cellulose and hemicellulose containing biomass is better than the charcoal. The concentration variation of the downdraft reactor showed that the CO and H₂ concentration increase with the increasing charcoal (up to 40%) with increasing temperature (800-1000°C) and pressure (25-35bar). On the contrary, an opposite trend for the case CO₂ concentration was observed with increasing the charcoal in the reactor. However, CH₄ concentration was relatively unchanged throughout the reactions of several co-gasification ratios. Consequently, the optimal yield of syngas (H₂:CO) ratio for three different co-gasification was found to be 1.10-1.55 after the biomass:charcoal mixture of 70:30 and 60:40 w/w for maximizing the benefits of the gasification process. Successively, the concentration of bioethanol production using yeast (*Saccharomyces cerevisiae*) and bacteria (*Clostridium butyricum*) were 15.28 mmol/L and 14.97 mmol/L, respectively. Thus, the available lignocellulosic biomass of EFB, FR and CS with by-product charcoal could be suited for co-gasification for syngas production, and further, it is also suited for the conversion of bioethanol through syngas fermentation using *Saccharomyces cerevisiae* and *Clostridium butyricum*. This research may contribute to affordable and environment-friendly syngas and bioethanol-based energy and to reduce the dependency on limited fossil-based fuels.

TABLE OF CONTENT



DECLARATION	
TITLE PAGE	
ACKNOWLEDGEMENTS	ii
ABSTRAK	iii
ABSTRACT	iv
TABLE OF CONTENT	v
LIST OF TABLES	xi
LIST OF FIGURES	xii
LIST OF SYMBOLS	xviii
LIST OF ABBREVIATIONS	xix
CHAPTER 1 INTRODUCTION	1
1.1 Research Background	1
1.2 Problem Statement	5
1.3 Objectives	6
1.4 Scope of the Study	7
1.5 Significance of the Study	8
1.6 Thesis Outline	9
CHAPTER 2 LITERATURE REVIEW	10
2.1 Global Energy and Its Demand	10
2.2 Biomass-based Energy	14
2.3 Energetic Utilization of Biomass	17

2.3.1	Syngas	18
2.3.2	Biofuels (Bioethanol)	22
2.4	Lignocellulosic Biomass	23
2.4.1	Types of Lignocellulosic Biomass	25
2.4.2	Composition of Lignocellulosic Biomass	25
2.5	Feedstocks Availability in Malaysia	28
2.6	Energy Conversion Routes from Lignocellulosic Biomass	28
2.6.1	Pyrolysis	29
2.6.2	Combustion	30
2.6.3	Gasification	31
2.6.4	Co-gasification	34
2.7	Simulation, Optimization and Modelling for Biomass Gasification	36
2.7.1	Comparative Analysis Using Simulation Software and Applications	36
2.7.2	Simulation, Optimization and Modelling using Aspen Plus®	38
2.8	Types of Gasifier Used for Gasification and Co-gasification	40
2.8.1	Fixed Bed Gasifier	41
2.8.2	Fluidized Bed Gasifier	44
2.8.3	Entrained Flow Gasifier	47
2.8.4	Selection of Gasifier	49
2.9	Biocatalyst Used for Syngas Fermentation	50
2.10	Syngas Fermentation System	54
2.10.1	Batch Culture	54
2.10.2	Fed-batch Culture	54
2.10.3	Continuous Culture	55
2.11	Microbial Pathway and Energy Conversion	55

2.12	Types of Fermenter Used for Syngas Fermentation	57
2.12.1	Continuous Stirred Tank Bioreactor	57
2.12.2	Bubble Column Reactor	58
2.12.3	Monolithic Biofilm Reactor	59
2.12.4	Trickle Bed Reactor	60
2.12.5	Membrane-based System Reactor	61
2.12.6	Selection of Bioreactor	62
2.13	Syngas Fermentation for Bioethanol Production	62
2.14	Effect of Syngas Fermentation for Bioethanol Production	63
2.14.1	Effect of Microbial Growth Phase	63
2.14.2	Effect of Organic Source	65
2.14.3	Effect of pH	65
2.14.4	Effect of Temperature	65
2.14.5	Effect of Syngas Flow Rate	66
2.14.6	Effect of Mass Transfer	66
2.14.7	Effect of Trace Metals	66
2.15	Summary	66
CHAPTER 3 METHODOLOGY		68
3.1	Samples Collection and Preparation	69
3.2	Feedstocks and Product Characterization	70
3.2.1	Proximate Analysis	70
3.2.2	Ultimate Analysis	71
3.2.3	X-ray Diffraction Analysis	71
3.2.4	Scanning Electron Microscopy and Energy-Dispersive X-ray Analysis	72

3.2.5	Field Emission Scanning Electron Microscopy and Energy-Dispersive X-ray Analysis	72
3.2.6	Transmission Electron Microscopy Analysis	72
3.2.7	Fourier Transform Infrared Analysis	72
3.2.8	X-ray Photoelectron Spectroscopy Analysis	73
3.2.9	In-situ Syngas Analysis Using Portable Gas Analyzer	73
3.2.10	Gas Chromatography-Thermal Conductivity Detector Analysis	73
3.2.11	Gas Chromatography-Mass Spectrometry Analysis	73
3.2.12	Nuclear Magnetic Resonance Analysis	74
3.3	Heating Value Calculation	74
3.4	Cold Gas Efficiency and Carbon Conversion Efficiency Calculation	75
3.5	Exergy Analysis	76
3.6	Assumptions for Simulation Using Aspen Plus®	77
3.7	Experimental Setup and Process of Co-gasification	78
3.8	Biocatalyst Preparation for Syngas Fermentation	81
3.8.1	Saccharomyces Cerevisiae Cell Growth Culture	81
3.8.2	Clostridium Butyricum Cell Growth Culture	82
3.9	Experimental Setup and Process of Syngas Fermentation	82
3.9.1	Syngas Fermentation Medium for Saccharomyces Cerevisiae	83
3.9.2	Syngas Fermentation Medium for Clostridium Butyricum	84
3.9.3	Syngas Fermentation Process for Bioethanol Production	84
3.9.4	Product Extraction and Analysis	85
CHAPTER 4 RESULTS AND DISCUSSION		87
4.1	Feedstocks Characterization	87
4.1.1	Proximate Analysis	87
4.1.2	Ultimate Analysis	92

4.1.3	X-ray Diffraction Analysis	96
4.1.4	Scanning Electron Microscopy Analysis	98
4.1.5	Field Emission Scanning Electron Microscopy and Energy-Dispersive X-ray Analysis	101
4.1.6	Transmission Electron Microscopy Analysis	103
4.1.7	Fourier Transform Infrared Analysis	104
4.1.8	X-ray Photoelectron Spectroscopy Analysis	105
4.2	Simulation by Aspen Plus®	111
4.2.1	Model Flowsheet for Co-gasification Using Aspen Plus®	111
4.2.2	Mechanism of Simulation for Biomass and Charcoal Co-gasification Using Aspen Plus®	112
4.2.3	Simulation for Lignocellulosic Biomass and Charcoal Co-gasification	113
4.2.4	Experimental Validation with Simulation	114
4.2.5	Economic Analysis Using Aspen Plus®	116
4.3	Syngas Production Through Co-gasification	117
4.3.1	Co-gasification of EFB of Palm Oil and Charcoal	117
4.3.2	Co-gasification of Forest Residue and Charcoal	125
4.3.3	Co-gasification of Coconut Shell and Charcoal	133
4.3.4	Co-product Analysis	141
4.3.5	By-product Analysis	149
4.3.6	Comparative Study on Co-gasification	150
4.4	Bioethanol Production Through Syngas Fermentation	154
4.4.1	Biocatalysts Preparation and Characterization	154
4.4.2	Effect of Syngas Fermentation	156
4.4.3	Bioethanol Production and Analysis	162

CHAPTER 5 CONCLUSION AND RECOMMENDATIONS	167
5.1 Conclusion	167
5.2 Recommendations	169
REFERENCES	170
LIST OF PUBLICATIONS	191
APPENDIX A Exergy Efficiency Calculation	202
APPENDIX B Procedure for Simulation USING Aspen Plus®	206
APPENDIX C NMR (¹H and ¹³C) for Co-product Tar	208
APPENDIX D GC-MS Fraction of Ethanol (Standard MS fraction (15:29:31:45) for ethanol (99.99%)).	214
APPENDIX E Syngas Composition Before and After Fermentation	215



UMP

LIST OF TABLES

Table 2.1	Types of biofuels and their characteristics.	22
Table 2.2	Potential lignocellulosic biomass source and their composition (% dry weight).	26
Table 2.3	Chemical reactions involved in biomass gasification.	33
Table 2.4	Comparative study on various types of gasifiers including their advantages and disadvantages.	49
Table 2.5	Production of liquid fuels by microbial syngas fermentation with various carbon sources and operational parameters.	51
Table 2.6	Reactions involved for acetic acid and ethanol production.	57
Table 3.1	Aspen Plus blocks with unit assumptions used for simulation of the co-gasification process of lignocellulosic biomass and charcoal.	78
Table 4.1	Proximate and ultimate analytical results of EFB, FR, CS and Charcoal compared to literature.	89
Table 4.2	Elemental weight percentage and the atomic percentage of EFB, FR, CS and Charcoal.	101
Table 4.3	Experimental results (syngas composition) were validated with simulation results at the temperature of 975°C and pressure 35 bar.	115
Table 4.4	Comparison between experimental and theoretical temperature during the gasification of EFB and co-gasification of EFB with Charcoal.	119
Table 4.5	Comparison between experimental and theoretical temperature during the gasification of FR (100%) and co-gasification of FR (70%) with Charcoal (30%).	127
Table 4.6	Comparison between experimental and theoretical temperature during the gasification of CS (100%) and co-gasification of CS (70%) with Charcoal (30%).	135
Table 4.7	Main chemical compounds of co-product tar produced from the co-gasification of CS and Charcoal.	143
Table 4.8	¹³ C NMR and ¹ H NMR data of co-product tar compounds generated from co-gasification of CS and Charcoal.	145
Table 4.9	¹ H NMR data of bioethanol generated from biocatalysts (<i>S. cerevisiae</i> and <i>C. butyricum</i>) based syngas fermentation.	165

LIST OF FIGURES

Figure 2.1	World energy consumption increases for fuels other than coal.	11
Figure 2.2	Non-OECD countries are projected to account for 64% of the 739 quadrillions Btu worldwide energy consumption by 2040.	12
Figure 2.3	Asia is projected to have significant increase in energy use of non-OECD regions.	12
Figure 2.4	World's total primary energy supply (TPES) from 1971 to 2015 by fuel.	13
Figure 2.5	Fuels shares from 1971 to 2015 by total primary energy supply (TPES).	13
Figure 2.6	Worldwide share of Bioenergy.	14
Figure 2.7	Share of renewables by category on transport, heat demand and electricity generation from 2010 to 2035.	15
Figure 2.8	Scenario of past, present and future bioenergy from 1995 to 2085.	16
Figure 2.9	Biomass feedstocks to the final product of syngas and ethanol for heat and power generation.	18
Figure 2.10	Lignocellulosic bio-conversions into value-added bioproducts.	24
Figure 2.11	Cellulose, hemicellulose and lignin structure of biomass cell.	24
Figure 2.12	Thermochemical and biochemical conversion routes for biomass to biofuels.	30
Figure 2.13	Schematic of the major steps involved in gasification in air and oxygen ambiance.	32
Figure 2.14	Co-gasification process for biomass and coal.	35
Figure 2.15	The flow diagram of the Aspen Plus process model.	40
Figure 2.16	Types of Gasifier used for the production of syngas.	41
Figure 2.17	Schematic diagram of fixed bed gasifiers: (a) updraft gasifier (b) downdraft gasifier (c) crossdraft gasifier.	42
Figure 2.18	Schematic diagram of fluidized bed gasifiers: (a) Bubbling fluidized bed gasifier (b) Circulating fluidized bed gasifier.	45
Figure 2.19	Schematic diagram of entrained flow gasifiers.	48
Figure 2.20	Wood-Ljungdahl pathway of acetogens and their metabolic end products.	56
Figure 2.21	Schematic diagram of continuous stirred-tank reactor (CSTR).	58
Figure 2.22	Schematic diagram of a bubble column reactor (BCR).	59
Figure 2.23	Schematics diagram of Monolithic biofilm reactor (MBR) system for syngas fermentation.	60
Figure 2.24	Schematic diagram of a trickle bed reactor (TBR).	61
Figure 2.25	Schematic diagram of membrane-based system reactor (MSR).	62

Figure 2.26	Microbial growth vs time for syngas fermentation.	64
Figure 3.1	Flowchart of research work plan.	68
Figure 3.2	Raw feedstocks for co-gasification: (a) EFB of palm oil, (b) Forest residue, (c) Coconut shell and (d) Charcoal.	69
Figure 3.3	Experimental setup of downdraft reactor for syngas production: (a) feedstocks (EFB, FR, CS and charcoal), (b) air blower (atmospheric air), (c) rotameter, (d) thermocouples, (e) downdraft reactor (including four zones), (f) gas flare points, (g) cyclone separator, (h) cooling heat exchanger, (i) filter, (j) clean gas sampling point, (k) gas sampling point by gas bag (l) temperature data logger, and (m) computer for data analysis.	79
Figure 3.4	Process for the conversion of syngas from lignocellulosic biomass.	81
Figure 3.5	Experimental setup for bioethanol production through syngas fermentation using yeast and bacteria.	83
Figure 3.6	Process for the conversion of bioethanol from syngas.	85
Figure 4.1	Ternary diagram based on VM, FC and Ash for EFB, FR, CS and Charcoal.	88
Figure 4.2	TGA Curves for EFB, FR, CS and Charcoal ('A' zone=Moisture content removal, 'B' zone=Cellulose and Hemicellulose decomposition and 'C' zone=Lignin decomposition).	90
Figure 4.3	DTG curves for EFB, FR, CS and Charcoal at a heating rate of 10 °/min.	91
Figure 4.4	Ternary diagram of C, H and O for EFB, FR, CS and Charcoal.	93
Figure 4.5	Van Krevelen diagram at the atomic ratio of H/C and O/C for EFB, FR, CS and Charcoal.	94
Figure 4.6	Higher heating value (MJ/kg) of feedstocks (EFB, FR, CS and Charcoal) compared with literature value.	95
Figure 4.7	Lower heating value (MJ/kg) of feedstocks (EFB, FR, CS and Charcoal) compared with literature value.	95
Figure 4.8	Comparison of X-ray diffraction spectra of feedstock samples (EFB, FR, CS and Charcoal).	97
Figure 4.9	SEM images for feedstock samples: (a) EFB of palm oil (b) Forest residue.	99
Figure 4.10	SEM images for feedstock samples: (a) Coconut shell and (b) Charcoal.	100
Figure 4.11	FESEM and EDX of feedstocks: (a) EFB of palm oil (b) Forest residue (c) Coconut shell (d) Charcoal.	102
Figure 4.12	TEM analysis of feedstocks: (a-b) EFB of palm oil (c-d) Forest residue (e-f) Coconut shell (g-h) Charcoal.	103
Figure 4.13	FTIR Spectrum of EFB, FR, CS and Charcoal.	105
Figure 4.14	Wide scan XPS curves for EFB, FR, CS and Charcoal.	106

Figure 4.15	X-ray photoelectron spectroscopy (XPS) narrow scan of C1s : (a) EFB of palm oil, (b) Forest residue (FR), (c) Coconut shell (CS) and (d) by-product Charcoal.	107
Figure 4.16	X-ray photoelectron spectroscopy (XPS) narrow scan of O1s : (a) EFB of palm oil, (b) Forest residue (FR), (c) Coconut shell (CS) and (d) by-product Charcoal.	108
Figure 4.17	X-ray photoelectron spectroscopy (XPS) narrow scan of N1s : (a) EFB of palm oil, (b) Forest residue (FR) and (c) Coconut shell (CS).	109
Figure 4.18	X-ray photoelectron spectroscopy (XPS) narrow scan of S2p : (a) EFB of palm oil, (b) Forest residue (FR) and (c) Coconut shell (CS).	110
Figure 4.19	Aspen Plus® flowsheet simulation model for the co-gasification process using lignocellulosic biomass and charcoal for a pilot scale Downdraft Gasifier.	112
Figure 4.20	Simulation mechanisms for co-gasification of biomass (EFB of palm oil, forest residue (FR), coconut shell (CS)) and charcoal in a pilot scale downdraft reactor.	113
Figure 4.21	Aspen Plus® simulation based on the parameters of temperature (500-1200 °C) and pressure (1-45 bar): (a) 1 bar (b) 5 bars (c) 15 bars (d) 25 bars (e) 35 bars (f) 45 bars.	114
Figure 4.22	Economic analysis of product syngas using Aspen Plus® simulator.	116
Figure 4.23	Temperature profile of various downdraft reactor zones (drying zone, pyrolysis zone, oxidation zone and reduction zone) with time during the co-gasification of EFB (70%) and charcoal (30%).	118
Figure 4.24	Syngas composition with various ratios of EFB of palm oil and Charcoal (100:0; 90:10; 80:20; 70:30 and 60:40).	120
Figure 4.25	H ₂ and CO yield (%) of syngas produced from co-gasification of EFB of and Charcoal with various ratios (100:0; 90:10; 80:20; 70:30 and 60:40).	121
Figure 4.26	Syngas ratio (H ₂ :CO) during the co-gasification of EFB of palm oil and Charcoal with various ratios (100:0; 90:10; 80:20; 70:30 and 60:40).	122
Figure 4.27	The syngas flame appearance of raw syngas (a) purified based syngas (b) during the co-gasification of EFB (70%) and Charcoal (30%).	123
Figure 4.28	Exergy efficiency during the co-gasification of EFB of palm oil and charcoal with various ratios (100:0; 90:10; 80:20; 70:30 and 60:40).	124
Figure 4.29	HHV (a) and LHV (b) of Syngas during the co-gasification of EFB of palm oil and Charcoal with various ratios (100:0; 90:10; 80:20; 70:30 and 60:40).	125

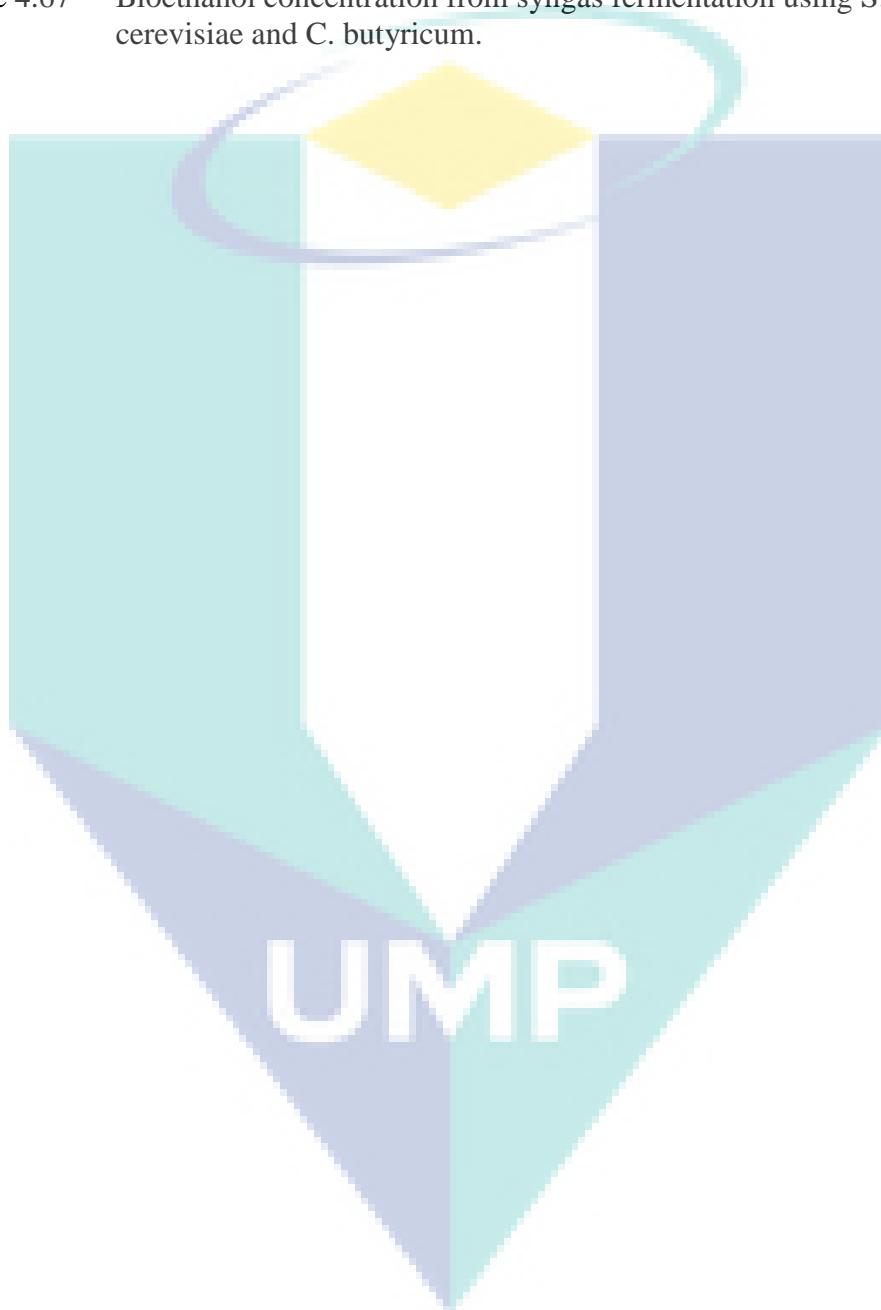
Figure 4.30	Temperature profile of various downdraft reactor zones (drying zone, pyrolysis zone, oxidation zone and reduction zone) with time during the co-gasification of FR (70%) and Charcoal (30%).	126
Figure 4.31	Syngas composition with various ratios of FR and Charcoal (100:0; 90:10; 80:20; 70:30 and 60:40).	128
Figure 4.32	H ₂ and CO yield (%) of syngas produced from co-gasification of FR and Charcoal with various ratios (100:0; 90:10; 80:20; 70:30 and 60:40).	129
Figure 4.33	Syngas ratio (H ₂ :CO) during the co-gasification of FR and Charcoal with various ratios (100:0; 90:10; 80:20; 70:30 and 60:40).	130
Figure 4.34	The flame appearance of raw and purified syngas during the co-gasification of FR (70%) and Charcoal (30%).	131
Figure 4.35	Exergy efficiency during the co-gasification of FR and Charcoal with various ratios (100:0; 90:10; 80:20; 70:30 and 60:40).	132
Figure 4.36	HHV (a) and LHV (b) of Syngas during the co-gasification of FR and Charcoal with various ratios (100:0; 90:10; 80:20; 70:30 and 60:40).	133
Figure 4.37	Temperature profile of various downdraft reactor zones (drying zone, pyrolysis zone, oxidation zone and reduction zone) with time during the co-gasification of CS (70%) and Charcoal (30%).	134
Figure 4.38	Syngas composition with various ratios of CS and Charcoal (100:0; 90:10; 80:20, 70:30 and 60:40).	136
Figure 4.39	Syngas ratio (H ₂ :CO) during the co-gasification of CS and Charcoal at various ratios (100:0; 90:10; 80:20, 70:30 and 60:40).	137
Figure 4.40	Syngas ratio (H ₂ :CO) during the co-gasification of CS and Charcoal with various ratios (100:0; 90:10; 80:20; 70:30 and 60:40).	138
Figure 4.41	The syngas flame appearance of raw (a) and purified (b) based syngas during the co-gasification of CS (70%) and Charcoal (30%).	139
Figure 4.42	Exergy efficiency for co-gasification of CS and Charcoal with the ratios of 100:0, 90:10, 80:20, 70:30 and 60:40.	140
Figure 4.43	HHV (a) and LHV (b) of Syngas during the co-gasification of CS and Charcoal with various ratios (100:0; 90:10; 80:20, 70:30 and 60:40).	141
Figure 4.44	Tar separation process from raw syngas (collected from co-gasification of CS and Charcoal).	142
Figure 4.45	SEM image with EDX of raw co-product tar produced from co-gasification of CS and Charcoal in the downdraft reactor.	144
Figure 4.46	GC-MS chromatogram of co-product tar produced from the co-gasification of CS and Charcoal.	144

Figure 4.47	SEM images of tar samples after thermal treatment: (a) at 700 °C (b) at 800 °C.	146
Figure 4.48	SEM images of tar samples after thermal treatment: (a) at 900 °C (b) at 1000 °C.	147
Figure 4.49	FTIR spectra of tar sample obtained from the co-gasification process: (a) before thermal treatment (b) thermal treatment at 700 °C (c) thermal treatment at 800 °C (d) thermal treatment at 900 °C and (d) thermal treatment at 1000 °C.	148
Figure 4.50	Oxides of by-product of charcoal produced from co-gasification of biomass and charcoal.	149
Figure 4.51	Comparative study on syngas concentration on the co-gasification of EFB with charcoal, FR with charcoal and CS with charcoal (70:30).	151
Figure 4.52	Comparative study on cold gas efficiency on the co-gasification of EFB with charcoal, FR with charcoal and CS with charcoal (70:30).	152
Figure 4.53	Comparative carbon conversion efficiency on the co-gasification of EFB with charcoal, FR with charcoal and CS with charcoal (70:30).	152
Figure 4.54	Comparative study on the heating value of syngas on the co-gasification of EFB with charcoal, FR with charcoal and CS with charcoal (70:30).	153
Figure 4.55	Growth Culture of <i>S. cerevisiae</i> in Petridish and Slant.	154
Figure 4.56	FESEM images of <i>S. cerevisiae</i> : (a) group of the colony (b) single colony.	155
Figure 4.57	Growth Culture of <i>C. butyricum</i> : (a) before inoculation (b) after inoculation at 37 °C for 24 h.	156
Figure 4.58	FESEM images of <i>C. butyricum</i> : (a) group of the colony (b) single colony.	156
Figure 4.59	Effect of treated and untreated syngas on CFU during <i>S. cerevisiae</i> based syngas fermentation.	157
Figure 4.60	Effect of treated and untreated syngas on CFU during <i>C. butyricum</i> syngas fermentation.	158
Figure 4.61	Temperature effect on syngas fermentation.	159
Figure 4.62	Effect of pH on syngas fermentation.	160
Figure 4.63	Effect of TOC on syngas fermentation.	161
Figure 4.64	Effect of syngas composition before and after syngas fermentation.	162
Figure 4.65	Syngas fermentation using <i>Saccharomyces Cerevisiae</i> : (a) ¹ H NMR, 500 MHz (CDCl ₃): δ = 3.75 (q, J = 7.00 Hz, 2H [CH ₂]), 2.19 (s, 1H [OH]), 1.28 (t, J = 3.70 Hz, 3H [CH ₃]). (b) S.	

cerevisiae-based bioethanol MS fraction
(15.01:29.03:31.02:45.01). 163

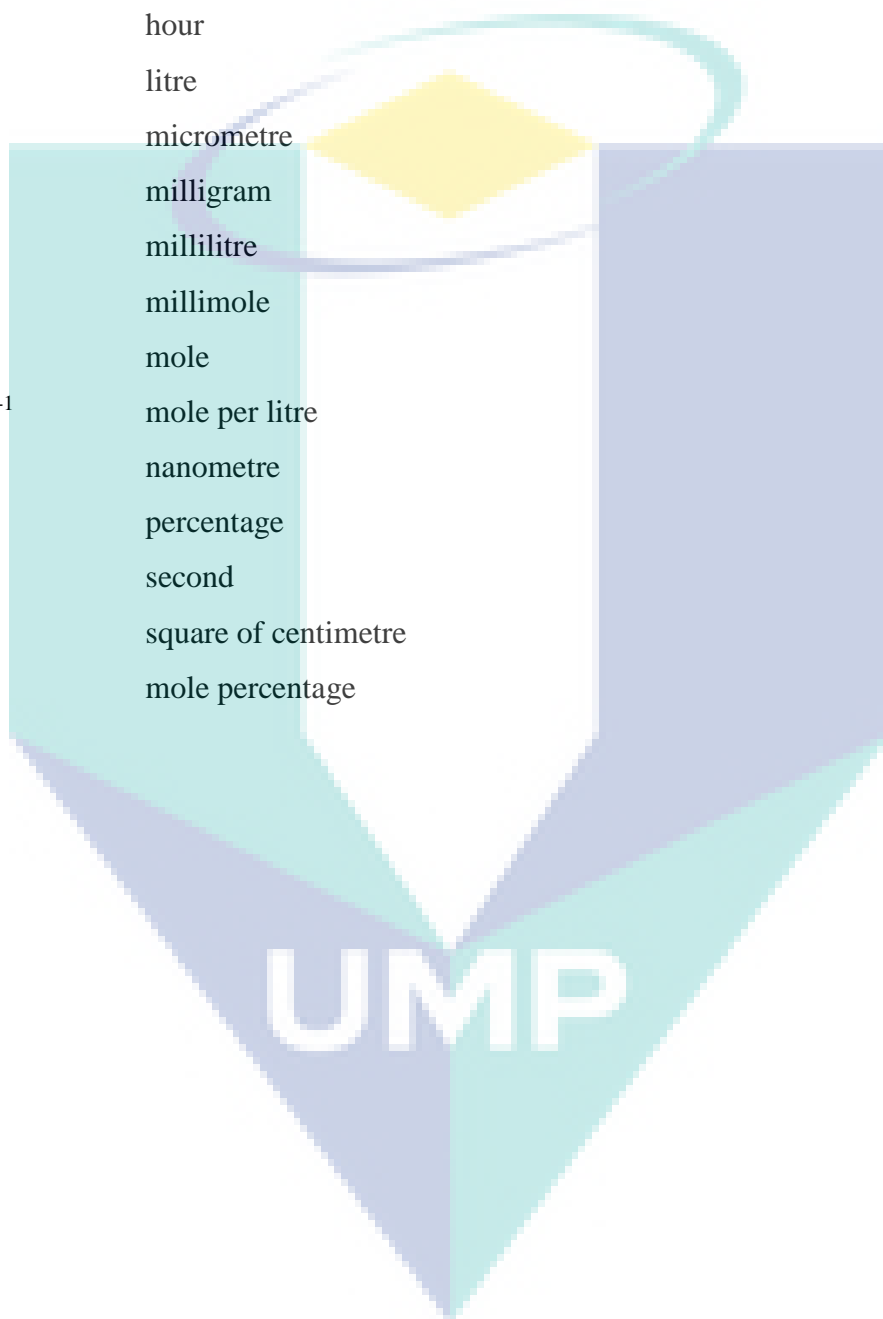
Figure 4.66 Syngas fermentation using *Clostridium Butyricum*: (a) ¹H NMR, 500 MHz (CDCl₃): δ = 3.75 (q, J = 7.00 Hz, 2H [CH₂]), 2.20 (s, 1H [OH]), 1.27 (t, J = 7.00 Hz, 3H [CH₃]). (b) *C. butyricum*-based bioethanol MS fraction (15.02:29.01:31.00:45.01). 164

Figure 4.67 Bioethanol concentration from syngas fermentation using *S. cerevisiae* and *C. butyricum*. 165

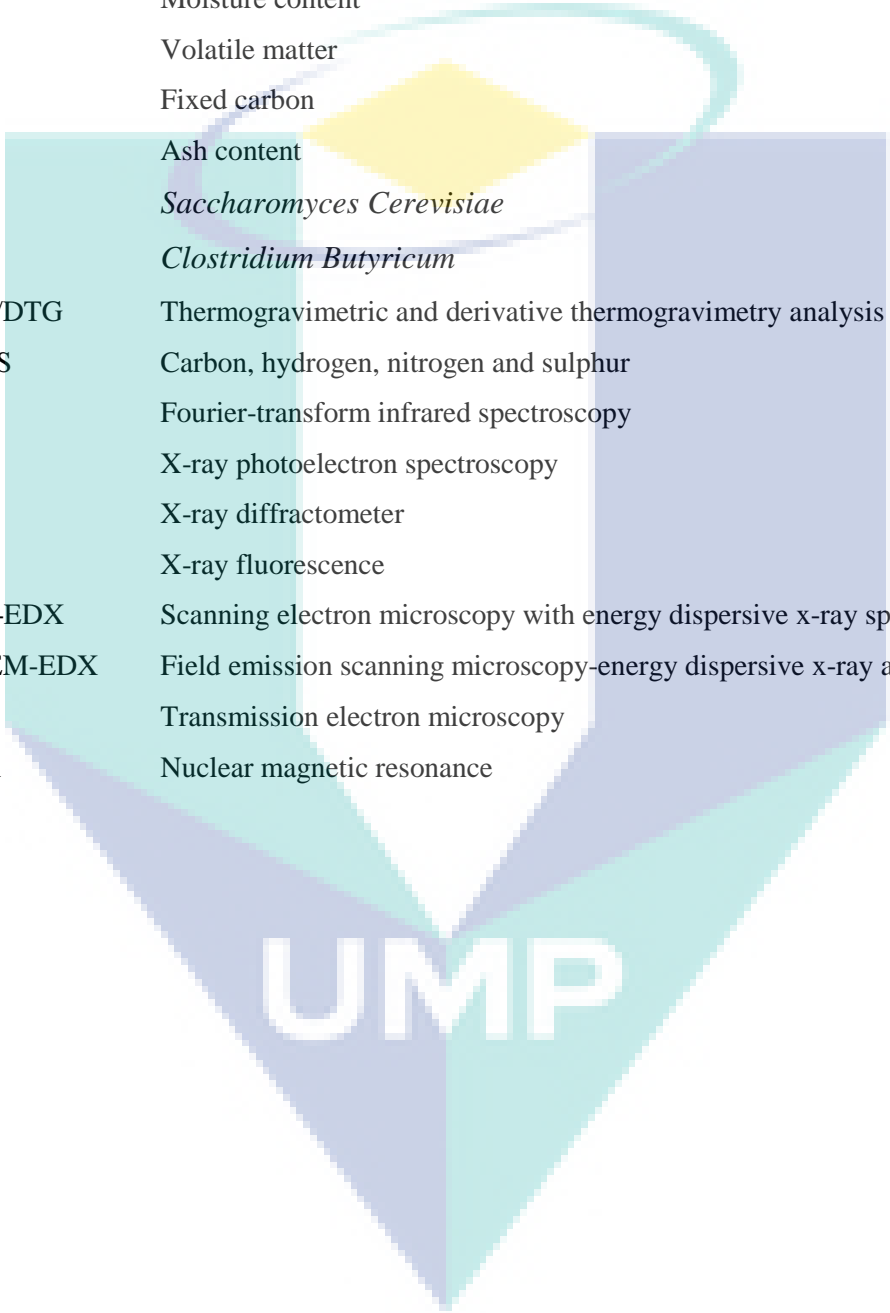


LIST OF SYMBOLS

°C	degree centigrade
g	gram
cm ⁻¹	per centimetre
h	hour
L	litre
µm	micrometre
mg	milligram
ml	millilitre
mmol	millimole
mol	mole
mol L ⁻¹	mole per litre
nm	nanometre
%	percentage
sec	second
cm ²	square of centimetre
mol%	mole percentage



LIST OF ABBREVIATIONS



EFB	Empty fruit bunch (of palm oil)
FR	Forest residue
CS	Coconut shell
MC	Moisture content
VM	Volatile matter
FC	Fixed carbon
AC	Ash content
S.C	<i>Saccharomyces Cerevisiae</i>
C.B	<i>Clostridium Butyricum</i>
TGA/DTG	Thermogravimetric and derivative thermogravimetry analysis
CHNS	Carbon, hydrogen, nitrogen and sulphur
FTIR	Fourier-transform infrared spectroscopy
XPS	X-ray photoelectron spectroscopy
XRD	X-ray diffractometer
XRF	X-ray fluorescence
SEM-EDX	Scanning electron microscopy with energy dispersive x-ray spectroscopy
FESEM-EDX	Field emission scanning microscopy-energy dispersive x-ray analysis
TEM	Transmission electron microscopy
NMR	Nuclear magnetic resonance

CHAPTER 1

INTRODUCTION

1.1 Research Background

Worldwide energy demand is increasing exponentially due to the rising trend of energy consumption, rapid growth of population, urbanization and industrial expansion which results in depletion of fossil fuels (coal, oil, and gas) (Kurniawan & Managi, 2018; Moriarty & Honnery, 2019); Paiman, Hamzah, Idris, Rahman, and Ismail (2018). More than 80% of global energy demand is covered by non-renewable energy resources, whereas renewable energy resources cover only 10-15% (Capuano, 2018; Singh & Sekhar, 2016). However, incessant advancement of petroleum exploitation technology and discovery of new natural resources, the increased production could not appease the required energy demand (Lee, Speight, & Loyalka, 2014; Sikarwar, Zhao, Fennell, Shah, & Anthony, 2017). As a result, there is a gap occurs between the demand and supply of these fuel resources. In this regard, Serrano-Ruiz (2017) mentioned that limited fossil fuels will be diminished in the near future. Moreover, Malek, Hasanuzzaman, Rahim, and Al Turki (2017) reported that in the last two decades, power consumption has been increased three times in five ASEAN countries (Malaysia, Indonesia, Philippine, Thailand, and Vietnam). Therefore, more attention has been taken to search for an alternative clean and sustainable energy sources to meet up the future energy demand.

Biomass is one of the most promising alternative energy sources for the production of bioethanol owing to future fuel security and environmental issues (Basu, 2018; Wyman, 2018). They reported that it contains a negligible amount of sulfur (S) and produces least ash debris which generates clean and sustainable energy. Gaurav, Sivasankari, Kiran, Ninawe, and Selvin (2017) also reported that biomass is the fourth largest available renewable energy resource that is reliance on fossil fuels and mitigates

global warming. Biomass-derived fuels (such as agricultural wastes, grasses, energy crops, forest and wood wastes, coconut shell, empty fruit bunch of palm oil, cocoa, sugarcane, industrial residues and municipal solid wastes) are employed as the raw materials for energy production (Catalán-Martínez, Domine, & Serra, 2018; Jin & Sutherland, 2018; Kamble, Saxena, Chavan, & Mendhe, 2018; Singh, Mahanta, & Bora, 2017). This biomass appears to be a potential source of energy due to their sustainability and carbon-neutrality to replace the existing non-renewable energy sources. Lignocellulosic biomass is the most favorable and fastest-growing renewable energy sources to generate bioenergy (Isikgor & Becer, 2015; Kundu, Chatterjee, Bhattacharyya, Roy, & Kaur, 2018). This type of biomass absorbs and stores energy from sunlight in the form of chemical energy through photosynthesis process. Lignocellulosic biomass is composed of three main components: cellulose (40-50 wt.%), hemicellulose (25-35 wt.%) and lignin (16-33 wt.%) (Cai et al., 2017). Generally, the biomass comprises chemical bonds of C-C, C-O and some other elements (Basu, 2018; Bhaskar et al., 2011). The main elements are carbon, hydrogen and oxygen that are bonded together and are fragmented by combustion or decomposition (Basu, 2018). Therefore, bioenergy containing biomass is converted into energy through thermochemical conversion of combustion, pyrolysis and gasification (Kundu et al., 2018). In terms of environmental consideration, biomass contained a minor amount of S which produce fewer ash particles and generate less air pollution in comparison with fossil fuels (Ahmad, Zawawi, Kasim, Inayat, & Khasri, 2016; Cai et al., 2017; Khatun, Monir, Arham, & Wahid, 2016). As a result, biomass combustion does not provide sulfur dioxide (SO₂) through emissions, which may cause acid rain. Samiran, Jaafar, Ng, Lam, and Chong (2016) reported that the use of biomass for energy production in Malaysia is not widespread yet. Suzuki, Tsuji, Shirai, Hassan, and Osaki (2017) also emphasized on bioenergy utilization from lignocellulosic biomass of empty fruit bunch of palm oil, forest residue and coconut shell. In this aspect, this biomass-based bioenergy is a suitable alternative for non-renewable energy sources in the future for Malaysia as well as globally.

Malaysia is the world's second-largest producer and exporter of palm oil after Indonesia and produces about 47% of the world's supply of palm oil (Kaman, Tan, & Lim, 2017; Mujah, 2016). Considering the total lifetime of oil palm tree plantation, only 10% by weight is converted to the ultimate product (palm oil and kernel oil); while the remaining 90% becomes biomass waste in the form of EFB, kernel shells, palm oil mill

effluent (POME), trunks and oil palm fronds (OPF) reported by Atnaw, Sulaiman, and Yusup (2013). Oil palm waste is reported to be the second largest biomass energy potential in this country, next to the forest residue (Suzuki et al., 2017). The huge amount of forest residues have been producing throughout the year from the forest of Malaysia (Osman, Othman, Karim, & Mazlan, 2014). Coconut is another major crops in Malaysia with 142,000 ha of planted land. The massive amount of solid wastes are generated annually, mostly in the form of fiber and shell (Suzuki et al., 2017). Hence, the conversion of this potential biomass into bioenergy is the most suitable option for future energy demand. Consequently, by-product charcoal is produced by the slow heating of biomass in the absence of oxygen (O₂) through biomass gasification (Kaman et al., 2017). This by-product charcoal is also the potential energy sources for better combustibility by co-firing with biomass (Yi et al., 2013).

Gasification is one of the most promising thermo-chemical conversion processes to recover energy from biomass (Molino, Chianese, & Musmarra, 2016; Samiran et al., 2016). There are some simulation softwares (Aspen Plus, Response Surface Methodology, MATLAB and Computational Fluid Dynamics) which are widely used for parametric optimization of gasification that reduce experimental time and cost (Anil, Rupesh, Muraleedharan, & Arun, 2016; Che, Li, Yang, Jia, & Zheng, 2012; Kaushal & Tyagi, 2017b). Energy conversion through gasification involves some frequent processes which are drying, pyrolysis, oxidation and reduction and yield products are obtained in three stages: low molecular weight liquids, gas fuels and solid residues (Molino et al., 2016; Sikarwar et al., 2016). This syngas is produced through the gasifiers; such as fixed bed gasifier (updraft, downdraft and crossdraft), fluidized bed gasifier (circulating and bubbling) and entrained flow gasifier (Oakey, 2015). Biomass gasification through downdraft gasifier is most widely used due to its high conversion efficiency of the producer syngas (Zhang, Zhao, Gao, Li, & Huang, 2015). The choice of the gasifier depends on feedstock type, size, moisture content, and gasifying agents (steam/oxygen/air) reported by Sansaniwal, Pal, Rosen, and Tyagi (2017). Among these, downdraft gasifier produces the least amount of tar, and reduction zone plays a vital role in the maximum conversion of tar and high-quality syngas (Chaurasia, 2018). Moreover, raw syngas is difficult to use directly as a power generation or transportation fuel purposes due to presence of tar and particle impurities. Widespread research on single biomass has already been carried out by downdraft gasifier (Sikarwar et al., 2016; Singh & Sekhar,

2016). However, co-gasification of biomass and charcoal by downdraft gasifier has not been studied yet. Therefore, downdraft gasifier is the best option for co-gasification of biomass and charcoal for this research, which could be considered as a potential fuel for syngas production (Sikarwar et al., 2017) and further syngas fermentation for bioethanol production (Hossain, Zaini, & Mahlia, 2017).

Co-gasification of lignocellulosic biomass from empty fruit bunch (EFB) of palm oil, forest residue (FR), coconut shell (CS) and charcoal by downdraft gasifier provides an opportunity to combine the advantages of the well-researched usage of biomass. The produced syngas is potential for the production of biofuels (such as ethanol) through syngas fermentation and further, it is used as transport fuels and electricity generation purposes (Sikarwar et al., 2017). The by-product CO₂ is also produced from this process and it could be used for enhancing the oil or gas recovery (Atia, 2016; Khatun et al., 2016), which may also take part to reduce the greenhouse gas content (Mikulcic, Klemeš, Vujanovic, Urbaniec, & Duic, 2016). Moreover, by giving the valorization of by-product charcoal which enhanced the economic and environmental validity of the lignocellulosic biomass to biofuels pathway, without being affected by fluctuating fossil fuel.

There are various types of biocatalysts are used for syngas fermentation. These biocatalysts are capable of bioethanol production through gas fermentation (Davis et al., 2018; Foo et al., 2017; Sayed & Abdelkareem, 2017). The advanced technique of syngas fermentation, syngas is used as a raw material that is produced from biomass gasification (Asimakopoulos, Gavala, & Skiadas, 2018; Sikarwar et al., 2017). Commonly, biocatalyst of yeast and bacteria are used for the production of bioethanol. The model biocatalysts that are usually used for bioethanol productions are *Clostridium sp.*, *Escherichia coli*, *Bacillus sp.* (bacteria), *Saccharomyces cerevisiae* (yeast) and *Trichoderma reesei*, *Fusarium oxysporum* (fungi) (Alfenore & Molina-Jouve, 2016). *Saccharomyces cerevisiae* is one of the most important biocatalysts because of its cost-effectiveness in comparison to other fermenting agents that are produced zero chemical wastes reported by Hossain et al. (2017). *Clostridium butyricum* is also an important biocatalyst because of its hydrogen productivity (Shen, Brown, & Wen, 2017; Zhang, Taylor, & Wang, 2016). For environmental considerations, bioethanol production by *S. cerevisiae* has been playing a key role in fermentation industry (Akhtar, 2016). This is

considered as an ideal biocatalyst for bioethanol production in the sugar-containing a nutrient medium.

In the literature, an insufficient work has been attempted through the detail characterization of EFB, FR, CS and charcoal, simulations for co-gasification using Aspen Plus®, syngas production using these feedstocks and biomass-based syngas fermentation for bioethanol production. According to the literature, there are insufficient study has been focused on syngas fermentation with *S. cerevisiae* for gas containing a nutrient medium, and very limited works with *C. butyricum* for syngas fermentation using biomass-based syngas. Therefore, the aim of this study is to produce clean, sustainable and environmental friendly syngas and bioethanol through the hybrid process of co-gasification (using lignocellulosic biomass and by-product charcoal) and syngas fermentation (using *S. cerevisiae* and *C. butyricum*).

1.2 Problem Statement

There are bottleneck works have been observed in terms of energy production from empty fruit bunch of palm oil, forest residue, coconut shell and by-product charcoal, although these biomasses are available in Malaysia. In the rural area, biomass burning in the open field causes environmental pollution and release greenhouse gases to the atmosphere which is one of the reasons for global warming. Although these lignocellulosic biomasses are stored energy through the photosynthesis process. However, existing practices are inefficient and environmentally unhealthy. Moreover, selected biomasses have not been characterized well for bioenergy potentiality yet, and insufficient work has been observed on parametric optimization for the production of syngas and bioethanol through co-gasification and syngas fermentation.

The co-gasification process involves some complex chemical reactions which are challenging to simulate properly and difficult to solve using algorithms. Moreover, experimental cost and time increase without any simulation. Although, Aspen Plus simulator has the facilities to see the warnings before running the simulations. Downdraft gasifier (DG) is usually used for syngas production because of its easy operation and low maintenance cost. However, the initial yield of syngas through biomass gasification is contained an unwanted co-product tar compounds, some impurities and ash content. As a result, syngas causes serious effects on further processing to other fuels due to the

presence of tar and particles. Consequently, impure syngas is difficult to use directly as for power generation or transporting fuels purposes. Moreover, produced syngas exists in the gaseous phase, and existing engines are needed for additional modification which is very expensive. Co-gasification of lignocellulosic biomass (EFB, FR and CS) with charcoal, and thereafter bioethanol from syngas fermentation using the biocatalyst of yeast (*S. cerevisiae*) and bacteria (*C. butyricum*) have not been studied yet. In the biochemical pathway, whole biomass including lignin is not converted into bioethanol. In addition, due to the complex pretreatment and high enzymes cost, the conventional fermentation process is not feasible.

Therefore, a gap exists on the co-gasification of lignocellulosic biomass (EFB, FR, CS) with charcoal for sustainable energy production with high efficiency. Moreover, by-product charcoal is attempted to reuse with biomass for the substitute of coal which enhanced the gasification process, and mineral nutrients for biocatalyst through syngas fermentation. Aspen Plus simulation is needed for parametric optimization of the process. In addition, tar-free syngas is needed to use for syngas fermentation by adding a purification system on the feed-batch mood bioreactor for the production of bioethanol. Thus, an alternative option is necessary for the production of clean and sustainable energy which could be the substitute for fossil fuel in the future.

1.3 Objectives

The main objective of this study is to produce bioethanol from co-gasification of lignocellulosic biomass with charcoal through syngas fermentation using yeast (*S. cerevisiae*) and bacteria (*C. butyricum*). The specific objectives and future outcomes from this study are summarized as –

- (a) To optimize the operating parameters (temperature, pressure) for syngas production using Aspen Plus® (V 8.6).
- (b) To produce syngas from feedstocks in a downdraft gasifier (DG) using co-gasification approach.
- (c) To perform the conversion of syngas to bioethanol using fermentation technique in a tar free bioreactor (TFB).

1.4 Scope of the Study

This study focuses on the two combine processes of thermochemical and biochemical for the production of syngas and bioethanol, respectively. This hybrid process utilizes the whole lignocellulosic biomass (including lignin) for the production of valuable fuels. Therefore, the produced clean and sustainable fuels can be used as transport fuels and power generation purposes for the fulfillment of future energy demand worldwide.

The mostly available three different types of lignocellulosic biomass of EFB, FR and CS are plenty in Malaysia that were characterized physiochemically in this research to find out their bioenergy potentiality. This study made a humble attempt for the co-gasification of biomass with by-product charcoal whether it is used as the substitute of coal in the future. The findings from characterization can be useful in assessing the optimum parameter for the co-gasification process and monitoring the thermochemical degradation of whole biomass as the reference data.

The simulation results using Aspen Plus® has directed the optimize parameters (temperature and pressure) for minimization of experimental cost and time. Moreover, economic analysis has been notified and evaluate optimum price of syngas.

The co-gasification approach of biomass with various ratios (0-40%) of by-product charcoal in a downdraft gasifier (DG) has clearly mentioned the optimized process and its mechanisms for the production of syngas. In addition, during the experimental study, syngas has been investigated by a portable online gas analyzer and further it was analyzed by a gas chromatography-thermal conductivity detector (GC-TCD). Moreover, the co-product tar has the opportunity to investigate reduction from syngas by thermal cracking at the temperature ranges from 700 °C to 1000 °C.

This research also focuses the biomass-based syngas fermentation that has been performed in a fed-batch mode fermentation technique and observed the concentration of bioethanol production considering various effects like syngas impurity, temperature, pH, TOC, CFU and syngas composition for optimizing the production efficiency. This study has been facilitated by adding a TFB for clean bioethanol production by using the biocatalyst of yeast (*S. cerevisiae*) and bacteria (*C. butyricum*). Finally, this study has the

scope to detect the yield by using nuclear magnetic resonance (^1H) and gas chromatography-mass spectrometry (GC-MS) analyzers. Additionally, from this research by-product charcoal has the opportunity to be reused both the thermochemical and biochemical process due to its valorization.

The ultimate results of this study are also anticipated to be applicable for effective bioenergy production. This research could be used for future advanced research and also for implementing the biomass conversion power plant projects by using a downdraft gasifier and a tar free bioreactor, and for further future advanced research as reference work. Moreover, these results would be beneficial to the peoples of rural areas where plenty of lignocellulosic biomass are available and for researchers who will research for the enhancement of bioethanol production.

1.5 Significance of the Study

The biomass-based syngas production from co-gasification through a pilot-scale downdraft gasification gasifier (50 kWth) using three different types of biomasses (EFB, FR, CS) with by-product charcoal has great importance for the generation of bioenergy (syngas). Limited works have been done by using these biomasses with natural coal and most of these studies were focused on the yield of syngas. Few researchers have focused on biomass gasification using pilot scale downdraft gasifier, optimization by using the simulator and kinetic reactions approach. Thus, in this approach, an Aspen Plus® (V 8.6) simulator was used to find out the precise parameters for process optimization and thereby minimized the experimental cost and ultimately attempted to the valorization of by-product charcoal. In this study, two different types of biocatalysts of yeast (*S. cerevisiae*) and bacteria (*C. butyricum*) were used for syngas fermentation that was not been used as biomass-based syngas yet. By-product charcoal was also reused in this study as a nutrient of yeast (*S. cerevisiae*) and bacteria (*C. butyricum*) during syngas fermentation. The obtained result in this work has a great advantage in the diverse areas of waste and biomass valorization, and ultimately more efficient clean and sustainable energy utilization for future energy demand.

1.6 Thesis Outline

This research work has been presented in this thesis and aims to produce syngas and bioethanol from the co-gasification of lignocellulosic biomass with charcoal through syngas fermentation using yeast (*S. cerevisiae*) and bacteria (*C. butyricum*). It also intended to apply the optimized parameters for co-gasification using Aspen Plus® (V8.6). The outline of this thesis is as follows: Chapter 1: Presented of the research background, problem statement, objectives of the study, scope of the study, significance of the study and the thesis outline. Chapter 2: Provided the theoretical parts that are related to this study. Chapter 3: Presented the procedures of co-gasification and syngas fermentation pathways adopted in the research. Chapter 4: Presented the characterization, optimized parameters for experimental works and produced syngas and bioethanol. Chapter 5: Concluded the research by agreeing on the results with the theoretical and experimental findings. Finally, some important suggestions that will make a new horizon for future researchers are included.



UMP

CHAPTER 2

LITERATURE REVIEW

This chapter represents the previous research interest with significant progress related to the biomass gasification and syngas fermentation for the production of syngas and bioethanol. Potential feedstocks for bioenergy production, gasification optimization using Aspen Plus® (V8.6) simulator, thermochemical conversion (gasification or co-gasification) for syngas production and syngas fermentation using biocatalysts (microorganism) for bioethanol production, and their parametric effects are critically discussed. The effects on syngas composition and bioethanol concentration based on the type of gasifier (reactor) and fermentor using various mixture of feedstocks are discussed. Moreover, co-gasification of lignocellulosic biomass with an alternative feedstock of by-product charcoal with their heating value and exergy efficiency, tar reduction from syngas and syngas fermentation mechanisms are also discussed. This chapter closes with a critical discussion on the opportunities and challenges of hybrid co-gasification and syngas fermentation process, and finally future research directions on syngas and bioethanol production.

2.1 Global Energy and Its Demand

Worldwide, ever-diminishing fossil-based fuels and its increasing demand require energy security that has become a public concern in recent time (Konur, 2018). These anxieties on energy crisis have required an alternative, clean and sustainable energy resources. Generally, energy is produced from renewable and non-renewable resources (Shankar & Shikha, 2017). They recommended that energy is directly related to the economic development of a nation that is facing the world today. In this emergency situation, the world needed to produce more energy from the most available energy resources (Gupta, De, Gautam, Dhar, & Pandey, 2018). Moreover, continuous uses of

fossil-based fuels (oil, gas, and coal) at the present rate is believed to present global warming that affected climate changes. Accordingly, Shankar and Shikha (2017) emphasized on the renewable energy sources that are used for the generation of electricity, water boiling, motor fuels, and off-grid energy services.

Presently, a major portion of energy is produced from non-renewable energy resources, whereas these are limited in their reserve. The main sources of these resources are oil, gas and coal that are usually stored within the surface or subsurface (Furuoka, 2017). When oil or gas are extracted from underground it required to be refined into gasoline so that it can be used in a vehicle and transported to the gas stations where it can be used by the consumers (Clews, 2016).

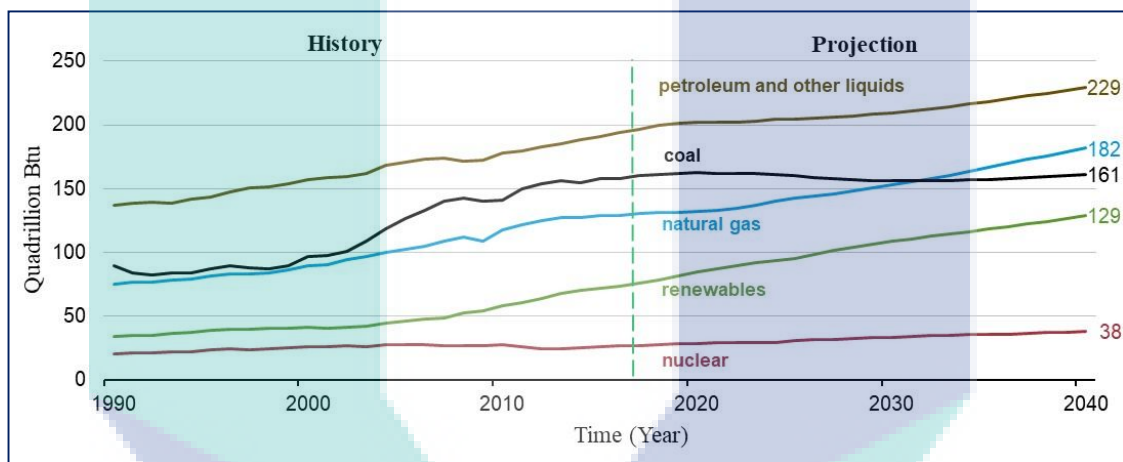


Figure 2.1 World energy consumption increases for fuels other than coal.

Source: International Energy Outlook (2018) Capuano (2018).

Capuano (2018) reported in EIA's International Energy Outlook 2018 that the world's energy consumption increases on average through 2040 for all type of fuels that are shown in Figure 2.1. In this report, it is mentioned that energy consumption in the non-OECD countries started to exceed OECD consumption in 2007 and is projected to reach approximately two-thirds of the 739 quadrillions Btu global energy consumption in 2040 (Figure 2.2). Figure 2.3 represents the largest increase in energy that has used by the non-OECD regions of Asia.

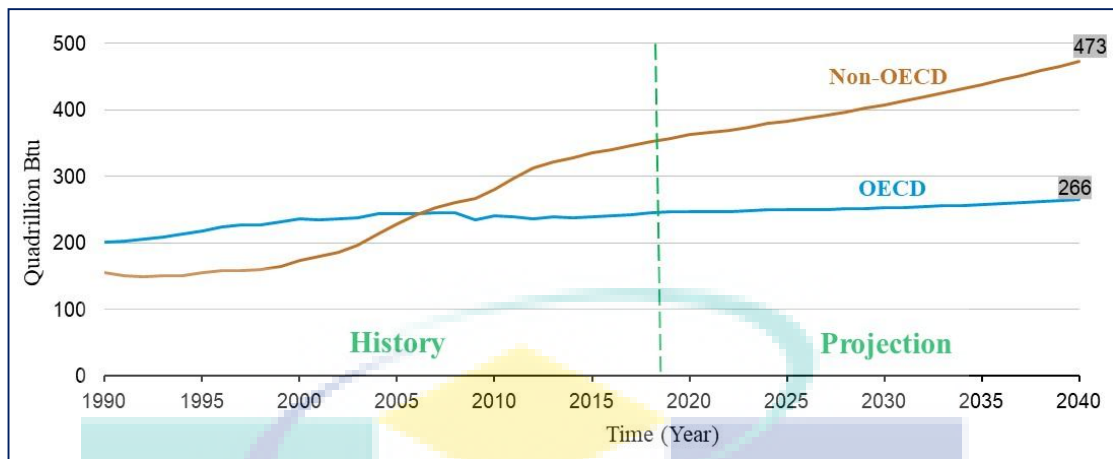


Figure 2.2 Non-OECD countries are projected to account for 64% of the 739 quadrillions Btu worldwide energy consumption by 2040.

Source: EIA, International Energy Outlook (2018) Capuano (2018).

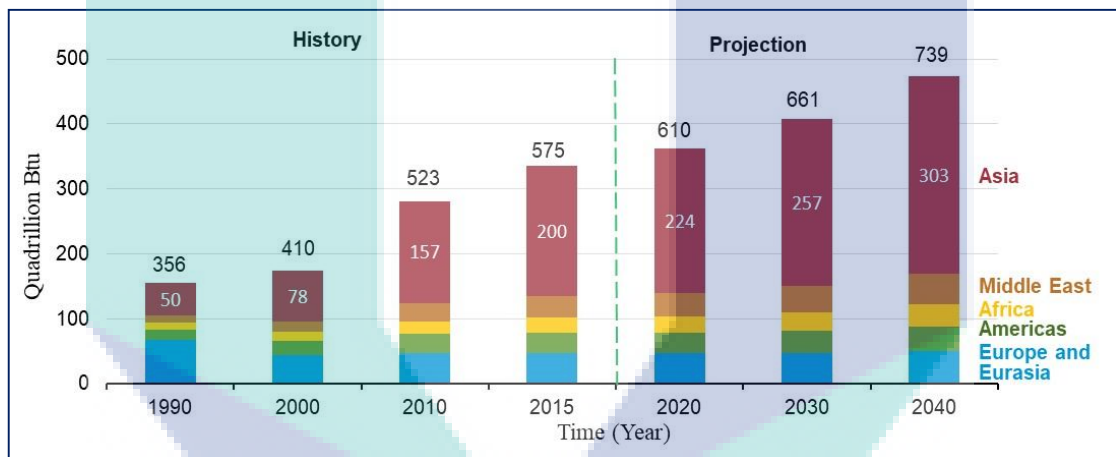


Figure 2.3 Asia is projected to have significant increase in energy use of non-OECD regions.

Source: International Energy Outlook (2018) Capuano (2018).

The total amount of electricity consumed worldwide was 12,116 TWh in 2000, 15,105 TWh in 2005, 16,503 TWh in 2008, and 19,504 TWh in 2013. At the end of 2014, the total installed electricity generating capacity globally was nearly 6.142 TW which only included generation connected to local electricity grids reported by Birol (2017). Moreover, there is an unpredictable amount of heat and electricity expended off-grid by isolated industries and villages. In 2014, the share of world energy consumption for power generation by source was natural gas (21.6%), natural coal (40.8%), hydro (16.4%), nuclear (10.6%), and other sources of solar, wind, geothermal, biomass, etc. (6.3%) and oil (4.3%). Natural gas and coal were the most consumed energy fuels for producing

power generation. In 2012, the world's electricity consumption was 18,608 TWh (Birol, 2017). World's total primary energy supply (TPES) by fuel from 1971 to 2015 are shown in Figure 2.4 and Figure 2.5.

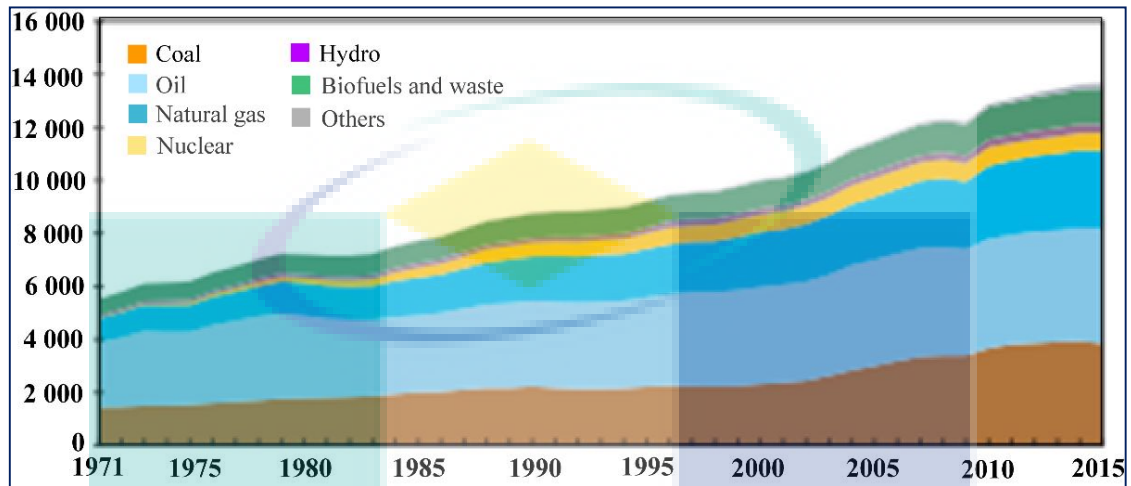


Figure 2.4 World's total primary energy supply (TPES) from 1971 to 2015 by fuel.

Source: Birol (2017).

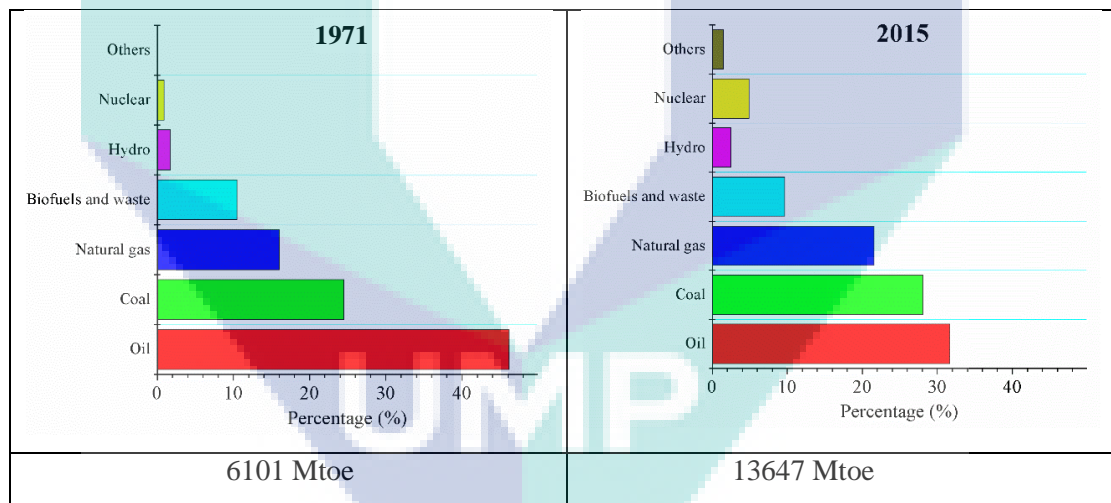


Figure 2.5 Fuels shares from 1971 to 2015 by total primary energy supply (TPES).

Source: Birol (2017).

In 2016, while the total world energy derived from around 80% of fossil fuels, 10% of biofuels, 5% of nuclear and 5% of renewable (hydro, wind, solar, geothermal), but only 18% of that total global energy was in the form of electricity reported by Janda and Tan (2017). They also mentioned that most of the other 82% was used for heat and transportation purposes.

2.2 Biomass-based Energy

The renewable energy sources that are commonly replaced by nature and derived directly from the sun (thermal, photo-chemical, photo-electric, etc.), indirectly from the sun (wind, hydropower, and photosynthetic energy stored in biomass), or from other natural movements and mechanisms of the environment (geothermal and tidal energy) (Ellabban, Abu-Rub, & Blaabjerg, 2014; Toklu, 2017). This type of energy resource does not include energy resources derived from fossil-based fuels, waste products from fossil sources, or waste products from inorganic sources. The technologies involved that turn these natural renewable energy sources into usable forms of energy-electricity, heat and fuels are represented graphically by Figure 2.6. Figure 2.7 represents the overview of renewable energy sources that shared the bioenergy worldwide.

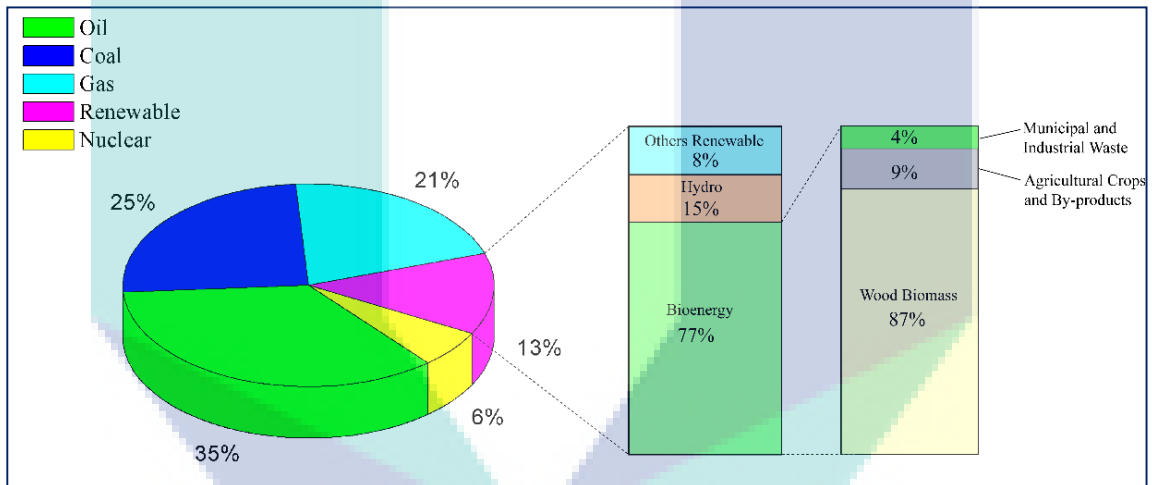


Figure 2.6 Worldwide share of Bioenergy.

Source: Toklu (2017).

In Figure 2.7, it has been observed that the renewable energy markets in electricity, heating and transportation sectors have been rising abruptly over the last few years. Ellabban et al. (2014) reported that the utilization of well-known technologies, such as hydro, as well as recent technologies (wind and solar system), has increased rapidly, which has improved and modified their technological design by minimizing its costs.

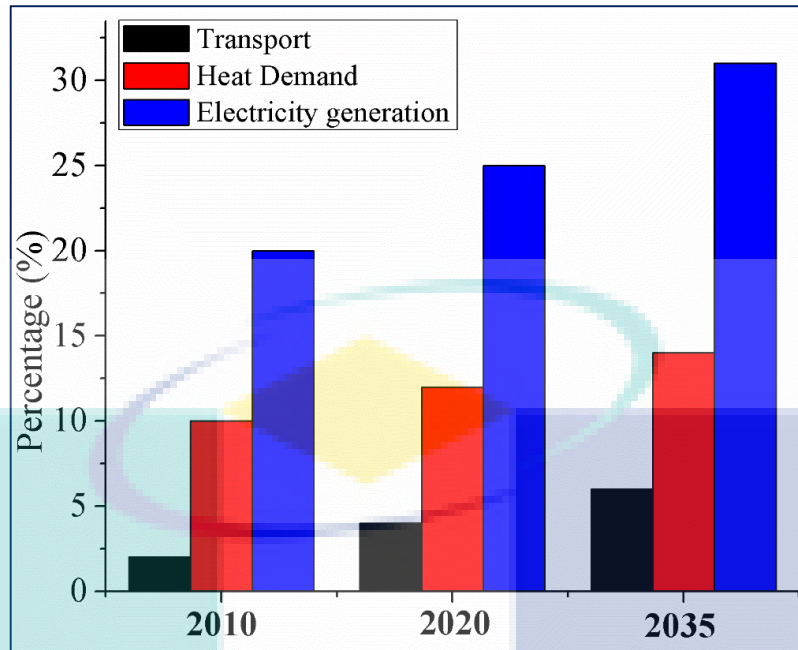


Figure 2.7 Share of renewables by category on transport, heat demand and electricity generation from 2010 to 2035.

Source: Ellabban et al. (2014).

Biomass refers to organic material that are mainly agricultural residues, grasses, energy crops, forest residues, wood residues and municipal paper wastes that are used for bioenergy production (Alfenore & Molina-Jouve, 2016; Singh et al., 2017). Biomass-based energy (bioenergy) is the conversion of biomass into useful forms of energy such as heat, electricity and liquid fuels (biofuels) reported by Kundu et al. (2018). Mostly available biomasses are usually used for energy production addressed by many researchers reported in the literatures (Atnaw et al., 2013; Atnaw, Sulaiman, & Yusup, 2017; Edrisi & Abhilash, 2016; Hassan, Lim, & Hameed, 2016; Kennes, Abubackar, Diaz, Veiga, & Kennes, 2016; Lee et al., 2014; Molino et al., 2016; Osman et al., 2014; Pambudi, Itaoka, Chapman, & Dinh; Richardson, Drobek, Julbe, Blin, & Pinta, 2015; Samiran et al., 2016; Sansaniwal et al., 2017; Sharma, Attanoor, & Dasappa, 2015). Shone and Jothi (2016) reported that leafy biomass are directly used for combustion or to extract the combustible gas using gasifiers. Moreover, Emami-Taba, Irfan, Wan Daud, and Chakrabarti (2013) studied the co-gasification effect of biomass, coal and their blends on the production of H₂, CO₂, CO, CH₄ and other hydrocarbons. They suggested that higher biomass ratio gives lower H₂ but produces higher CO, CO₂, CH₄ and hydrocarbons. In the contrary, the higher ratio of biomass gives lower charcoal, H₂S, and NH₃, although it produces a higher yield of tar compounds.

In the literature, Sansaniwal et al. (2017) reported that thermochemical conversion of biomass was familiarized since 1800s, especially for cooking and lighting purposes. Anex et al. (2010) studied on the techno-economic comparison of biomass into transportation fuels through pyrolysis, gasification, and biochemical pathways and later on Brown, Thilakaratne, Brown, and Hu (2013) also studied on the techno-economic analysis of biomass to transportation fuels and electricity via fast pyrolysis and hydroprocessing. Subsequently, Samiran et al. (2016) performed the gasification process for the production of syngas from biomass materials. They informed that produced syngas is mainly composed of CO and H₂, which are usually used as a fuel source for power generation and transport fuels. They also mentioned that biomass characterization is needed prior to gasification in order to choose a suitable method for specific biomass. Recently, Reddy and Vinu (2018) reported that the quality of yield products (syngas and liquid oils) and gasification process efficiencies depend on the operating parameters, that in turn depend on the characterization of feedstocks. Moreover, Kennes et al. (2016) reported biofuel conversion is obtained from biomasses and wastes through the fermentation process by two major routes: hydrolytic route and thermochemical route.

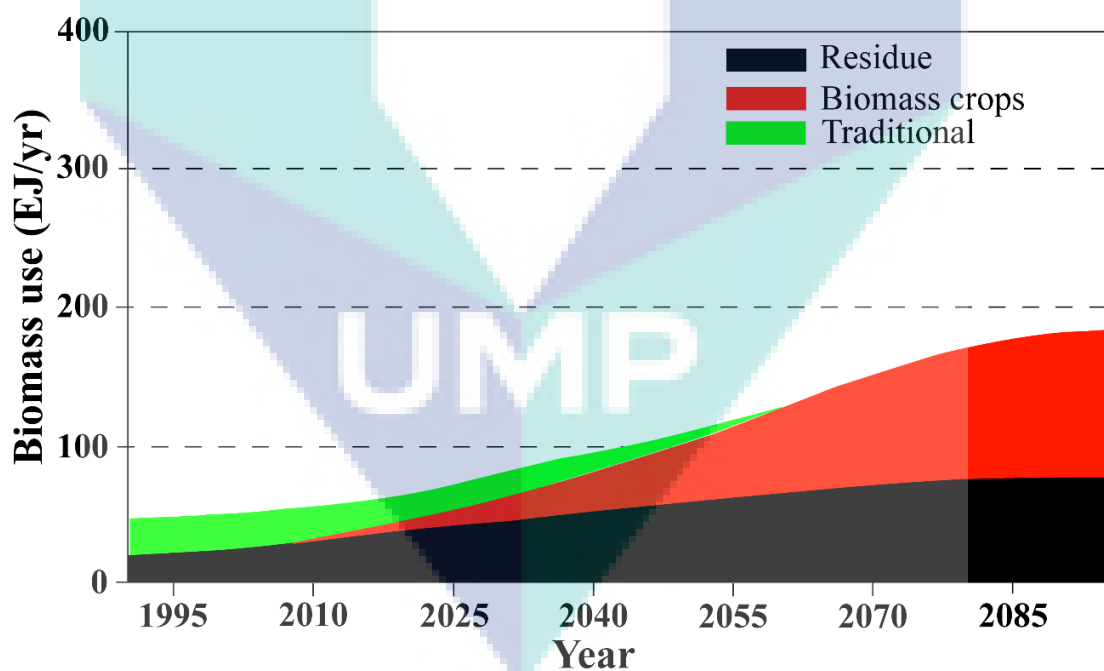


Figure 2.8 Scenario of past, present and future bioenergy from 1995 to 2085.

Source: Speight (2011).

Therefore, biomass-based energy is the most promising and potential renewable energy sources to fulfill the global energy requirements in the future. Accordingly, in the last few decades, every government emphasized the application of bioenergy in the transportation sector and for combined heat and power (CHP). In the 1990 s, about 50 EJ of bioenergy was generated from biomass, which is approximately 9% of the total energy consumption globally, and around 3 EJ out of this was used as the transporting fuels (Biol, 2017). Therefore, the application of biomass has been increasing every year and is expected its importance in coming years is reported by Konur (2018). Considering its importance, governments and organizations have been improving biomass conversion techniques by modifying their strategies, rules and legislation for the production of heat, power and biofuels (Searle & Malins, 2015). Speight (2011) reported that potential part of bioenergy by 2050 would be about 100 EJ, which will further rise to 190 EJ by 2085, as represented in Figure 2.8. Thus, this would be vast potential of biomass-derived bioenergy, which could not only contribute to ease the requirement for fossil-based fuels (oil, gas, coal, etc.) although it also leads to the development and expansion of rural areas with fewer adverse environmental impact.

2.3 Energetic Utilization of Biomass

There are three different categories of primary fuels that are produced from biomass through the thermochemical conversion processes (Basu, 2010, 2018). These biomass-based fuels are as follows:

- (a) Solid products: The solid products are charcoal, torrefied biomass.
- (b) Liquid products: The liquid products are bioethanol, methanol, biodiesel, vegetable oil and pyrolysis oil.
- (c) Gaseous products: The possible gaseous products are biogas (CH_4 , CO_2), producer gas (CO , H_2 , CH_4 , CO_2), syngas (CO , H_2), substitute natural gas (CH_4).

Basu (2018) also reported that these biomass-based fuels are usually used as electricity generation, heat energy production, transportation fuels, other chemicals production (fertilizer, synthetic fiber etc.) purposes. Figure 2.9 represents the biomass-based feedstock conversion process to the final product of syngas and ethanol including heat and power generation.

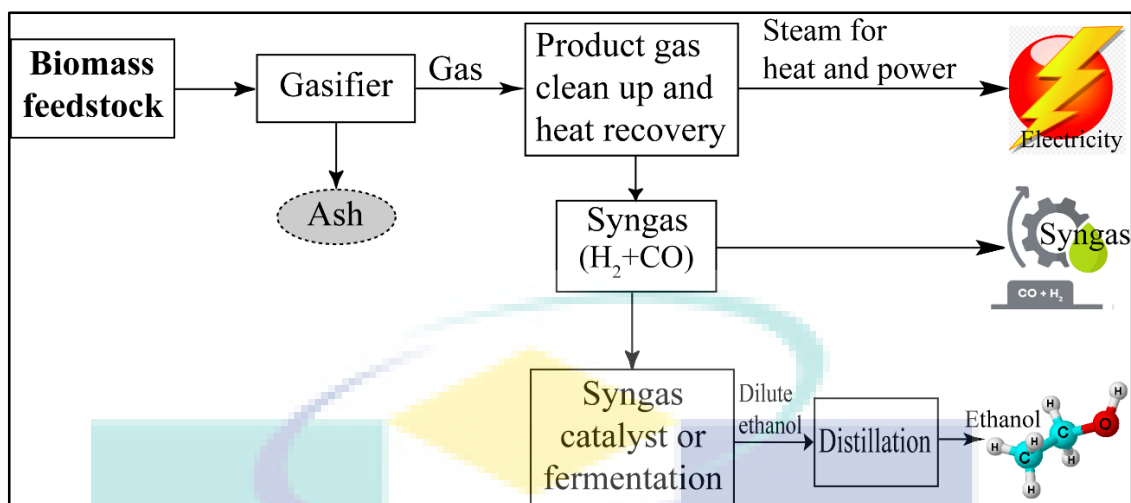


Figure 2.9 Biomass feedstocks to the final product of syngas and ethanol for heat and power generation.

Source: De, Agarwal, Moholkar, and Thallada (2018).

2.3.1 Syngas

Syngas (or synthetic gas) is the key product produced from biomass gasification or co-gasification. It usually consists of hydrogen (H_2), carbon monoxide (CO), carbon dioxide (CO_2), methane (CH_4), nitrogen (N_2) and some other compounds like C_2H_4 , C_2H_6 , NH_3 , H_2S , and tar (Kundu et al., 2018; Ramos, Monteiro, Silva, & Rouboa, 2018). However, syngas contained various co-products (high molecular weight compounds) during gasification that can be expected along with the syngas. Common by-products are ash (solid product) and charcoal, co-products are tars (liquid products) and ethane, benzene, hydrogen sulfide, sulfur dioxide, ammonia, nitrogen, hydrogen cyanide, nitrous oxide, methane, acetylene, ethylene etc. (gaseous products) (Adhikari, Abdoulmoumine, Nam, & Oyediji, 2017; Beagle, Wang, Bell, & Belmont, 2018; Ramos et al., 2018; Susastriawan & Saptoadi, 2017; Zhang & Zheng, 2016). They reported that the quality of syngas is affected by some important factors such as reactor type, fuel type, gasification medium (steam or air) and operational parameters (temperature, pressure) whereas fuel type has the most significant impact.

2.3.1.1 Syngas Impurities

There are many types of impurities commonly observed in syngas during gasification. The most common unwanted syngas impurities are as follows:

Impurity of Particles

Dust is a fine-grained particle (organic or inorganic) which is produced with syngas during gasification. It is primarily affected by the quality of the biomass-based syngas (Abdoulmoumine, Adhikari, Kulkarni, & Chattanathan, 2015). During the thermal conversion of biomass, the diameter of the particle decreased by increasing gasification temperature. However, the reduction of particle-size is significantly affected by elutriation, especially when feedstocks are fragmented. Moreover, temperature sensitively changes its chemical properties and finally increases residual solid content. These factors are the type of gasifying feedstocks, types of reactor and various operational parameters like temperature, pressure and gasifying agents reported by Rauch, Hrbek, and Hofbauer (2014). The cyclone separator is commonly attached with the gasifier to separate particles from the syngas as suggested by Nwokolo, Mamphweli, and Makaka (2016).

Impurity of Tar Compounds

Tar is a black, viscous, flammable, liquid hydrocarbons condensed during gasification from biomass, charcoal or coal. It is the most important co-product that produces syngas during biomass gasification (Valderrama Rios, González, Lora, & Almazán del Olmo, 2018). The level of unwanted co-product of tar is depended on some factors. Sometimes these compounds clogged the transportation engines when it is used directly. This co-product is also used for road-making, coating and preserving the timbers (Rakesh & Dasappa, 2018). The quality is affected by temperature, equivalent ratios and residence time is promoted by thermal cracking treatment. In this regards, temperature plays an important role in the elimination of tar content in the syngas. The tar concentration decreased due to increased in temperature. The equivalent ratio is another significant parameter that increased the oxidation reactions during char volatilization. Therefore, the concentration of tar increased by increasing the equivalent ratios as reported by Adhikari et al. (2017).

Impurity of NH_3

Ammonia (NH_3) is a compound of nitrogen and hydrogen which is also formed during the production of syngas through gasification. This type of impurities occurred due to the presence of nitrogen that exists in the biomass or coal. It also depends on the

concentration of nitrogen in various feedstocks (Valderrama Rios et al., 2018). In addition, the gasification operating parameters impact on the yield of nitrogenous impurities. The existence of steam during gasification increases the formation of NH_3 . However, the quantity of sulfur-based impurities in biomass producer gas is in lower quantity compared to coal producer gas.

Impurity of H_2S and COS

H_2S and COS are the two poisonous and flammable syngas impurities which affected the property of syngas. As a result, these gases are involved in various reactions with H_2S and other sulfur impurities during gasification which affected the quality of syngas (Valderrama Rios et al., 2018).

Impurity of Mercury

Mercury is a toxic impurity that occurs in the produced syngas. It comprises several heavy metals such as Hg, As, Se, Cu, Pd, Cd, and Zn that are found in producer syngas in trace amount. Moreover, it is more difficult to eliminate oxidized Hg in the form of HgS reported by Sikarwar et al. (2017).

Therefore, the quality of syngas depended on the presence of these impurities in the syngas. As a result, syngas cleaning is required for chemical production process while combustion on high ranked coal-fired power stations almost requires no cleaning. Thus, it is expected that the syngas for biological fermentation process (syngas fermentation) towards ethanol production required some cleaning.

2.3.1.2 Syngas Cleaning Process

There are various types of cleaning process used for syngas purification. The most important syngas cleaning process is as follows:

Wet scrubbing

This is one of the most effective processes for eliminating particles from syngas. This process occurred by introducing the syngas with a scrubbing liquid (ie. water). In this process, purified syngas is separated enormously and particles are collected with the scrubbing liquid (Sikarwar et al., 2016).

Catalytic tar removal

The tar concentration is removed by catalytic cracking of biomass over the char supported Ni catalyst at a lab-scale fixed bed reactor. Hu et al. (2018) reported in their study and investigated the effects of catalytic cracking temperature, Ni loading and gas residence time on product distribution and gas composition. Subsequently, they suggested that the optimum catalytic cracking temperatures are at 800 °C of 6 wt% Ni loading and 0.5 s gas residence time. Baidya, Cattolica, and Seiser (2018) also reported on the high-performance of Ni-Fe-Mg catalyst for tar removal in producer gas.

Thermal tar removal

Tar removal efficiencies of thermal tar decomposition combined with physical tar adsorption by using a reformer as the first step and a fixed-bed adsorber as the second step. The required temperature for thermal tar decomposition is about 800 °C (Guan, Kaewpanha, Hao, & Abudula, 2016). Meanwhile, high temperature has a strong influence on tar decomposition. The gasifying tar is efficiently decayed which improved the efficiency of tar elimination, either steam or air is introduced into the reactor. Consequently, tar decomposition has the elimination of tar compounds from the produced syngas that avoided the damage to downstream equipment.

Tar removal by oil washing

This process is also used for the reduction of tar from biomass-based syngas (Hu et al., 2018). Unyaphan, Tarnpradab, Takahashi, and Yoshikawa (2017) reported that the improvement of tar removal performance of oil scrubber is used by producing microbubbles.

Chemical absorption

This technique is applicable for the absorption process where atoms, molecules or ions meets some bulk phase-liquid or solid materials. Recently, Pallozzi, Di Carlo, Bocci, and Carlini (2018) suggested on the combined gas conditioning and cleaning process for the reduction of tars compounds during biomass gasification.

2.3.2 Biofuels (Bioethanol)

Biofuels (methanol, ethanol, dimethyl ether, synthetic natural gas, hydrogen) are produced from syngas fermentation and syngas is obtained from biomass gasification (Molino, Larocca, Chianese, & Musmarra, 2018). It is classified as primary and secondary biofuels based on their type, origin and production techniques. The primary biofuels are natural and unprocessed biomass such as wood (wood chips, pellets) and landfill gas. These are mainly used by direct combustion for heating and production of electricity. The secondary biofuels are produced by processing of biomass, for example, bioethanol, biodiesel, methanol, biogas etc. (Nigam & Singh, 2011).

Table 2.1 Types of biofuels and their characteristics.

Parameters	1 st Generation Biofuels	2 nd Generation Biofuels	3 rd Generation Biofuels
Source (feedstocks)	Generated from food crops: corn, wheat, sugarcane, soya beans, sugar beet, animal fat, cooking oil, etc.	Generated from non-food crops: agricultural wastes, lignocellulosic municipal wastes, vegetable oil, etc.	Generated from algae and other microbes: algae, seaweeds, etc.
Manufacturing method	Starch fermentation or ABE fermentation process. Transesterification of plant oils; Anaerobic fermentation	Enzymatic hydrolysis; Thermochemical processes followed by synthesis	Biochemical and thermochemical methods can be used
Biofuel products	Bio-alcohol such as ethanol, propanol, butanol (made from starches of wheat, corn, sugar cane, molasses, potatoes, other fruits). Biodiesel (made from oils and fats including animal fats, vegetable oils, nut oils, herp, and algae). Green diesel (made from hydrocracking oil and fat feedstock)	Bioethanol/biobutanol/ biodiesel (usually made from wood, grass, or inedible parts of plants. Methanol (made from inedible plant matter). Fischer-Tropsch biodiesel (made from waste from paper and pulp manufacturing). Dimethylfuran (made from fructose and some vegetables).	Bioethanol from algae and sea weeds. Biohydrogen (made from algae breaking down water)
Energy Density	Up to 48 MJ/kg	Up to 38 MJ/kg	Up to 123 MJ/kg
Greenhouse Gas CO ₂ (kg/kg)	Up to 3.4	Up to 2.85	Similar to 1 st generation fuels

Source: Dalena, Senatore, Tursi, and Basile (2017); Oumer, Hasan, Baheta, Mamat, and Abdullah (2018).

Therefore, biofuels are typically categorized into three major groups: 1st generation, 2nd generation and 3rd generation biofuels (Oumer et al., 2018). Every generation contained of distinct types of fuels. This classification is usually based on the source from which the fuel is originated. The composition of the biofuels does not vary with the change of generation. Table 2.1 shows the different types of biofuels and their characteristics. Tsuchida, Tsukagoshi, and Ueyama (2017) reported on microbial growth methods for the production of bioethanol. Moreover, various types of yeast strains through fermentation process considering factors affecting bioethanol production and immobilization of yeasts are responsible for better bioethanol production (Mohd Azhar et al., 2017).

2.4 Lignocellulosic Biomass

Arevalo-Gallegos, Ahmad, Asgher, Parra-Saldivar, and Iqbal (2017) reported that lignocellulose-based biomass is the most potential sources for the production of high-value marketable and sustainable products (Figure 2.10). These type of biomass comprises three main polymers: cellulose (38-54%), hemicellulose (24-36%) and lignin (15-25%) depending on plant species (Figure 2.11) (Sadhukhan, Ng, & Hernandez, 2014; Smith, Pecha, Helms, Scudiero, & Garcia-Perez, 2017; Wang S. R., Dai G. X., Yang H. P., & Luo Z. Y., 2017). Celluloses and hemicelluloses are composed of polysaccharides of C6 and C5 sugar monomers (glucose, mannose, arabinose, xylose etc.), respectively, connected by β -(1-4)-glycosidic linkages (Sadhukhan et al., 2014). The lignin compounds are polymers of para-hydroxyphenyl (H lignin), guaiacyl (G lignin) and syringyl (S lignin) alcohol (Sadhukhan et al., 2014).

The lignocellulosic materials for bioethanol production involve some important steps, such as pre-treatment, hydrolysis, followed by fermentation and ultimate ethanol purification (Haq et al., 2016). The hybrid process of thermochemical and biological which involved in potential feedstocks for liquid and gaseous biofuel production (Claypool & Simmons, 2016).

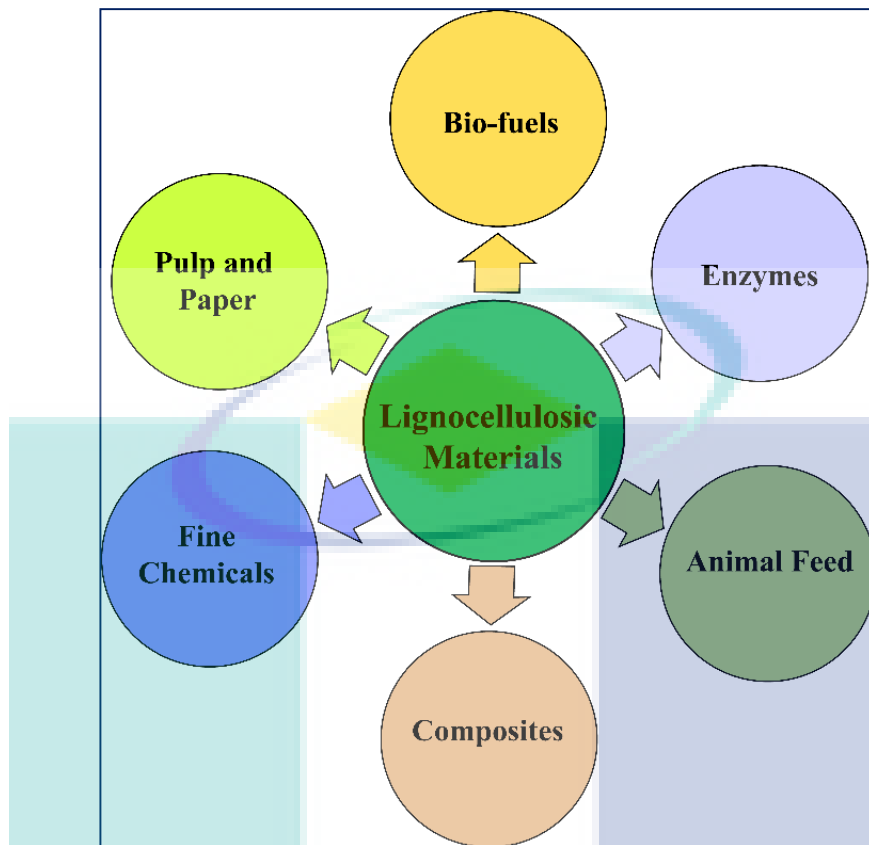


Figure 2.10 Lignocellulosic bio-conversions into value-added bioproducts.

Source: Arevalo-Gallegos et al. (2017).

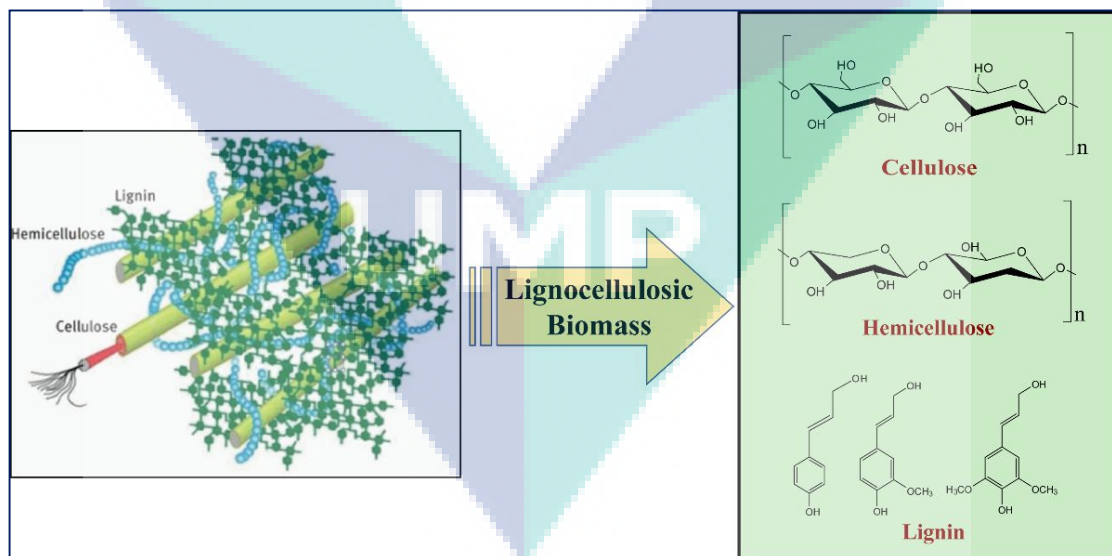


Figure 2.11 Cellulose, hemicellulose and lignin structure of biomass cell.

Source: Wang Shurong, Dai Gongxin, Yang Haiping, and Luo Zhongyang (2017).

2.4.1 Types of Lignocellulosic Biomass

There are various types of lignocellulosic biomass that are used for bioenergy production (Shankar & Shikha, 2017). The common types of lignocellulosic biomasses are wood, wood waste, straw, manure, sugarcane and many other by-products from a wide spectrum of agricultural practices. Lauri et al. (2014) reported that woody biomasses (forest and agricultural waste) are mostly available that cover an important part of the global potential energy consumption in 2050. They mentioned that total estimated world's wood-based energy supply was around 0-23 Gm(3)/year (0-165 EJ/year) and the energy prices were within the ranges of 0-30\$/GJ (0-216\$/m(3)). They also reported that by adding household fuel wood to energy wood, the woody biomass fulfilled 2-18% of world's energy consumption in 2050. Atnaw, Sulaiman, and Yusup (2017) mentioned that biomass materials have an initial moisture content as high as 70% on a mass basis. They also reported that major characteristics of biomass materials are included as moisture content, bulk density, a proportion of fixed carbon, volatile matter, ash content and elemental composition. These characterizations are needed before going to gasification to enhance their energy efficiency. Singh et al. (2017) also reported that biomass samples of *Impereta cylindrica*, *Eragrostis airoides*, *Typha angustifolia L.*, *Arundinella khasiana* Nees ex Steud, and *Echinochloa stagnina* (Retz.) *P. Beauv* were characterized based on the proximate, ultimate and compositional analysis.

2.4.2 Composition of Lignocellulosic Biomass

In the literature, it is mentioned that the entire biomass comprises approximately 70% of cellulose and hemicelluloses that are tightly linked to the lignin component by covalent and hydrogenic bonds. As a result, the structure is highly robust and resistant to any treatment reported by Limayem and Ricke (2012). Wang S. R. et al. (2017) suggested that cellulose usually formed rigid microfibrils which is the skeleton of the plant cell wall and the inner cell is filled with the amorphous type of hemicellulose and linking material of lignin. They also reported that cellulose connects with hemicellulose and lignin which included both hydrogen and covalent bonds. The potential lignocellulosic feedstocks and their composition are summarized in Table 2.2.

Table 2.2 Potential lignocellulosic biomass source and their composition (% dry weight).

Lignocellulosic Biomass	Hemicelluloses	Cellulose	Lignin	Others (ash)
Agricultural residues	25-50	37-50	5-15	12-16
Hardwood	25-40	45-47	20-25	0.80
Softwood	25-29	40-45	30-60	0.50
Grasses	35-50	25-40	-	-
Waste papers from chemical pulps	12-20	50-70	6-10	-
Switch grass	30-35	40-45	12	-

Source: Limayem and Ricke (2012).

2.4.2.1 Cellulose

The cellulose is an organic compound with a formula of $(C_6H_{10}O_5)_n$ and is originated in the cellular structure of biomass. It keeps structure and strength to the cell walls of plants. A comparatively very strong interaction between neighboring cellulose molecules in dry fibers due to the presence of the hydroxyl (-OH) groups which stick out from the chain form intermolecular hydrogen bonds (Figure 2.11). Yu, Paterson, Blamey, and Millan (2017) and Zhang Jing et al. (2015) reported that it mainly formed condensables and was less dependent on heating rate, decomposition is sharp with low temperature and its behavior is typical of linear polymers. It comprises of thousands of d-glucose monomers and is the largest single component of lignocellulosic biomass.

2.4.2.2 Hemicellulose

Hemicellulose is an amorphous and variable structure formed of heteropolymers including hexoses (d-glucose, d-galactose and d-mannose) as well as pentose (d-xylose and l-arabinose) and contained sugar acids (uronic acids), d-glucuronic, d-galacturonic and methylgalacturonic acids (Limayem & Ricke, 2012). Its backbone chain is mainly composed of xylan β (1→4)-linkages that include d-xylose (nearly 90%) and l-arabinose (approximately 10%) (Gírio et al., 2010). Moreover, branch frequencies are vary depending on the nature and the source of feedstocks. The hemicelluloses of softwood are usually glucomannans while hardwood hemicellulose is more frequently composed

of xylans (Gírio et al., 2010). Although the most abundant component in hemicellulose and xylan composition still varies in each feedstock.

The content of hemicellulose and species of polysaccharides greatly depends on the sources of biomass. Hardwood, softwood, and herbaceous plants have hemicellulose contents of 10–15%, 18–23% and 20–25%, respectively (Chen, 2014). The polysaccharides in hardwood hemicellulose include glucuronoxytan, xyloglucan and glucomannan, while softwood hemicellulose is primarily composed of xyloglucan, arabinoglucuronoxytan and galactoglucomannan, and the herbaceous hemicellulose primarily consists of glucuronoarabionxytan and xyloglucan reported by Limayem and Ricke (2012). The chemical structure of the hemicellulosic component is shown in Figure 2.11.

2.4.2.3 Lignin

Lignin is composed of three phenolic monomers of phenyl propionic alcohol namely, coumaryl, coniferyl and sinapyl alcohol. Forest woody biomass is primarily composed of cellulose and lignin polymers. Softwood barks have the highest level of lignin (30–60%) followed by the hardwood barks (30–55%) while grasses and agricultural residues contain the lowest level of lignin (10–30% and 3–15%, respectively) as reported by Limayem and Ricke (2012). On the contrary, crop residues such as corn stover, rice and wheat straws are comprised mostly of a hemicellulosic heteropolymer that includes a large number of 5-carbon pentose sugars of primarily xylose. Lignin components are important because of their dilution effect on the process once solids are added to a fed-batch hydrolytic or fermentation bioreactor in addition to their structure and concentration effects that are affected to potential hydrolysis (Ladisich, Mosier, Youngmi, Ximenes, & Hogsett, 2010). The adsorption of lignin to cellulase needed a higher enzyme loading because of this binding generates a non-productive enzyme attachment and limits the accessibility of cellulose to cellulase (Chen et al., 2006). Moreover, phenolic groups are formed from the degradation of lignin. These components substantially deactivate cellulolytic enzymes and hence influence enzymatic hydrolysis. This negative impact caused by lignin has led to an interest in lowering the lignin negative effect. Chen et al. (2006) reported that lignin modification via genetically engineering practices are targeting its biosynthetic pathways could considerably reduce lignin formation and improve ethanol yield. Retaining the lignin could have benefits as

Limayem and Ricke (2012) have suggested that lignin components are once recovered from biofuel that could be a potential energy self-sustaining source to retain biorefineries financial solvency.

2.5 Feedstocks Availability in Malaysia

In Malaysia, biomass-based bioenergy has become gaining much attention day by day. There are various kinds of biomass-based feedstocks which are available in Malaysia. Ozturk et al. (2017) worked on potential biomass feedstocks in Malaysia for bioenergy production. They reported that the annual product of bioenergy of 168 million tons (approx.) of biomass, timber, oil palm waste, coconut trunk fibers, rice husks, sugarcane wastes and municipal solid wastes in Malaysia. Among these, 58 million tons (approx.) comes from palm oil mill effluent. They also suggested that by utilizing these biomasses, the economic condition of this country will be higher by the year 2020. Sadhukhan et al. (2018) studied on the strategic pathway for Malaysia on the role of bioenergy, biorefinery and bio-economy in sustainable development. This country planned to reduce emissions by using forestry and agricultural resources up to 40% by 2020 from 2005 level. The authors stated that palm oil industry plays a vital role by contributing to gross national income in Malaysia. Oil palm EFBs as a promising and sustainable non-edible feedstock for biofuels production in Malaysia (Derman, Abdulla, Marbawi, & Sabullah, 2018). This EFBs is one of the potential biomass wastes, that can be utilized as the raw material for bioethanol production. They also reported that EFB based liquid biofuels such as bioethanol can cover for cleaner earth together with fewer dependency on fossil fuels. Every year this country produces a huge amount of lignocellulosic waste from the oil palm industry, that are potential to be converted to second-generation bioethanol (Ozturk et al., 2017).

2.6 Energy Conversion Routes from Lignocellulosic Biomass

There are several routes to convert biomass into useful biofuels depending on the biomass characteristics and the requirement of the end product and its applications. For woody biomass, the most common application is thermochemical conversion route viz. combustion for the production of heat energy while through gasification both heat and power generation requirements can also be met more effectively, efficiently and environment-friendly besides the biofuels production through pyrolysis for transportation

and related applications. Among all the three main routes, gasification has been considered to be a more attractive process to exploit the energy from certain renewable and non-renewable biomass with better conversion efficiency for various end products such as heat, electricity, transportation fuels etc. (Kundu et al., 2018). Reddy and Vinu (2018) reported that gasification and pyrolysis is the promising energy conversion route from complex feedstocks like lignocellulosic biomass and coal. Since gasification is the thermochemical conversion of solid biomass into combustible fuel in the presence of oxidant carried out in a reactor called gasifier or reactor. Hence, it can convert the solid biomass into different fuels such as liquid and gas which may be further synthesized for various applications including heating, cooking, power generation, transportation and so on. The major thermochemical conversion routes of biomass are shown in Figure 2.12.

2.6.1 Pyrolysis

Pyrolysis is the decomposition of biomass at the temperature and pressure of 375 °C-525 °C and 5-10 bar, respectively in the absence of air. In this process, biomass is converted into solid charcoal, liquid oils and gaseous compounds through four thermal stages of drying (100 °C), initial stage (100-300 °C), intermediate stage (>200 °C) and final stage (300-900 °C) as reported by Basu (2010). The main product of slow pyrolysis is charcoal. Therefore, it is not considered for hydrogen production. Gaseous co-products of pyrolysis includes of H₂, CO, CH₄, CO₂ and other gases depending on the organic nature of the biomass.

Wang S. R. et al. (2017) informed the pyrolysis mechanisms of lignocellulosic biomass with its conversion pathways for the production of biofuels and bio-based chemicals. They explained on the thermochemical characteristics and reported on cellulose, hemicellulose and lignin properties that are responsible for their pyrolysis behavior, distribution of building blocks and their functional groups. They also emphasized on the production of biofuels of aromatic or aliphatic hydrocarbons, and value-added chemicals such as anhydrosugars and furans, by catalytic pyrolysis.

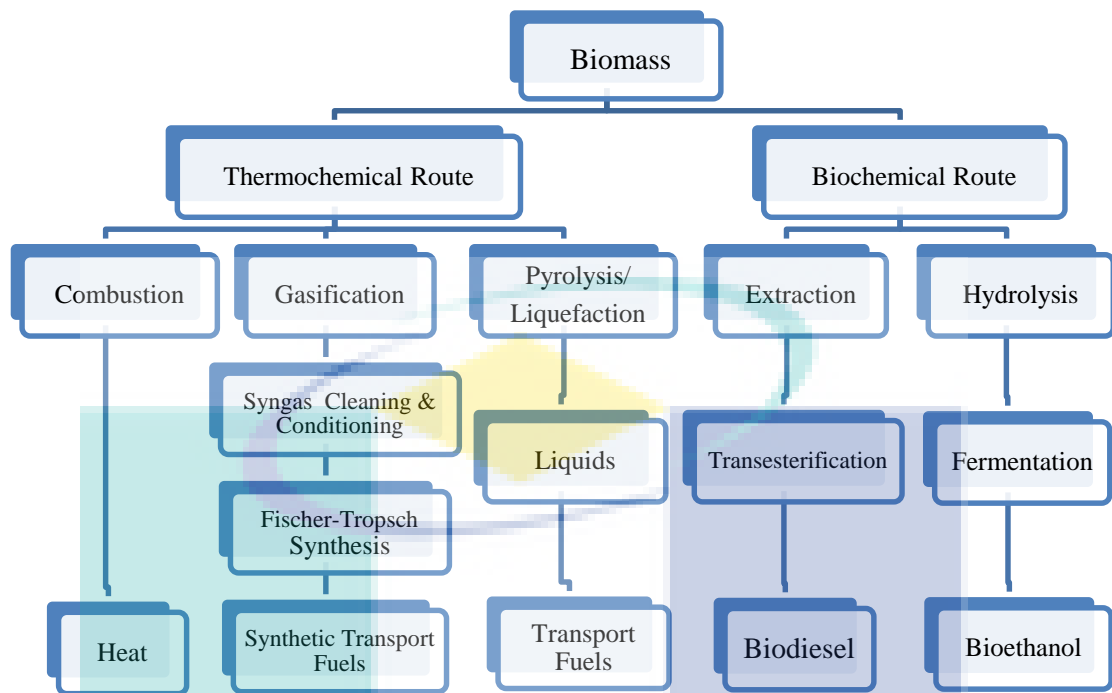


Figure 2.12 Thermochemical and biochemical conversion routes for biomass to biofuels.

Source: Sikarwar et al. (2017).

2.6.2 Combustion

The most important biomass conversion route of combustion involves the relatively high-temperature thermo-chemical conversion of biomass in excess air into CO₂ and steam within the temperature ranges from 800 °C to 1000 °C (Basu, 2010, 2018). Biomass is converted into the combustible mixture of CO, H₂, CO₂, and CH₄ gases. In this process, the chemical energy of biomass is fluently decomposed and converted into heat that is used for heating and electricity purposes. In addition, biomasses are co-fired with coal in a coal-fired power plant (Kuo, Chen, & Wu, 2014). They also mentioned that when the percentage of the biomass is more than 10% then biomass and coal are burned separately in different boilers known as parallel co-firing.

This combustion process is the oldest utilization of biomass and civilization began with the discovery of fire. The burning of forest wood taught humans how to cook and how to be warm (Basu, 2018). Chemically, combustion is an exothermic reaction between oxygen and hydrocarbon in biomass. In addition, biomass is converted into two major stable compounds of H₂O and CO. In this process, about 90% of heat energy is released through some reactions from biomass. In rural areas, biomass is used for the production

of heat for cooking purposes. Moreover, industrial heating is also produced by steam generated in biomass-fired boilers. Electricity, the foundation of all modern economic activities, were generated from biomass combustion (Ruiz, Girón, Suárez-Ruiz, & Fuente, 2017). The most common practice involves the generation of steam by burning biomass in a boiler and the generation of electricity through a steam turbine. In some places, electricity is produced by burning combustible gas derived from biomass through gasification (Sikarwar et al., 2016).

2.6.3 Gasification

Gasification is the thermochemical conversion of biomass that converted it into a gaseous product of synthetic gas or syngas in an oxygen-deficient environmental condition (Aydin, Yucel, & Sadikoglu, 2018; Basu, 2010, 2018). Produced syngas mainly consists of carbon monoxide and hydrogen. It can be considered as the intermediate stage between pyrolysis and combustion. The most common type of gasifier used for gasification is a fixed bed, fluidized bed and entrained flow gasifier. The produced gas is usually used as gas engines, micro-turbines, fuel cells and gas turbine (Basu, 2010). They also mentioned that the biomass gasification process is completed with some complex chemical reactions which occurred at gasifier zones.

Baruah and Baruah (2014) reported that biomass gasification is categorized based on their physical structure; such as fixed bed gasifier (downdraft and updraft), fluidized bed gasifier (circulating and bubbling) and entrained flow gasifier (Oakey, 2015). The choice of the gasifier is usually depended on the feedstock type, size, moisture content and end product with the interaction system of steam/oxygen/air (Sansaniwal et al., 2017). Commercially different types of gasifiers are used for energy production. Among them, downdraft, fluidized bed, updraft and other gasifiers are covered by 75%, 20%, 2.5% and 2.5% respectively. Gas produced through downdraft gasifier contains unwanted by-products such as tars, impurities and ash (Samiran et al., 2016; Singh & Sekhar, 2016). Patra and Sheth (2015) mentioned that downdraft gasifier has the maximum power production capacity up to 5 MW. Gao, Zhang, Li, and Yu (2016) developed a model for biomass gasification in an entrained flow gasifier using the intrinsic reaction rate. They observed that the relative errors for volumetric concentrations are within the range of 1-18% and lower heating value, gas production, cold gas efficiency and carbon conversion efficiency are within the ranges of 1-13%, 1-8%, 1-12% and 1-11%, respectively.

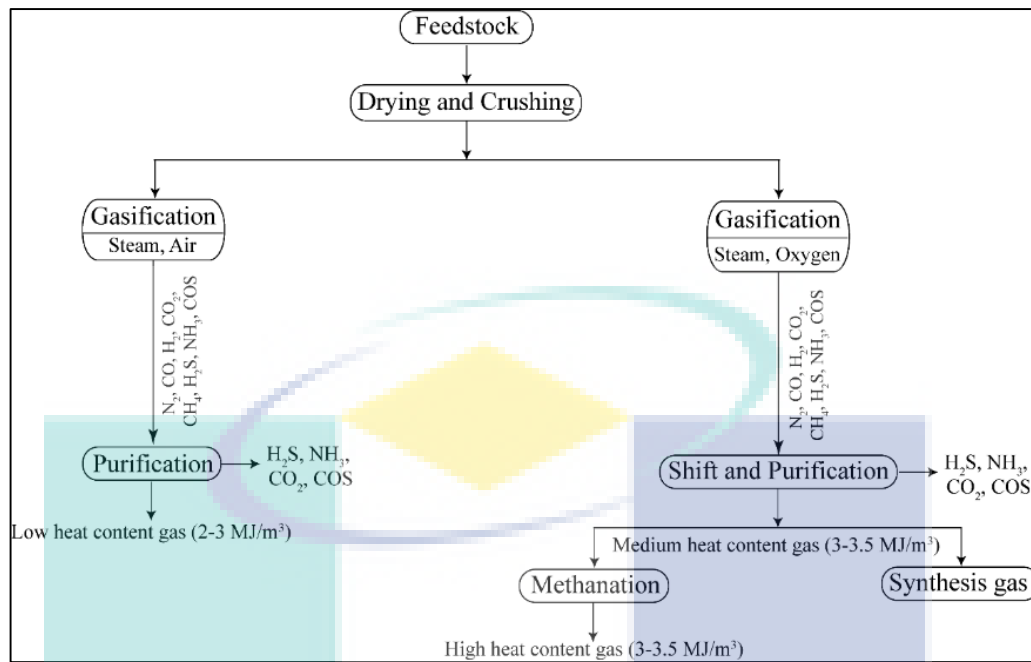


Figure 2.13 Schematic of the major steps involved in gasification in air and oxygen ambience.

Source: De et al. (2018).

The drying phase involves evaporation of moisture content from biomass. In this zone, the gasifier is at a lower temperature in the range of 100-150 °C and part of this vapour is converted to H_2 during gasification (Atnaw, Sulaiman, & Yusup, 2017; Aydin et al., 2018). The biomass is beginning to pyrolysis at the temperature ranges from 200 °C to 500 °C (Aydin et al., 2018). At this stage, thermal disintegration of biomass into volatile gases and char are formed. The proportion of these components is influenced by the chemical composition of biomass being fed and the operation conditions of the gasifier. Subsequently, there is an oxidation zone where the pyrolysis products move into hotter zone. Air is inserted into the oxidation zone under starved O_2 conditions. The oxidation takes place at temperatures to reach up to 1200 °C (Atnaw, Sulaiman, & Yusup, 2017; Aydin et al., 2018) and possible reactions (Sharma et al., 2015) occurred are shown in Table 2.3. The products from the oxidation zone move into the reduction zone where there is lack of O_2 , leading to a reduction of reactions between the hot gases and char. In this zone, the sensible heat of the gases and char is converted into the stored chemical energy in the syngas. Therefore, the temperature of the gases is reduced and ranges from 650 °C to 900 °C (Aydin et al., 2018; Sharma et al., 2015; Wei, 2005). Figure 2.13 represents the typical gasification process which involves primary treatment, reaction and

flue emissions which include ammonia and carbonyl sulphide (COS) reported by De et al. (2018).

Table 2.3 Chemical reactions involved in biomass gasification.

Name of reactions	Chemical reactions	No. of equation
Overall reaction	$CH_xO_y(\text{biomass}+\text{charcoal})+O_2(\text{atmospheric air})$ $=CH_4+CO+CO_2+H_2O(\text{untreated steam})+C(\text{char})+\text{tar}$	2.1
Char combustion		
Partial combustion	$C+\frac{1}{2}O_2=CO; \Delta H=-111\text{KJ/mol}$	2.2
Total combustion	$C+O_2=CO_2; \Delta H=-394\text{KJ/mol}$	2.3
Char gasification		
Boudouard equilibrium	$C+CO_2=2CO; \Delta H=173\text{KJ/mol}$	2.4
Water-gas reaction	$C+H_2O=CO+H_2; \Delta H=131\text{KJ/mol}$	2.5
Methanation reaction	$C+2H_2=CH_4; \Delta H=-75\text{KJ/mol}$	2.6
Homogeneous reactions		
CO oxidation	$CO+\frac{1}{2}O_2=CO_2; \Delta H=-283\text{KJ/mol}$	2.7
H ₂ oxidation	$H_2+\frac{1}{2}O_2=H_2O; \Delta H=-283\text{KJ/mol}$	2.8
CH ₄ oxidation	$CH_4+2O_2=CO_2+2H_2O; \Delta H=206\text{KJ/mol}$	2.9
Water-gas shift reaction	$CO+H_2O=CO_2+H_2; \Delta H=-41\text{KJ/mol}$	2.10
Methanation	$CO+3H_2=CH_4+H_2O; \Delta H=-41\text{KJ/mol}$	2.11

Source: Oh et al. (2018); Sansaniwal et al. (2017); Sikarwar et al. (2017).

The gasification mechanisms usually occur through some complex chemical reactions during biomass gasification reported by some researchers (Oh et al., 2018; Sansaniwal et al., 2017; Shayan, Zare, & Mirzaee, 2018; Sikarwar et al., 2017). During the co-gasification process, fuel-mixture involved to reach a high temperature that is caused by both physical and chemical changes throughout a series of chemical reactions (Table 2.3) and it is occurred inside the downdraft reactor. These primary chemical reactions that were associated with syngas composition. These reactions were affected by the reactivity of feedstocks. Moreover, the reactivity of fuels depends on its molecular structure (Patel, Patel, Varia, & Patel, 2017). The rate of reaction influenced by the nature of feedstocks. Furthermore, due to the interaction by adding coal to biomass can also change the gasification reaction rate as reported by Saw and Pang (2013). Such interaction may cause changes in the microstructure of the feedstock, which affected the mass

transfer and reaction rate (Saw & Pang, 2013). Therefore, gasification reactions were more efficient due to optimized fuel mixtures.

2.6.4 Co-gasification

Moghadam et al. (2014) studied on the co-gasification process for the production of syngas such as kernel shell (PKS) and polyethylene waste blend in a catalytic steam and the optimized temperature was 800 °C, P/B ratio: 0.3 w/w and S/F ratio: 1 w/w, the total syngas yield and hydrogen yield was 422.40 g syngas/kg feedstock and 135.27 g H₂/kg feedstock, respectively. Patel et al. (2017) reported on the co-gasification of lignite and waste wood mixtures in an atmospheric pilot-scale (10 kW) downdraft gasifier, where 22 to 25 mm particle size was found to be suitable, and waste wood-lignite mixture ratios was 10%–90%, 20%–80% and 30%–70% (w/w). The energy efficiency, lower heating value (LHV) of gas and gas yield increased by 8.92%, 11.66%, 6.31% and 9.33%, respectively. Currently, the work was performed successfully on the co-gasification of EFB with charcoal, FR with charcoal and CS with charcoal for syngas production (Monir, Abd Aziz, Kristanti, & Yousuf, 2018a, 2018b, 2018c; Monir, Yousuf, Aziz, & Atnaw, 2017). Sansaniwal et al. (2017) also reported that the gases obtained during the downdraft gasification were due to consumption of 99% of the tar. The process itself led to low particulate and tar content in the gas and hence, suited for small scale power generation applications. At the end of pyrolysis zone, the gases obtained in the absence of O₂ are CO₂, H₂O, CO, and H₂, called flaming pyrolysis. They also reported that downdraft gasifier is superior in quality for syngas production due to sustainable production of combustible fuels and energy effectiveness, although downdraft gasifier is suitable for low moisture content feedstock (Susastriawan & Saptoadi, 2017). According to the literature, Atnaw, Sulaiman, Singh, et al. (2017) reported that modeling and parametric study maximizes the heating value of gasification of syngas, major output parameters that were considered with respect to the main operating parameters of temperature, equivalence ratio (ER) and moisture content.

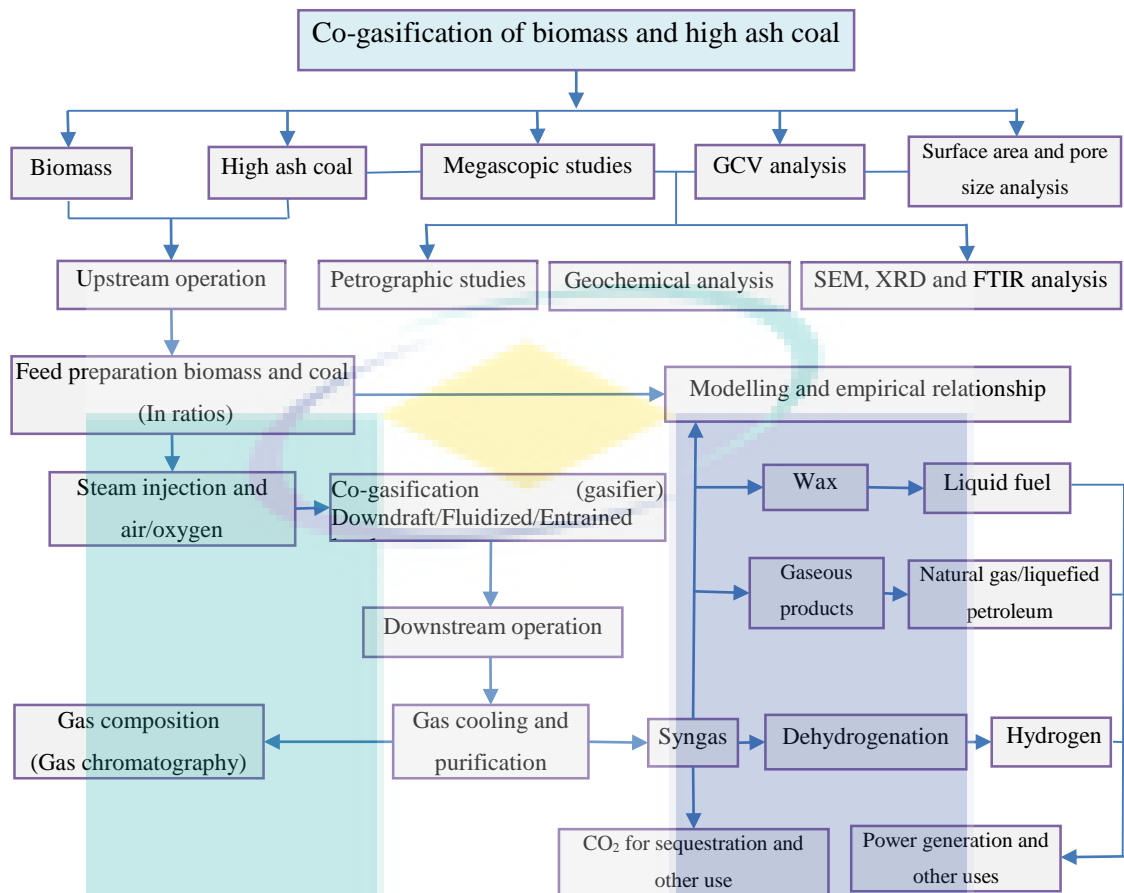


Figure 2.14 Co-gasification process for biomass and coal.

Source: Kamble et al. (2018).

Environmental consideration is one of the most important reasons for the conversion of energy. Most of the cases it is observed that non-renewable (i.e. coal) energy source-based resources produces toxic gases that may affect the environment. From the environmental point of view, renewable energy sources (biomass) consist of less toxic elements than coal. On the other hand, during gasification of single feedstocks that produce by-product other than gases like CO₂ than the syngas (CO and H₂). Thus, the main target of co-gasification is to improve the quality of product syngas. Many researchers worked on various types of the feedstocks and optimized the parameters for reduction of toxic gases. The co-gasification process improves the quality of product gases that are environmentally sustainable. Kamble et al. (2018) investigated the co-gasification-based projects that are well-thought-out under clean technology alternatives which has a relatively fewer environmental impact (Figure 2.14). They also suggested that product gases contain toxic component like carbon monoxide that is very hazardous

to the human body. It also tends to combine with the haemoglobin of the blood which prevents oxygen absorption and distribution in the human body.

Therefore, during gasification more attention has been needed, and no leakage is allowed during running the process. Subsequently, other toxic gases of SO_x and NO_x are needed for separation of the producer gas before further fuel conversion. Sometimes, co-product of tar compounds from the reactor as well as in the product gas is also toxic and environmentally hazardous (Kamble et al., 2018). This process is usually performed at a high temperature, and as a result, the whole body of the equipment is usually hot and required insulation to minimize the risks of burns. In addition, product gas contains a significant proportion of hydrogen and has the risk for an explosion if it outs the air and mixed at a particular ratio. The ash content is also hazardous to the agricultural lands. They may disposed properly with no environmental effects. Nevertheless, the disposal of toxic tar compounds obtained from a large number of reactors can have unwanted environmental effects (Widjaya, Chen, Bowtell, & Hills, 2018).

2.7 Simulation, Optimization and Modelling for Biomass Gasification

2.7.1 Comparative Analysis Using Simulation Software and Applications

Several commercial software is widely used for simulating biomass gasification process mainly including stoichiometric calculation software HSC, large-scale general chemical flow simulation software Aspen Plus, response surface methodology (RSM), a high-performance language for technical computing software MATLAB[®] and computational fluid dynamics (CFD) software Fluent etc (Anil et al., 2016; Che et al., 2012; Kaushal & Tyagi, 2017b). There are some advantages of computer-aided simulation which is to quickly test the performance of synthesized process flowsheets and run the process synthesis activities. It can be coordinated with process synthesis to develop optimum integrated designs by minimizes experimental and scale-up efforts. Among these, RSM is an applicable statistical tool that has been implemented both statistical and mathematical methods to develop, improve and optimize the gasification process. It also analyses some responses of importance that is either adopted by some variables (Morero, Groppelli, & Campanella, 2017; Sarrai et al., 2016). The Aspen Plus simulator is usually used to avoid complex processes and develop the simplest possible model that incorporates the principal gasification reactions and the gross physical

characteristics of the reactor have developed models (Atnaw, Sulaiman, & Yusup, 2011). In addition, Sadhwani, Adhikari, Eden, and Li (2018) performed a process model for the prediction of steady state performance of biomass- CO₂ gasification in a fluidized bed gasifier using the ASPEN PLUS simulator. This model focuses on both hydrodynamic parameters and reaction kinetic modeling. Inayat, Ahmad, Mutalib, and Yusup (2010) reported the impact of temperature, steam to biomass ratio and sorbent/biomass ratio on hydrogen (H₂) production performance in a steam gasification using a simulation model developed in MATLAB[®]. They investigated that with increase in temperature and steam to biomass ratio, the hydrogen concentration and yield increases and the thermodynamic efficiency decreases. Che et al. (2012) reported that based on domestic and foreign summarization of numerical simulation technology application in the gasification of biomass, the two frequently-used softwares are the large-scale industry flowsheet simulation software Aspen Plus and the computational fluid dynamics software Fluent. There are many dissimilarities between them to simulate gasification process, such as the principle of simulation, the foundation of simulation, the input and output of data and so on. The key differences between the kinetic model and the revised chemical kinetics used in the CFD model are mainly with the values of the frequency factor and activation energy (Kumar & Paul, 2019). The 2D modelling and simulation of biomass gasification in a bubbling fluidized bed gasifier using CFD solver ANSYS FLUENT 15.0 and it developed model for the prediction of some effects like equivalence ratio, steam to biomass ratio, steam temperature and air preheating on product gas composition as reported by Anil et al. (2016).

The biomass is defined as unconventional component in Aspen Plus, consequently, feedstocks characterization data from the proximate and elemental analysis can be input directly. The other gas components produced in the reaction process are defined as conventional components, and they can be found in the software database. Compared with Aspen Plus, the non-premixed combustion model is used to define the biomass in CFD. The simulated model is more complex. For Aspen Plus, the simulation outcome is displayed in tabular form. In the table, concentration of each component can be exhibited, even the output components of each block. However, the outcome for CFD is the concentration cloud map of each component. Therefore, the post processing software must be needed to process it. Moreover, the details of flow condition of the

biomass, granule in the gasifier, distributions of temperature, pressure and gas composition can be revealed with cloud map, which is favourable to analyse the gasification process.

2.7.2 Simulation, Optimization and Modelling using Aspen Plus®

Aspen Plus® is a problem-oriented process simulation program that is used to facilitate the physical, chemical and biological calculations reported by Kaushal and Tyagi (2017a). They stated that to model the chemical processes that involve solid, liquid and gaseous streams under a specific condition by using mass and energy balance equations and phase equilibrium database. Aspen plus solving algorithms are more complex than Aspen Hysys because of that that is very probable to see warnings. Over the years Aspen Plus has made model creation and upgradation easier and small sections of complex and integrated systems can be created and tested as separate modules before they are integrated as reported by some researchers (Ismail, Abbas, Azizi, & Zeaiter, 2017; Kaushal & Tyagi, 2017b; Peters, Banks, Bridgwater, & Dufour, 2017). This simulator is used to simulate a variety of processes, for example, methanol synthesis, indirect coal liquefaction processes, integrated coal gasification combined cycle (IGCC) power plants, atmospheric fluidized-bed combustor processes, compartment fluidized-bed coal gasifiers, coal hydrogasification processes and coal gasification simulation (Kaushal & Tyagi, 2017b).

Aspen Plus® simulator is used for optimizing the gasification parameters (temperature and pressure) within the existing libraries. The co-gasification process is needed to simulate based on some assumptions (Table 3.1). In this regards, experimental results are validated against the simulation results. It also minimizes experimental cost and time. Therefore, the simulation seems to be a suitable option for the valuation of product syngas and also the indication of co-gasification behavior. In the literature, some works have been done for the modeling and simulation of biomass gasification using Aspen Plus® (Ali, Gadalla, Abdelaziz, Hulteberg, & Ashour, 2017; Darmawan, Hardi, Yoshikawa, Aziz, & Tokimatsu, 2017; Kaushal & Tyagi, 2017b; Peters et al., 2017; Zhang, Pang, & Levi, 2017). Although the simulation and modeling of biomass gasification are reported in the literature, there have been bottleneck works that has been done on the key parameter optimization for the co-gasification of lignocellulosic biomass and charcoal. The benefit of this simulation refers to the precise relationship between temperature, pressure and mole fractions. At the end of the simulation, optimized pressure

and temperature are set for the co-gasification experiment (Nikoo & Mahinpey, 2008). Mathieu and Dubuisson (2002) modelled wood gasification in a fluidised bed using Aspen Plus. The model was based on the minimisation of the Gibbs free energy and the process was uncoupled in pyrolysis, combustion, Boudouard reaction and gasification.

The main simulation principle of Aspen Plus is to use the basic property relationship of systemic substance (the balance of mass and energy, velocity coefficient, the reaction, the transfer of mass and heat and all kinds of equilibrium relationship) to simulate and predict the material's flow rate, composition and property, thus to optimize the condition of operation and structure of reactor and so on. According to the property of thermo chemistry conversion process occurred in gasifier, different unit operation models can be used to simulate the different processes. For example, the RYield block is used to simulate the pyrolysis process of biomass. The Gibbs block, which is based on Gibbs energy minimization principle, is used to simulate the Oxidation-Reduction process. Then all kinds of blocks are connected together with material flow, heat flow or work streams to form a flowsheet. Mehrpooya, Khalili, and Sharifzadeh (2018) has developed a model for exergy analysis of the biomass gasification process (Based on the various biomass sources) which is showed in Figure 2.15. In this flowsheet represents the biomass at 298 K and 1 atm is mixed with the produced solids in the process, 9, and inputs the drying reactor. In this reactor, moisture content is evaporated through hot air (363 K, 1 atm). The produced hot gases separates in this dry reactor, 1, follows to the dry flash., Vapor phase is removed from the solid in this separator and leave the reactor as stream 3. Subsequently, dry biomass, 2, enters the decomposition reactor. The biomass decomposition is completed based on the RYield reactor at 394 K and 1 atm. The biomass is converted to C, O₂, H₂, S, N₂ and ash content. Outlet stream, 4, and steam at 900 K and 1 atm for production of syngas enter the gasifier. The R-Gibbs reactor model at 900 K and 1 atm is used for simulation. The produced syngas is separated, the outlet stream, 5, follows to the cyclone 1. The remained solid stream, 7, is tar. Tar and steam at 723 K and 1 atm enter the final combustion reactor and C and syngas are produced. Moreover, for separation of the C, stream 8 follows to the second cyclone. After separation, the remained C, 9, is returned to the process and is mixed with fresh biomass. The outlet syngas, 6, is at high temperature. The produced synthesis gas streams are mixed in mixer 1 (Figure 2.15).

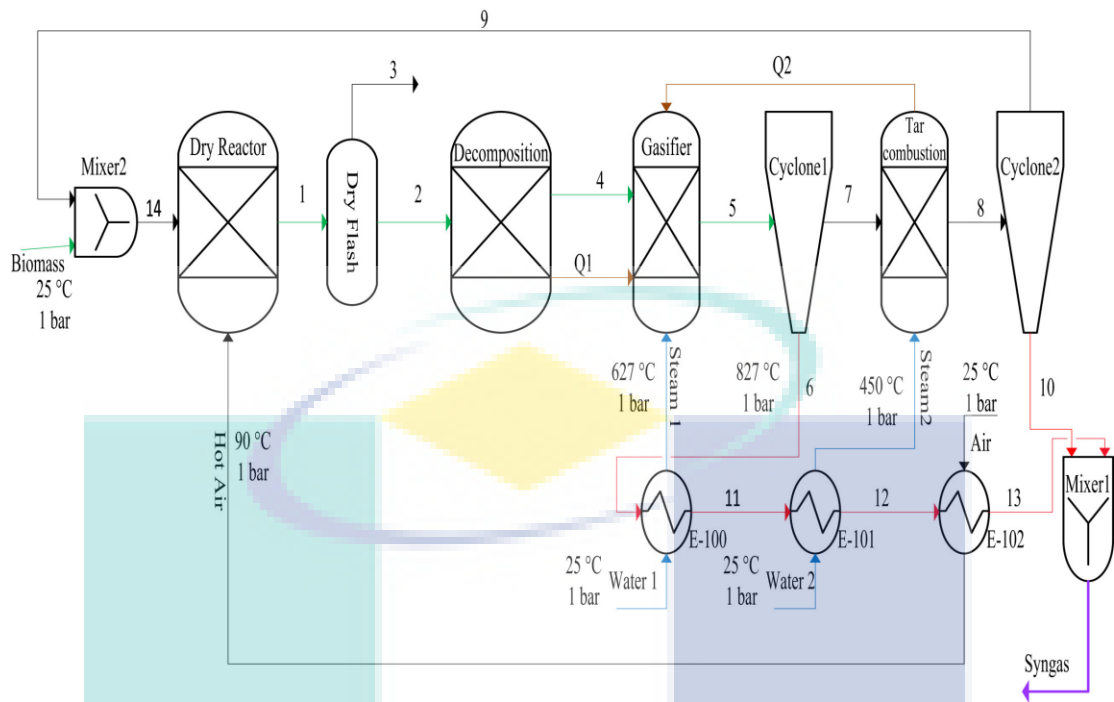


Figure 2.15 The flow diagram of the Aspen Plus process model.

Source: Mehrpooya et al. (2018).

2.8 Types of Gasifier Used for Gasification and Co-gasification

There are various types of gasifiers used for the production of syngas that is shown in the following flowchart (Figure 2.16) as reported by De et al. (2018). These are categorized based on some parameters, conditions and type of instrument. These are usually used for gasification and co-gasification considering various types of feedstocks with various ratios. Some researchers express the variations in the occurrence of reactions considering the type of gasifiers, the process involved in the reactor zones, the presence and absence of reagents and temperatures of the coaxing process. Therefore, the choice of a specific reactor requires a specific mixture of variables from the feedstock type to the recommended gas properties. As such co-gasification of coal and biomass has performed in the three main types of gasifiers in several countries (De et al., 2018). These have sustained to operate agreeably without obtaining any operational troubles considering that few plants that are indirectly cofired coal and biomass.

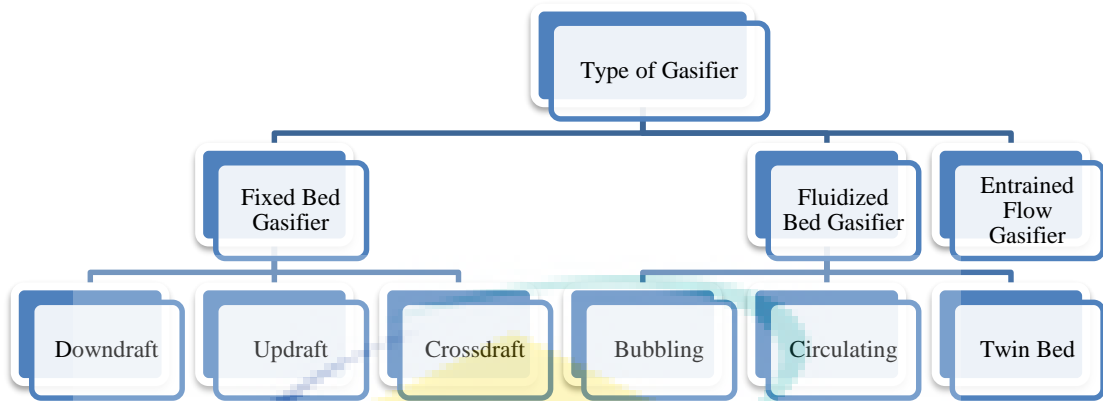


Figure 2.16 Types of Gasifier used for the production of syngas.

Source: De et al. (2018).

2.8.1 Fixed Bed Gasifier

The fixed bed gasifiers are categorized as updraft, downdraft and crossdraft gasifier are shown in Figure 2.17. The schematic diagram of an updraft gasifier is represented in Figure 2.17 which consists of a fixed bed of biomass fuel where the gasifying agent flows. Fuel in the form of large particles is loaded into the top of the gasifier. The gasifying agent is introduced at the bottom of the gasifier. The fuel moves slowly from top to the bottom and react with the gasifying agent which flows counter currently upward in the gasifier. Therefore, the updraft gasifier is also called counter current gasifier (Figure 2.17a). Typical reaction zones of an updraft gasifier are shown in Figure 2.17a. The fuel moves down through a drying zone where the moisture content is removed from the fuel, followed by a pyrolysis zone where volatiles are evaporated from the fuel and char is produced. Water vapor goes upward and leaves the gasifier along with the product gas. Char continues to move downward and gets reduced in the gasification zone and finally it is combusted in the oxidation zone where the gasifying agent is introduced. Because of high temperature (up to 1200 °C) in the oxidation zone, ash is mostly removed as a liquid. Here, the risk of ash fusion or solidification of slag is less due to the presence of oxidation zone at the bottom of the reactor which prevents the blockage in the flow path of the reactor when proceeding to the zone with lower temperature.

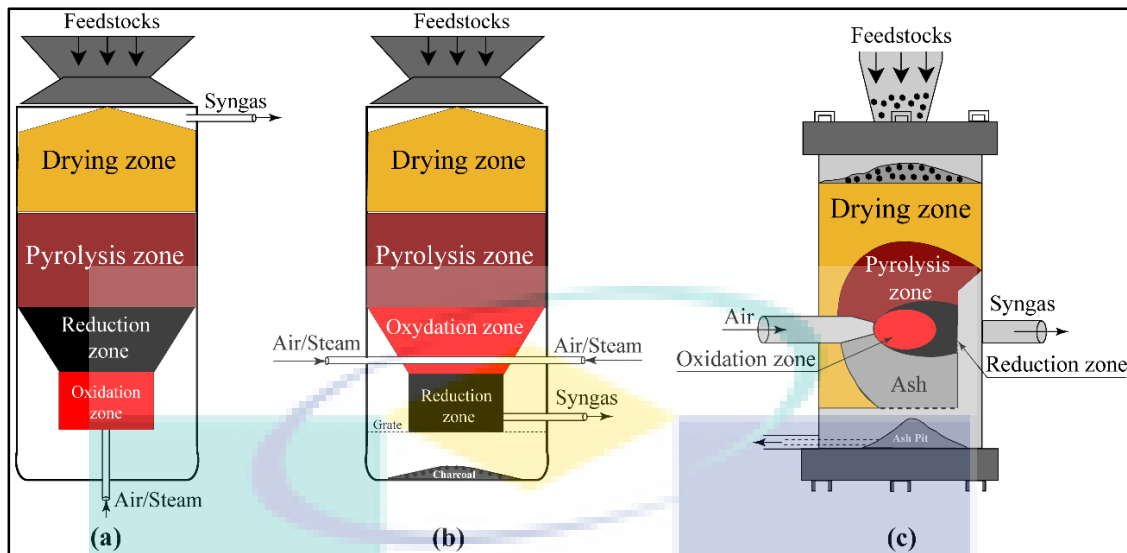


Figure 2.17 Schematic diagram of fixed bed gasifiers: (a) updraft gasifier (b) downdraft gasifier (c) crossdraft gasifier.

Source: De et al. (2018)

The gaseous pyrolysis products are carried upwards by the upward flowing hot gas stream. The product gas from the gasifier consists mainly of the pyrolysis products and the gaseous products from char reduction and oxidation reactions. The product gas passes over a relatively cold drying region before exit. The fuel used for these types of gasifiers must have a high mechanical strength and should form a porous bed. The thermal efficiency of this type of gasifier is high but the throughput is relatively low. As the pyrolysis product passes over a relatively cold drying zone but not through the high-temperature oxidation zone, the exit gas temperature is relatively low. Due to relatively low gas temperature, the production of tar (~ 50 g/Nm) is significant from these types of gasifiers (Basu, 2018).

Figure 2.17b shows the schematic diagram of a downdraft gasifier. Here, the solid fuel is introduced from the top, the gasifying agent is introduced at some intermediate level, and the product gas is taken out from the bottom. As the solid fuel and the gas move in the same direction, the downdraft gasifier is also called co-current gasifier. The product gas leaves the downdraft gasifier at high temperature. Heat from the product gas is generally recovered by preheating the gasifying agent which may result in higher efficiency almost equivalent to the updraft gasifier. Tar which is produced in downdraft gasifier passes through a hot bed of char which converts much of the tar to the gaseous product. Typical reaction zones of a downdraft gasifier are shown in Figure 2.17b. Fuel

is introduced from the top gets dried in the drying zone. The water vapor produced during drying flows downward and adds to the water vapor formed in the oxidation zone. Some amount of water vapor reacts with the char in the reduction zone and rest leaves the gasifier with the product gas. Then the fuel comes to the pyrolysis zone where char and gaseous species are produced. The pyrolysis products (gas and char) flow downwards into the oxidation zone. As can be seen from Figure 2.17b there is a throat in the oxidation zone where the gasifying agent is introduced and the oxidation reactions take place. The pyrolysis gas and char are partially combusted in the oxidation zone, and a sharp rise in the temperature occurs. The products from the oxidation zone move downward into the reduction zone. In the reduction zone, the gases and char coming from the oxidation zone get reduced and finally a combustible fuel gas is produced. The sensible heat of gases and char provide the heat required for reduction reactions. In downdraft gasifier, the reaction products are thoroughly mixed in high-temperature turbulent oxidation zone around the throat which helps in tar conversion. Some tar conversion also takes place below the throat on a residual charcoal bed where the gasification process is completed. As a result of tar conversion, tar production in downdraft gasifiers is less than in the case of updraft gasifiers. In these types of gasifiers, the maximum fuel size is limited to the size of the throat. The arrangement of the reaction zones in downdraft gasifier restricts the use of high ash fuel. In this type of gasifier, some of the ash constituents may melt at the high-temperatures oxidation zone which could form bigger lumps upon cooling in the gasification zone. These lumps formation frequently put obstruction to the overall flow of solid and also to the ash discharge at the bottom of the gasifier.

Figure 2.17c shows the schematic diagram of a cross-draft gasifier. Here, the fuel is introduced from the top of the gasifier. The gasifying agent is introduced from one side of the gasifier, and the product gas is taken out from the other side. The exit of the product gas and the entry of the gasifying agent are kept almost at the same level. As the fuel moves down through the gasifier, it is dried, devolatilized, pyrolyzed, and finally gasified before leaving the gasifier. The oxidation zone is located near the entry of the gasifying agent, and the gasification zone is located near the exit. The pyrolysis zone is located above the oxidation/reduction zone, and the drying zone is located above the pyrolysis zone. In cross-draft gasifier ash bin, oxidation zone and reduction zone are separated which impose the restriction for using a different type of fuels. The exit gas temperature

in cross-draft gasifier is very high which has an effect on gas composition like it produces gas with higher carbon monoxide content and low hydrogen and methane content.

2.8.2 Fluidized Bed Gasifier

Fluidization is the operation by which a bed of solid particles is transformed into a fluid-like state by the application of gas. The fluidized bed system requires the feedstock to be finely ground into small particles, and the gasifying and fluidizing gases are introduced through a distributor plate near the bottom of the reactor (Sikarwar et al., 2016; Zhou, Rosén, & Engvall, 2016). In fluidized bed gasifier, the drying, pyrolysis, oxidation, and reduction zones are not apparent at any specific region of the gasifier like in fixed bed gasifiers. These processes occur in the entire gasifier, and thus the fluidized bed gasifiers are the more homogeneous type of reactors. In a fluidized bed gasifier, the gasifying agent also acts as the fluidizing agent to fluidize the particle bed. The distinct advantages of fluidized bed over fixed bed gasifiers are uniform and controllable temperature due to excellent gas-solid mixing, high carbon conversion rate, low tar production, flexibility in terms of use of different types of fuel, feed rate, particle size, and moisture content. In fluidized bed gasifiers, reaction rates are much faster than in the fixed bed gasifiers because of intimate gas-solid contact and the increased solids surface area resulted from smaller particle size. Because of the aforementioned features, scale-up and operation of the fluidized bed gasifiers are much easier. The fluidized bed gasifiers are designed to be accompanied by a cyclone separator downstream of the gasifier to capture the particles that are entrained by gas and leave the gasifier as a result of the fluidity of the bed and the velocity of the gas rising through the bed as in Figure 2.18. After separation, these particles are either recycled back into the gasifier or removed from the gasifier. Most of the problems associated with the fixed bed gasifiers could be overcome in fluidized bed gasifiers. Therefore, fluidized bed gasifiers are more popular than fixed bed gasifiers. The most common type of fluidized bed gasifier is bubbling fluidized bed gasifier and circulating fluidized bed gasifier as shown in Figure 2.18.

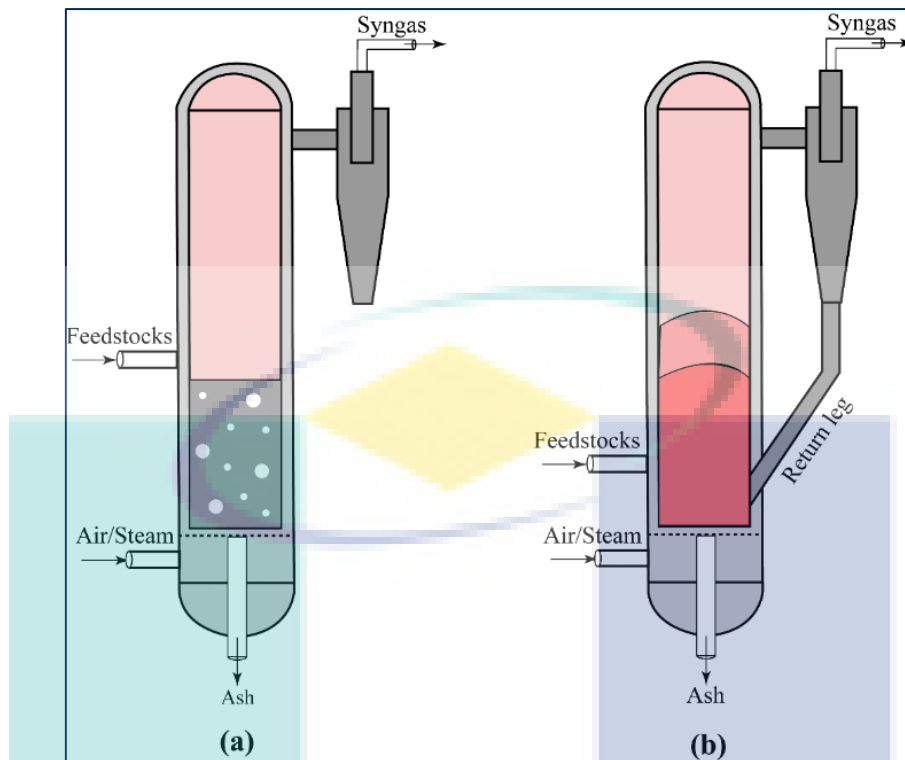


Figure 2.18 Schematic diagram of fluidized bed gasifiers: (a) Bubbling fluidized bed gasifier (b) Circulating fluidized bed gasifier.

The residence time of fuel particles in fluidized bed gasifiers is generally less than that of fixed bed gasifiers. However, the residence time may be increased by re-circulating the particles again and again, like in circulating fluidized bed gasifiers. Fluidized bed gasifiers are suitable for small to medium scale (500 kW to 50 MW) application. Although the fluidized bed gasifiers are used for gasification of both coal and biomass, they are becoming more popular for biomass gasification due to a lower gasification temperature of biomass compared to coal (Basu, 2018).

Figure 2.18a presents the schematic diagram of a bubbling fluidized bed gasifier. In a typical reactor with solid particles, when the velocity of fluidizing gas is increased, a situation is reached when the solid particles are just suspended by the upward flowing gas. At this situation, the drag force between particles and fluid counterbalance the weight of particles and the pressure drop between any two points along the height of the bed equals the weight of fluid and particles in that section. At this point, the bed is called to be at the minimum fluidization condition and the corresponding velocity is called the minimum fluidization velocity. With an increase in velocity beyond the minimum fluidization velocity, bubble formation starts. These small bubbles grow in size while traveling through the bed. On the way up through the bed, bubbles withdraw particles

from surroundings and thereby set the particles in motion. On reaching the bed surface, bubbles burst and particles splash into freeboard region. However, the bed of particles does not expand much beyond its volume at the minimum fluidization condition. Such a bed is called bubbling fluidized bed. In bubbling fluidized bed gasifier, generally, an inert bed material is used where the gasification of fuel takes place. Solid fuel is introduced either from the top of the gasifier on the bed of particles or deep inside the bed. The deeper introduction of the fuel into the gasifier will allow sufficient residence time for fine fuel particles that would otherwise be entrained by the fluidizing gas. In bubbling fluidized bed, the volume flow rate of the gasifying or fluidizing agent is such that its velocity is sufficient to suspend the solid particles but not high enough to blow them out from the gasifier. The result is a bed of solids which simulate a boiling action ensuing intimate contact between solid and gas which lead to a uniform temperature distribution inside the gasifier. Solid particles flow rapidly and repeatedly from bottom to top of the bed and back again, while the gas flows up through void space in between solid particles and in the bubbles with higher velocity. Some of the small particles are transported with the gas and leaves the gasifier at the top. A cyclone separator is used to trap these particles that exit from the fluidized bed gasifier, and these particles are either returned to the bed of the gasifier or removed from the system as fly ash. But, most of the fine ash particles fall back to the bed and can be continuously removed from the bottom of the gasifier as bottom ash. In bubbling fluidized bed gasifier, the height of the freeboard region should be enough to restrict bed materials from blown out of the system. The tar production in bubbling fluidized bed gasifier is less than the updraft gasifier but more than the downdraft gasifier.

The rate of gasification and the movement of particles in bubbling fluidized bed gasifier largely depend upon the size of fuel particles. With small particles, the gasification process is rapid and it might be complete near the fuel feeding zone before reaching to the center of the bed, resulting in oxygen slip and a void center in the bed. For this reason, fuel feeding is done through multi-feeding points in bubbling fluid bed gasifier. The typical superficial gas velocity in a bubbling fluidized bed is around 12 m/s.

Figure 2.18b shows the schematic of a circulating fluidized bed gasifier. Generally, it consists of a high-velocity riser, a cyclone separator, a downcomer, and a loop-seal/L-valve. If the velocity of the gasifying agent is increased beyond the bubbling

fluidized bed, solid particles are distributed across the whole riser height and most of the particles are entrained by the gas. Particles are separated from the gas with the help of cyclone separator, come down through the loop-seal through the downcomer, and return to the bottom of the riser, forming a solids circulation loop. Then it becomes a circulating fluidized bed or fast fluidized bed gasifier. In circulating fluidized bed, particles arrested by cyclone separator are generally fed back to the riser either by using a loop-seal or L-valve. The solid circulation flux is controlled by the gas velocity in the riser and as well as in the loop-seal. The driving force for the solid circulation is the pressure difference in different parts of the circulating fluidized bed system. The higher gas velocity in circulating fluidized bed results in more intense mixing of the gas and particles in the bed which provides excellent gas-solid contact. The high relative velocity between the gas and particles also enables it for very high heat and mass transfer rates within the circulating fluidized bed system. Unlike bubbling fluidized bed, there is no distinct separation between dense particle zone and dilute particle zone. The advantage of circulating fluidized bed over bubbling fluidized bed is mainly due to the longer overall residence time. The residence time of solid particles in the circulating fluid bed gasifier is determined by the solids circulation rate, collection efficiency of the solids in the cyclone separator, and the number of circulations. In a circulating fluidized bed gasifier, a fuel particle generally takes 110 s to complete one circulation, and thus, the total residence time could be as high as 10,000 s by re-circulating many times. Due to higher gas velocity and recycling of the particles, complete mixing could be achieved regardless of fuel type. Generally, the circulating fluidized bed designs are more flexible but are still limited by the amount of fine particles that can be processed. The typical gas velocity in a circulating fluidized bed may vary from 5 to 10 m/s.

2.8.3 Entrained Flow Gasifier

The schematic diagram of an entrained flow gasifier is shown in Figure 2.19. The solid fuel and the gasifying agent are fed from the top and they flow co-currently to the gasifier. Very fine fuel particles are required for entrained flow gasifier compared to the fluidized bed gasifiers. Oxygen or air both can be used as the gasifying agent, but most of the commercial plants use oxygen as the gasifying agent. Here, the velocity of the gasifying agent is even higher than in circulating fluidized bed gasifier. The small fuel particles are entrained by the gasifying agent, and they flow through the gasifier in a dense

cloud. The residence time of particles is very less which requires the entrained flow gasifier to be operated at high temperature (about 1200 to 1500 °C) (Basu, 2018).

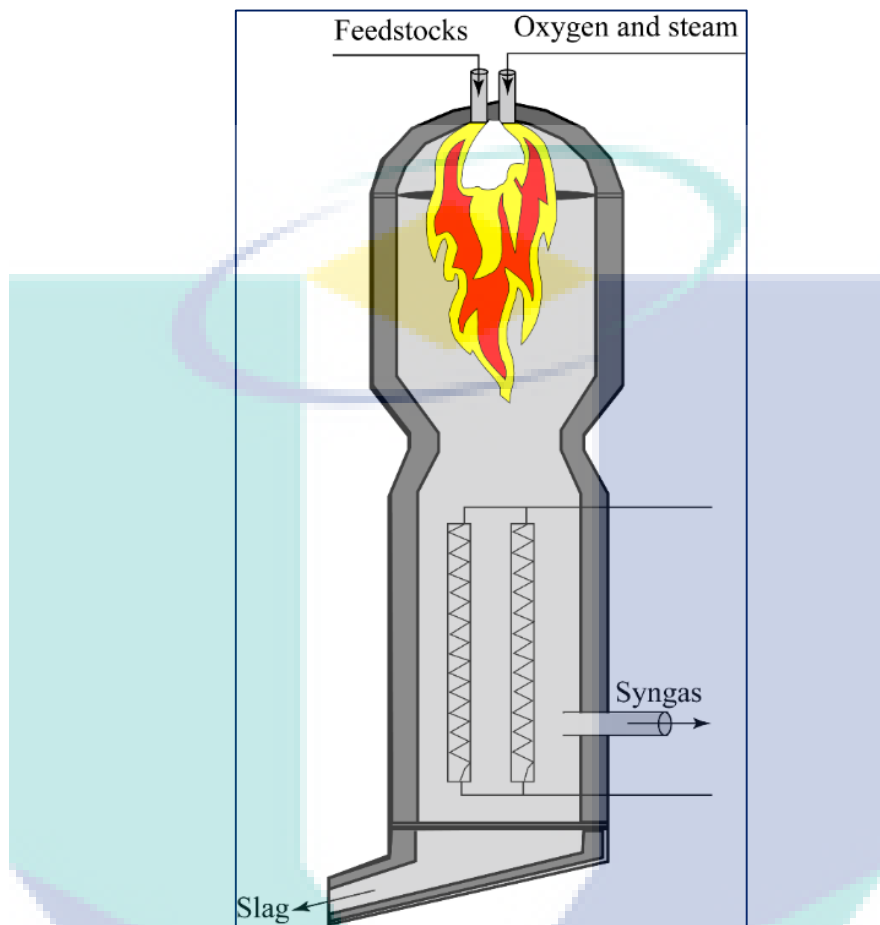


Figure 2.19 Schematic diagram of entrained flow gasifiers.

High temperature and extremely turbulent flow inside the gasifier cause rapid fuel conversion which also allows high throughput. The gasification reactions occur at a very high rate. Product gas from entrained flow gasifier contains a lesser amount of tar and condensable gases due to high-temperature operation. The major part of the ash is removed as slag because the operating temperature of the gasifier is well above the ash fusion temperature. It has the ability to gasify any type of fuels. However, fuels with low moisture and ash content are favored to reduce oxygen consumption. Entrained flow gasifiers are suitable for the large-scale application (>100 MW). It is a well-researched and developed technology for gasification of fossil fuel like coal, refinery waste. The entrained flow gasification technology has been commercialized in large-scale integrated gasification combined cycle (IGCC) coal power plants. In most cases, the gasifiers are operated under pressure (~20–50 bar) with pure oxygen and with capacities in the order

of several hundreds of MW. However, the application of entrained flow gasifiers in biomass gasification is still under development. Most of the integrated gasification combined cycle (IGCC) plants installed worldwide used the entrained flow gasification technology (Darmawan et al., 2017).

2.8.4 Selection of Gasifier

Guangul, Sulaiman, and Ramli (2012) reported that several factors have been considered for the selection of gasifiers. They reported that the most important factors are the type of feedstocks, cost of fabrication, feedstock elasticity, ease of operation, cold gas efficiency, tar content, lower heating value (LHV) and application versatility of syngas. The comparison of various types of gasifiers for the production of syngas using different types of feedstocks are shown in Table 2.4. The downdraft gasifier is more suitable for syngas production with less amount of co-product of compounds. This type of gasifier is appropriate to handle solid fuels with an ash content of <5% and moisture content < 20% as reported by Aydin et al. (2018).

Table 2.4 Comparative study on various types of gasifiers including their advantages and disadvantages.

Type of Gasifier		Advantages	Disadvantages
Fixed Bed Gasifier	Downdraft	<ul style="list-style-type: none"> ▪ Flexible adaptation of gas production to loads ▪ Low sensitivity to charcoal dust and tar content of the fuel ▪ Low entrainment of particulates ▪ Simple and easy control systems ▪ Simplicity and ease of operation ▪ Wear rate is minimal, as a result, maintenance cost is reduced 	<ul style="list-style-type: none"> ▪ Design tends to be tall ▪ Not feasible for the very small particle size of fuel (size requirement relatively strict) ▪ Only limited to small-scale applications (scale-up not feasible) ▪ Unable to handle feedstock with high moisture and ash contents ▪ Inability to operate on a number of unprocessed feedstocks
	Updraft	<ul style="list-style-type: none"> ▪ Small pressure drops ▪ Good thermal efficiency ▪ Little tendency towards the formation of slag 	<ul style="list-style-type: none"> ▪ High sensitivity to tar and fuel moisture content ▪ Startup of internal combustion (IC) engine require a relatively long time ▪ Poor reaction capability with heavy gas loads

Table 2.4 Continued

Type of Gasifier	Advantages	Disadvantages
Crossdraft	<ul style="list-style-type: none"> ▪ Short design height ▪ Very fast response time to load ▪ Flexible gas production 	<ul style="list-style-type: none"> ▪ Highly sensitive to slag formation ▪ High pressure drops ▪ Poor reduction in CO₂ ▪ Limited to low ash materials such as wood and charcoal
Fluidized Bed Gasifier	<ul style="list-style-type: none"> ▪ Excellent gas to solid contact ▪ Excellent heat transfer characteristics ▪ High rates of heat and mass transfer ▪ Good temperature control ▪ Large heat storage capacity ▪ A good degree of mixing 	<ul style="list-style-type: none"> ▪ The increased tar production rate ▪ Poor response to changes in load ▪ Incomplete carbon burn-out ▪ The possibility of scale-up is minimal ▪ Complicated and expensive control systems ▪ High capital and operational costs
Entrained Flow Gasifier	<ul style="list-style-type: none"> ▪ High throughput and rapid feed conversion as a consequence of the high temperature and pressure characterized by the process ▪ The feedstock can be fed in dry or slurry form 	<ul style="list-style-type: none"> ▪ Water is introduced into the gasifier due to slurry feedstock, which results in reduced thermal efficiency ▪ High temperature increases the wear rate

Source: Anukam, Mamphweli, Reddy, Meyer, and Okoh (2016); Basu (2018); Patra and Sheth (2015); Vassilev, Vassileva, and Vassilev (2015).

2.9 Biocatalyst Used for Syngas Fermentation

There are various types of biocatalysts (microorganisms) used for syngas fermentation (Sun, Atiyeh, Kumar, Zhang, & Tanner, 2018). Yeast and bacteria are the common biocatalysts that are used for chemical and biofuel production through syngas fermentation (Davis et al., 2018; Foo et al., 2017; Sayed & Abdelkareem, 2017). Microorganisms are unable to degrade the lignocellulosic biomass entirely through the direct fermentation of biomass which contained lignin. However, microorganisms are capable to produce biofuel from biomass-based syngas (Asimakopoulos et al., 2018; Molitor, Marcellin, & Angenent, 2017). Moreover, biomass-based syngas contains some impurities like tar (higher hydrocarbon) and small particles (Al-Rahbi & Williams, 2017; Kuba & Hofbauer, 2018; Moon et al., 2017). Due to the presence of these impurities,

syngas is not capable to be used as the transporting fuels without purification and there are needed to change or modify the existing engines (Mansfield & Wooldridge, 2015; Xu, Tree, & Lewis, 2011). As a result, syngas conversion into fuels and other chemicals by using some special type of microorganisms is the appropriate option for future energy demand (Henstra, Sipma, Rinzema, & Stams, 2007).

At present, syngas fermentation is attracting more attention in order to enhance the yield of product using microorganisms by optimizing the bioreactor operational parameters (Drzyzga et al., 2015). Mesophilic and thermophilic microorganisms are categorized for the syngas fermentation based on the fermentation process. The common microorganisms that are usually used for syngas fermentation like *Clostridium autoethanogenum*, *Clostridium carboxidivorans*, *Acetobacterium woodii*, *Clostridium ragsdalei*, *Butyribacterium methylotrophicum*, *Clostridium ljungdahlii* etc. (Acharya, Roy, & Dutta, 2014). Heiskanen, Virkajärvi, and Viikari (2007) mentioned that the bioethanol production through syngas fermentation is more efficient by using biological catalysts (microorganisms) (*Acetobacterium woodii* and *Clostridium carboxidivorans*) than chemical catalysts (copper, cobalt or iron). The detailed list of common microorganisms and their optimum condition of temperature, pH level, yield products for syngas fermentation are shown in Table 2.5.

Table 2.5 Production of liquid fuels by microbial syngas fermentation with various carbon sources and operational parameters.

Microorganisms	Syngas composition	Fermentation mode	T _{opt} (°C)	pH _{opt}	Products	Reference
Mesophilic bacteria						
<i>Clostridium autoethanogenum</i>	CO:CO ₂ :H ₂ :N ₂	Fed-batch	30	6	Acetic acid, ethanol	(Lagoa-Costa, Abubackar, Fernández-Romasanta, Kennes, & Veiga, 2017)
<i>Clostridium autoethanogenum</i>	CO:H ₂ :CO ₂	Batch	37	5.8	Ethanol	(Liew et al., 2017)
<i>Clostridium autoethanogenum</i>	CO:H ₂ :CO ₂ :N ₂	Batch	37	6	Bioethanol	(Xu et al., 2017)
<i>Acetobacterium woodii</i>	CO:H ₂ :CO ₂	Batch	30	6.8	Acetate	(Munasinghe & Khanal, 2011a)
<i>Acetobacterium woodii</i>	CO ₂	Batch	30	7.0	Acetate	(Hoffmeister et al., 2016)

Table 2.5 Continued

Microorganisms	Syngas composition	Fermentation mode	T _{opt} (°C)	pH _{opt}	Products	Reference
Mesophilic bacteria						
<i>Butyribacterium methylotrophicum</i>	CO	Batch	37	6	Ethanol, acetate, butyrate, butanol	(Munasinghe & Khanal, 2011a)
<i>Clostridium carboxidivorans</i>	CO:H ₂ :CO ₂	Batch	38	6.2	Acetate, ethanol, butyrate, butanol,	(Munasinghe & Khanal, 2011a)
<i>Clostridium carboxidivorans</i>	CO:CO ₂ :H ₂ :N ₂	Continuous	33	5	Acids and alcohols	(Abubackar, Veiga, & Kennes, 2018)
<i>Clostridium ragsdalei</i>	CO:H ₂ :CO ₂	Fed-batch	37	5.5	Ethanol	(Sun, Atiyeh, Kumar, & Zhang, 2018)
<i>Clostridium ragsdalei</i>	CO:CO ₂ :H ₂ :N ₂	Semi-continuous	37	5.8 - 4.6	Ethanol	(Devarapalli, Atiyeh, Phillips, Lewis, & Huhnke, 2016)
<i>Clostridium ljungdahlii</i>	CO:CO ₂ :H ₂	Batch	37	6.8	Acetic acid, ethanol	(Kim, Park, Lee, & Yun, 2014)
<i>Clostridium ragsdalet</i>	CO:H ₂ :CO ₂	Batch	37	5.7-6.4	Acetate, ethanol	(Sun, Atiyeh, Kumar, & Zhang, 2018)
<i>Eubacteriumlimosum</i>	CO:H ₂ :CO ₂	Batch	38-39	7.0-7.2	Acetate	(Munasinghe & Khanal, 2011a)
<i>Mesophilic bacterium</i>	CO:CO ₂ :N ₂	Batch	37	5.7-5.8	Acetate, ethanol, butyrate, butanol	(Lewis, Tanner, & Huhnke, 2007)
Thermophilic bacteria						
<i>Clostridium thermocellum</i>	N ₂ :CO ₂ :H ₂	Batch	55	7.0	Ethanol	(Tian et al., 2016)
<i>Moorella thermoacetica</i>	CO:H ₂ :CO ₂	Batch	55	6.8-6.8	Acetate	(Molitor et al., 2017)
<i>Moorella thermoautotrophica</i>	CO:H ₂ :CO ₂	Batch	58	6.1	Acetate	(Sakai et al., 2004)

Alfenore and Molina-Jouve (2016) reported that microorganisms (yeast, bacteria and fungi) are used for the conversion of lignocellulosic biomass for the production of biofuels. The model biocatalysts that are used for biofuel productions are *Escherichia Coli*, *Bacillus Sp.*, and *Clostridium Sp.*, *S. cerevisiae*, and *Trichoderma Reesei* and *Fusarium Oxysporum*. Matsushika, Inoue, Kodaki, and Sawayama (2009) reported that the most effective microorganism is *S. cerevisiae* for hexose sugar fermentation which shows a high yield of ethanol production, and high tolerance to ethanol present in the lignocellulosic materials. Some strains of *S. cerevisiae* that ferment xylose into ethanol, but yield product of ethanol is less compared to glucose fermentation using *S. cerevisiae* as studied by Lin et al. (2012). Saravanakumar, Senthilraja, and Kathiresan (2013) reported to emphasis on the mangrove-derived marine *S. cerevisiae* that is suitable for ethanol production. Liao, Mi, Pontrelli, and Luo (2016) mentioned on the production of next-generation biofuels, based on the ability of bacteria and fungi to be used lignocellulose through direct CO₂ conversion by microalgae. In this regards, Hossain et al. (2017) also stated their opinion that yeast fermentation is the cheapest and conventional method. It is cost effective in comparison to other fermenting agents and also it has acknowledged fermentation capability and produced zero chemical wastes. Kennes et al. (2016) informed that hydrolytic treatment used enzymes to convert the cellulose polymer to simple, fermentable, sugars, mainly glucose where simple sugars obtained from hemicellulose and cellulose are then fermented by yeasts to bioethanol. They also mentioned that feedstock is gasified by thermochemical alternative and yield product of syngas comprised of CO, CO₂ and H₂ which were fermented anaerobically, usually by *Clostridia Sp.*, to ethanol or other yield products. Another research conducted by Akhtar (2016) mentioned that for the environmental consideration the end product (ethanol) on biofuel production by *S. cerevisiae* plays a key role. Shen et al. (2017) informed that *C. carboxidivorans* also plays an important role in the production of bioethanol. Recently, Kanchanasuta, Prommeenate, Boonapatcharone, and Pisutpaisal (2017) reported that biohydrogen was produced by adding of *C. butyricum* into non-sterile food waste.

2.10 Syngas Fermentation System

For the performing of syngas fermentation system microorganisms are grown in batch, fed-batch and continuous culture systems in a bioreactor (Asimakopoulos et al., 2018). These microbial growth cultivation systems are as follows:

2.10.1 Batch Culture

Batch culture is a closed system where there is no interaction between the system and surrounding during the fermentation process (Collet, Ng, & Aston, 2018). In this technique, fermentation broth medium is prepared initially and then the cultured organism is inoculated to the medium. During the process, the reactor is bubbling though no further additions of the medium are made. Once a production cycle is ended, the consumed medium is removed to add fresh medium. The cultivation medium is prepared and sterilized before fermentation run. In this cultivation, microorganisms are inoculated into the bioreactor before the process started. Since there is no fresh media is added after the experimental run, the concentration of nutrition decreased continuously (Asimakopoulos et al., 2018). The volume of culture usually remains constant. Batch fermentation gives characteristics growth curve with lag phase, exponential phase, stationary phase and death phase. Conclusively, the microbial cells to grow and produces the yield product. The conversions of substrate occur completely which is the main advantages of this system (Alzate, Toro, & Peña, 2018). It has properly sterilized and low risk of infection from the microbial strain. The disadvantages of this system are the labour cost is high. Every batch system is needed to be sterilized, growth and cleaning the system.

2.10.2 Fed-batch Culture

The fed-batch (or semi-closed) system is a culture where substrates are inoculated to the bioreactor after some interval (Gaikwad et al., 2018). In this system, nutrient media is prepared, and organisms are inoculated to the broth medium and then incubated. In the course of incubation, nutrients are fed at given intervals. As a result, the volume of culture is continuously increased. This technique is applicable to various fermentation processes when some nutrients, though essential for biomass growth, may inhibit the microbial growth if their concentration is too high (Buruiana, Vizireanu, Garrote, & Parajó, 2014). In this case, lower initial concentrations of these nutrients are adopted by adding them

continuously or discontinuously during the process. The parameters like temperature, pH, substrate inoculation interval time are needed to be investigated. The growth phase of the microorganisms is monitored enormously. The toxic and concentrated microorganisms are suitable for this fermentation system (Asimakopoulos et al., 2018). More attention should be necessary when toxic microorganisms are used. Experiment handling is not an easy task. Sometimes microorganisms are expensive.

2.10.3 Continuous Culture

A continuous (or open) system is a culture allowing the continuous production of products. This system is feasible for syngas fermentation, especially for industrial purposes. Fresh sterile medium is fed continuously to the vessel and spent fermentation medium is continuously removed. As a result, the volume always remains constant within the fermenter (Collet et al., 2018). The bacterial growth occurs mainly during the log phase. Substrates are gone through the bioreactor continuously. The continuous fermenters allow a steady-state microbial growth if the input flow rate is kept constant. Under steady-state conditions, the microbial cell density remains constant. This system works all the time. As a result, labour cost always low and perfect utilization of the bioreactor. Moreover, productivity is high and maintained constant product quality (Abubackar et al., 2018). The substrate must be inoculated continuously for the continuous production of the product. Sometimes, the selected microorganisms are contaminated with the non-producing microbial strain.

2.11 Microbial Pathway and Energy Conversion

The syngas fermentation for the production of acetic acid and bioethanol, CO, H₂ and CO₂, followed a series of elementary chemical reactions (Table 2.6). Each reactions involved the microbial metabolism process in a specific location within the cell, either free in the cytoplasm, together with the surface of the cell membrane or embedded in the membrane (Henstra et al., 2007). The cells act individually, but integral action of all cells sets conditions in the fermentation bulk liquid. The reactions occur under certain condition (pH, temperature) for different microorganisms (Asimakopoulos et al., 2018). The inorganic substrates, CO, H₂ and CO₂, are converted to acetylCoA and then organic products of acetic acid and ethanol (Figure 2.20). Moreover, acetyl-CoA is transferred to complex organic cell components, carbohydrates, proteins and lipids. Though, most of

the gas molecules provide the energy for cell function. As a result, the yields are acetic acid and ethanol (Phillips, Huhnke, & Atiyeh, 2017).

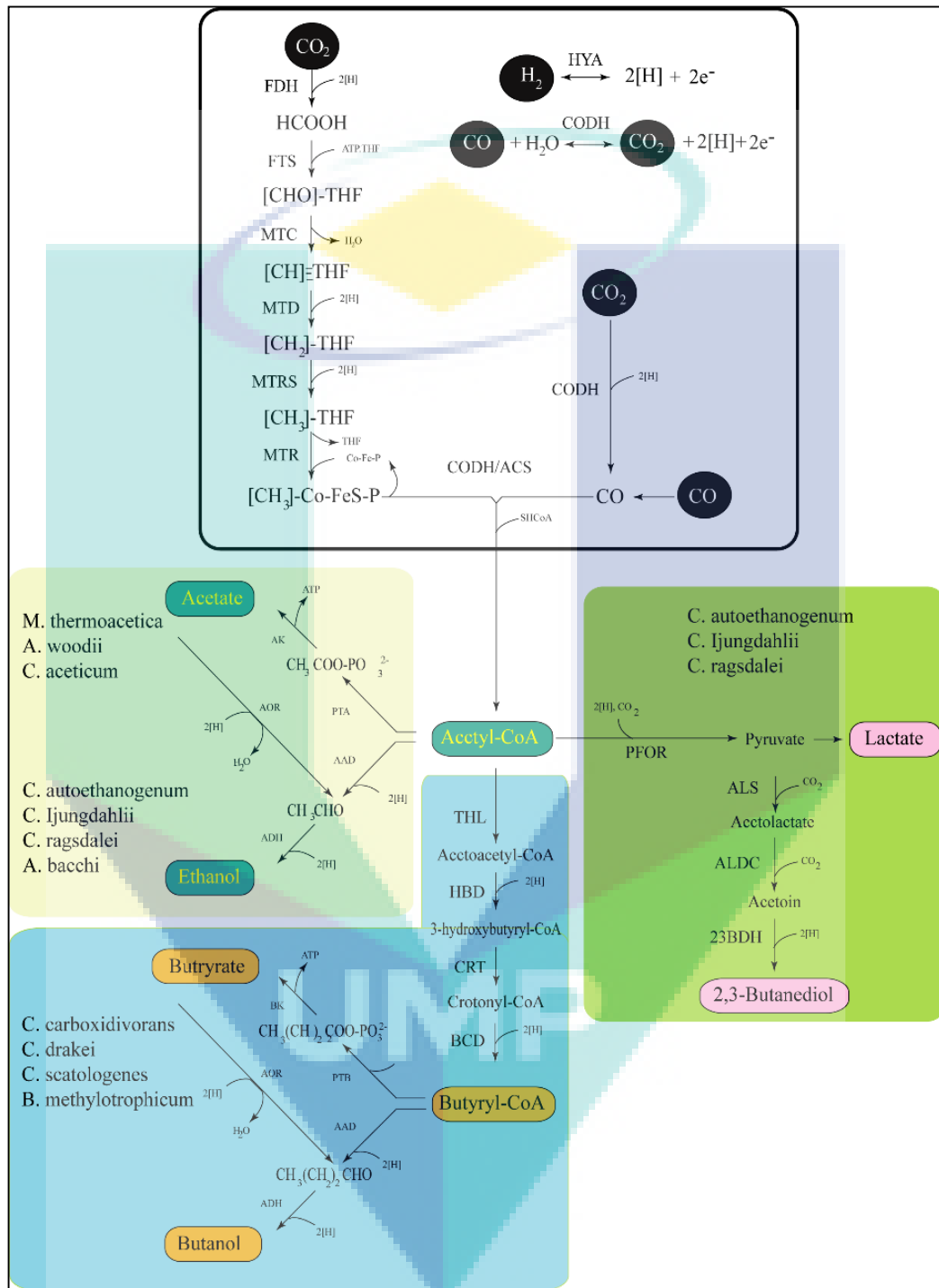


Figure 2.20 Wood-Ljungdahl pathway of acetogens and their metabolic end products.

Source: Chen and Henson (2016).

Table 2.6 Reactions involved for acetic acid and ethanol production.

Reactions	Products	Equation No.
$4 \text{ CO} + 2 \text{ H}_2\text{O} \rightarrow \text{CH}_3\text{COOH} + 2 \text{ CO}_2$	Acetic Acid	2.12
$3 \text{ CO} + \text{ H}_2 + \text{ H}_2\text{O} \rightarrow \text{CH}_3\text{COOH} + \text{ CO}_2$		2.13
$2 \text{ CO} + 2 \text{ H}_2 \rightarrow \text{CH}_3\text{COOH}$		2.14
$\text{CO} + 3 \text{ H}_2 + \text{ CO}_2 \rightarrow \text{CH}_3\text{COOH} + \text{ H}_2\text{O}$		2.15
$\text{H}_2 + 2 \text{ CO}_2 \rightarrow \text{CH}_3\text{COOH} + 2 \text{ H}_2\text{O}$		2.16
$6 \text{ CO} + 3 \text{ H}_2\text{O} \rightarrow \text{CH}_3\text{CH}_2\text{OH} + 4 \text{ CO}_2$	Ethanol	2.17
$5 \text{ CO} + \text{ H}_2 + 2 \text{ H}_2\text{O} \rightarrow \text{CH}_3\text{CH}_2\text{OH} + 3 \text{ CO}_2$		2.18
$4 \text{ CO} + 2 \text{ H}_2 + \text{ H}_2\text{O} \rightarrow \text{CH}_3\text{CH}_2\text{OH} + 2 \text{ CO}_2$	Ethanol	2.19
$3 \text{ CO} + 3 \text{ H}_2 \rightarrow \text{CH}_3\text{CH}_2\text{OH} + \text{ CO}_2$		2.20
$2 \text{ CO} + 4 \text{ H}_2 \rightarrow \text{CH}_3\text{CH}_2\text{OH} + \text{ H}_2\text{O}$		2.21
$\text{CO} + 5 \text{ H}_2 + \text{ CO}_2 \rightarrow \text{CH}_3\text{CH}_2\text{OH} + 2 \text{ H}_2\text{O}$		2.22
$6 \text{ H}_2 + 2 \text{ CO}_2 \rightarrow \text{CH}_3\text{CH}_2\text{OH} + 3 \text{ H}_2\text{O}$		2.23
$\text{CO} + \text{ CO}_2 + 6\text{H}^+ + 6\text{e}^- \rightarrow \text{CH}_3\text{COOH} + \text{ H}_2\text{O}$	Acetic Acid	2.24
$\text{CO} + \text{ CO}_2 + 10\text{H}^+ + 10 \text{ e}^- \rightarrow \text{CH}_3\text{CH}_2\text{OH} + 2\text{H}_2\text{O}$		Ethanol

Source: Phillips et al. (2017).

2.12 Types of Fermenter Used for Syngas Fermentation

A fermenter is basically a device in which the microorganisms are cultured for the production of desired products. This system is usually designed to give the right environment for optimal microbial cell growth and their metabolic activity of the organisms. There are various types of fermenter used for syngas fermentation (Acharya et al., 2014; Munasinghe & Khanal, 2011b).

2.12.1 Continuous Stirred Tank Bioreactor

The continuous stirred-tank reactor (CSTR) is one of the most familiar fermenters used for syngas fermentation (Figure 2.21). In this system, one or more reactants (inlet syngas, nutrients) are introduced into a reactor equipped with an agitator fixed with stirrer bars and the ultimate products are removed continuously (Sikarwar et al., 2017). The agitator rotates the stirrer bar to ensure perfect mixing of inlet syngas, nutrients and the

fermentation broth uniformly throughout the whole fermentation (Asimakopoulos et al., 2018; Henstra et al., 2007). As a result, the composition of the product is uniform.

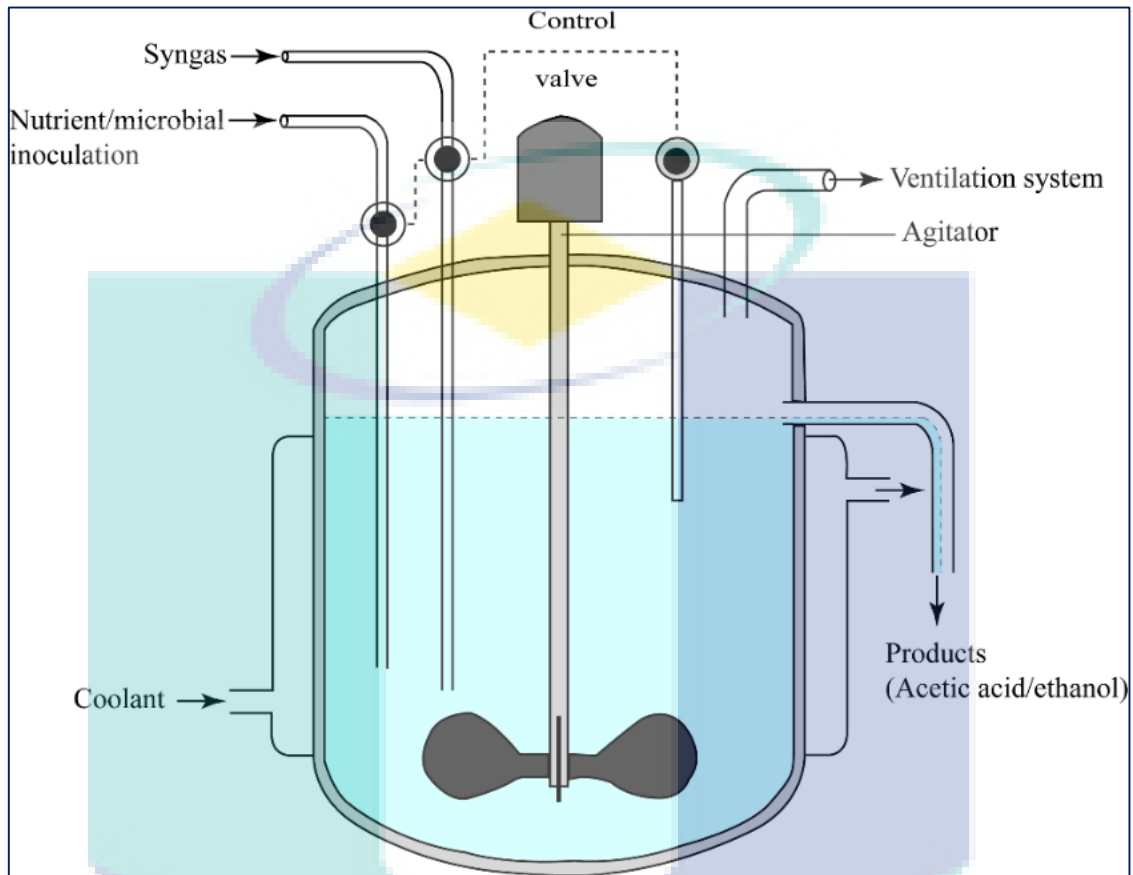


Figure 2.21 Schematic diagram of continuous stirred-tank reactor (CSTR).

2.12.2 Bubble Column Reactor

The bubble column reactors (BCR) is comprised of a vessel containing a liquid or a liquid-solid suspension at the bottom which has the capabilities for the distribution of gas. The schematic diagram of the bubble column reactor is shown in Figure 2.22. This type of fermenter is usually used in the chemical and biochemical industries where the reactions involved as oxidation, fermentation chlorination, Fischer–Tropsch synthesis polymerization, hydrogenation, wastewater treatment etc. This type of fermenter used because of its excellent heat and mass transfer characteristics, less operational cost and durability of any type of solid material (Holland, 2015). In addition, this fermenter has the facilities for the addition or removal of any catalyst from the column. Nevertheless, there are some limitation or challenges which are associated with the fermenter (Asimakopoulos et al., 2018). The syngas, enters the inlet to the column through the gas sparger in the bottom of the column. When the column gas forms, separate bubbles rise

and spread-out due to their buoyancy. It also induces motion of the continuous liquid phase as reported by Holland (2015).

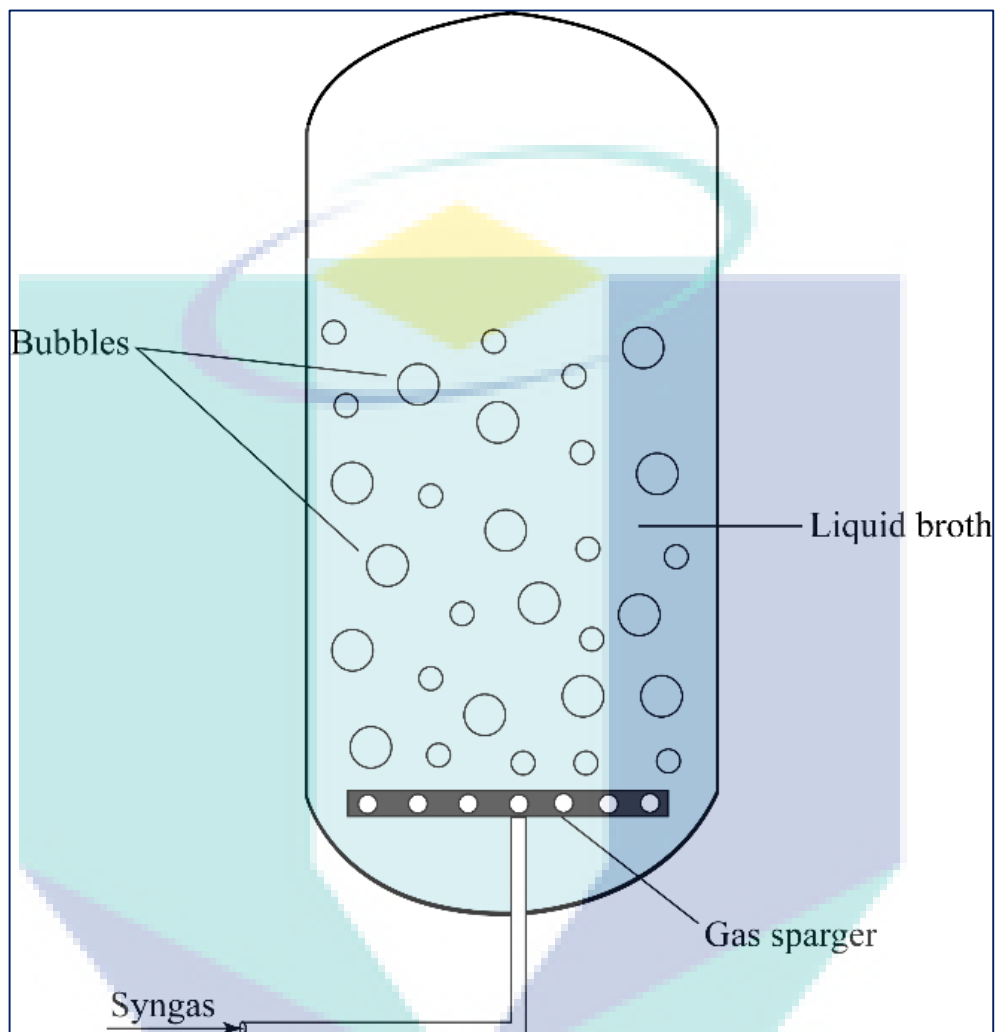


Figure 2.22 Schematic diagram of a bubble column reactor (BCR).

2.12.3 Monolithic Biofilm Reactor

Monolithic biofilm reactor (MBR) is one type of fermenter which integrates a cordierite monolithic packing material within a bubble column. It provides a perfect way to sustain the high cell density with the efficiency of high mass transfer capacity. The monolithic column was fixed inside the plexiglass column by two symmetrical block rings located at the top and bottom of the monolithic column. The monolithic column was covered with an insulation sheet to minimize heat loss. The broth was circulated between the column and the vessel during syngas fermentation (Asimakopoulos et al., 2018; Henstra et al., 2007). The disadvantages of the fermenter are clogging due to biofilm formation during the biological process. The schematic diagram of the

monolithic biofilm reactor is shown in Figure 2.23. In addition, a bubble column reactor was also established as a control to gauge the mass transfer and syngas fermentation performance. The parameters of the column and the operational conditions were identical to MBR as reported by Shen, Brown, and Wen (2014a).

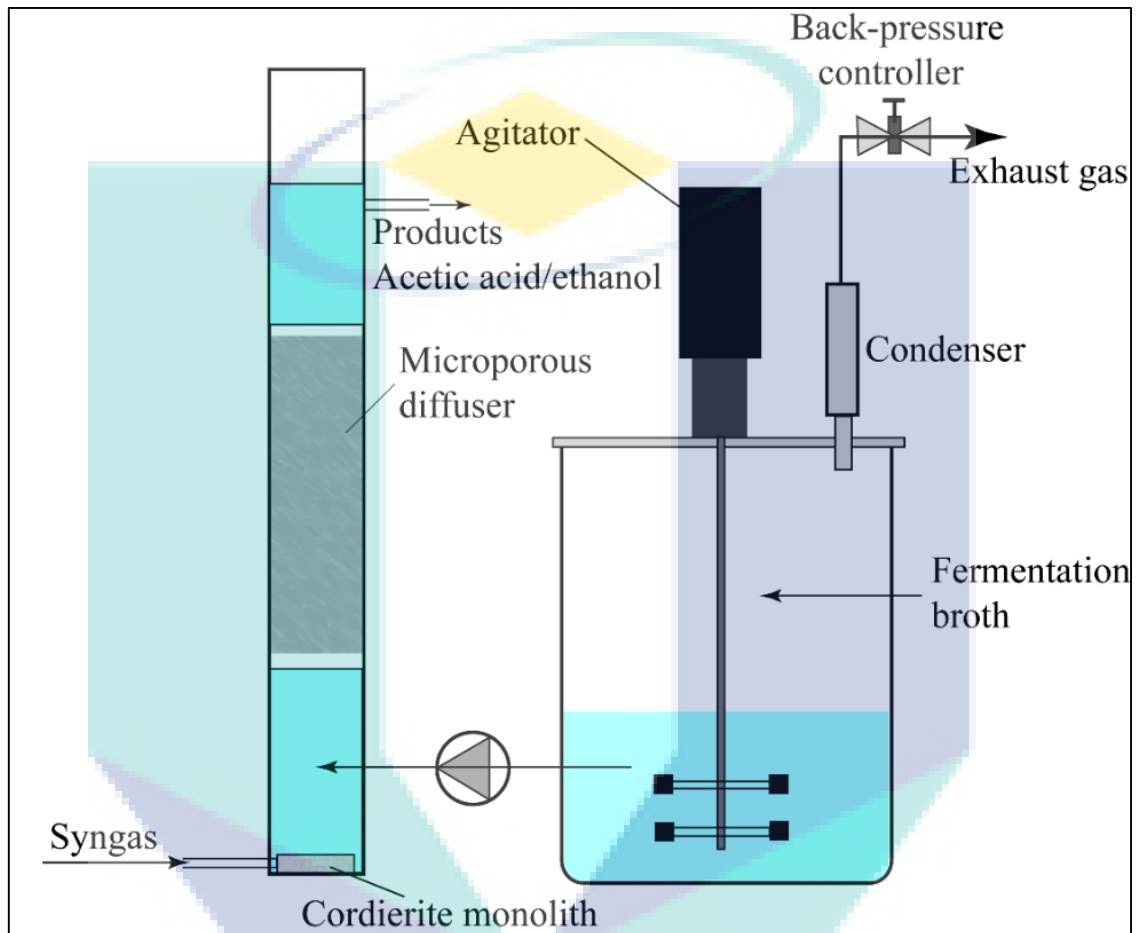


Figure 2.23 Schematics diagram of Monolithic biofilm reactor (MBR) system for syngas fermentation.

2.12.4 Trickle Bed Reactor

The trickle-bed reactor (TBR) is one type of chemical reactor which involved the downward movement of a liquid and the downward or upward movement of syngas over a catalytical packed bed. The schematic diagram of this type of fermenter is shown in Figure 2.24. This bed is intrinsically nonstop in operation. Due to the low operating cost, nominally plug flow both gas and liquid phase, it occurs good control over the process and maintains good product quality. It has a random packed catalytical bed. As a result, it has the ability to inherently a single production plant or single catalytical plant. In addition, it has no heat transfer facilities within the bed. Therefore, the designs for trickle

bed and batch plants are based on various flow rates, and design specification and cost extrapolations (Asimakopoulos et al., 2018).

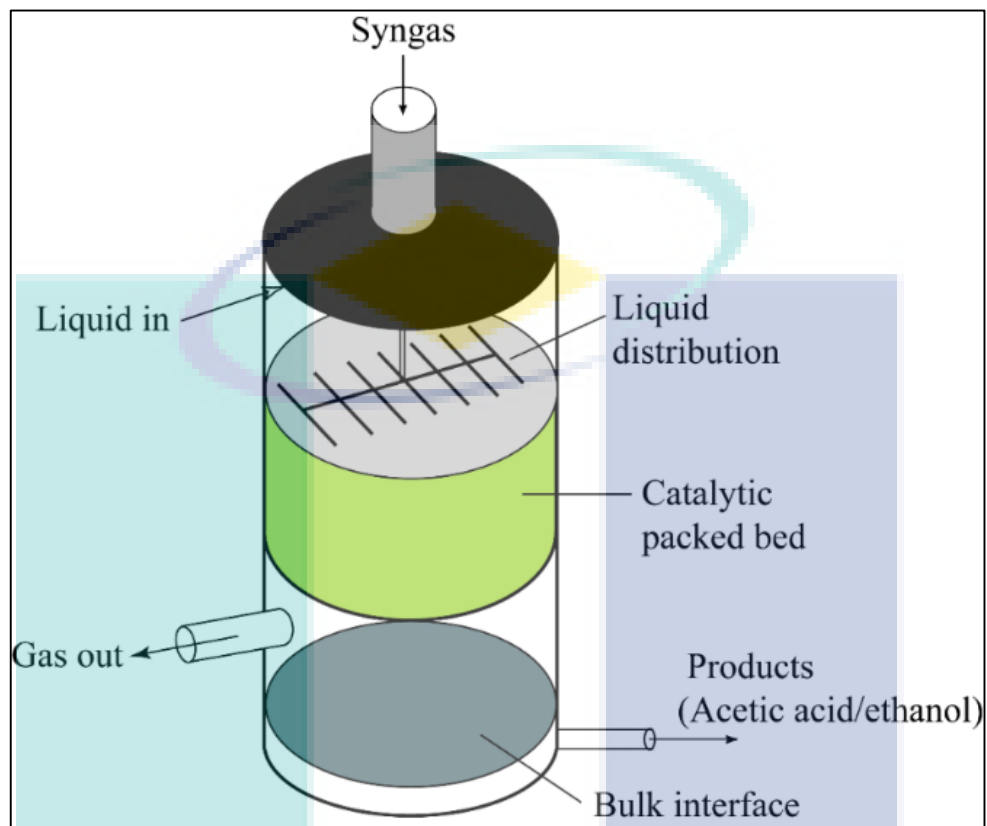


Figure 2.24 Schematic diagram of a trickle bed reactor (TBR).

Source: Stitt (2002).

2.12.5 Membrane-based System Reactor

The schematic design of the membrane-based system reactor (MSR) is shown in Figure 2.25. It compared the fuel processor which generate H_2 by the dilution of CO_2 and similar types of gases. This type of fermenter allows the fuel cell to operate at high voltage electricity and fuel consumption factors, that reduces the degradation rates due to the CO harming. This type of bioreactor has significant advantages to achieving a maximum yield product and reaction rate (Asimakopoulos et al., 2018). It has also the maximum tolerance to toxic compounds that exist in the syngas (tar, acetylene, NO_x , O_2).

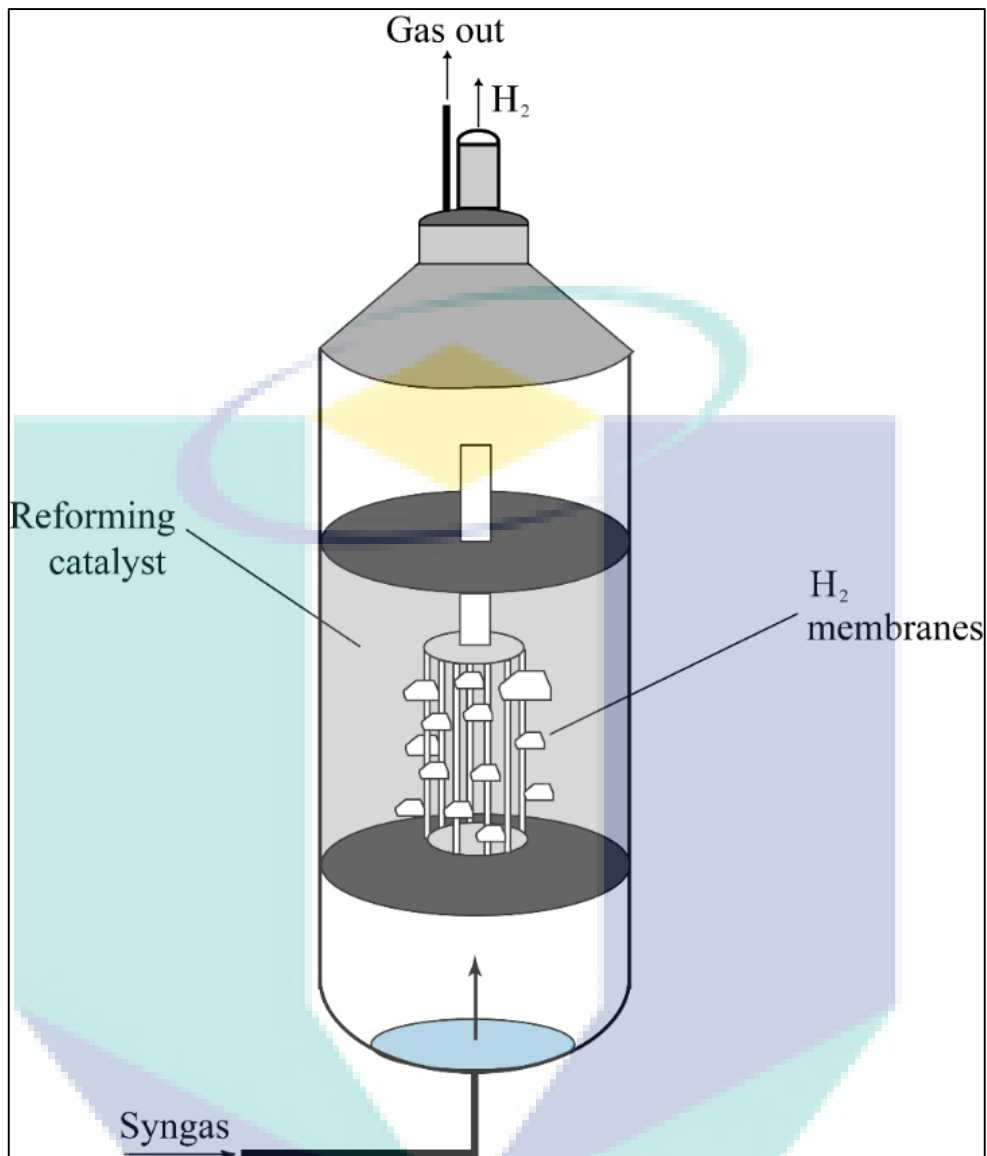


Figure 2.25 Schematic diagram of membrane-based system reactor (MSR).

2.12.6 Selection of Bioreactor

The selection criteria for the uses of a bioreactor for syngas fermentation is based on some important criteria. The most important factors for the choice of bioreactor are type of microorganisms, type of syngas, type of nutrients, raw syngas purification facilities, fermentation system and expected yield products (Collet et al., 2018; Henstra et al., 2007; Phillips et al., 2017).

2.13 Syngas Fermentation for Bioethanol Production

Sikarwar et al. (2017) reported that biofuels are categorized as first generation, second generation, third generation and fourth generation based on biomass types and

process employed. The first generation of biofuels which are bio-methanol, bio-ethanol, bio-propanol, bio-butanol, fatty acid esters, etc., are converted from simple sugars, starch, fats and vegetable oils (Naik, Goud, Rout, & Dalai, 2010). Inderwildi and King (2009) stated that the second generation biofuels, such as ethanol are produced from lignocellulosic biomass. The third and fourth generation of biofuels products used the 'algae-to-biofuel' strategy. In third generation technologies, algae biomass is treated for biofuel production, whereas the fourth generation approach utilizes metabolic engineering of algae for generating biofuels from oxygenic photosynthetic microbes and creating artificial carbon sinks (Lü, Sheahan, & Fu, 2011). Second generation bioethanol production is cost-effectiveness compared to fossil fuels (Kennes et al., 2016). Rastogi and Shrivastava (2017) reported that utilization of lignocellulosic biomass for the production of various energy forms (second generation fuels) like biogas, biodiesel, bioethanol, etc has been increased day by day. Different types of syngas fermentation reactors are used for bioethanol production. These are Continuous Stirred Tank Reactor (CSTR), Bubble Column Reactor (BCR), Monolithic Biofilm Reactor (MBR), Trickle Bed Reactor (TBR), Microbubble Dispersion Stirred-tank Reactor (MDSR) and Membrane-based System Reactor (MSR) as reported by Acharya et al. (2014). The ethanol production can be increased by proper reactor designs, which allow proper mass transfer rates, choice of biocatalysts with optimizing yields and efficient recovery methods (Shen, Brown, & Wen, 2014b). Shen et al. (2017) stated that horizontal rotating packed bed (h-RPB) reactor was more effective compared to CSTR for bioethanol production.

2.14 Effect of Syngas Fermentation for Bioethanol Production

2.14.1 Effect of Microbial Growth Phase

Microbial growth is the division of one microorganism into two daughter cells in the syngas fermentation process (Vinícius de Melo Pereira, Soccol, Brar, Neto, & Soccol, 2017). During the whole process, five individual phases indicated the microbial cell growth for the production of bioethanol or other liquid fuels (Figure 2.26).

2.14.1.1 Lag phase

When microorganisms are introduced into the fresh culture medium. In this phase, usually, no increasing number of microbial cells occur. Therefore, this period is called the lag phase.

2.14.1.2 Log phase

In this phase, microorganisms are growing and dividing at the maximal rate. The exponential increase in the number of living microbial cells in this phase is observed.

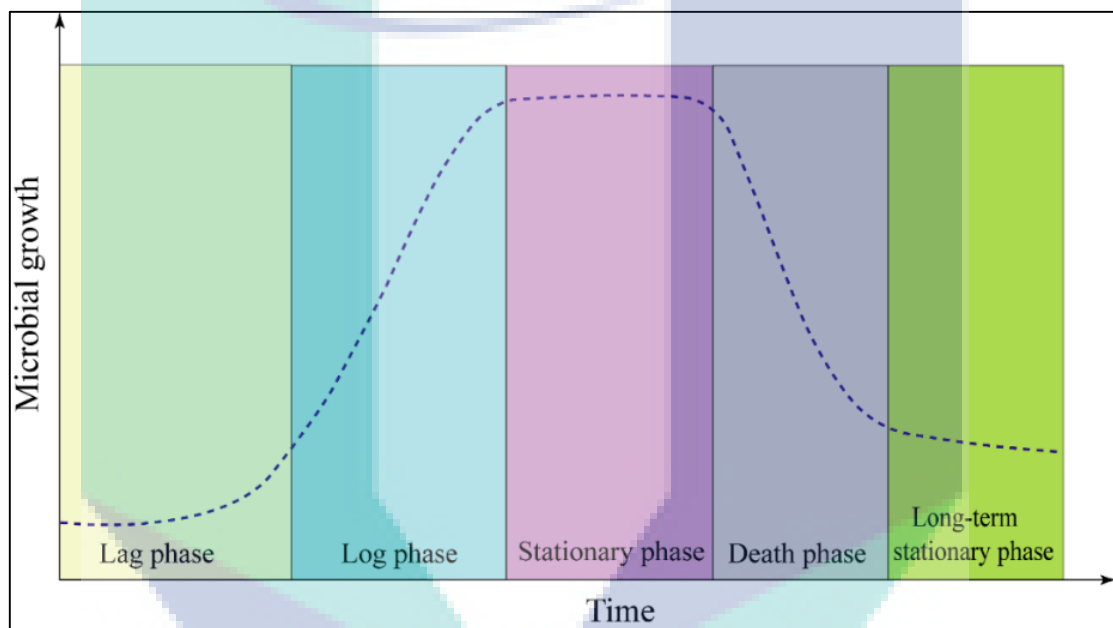


Figure 2.26 Microbial growth vs time for syngas fermentation.

2.14.1.3 Stationary phase

The microbial cell production ceases, and the growth curve becomes horizontal. As a result, a plateau in a number of living microbial cells, the rate of cells division and death are roughly equal.

2.14.1.4 Death phase

The decline in visible cells, following stationary phase is called the death phase (Casolari, 2018).

2.14.1.5 Long-term stationary phase

At the end of the death phase, most of the microorganisms died and the dead cells released nutrients to the environment.

2.14.2 Effect of Organic Source

The most important effect of syngas fermentation is the source of substrate. The organic matter containing biomass-based syngas is recently used for biofuel production (Phillips et al., 2017). The carbonic acid and carbonate formation are depending on the concentrations of carbon dioxide and high acetate, which may potentially inhibit microbiological actions in the fermentation media. Biomass-based syngas can constrain hydrogen production and adapt product distribution of ethanol and acetate as reported by Sun, Atiyeh, Kumar, and Zhang (2018). It has the potential to maintain microbial cells in an inactive stage during biofuel production.

2.14.3 Effect of pH

The pH level is another vital factor that is affected by syngas fermentation. It depends on the fermentation medium, nutrient or substrate. Subsequently, the productivity of ethanol or acetic acid from biomass-based syngas depends on the pH level (Zhang et al., 2016). It also affects the substrate metabolism as well as other parameters (pH, membrane and proton motive force). The biological actions are also affected by small changes in pH (Henstra et al., 2007). Obviously, large changes in pH can lead to the death of microbes, or at least can inhibit the generation of the desired products. The acetogenic bacteria are widely used in syngas fermentation where the ethanol production level is high at lower pH levels. The optimum pH value for the generation of acetate is from 5 to 7 (growth level), whereas for ethanol it is 4-4.5 (non-growth level) by using specific types of bacteria (Asimakopoulos et al., 2018; Henstra et al., 2007).

2.14.4 Effect of Temperature

This parameter is one of the key factors that also affected the production of biofuels. The specific type of microorganisms survived on a specific temperature. The optimum temperature for mesophilic microorganisms is needed to be maintained within the ranges of 37-40 °C, whereas the thermophilic bacteria, it is 55 °C to 80 °C (Acharya et al., 2014; Asimakopoulos et al., 2018).

2.14.5 Effect of Syngas Flow Rate

The microbial growth rate and its metabolic activities are affected by the substrates used in the syngas fermentation. Moreover, the partial pressures of syngas components are needed to be controlled and maintained at an optimum rate (Alzate et al., 2018).

2.14.6 Effect of Mass Transfer

The critical factor for syngas fermentation is limiting the mass transfer rate for gas to liquid. The efficiency of mass transfer rate among different fermenter is compared by the evaluation of gas-liquid volumetric mass transfer coefficient (Alzate et al., 2018). This factor also gives information about the hydrodynamic condition of the bioreactor. Therefore, the design of the bioreactor is very much important for syngas fermentation.

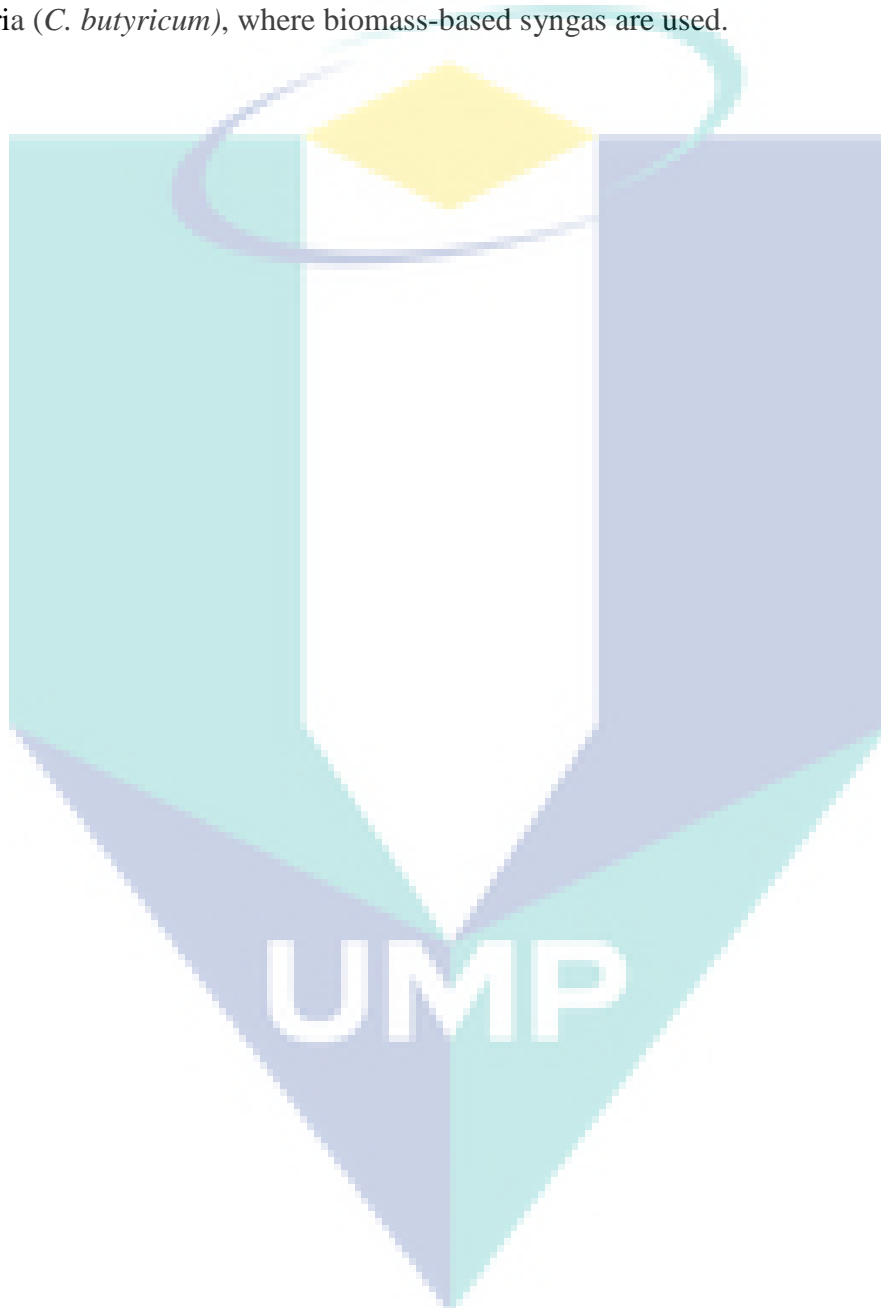
2.14.7 Effect of Trace Metals

The biomass-based syngas contained some trace metals that acted as an impurity. It effects the microbial growth during the syngas fermentation (Mansfield & Wooldridge, 2015). It has the ability to adopt an iron concentration of ten times higher in comparison to the standard medium used for the fermentation of *Clostridium carboxidivorans*. As a result, ethanol production is doubled, and the production of acetic acid and butyric acid is reduced.

2.15 Summary

From the literature review, it is concluded that no study has been done on the co-gasification of lignocellulosic biomass (EFB of palm oil, forest residue and coconut shell) with charcoal in terms of energy production. There is a limited reserve of fossil fuels and it will be diminished in future. Biofuel production from lignocellulosic biomass could be a sustainable alternative for future energy demand. By-product charcoal could be the proper substitute for coal in the future. Aspen plus simulation could be used to optimized the gasification parameters (temperature, pressure) which reduces the experimental cost and time. From the literature, coal was co-gasified with biomass, because it contains more fixed carbon than biomass, which enhances the combustion time. As a result, higher energy syngas can be obtained by optimizing the ratio of biomass and charcoal through

co-gasification process. Downdraft gasifier could be used to perform the co-gasification experiment due to its ease operation and relatively high energy efficiency. Before going to bioenergy production, characterization of feedstocks and simulation for the experimental run are needed. From the literature, it is also found that there has been no studied on the syngas fermentation using the biocatalyst of yeast (*S. cerevisiae*) and bacteria (*C. butyricum*), where biomass-based syngas are used.



CHAPTER 3

METHODOLOGY

This study has been done based on the specified research objectives. According to the complete research work plan, detail activities are shown in the following flowchart (Figure 3.1).

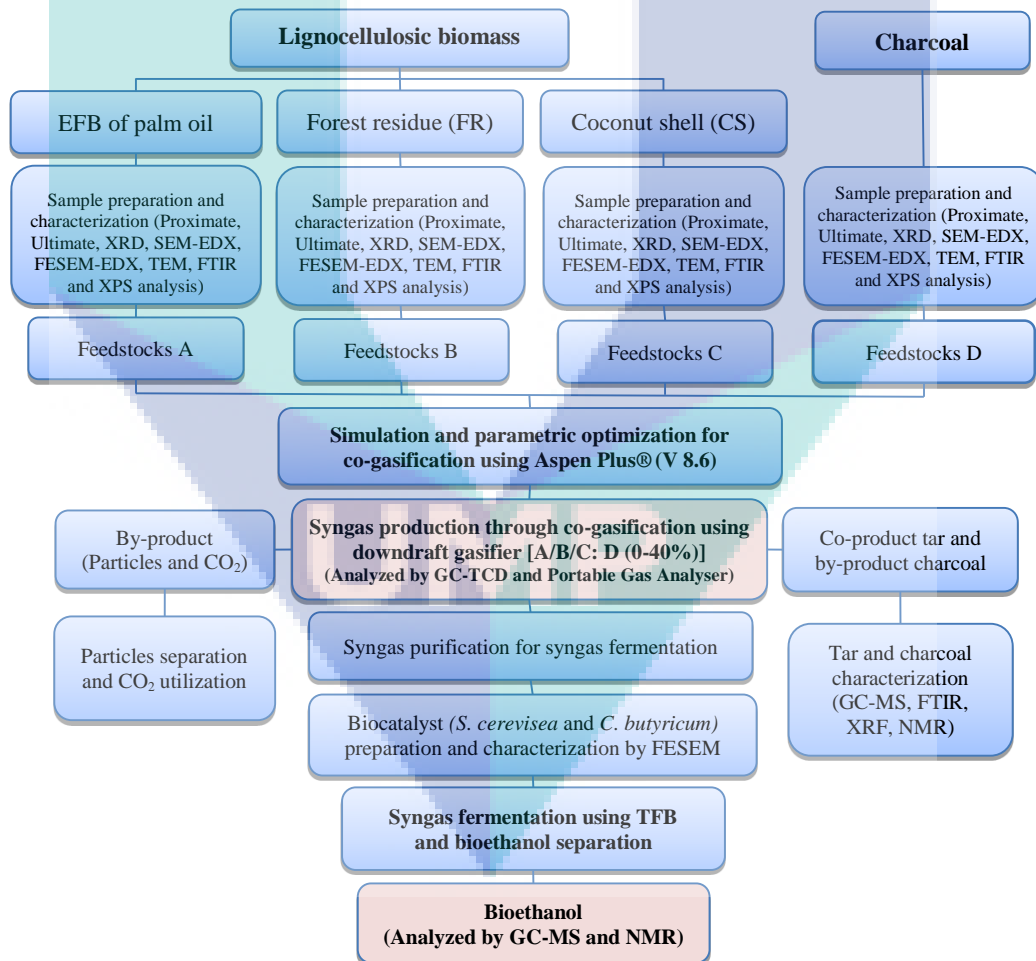


Figure 3.1 Flowchart of research work plan.

This flowchart represents the hybrid process of co-gasification and syngas fermentation for the production of syngas and bioethanol, respectively. The used feedstocks for co-gasification were empty fruit bunch of palm oil, forest residue, coconut shell and charcoal, and used biocatalysts (microorganisms) for syngas fermentation were *S. cerevisiae* and *C. butyricum*. All feedstocks, yield products, co-products and by-products were characterized using various analysis that discussed in detail in this chapter.

3.1 Samples Collection and Preparation

The lignocellulosic biomass of empty fruit bunch (EFB) of palm oil (processed), forest residue (FR) and coconut shell (CS) were collected from palm oil mill industry (LKPP Corporation Sdn Bhd, Kilang Sawit, Lepar, Lebuhraya Tun Razak), forests and local market nearby Gambang area, Kuantan, Pahang, Malaysia, respectively. The collected forest residue comprised of softwood to hardwood category (*Shorea Spp.*, *Dipterocarpus Spp.*, *Scaphium Spp.*, *Intsia Spp.* etc.). Charcoal was collected from previous wood-based biomass gasification that was produced as a by-product.



Figure 3.2 Raw feedstocks for co-gasification: (a) EFB of palm oil, (b) Forest residue, (c) Coconut shell and (d) Charcoal.

In this study, collected feedstocks (Figure 3.2) were chopped (avg. $l \times w \times h = 20 \times 20 \times 10$) and kept under the sun (15 days) to maintain their freshness. Subsequently, dried samples were placed in a sample bag to avoid any kind of contamination. The feedstocks size was an average dimension of 20 mm square with 10 mm thick for performing the gasification process through a downdraft gasifier (At Naw et al., 2013). Moreover, feedstocks were crushed by a high-speed rotary cutting mill and then sieved to the desired particle size ($<45 \mu\text{m}$ /Pan) to obtain better analytical results for characterization.

3.2 Feedstocks and Product Characterization

The feedstock samples were characterized for bioenergy potentiality before the experimental run. The proximate analysis was performed by thermogravimetric (TGA) and derivative thermogravimetry (DTG) analysis, and ultimate analysis was done using elemental (CHNS) and X-ray fluorescence (XRF) analysis. The morphological structure (size, shape, regularity and agglomeration of nanoparticles and cellulose) and functional groups of EFB, FR, CS and charcoal were investigated by fourier-transform infrared spectroscopy (FTIR), field emission scanning microscopy-energy dispersive x-ray analysis (FESEM-EDX), transmission electron microscopy (TEM) and x-ray photoelectron spectroscopy (XPS) analysis. The initial product of syngas was produced through co-gasification of biomass and charcoal. It was insitu analyzed by portable gas analyzer and further, it was analyzed by online gas chromatography-thermal conductivity detector (GC-TCD). The newly cultured biocatalyst (*S. cerevisiae* and *C. butyricum*) were characterized by FESEM analysis. Subsequently, the yield of bioethanol was produced through syngas fermentation that was characterized using gas chromatography-mass spectrometry (GC-MS) and nuclear magnetic resonance (NMR) analysis. The by-product charcoal was also characterized by XRF analysis and co-product tar compounds were identified by scanning electron microscopy with energy dispersive X-ray spectroscopy (SEM-EDX), FTIR, GC-MS and NMR (^1H and ^{13}C) analysis.

3.2.1 Proximate Analysis

The proximate analysis of EFB, FR, CS and charcoal were carried out by thermogravimetric (TGA) and derivative thermogravimetry (DTG) analyzer (Brand: Mettler Toledo, Model: TGADSC1). This analysis was used for the determination of

relative percentage of moisture content (MC), volatile matter (VM), fixed carbon (FC) and ash content (AC) in the feedstock samples (Atnaw, Sulaiman, & Yusup, 2017). Prior to the analysis, a 10 mg of a powder sample of each dried EFB, FR, CS and charcoal were placed in a small alumina crucible and weighted individually. The high temperature furnace was set starting at 25 °C to a maximum temperature of 1000 °C. The heating rate was 100/min under 30 ml/min N₂ purging. The VM fraction was considered within the temperature ranges of 200 °C and 500 °C (Aydin et al., 2018). The ignition and peak temperature of each feedstock samples were detected by first derivative of the TGA curve called DTG curve.

3.2.2 Ultimate Analysis

The ultimate analysis was performed by CHNS elemental analyzer (Brand: Agilent, Model: 780A) to determine the elemental composition of carbon (C), hydrogen (H), oxygen (O), nitrogen (N) and sulphur (S) of EFB, FR, CS and charcoal samples. The O was calculated by subtraction method. During this analysis, approximately a 2 mg of very fine dried samples were placed in a tin capsule and crimped. In this analysis, the oxidation temperature was set as 1000 °C and used as carrier gas was helium (He). The elemental composition of all samples was given in percentage (%).

The XRF was used to determine the oxide groups of by-product charcoal. This analysis has investigated the chemistry of charcoal by measuring the fluorescent X-ray that emitted from the sample when it is excited by a primary X-ray source using XRF analyzer (Brand: Bruker, Model: S8 Tiger). Each of the elements presented in a sample that produces a set of characteristic fluorescent X-rays which was unique for that specific element.

3.2.3 X-ray Diffraction Analysis

The XRD analysis was carried out by an X-ray diffractometer (Brand: Bruker, Model: D8 Advance). In this analysis, Cu-K α radiation (wave length, $\lambda = 0.15418$ nm) was used as the source. All feedstock samples were characterized to know the characteristics of solid (crystalline or amorphous). The X-ray diffraction patterns were set for the 2θ range of 10 to 80° with 2θ of 5° per minute. The crystal dimension was estimated by using the Scherrer equation reported by Baharuddin et al. (2013).

3.2.4 Scanning Electron Microscopy and Energy-Dispersive X-ray Analysis

In this study, SEM-EDX analysis (Brand: Fei, Model: Quanta 450) was used for feedstock samples and co-product tar samples to identify the elemental and morphological features. Bahng, Mukarakate, Robichaud, and Nimlos (2009) reported that scanning electron microscopy (SEM) and transmission electron microscopy (TEM) are the most important techniques for the analysis of micro-structural morphology of samples and also their transformations that occurred during thermal degradation of the biomass. In this analysis, electron beam was scanned over the surface of the samples to create an image. It can also be used to achieve the information of co-product tar samples regarding the surface topography and composition.

3.2.5 Field Emission Scanning Electron Microscopy and Energy-Dispersive X-ray Analysis

The high resolution images and elemental composition were obtained from TEM-EDX analysis (Brand: Jeol, Model: JSM-7800F). The morphology of EFB, FR, CS and charcoal were characterized by FESEM-EDX spectra and obtained a SIRION200 Schottky field emission scanning electron microscope (SFE-SEM) that were equipped with a Rontec EDX system. The detected samples were rinsed with deionized water and dried in air, then coated with Pt to make the samples conductive before loading into the instrument. Images were obtained with an acceleration voltage of 5 kV or 10 kV.

3.2.6 Transmission Electron Microscopy Analysis

The TEM analysis was performed by examining the morphological structure (size, shape, regularity and agglomeration of nanoparticles and cellulose) of EFB, FR, CS and charcoal using high resolution transmission electron microscope (Brand: Fei, Model: Tecnai-G2-20-Twin), operated at an acceleration voltage of 200 K.

3.2.7 Fourier Transform Infrared Analysis

The FTIR analysis was used to determine the particular functional groups existed within the feedstocks and co-product tar samples. All spectra were identified with an FTIR spectrometer (Brand: Perkin Elmer, Model: Spectrum 100) in a transmission mode and scanned over the range between 400 and 4000 cm^{-1} wavenumber with a resolution of 4 cm^{-1} . Potassium bromide (KBr) was mixed with pellets of selected samples at the ratio

of 10:1 and a rate of 0.5 cm/s. The background scans were also collected prior to spectra measurement. The FTIR spectral sets of data were analyzed by using Principle Component Analysis (PCA) to study the chemical variations (Cantero-Tubilla et al., 2017).

3.2.8 X-ray Photoelectron Spectroscopy Analysis

The XPS analysis was used to identify the chemical composition and its binding energies for all feedstock samples using a PHI 5000 VersaProbeII Scanning X-ray photoelectron spectroscopy (XPS) Microprobe (Model: 5000 VersaProbeII). The used X-ray was 100 μ , 25W, 15KV and proton energy was 1486.6eV. For survey scan (usually wide scan) from 0eV to 1100eV binding energy, pass energy used: 117.40eV and in the narrow scan for each element appears in survey scan, binding energy was depended on each element, pass energy was used as 29.350 eV.

3.2.9 In-situ Syngas Analysis Using Portable Gas Analyzer

An online portable gas analyzer (Brand: SA, Model: IRCD4) was used to investigate the composition of produced gases (H₂, CO, CO₂ and CH₄) for insitu measurement (Sensor type: Infrared and Electrochemical). The analyzer was calibrated, allows the concentration measurement of CH₄: (1-100)% vol. (\pm 0.5%) of displaced value, CO₂: (0-100) % vol. (\pm 0.5%) of displaced value; CO: (0-1000) ppm and H₂: (0-1000) ppm.

3.2.10 Gas Chromatography-Thermal Conductivity Detector Analysis

The GC-TCD online gas analyzer (Brand: Shimadzu, Model: GC-2014) was also used to analyze the produced syngas more precisely. The attached TCD sensor changes the thermal conductivity of the column that compares the reference flow of carrier gas (helium). The analyzed gases were mainly nitrogen (N₂), hydrogen (H₂), carbon dioxide (CO₂), carbon monoxide (CO), methane (CH₄), etc. During analysis, the injected volume of syngas was 1 μ L.

3.2.11 Gas Chromatography-Mass Spectrometry Analysis

The GC-MS analyzer (Brand: Agilent, Model: 7890A) was used to identify different substances within the test samples. During the analysis, the initial and final

temperatures were set as 70 °C and 325 °C, respectively. The heater temperature was set at 300 °C, the pressure was 8.81 psi, and the flow rate was programmed as 1 mL/min for 0 min and 3 mL/min for 5 min (post run). The total run time was 29.614 min. The MS was operated in the scan mode mass ranges from 40 amu to 600 amu.

3.2.12 Nuclear Magnetic Resonance Analysis

The NMR (¹H and ¹³C) analyses were carried out to identify the nature and type of organic compounds in co-product tar samples produced from co-gasification, and yield of bioethanol produced from syngas fermentation. ¹H NMR (500 MHz) and ¹³C NMR (100 MHz) spectra were recorded using BRUKER-500/400 spectrometer (Model: Bruker Ultra Shield Plus 500 MHz). The ¹H NMR chemical shifts were stated relative to CDCl₃ (TMS, 0.00 ppm). The ¹³C NMR chemical shifts were reported relative to CDCl₃ (77.0 ppm). The used solvent for tar and ethanol samples were acetone and CDCl₃, respectively that was used during NMR analysis.

3.3 Heating Value Calculation

The heating value is one of the most important fuel property for feedstock samples which quantified the energy content. The heating value of solid biomasses (EFB, FR and CS) and charcoal were calculated based on proximate and ultimate analytical results. This analysis was also used to identify the energy content for thermochemical conversion of selected feedstocks. The higher heating value (HHV) was calculated using the following Eq. 3.1. A similar equation was used for this HHV calculation that is reported by Channiwala and Parikh (2002).

$$\text{HHV}_{\text{feedstock}} = 0.3491M_C + 1.1783M_H + 0.1005M_S - 0.1034M_O - 0.0151M_N - 0.0211M_{AC} \quad 3.1$$

Where, $\text{HHV}_{\text{feedstock}}$ = Higher heating value for feedstock (MJ/kg);

M_C, M_H, M_S, M_O, M_N and M_{AC} = Mass percentage of carbon, hydrogen, sulfur, oxygen, nitrogen and ash content for feedstock, respectively.

The lower heating value (LHV) was calculated by deducting the heat of evaporation of water vapor from the HHV was estimated by the Eq. 3.2 (Basu, 2010, 2018).

$$\text{LHV}_{\text{feedstock}} = \text{HHV}_{\text{feedstock}} - h_g \left(\frac{9H}{100} + \frac{MC}{100} \right) \quad 3.2$$

Where, $LHV_{\text{feedstock}}$ =Lower heating value of feedstock (MJ/kg) .

H and MC=Hydrogen and moisture content percentage of feedstock, respectively;

h_g =Latent heat of steam (2.260 MJ/kg) .

The LHV and HHV of produced syngas were calculated using equations Eq. 3.3 and Eq. 3.4 (Shahbaz et al., 2017; Valdés, Marrugo, Chejne, Montoya, & Gómez, 2015).

$$LHV_{\text{syngas}}=(H_2 \times 25.7 + CO \times 30 + CH_4 \times 85.4) \times 0.0042 \quad 3.3$$

Where, LHV_{syngas} =Lower heating value of syngas (MJ/kg) .

H_2 , CO and CH_4 =Hydrogen, carbon monoxide and methane percentage of syngas (mol %), respectively.

$$HHV_{\text{syngas}}=(H_2 \times 30.52 + CO \times 30.18 + CH_4 \times 95) \times 0.0041868 \quad 3.4$$

Where, HHV_{syngas} =Higher heating value of syngas (MJ/kg) ;

H_2 , CO and CH_4 = Hydrogen, carbon monoxide and methane percentage of syngas (mol %), respectively.

3.4 Cold Gas Efficiency and Carbon Conversion Efficiency Calculation

In this study, total carbon in the feedstocks (biomass and charcoal) were converted into product syngas (CO , CO_2 , CH_4 , etc.) which contained carbon. Based on the feedstocks and produced syngas composition, cold gas efficiency (E_{CG}) and carbon conversion efficiency (E_{CC}) were calculated using the equations of Eq. 3.5 and Eq. 3.6 (Shahbaz et al., 2017; Valdés et al., 2015):

$$E_{CG} = \left(\frac{LHV_{\text{syngas}}}{LHV_{\text{biomass}}} \right) \% \quad 3.5$$

Where, E_{CG} =Cold gas efficiency (%);

LHV_{biomass} =Lower heating value of feedstock ($\frac{MJ}{kg}$);

LHV_{syngas} =Lower heating value of produced syngas ($\frac{MJ}{kg}$).

$$E_{CC} = \left(\frac{\text{Moles of carbon produced}}{\text{Moles of carbon in feed}} \right) \% \quad 3.6$$

Where, E_{CC} =Carbon conversion efficiency (%).

3.5 Exergy Analysis

The exergy analysis was performed to estimate the energy quality of feedstocks based on the second law of thermodynamics (Roy & Ghosh, 2017). This analysis provides some efficient parameters to optimize the performance of the reactor system. Exergy efficiency is expressed (Eq. 3.7) as follows (Patel et al., 2017):

$$\eta_{ex} = \frac{Ex_{prod}}{Ex_{feedstocks} + Ex_{agent}} \quad 3.7$$

Where, Ex_{prod} and $Ex_{feedstocks}$ = The exergies of produced syngas and inlet feedstocks, respectively, while Ex_{agent} is the exergy of gasifying agent (i.e. air).

In this study, atmospheric air was used as a gasifying agent and injected to the reactor system using an air blower. As a result, for the estimation of exergy efficiency, the gasifying agent was neglected (Prins & Ptasiniski, 2005). Therefore, overall exergy of produced syngas (Ex_{prod}) remains physical exergy, chemical exergy, potential exergy and kinetic exergy. However, potential and kinetic exergy have their independent temperature and pressure. Consequently, their contribution to overall exergy was irrelevance. Therefore, the physical and chemical exergy had two major contributors that were considered for the calculation of overall exergy is shown in Eq. 3.8.

$$Ex = Ex_{phy} + Ex_{chem} \quad 3.8$$

Where, Ex = Overall exergy
 Ex_{phy} = Physical exergy
 Ex_{chem} = Chemical exergy

The generalized equation of Eq. 3.9 for the estimation of specific physical exergy are as follows:

$$\epsilon_{ph} = (h - h_0) - T_0(s - s_0) \quad 3.9$$

Where, h and s = Enthalpy and entropy at any temperature (T) and pressure (P);
 h_0 and s_0 = Enthalpy and entropy at dead state ($T_0 = 298.15$ K, $P_0 = 1$ atm.).

Eq. 3.10 represents for the calculation of specific chemical exergy of an ideal gas mixture are as follows:

$$\varepsilon_{ch,m} = \sum_i x_i \varepsilon_{ch,i} + RT_0 \sum_i x_i \ln x_i \quad 3.10$$

Where, x_i =Mole fraction of i^{th} species;

R =Universal gas constant;

$\varepsilon_{ch,i}$ =Standard chemical exergy of i^{th} species in KJ/kmol

The exergy of feedstocks (EFB, FR, CS and charcoal) with the mass ratio of $2.67 > O/C > 0.667$ were calculated by equation Eq. 3.11 (Patel et al., 2017).

$$\varepsilon_{fm} = (LHV_{fm} + 2442 \times W_{fm})\beta \quad 3.11$$

Where, LHV_{fm} =Lower heating value of fuel (biomass and charcoal) mixture;

W_{fm} =Mass fraction of moisture in the fuel (biomass and charcoal) mixture.

The Eq. 3.12 was used to calculate the value of β by comparing the mass fraction of H, C, O and N.

$$\beta = \frac{1.0438 + 0.1882 \frac{H}{C} - 0.2509 \frac{O}{C} \left[1 + 0.7256 \frac{H}{C} \right] + 0.0383 \frac{N}{C}}{1 - 0.3035 \frac{O}{C}} \quad 3.12$$

Where, H, C, O and N= Mass fraction of hydrogen, carbon, oxygen and nitrogen, respectively.

3.6 Assumptions for Simulation Using Aspen Plus®

In this study, an Aspen Plus® simulator (V 8.6) was used for optimizing the co-gasification parameters (temperature and pressure). Prior to the co-gasification run, it was required to reduce the experimental number, time and cost. Some assumptions were considered to perform the simulation is shown in Table 3.1. Proximate and ultimate analytical results of feedstock samples that were corresponding to the required temperatures for cellulose, hemicellulose and lignin decomposition were used as the input parameters to run the simulation. Experimental results were validated against the simulation results. In this regard, the simulation seems to be an appropriate option for the valuation of product syngas and an indication of co-gasification behavior. This simulation refers to the precise relationship between temperature, pressure and mole fractions (Keche, Gaddale, Tated, & Policy, 2015). At the end of the simulation, optimized pressure and temperature were set and the experiments were run for co-gasification.

Table 3.1 Aspen Plus blocks with unit assumptions used for simulation of the co-gasification process of lignocellulosic biomass and charcoal.

Aspen Plus Block ID	Description	Assumptions
MIXER	Blended of lignocellulosic biomass and charcoal	<ul style="list-style-type: none"> ▪ Lignocellulosic biomass of EFB, FR and CS comprises only carbon (C), hydrogen (H) and oxygen (O)
RSTOIC	Removal of moisture content from feedstocks	<ul style="list-style-type: none"> ▪ By-product charcoal contains only C
RYIELD	Elemental decomposition and distribution	<ul style="list-style-type: none"> ▪ Feedstocks for co-gasification are considered as lignocellulosic biomass and charcoal (100:0; 90:10; 80:20; 70:30 and 60:40)
BLOWER	Atmospheric air pass through the reactor (oxidation zone)	<ul style="list-style-type: none"> ▪ Co-gasification process is isothermal and steady state
RGIBBS	Models are single-phase chemical equilibrium by reducing Gibbs free energy that are subjected to material balance constraints	<ul style="list-style-type: none"> ▪ Feedstocks devolatilization is instantaneously and volatile matter contains CO₂, CO, H₂, H₂O and CH₄
CYCLONE	Solid particles are separated from syngas	<ul style="list-style-type: none"> ▪ Produced gases are considered as ideal ▪ Temperature (T) and pressure (P) is uniformly distributed inside the reactor
COOLER	High temperature syngas is converted into room temperature syngas	<ul style="list-style-type: none"> ▪ By-product tar compounds and ashes are not considered
SEPARATOR	By-product tars are separated from syngas	<ul style="list-style-type: none"> ▪ Gasifying agent is considered as atmospheric air (O₂) ▪ Property method: NRTL-(Remon) with ideal gas and Henry law.

3.7 Experimental Setup and Process of Co-gasification

The downdraft gasifier (DG) was used for the experiment of co-gasification using a various mixture of lignocellulosic biomass and charcoal (100:0, 90:10, 80:20, 70:30 and 60:40) are shown in Figure 3.3. The capacity of the thermal output of this pilot-scale DG was 50 kW. The body of the reactor was made of mild steel (MS) sheet having a thickness of 10 mm. The dimension (height and diameter) of the reactor was 1000 mm and 400 mm, respectively. The slope angle of the neck or throat was $\sim 70^\circ$ that provided near the grate inside the reactor in order to ensure frequently down the flow of the feedstocks due to the gravitational attraction (Atnaw, Kueh, & Sulaiman, 2014; Atnaw et al., 2013).

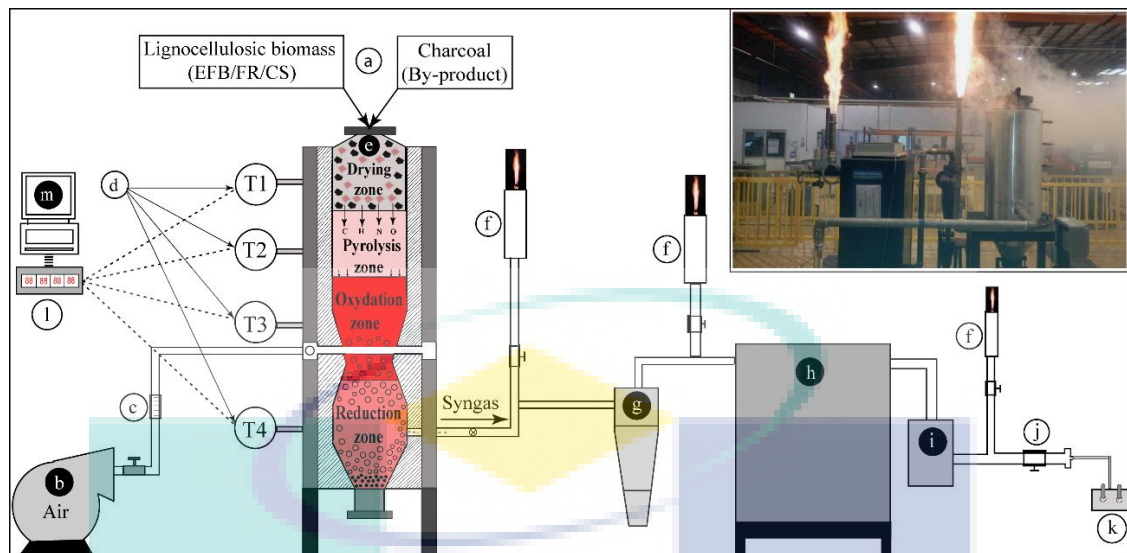


Figure 3.3 Experimental setup of downdraft reactor for syngas production: (a) feedstocks (EFB, FR, CS and charcoal), (b) air blower (atmospheric air), (c) rotameter, (d) thermocouples, (e) downdraft reactor (including four zones), (f) gas flare points, (g) cyclone separator, (h) cooling heat exchanger, (i) filter, (j) clean gas sampling point, (k) gas sampling point by gas bag (l) temperature data logger, and (m) computer for data analysis.

The reactor comprises four zones from top to bottom: (a) drying zone, (b) pyrolysis zone, (c) oxidation zone, and (d) reduction zone. These zones were connected with a data logger through K-type thermocouples for real-time data acquisition and continuously recorded temperature profile separately. The K-type thermocouples were mounted in the middle section along the gasifier wall at 200 mm interval. This reactor was also connected with an air blower which has the facilities of inlet the atmospheric air, a rotameter which control the air flow rate, gas flare point that investigated the quality syngas flame, a cyclone separator which separated smaller particles from product gas, a heat exchanger that cooled down the hot syngas, an online portable gas analyzer which monitored in-situ yield gas composition (CO , CO_2 , H_2 and CH_4) (Figure 3.3). The air flow rate capacity of the blower was upto $60 \text{ m}^3\text{h}^{-1}$. An inlet air pipe was connected with the reactor to flow the air into the oxidation zone that was coming through the air blower. The cyclone separator was the first purification unit of the system that obtained between the reactor and heat exchanger. The main purpose of this purification system was to remove the fine carbon reached particles that leaving the producer syngas (Atnaw et al., 2013). Ultimately, hot syngas was cooled down to room temperature through the heat exchanger. The major optimized output parameter (i.e., heating value of syngas) was considered with respect to the main operating parameters (i.e., temperature, pressure,

feedstocks ratio and moisture content) (Atnaw, Sulaiman, & Yusup, 2017). Product gas was collected and stored by gas sample bags for further precise analysis using gas chromatograph-thermal conductivity detector (GC-TCD).

During the co-gasification run, feedstocks were passed through four zones inside the downdraft reactor from drying zone to reduction zone. In the drying phase, moisture was evaporated. The temperatures were above 100 °C and part of this vapour might be converted to hydrogen during gasification and rest ends up as moisture in the produced syngas. Subsequently, the feedstocks were started to be pyrolyzed at the temperature of ~200 °C (Basu, 2018; Wei, 2005). At this stage, thermal disintegration of the feedstocks started and it was converted into volatile gases and char. The proportion of these components was influenced by the chemical composition of feedstock being fed. It was also influenced by the operational conditions of the reactor. Subsequently, there was an oxidation zone where the pyrolyzed products were stimulated into the hotter zone. Atmospheric air was injected into the oxidation zone under starved oxygen conditions. The oxidation occurred at the temperature ranges from 700-1000 °C (Basu, 2010; Wei, 2005) and possible reactions happened during the co-gasification experiments. After that, the products were transferred into the reduction zone where there is oxygen deficiency, leading to reduction reactions between the hot gases and char. In this zone, the sensible heat of the gases and char was converted into the stored chemical energy in the syngas. Therefore, the temperature of the gases was reduced during this process. The process for syngas production from lignocellulosic biomass through gasification is illustrated in Figure 3.4.

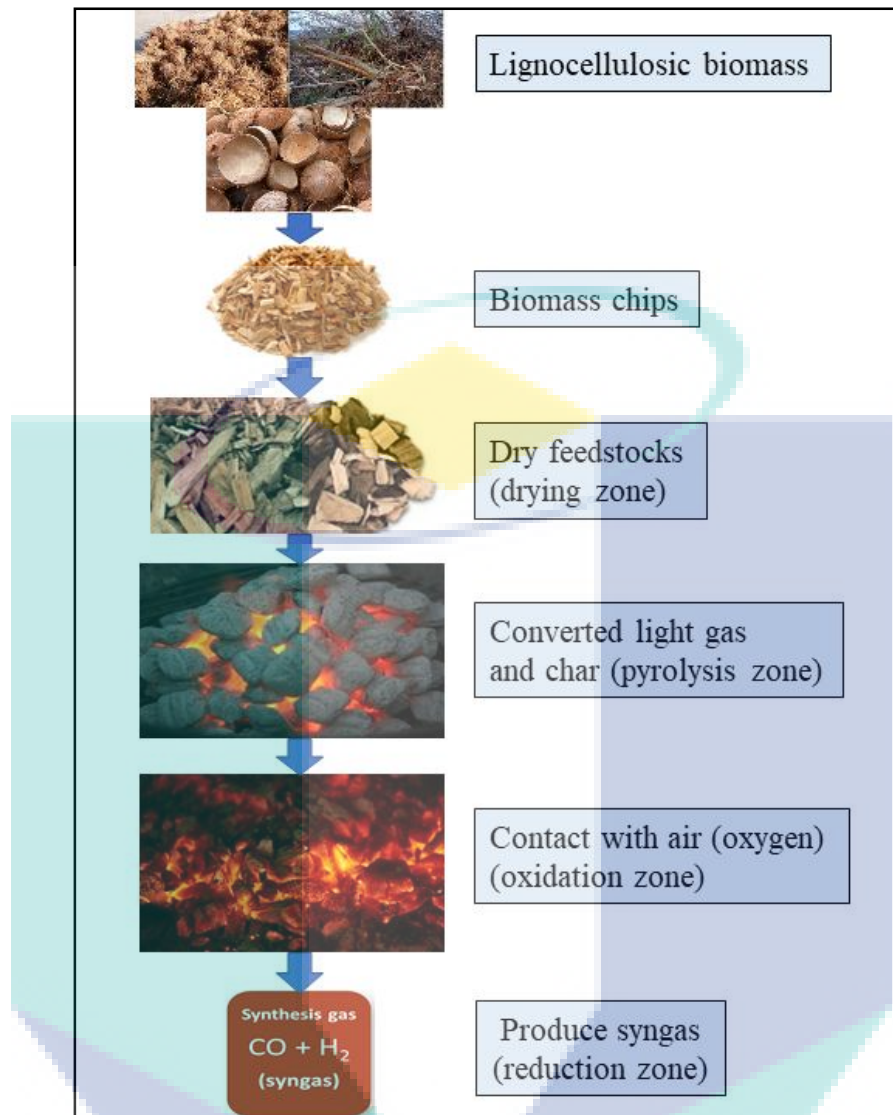


Figure 3.4 Process for the conversion of syngas from lignocellulosic biomass.

3.8 Biocatalyst Preparation for Syngas Fermentation

There were two different types of biocatalysts (*Saccharomyces cerevisiae* and *Clostridium butyricum*) were obtained from the laboratory of Biochemical Engineering, International Islamic University Malaysia (IIUM), Malaysia. Subsequently, *S. cerevisiae* and *C. butyricum* were cultured freshly that were used for syngas fermentation.

3.8.1 *Saccharomyces Cerevisiae* Cell Growth Culture

The *Saccharomyces cerevisiae* was freshly cultured in a 10 mL agar slants containing glucose (10 g/L), yeast extract (10 g/L), peptone (10 g/L) and agar (2%, w/v) as a growth medium to maintain the stock culture (Islam et al., 2018). Subsequently, the

medium was sterilized by autoclaving at 121°C for 20 minutes. The *S. cerevisiae* was sub-cultured in the petri plate to grow up the new cells. The inoculum was prepared by dissolving 10 loops of *S. cerevisiae* from sub-cultured cells in 10 mL of deionized (DI) water. The inoculum process was performed under the biosafety hood to protect any kind of contamination. When this process was completed, these were placed inside the incubator to maintain its temperature. The incubator temperature was set at 37 °C for new cells growth of *S. cerevisiae* for 24 hrs and stored at 4 °C for further uses of syngas fermentation.

3.8.2 *Clostridium Butyricum* Cell Growth Culture

The Reinforced Clostridial Medium (RCM) containing (g/L) yeast extract 3.0; lab-lemco powder 10.0; peptone 10.0; soluble starch 1.0; glucose 5.0; cysteine hydrochloride 0.5; sodium chloride 5.0; sodium acetate 3.0; and agar 0.5 were used and mixed with DI water at a ratio of 38 g/L. Then, the medium was sterilized by autoclaving at 121°C for 20 minutes. Prior to cultivation *C. butyricum* was reactivated by transferring 2 mL of the stock culture into 20 mL of RCM. The cultural serum bottle was flushed with nitrogen gas (N₂) for 2 minutes to create anaerobic condition and incubated at 37 °C for 24 hrs and stored at 4 °C. The prepared *C. butyricum* cell was used for further syngas fermentation.

3.9 Experimental Setup and Process of Syngas Fermentation

The experiment for syngas fermentation was performed by a tar free bioreactor (TFB) in the fed-batch system (Figure 3.5). The first step of the bioethanol production process takes place, where biomass-based syngas was produced from the co-gasification of lignocellulosic biomass and charcoal. In this syngas fermentation study, forest residue (70%) and charcoal (30%) producing syngas were used (Patel et al., 2017). The main composition of syngas were hydrogen (13.05, % Mole), carbon monoxide (22.92, % Mole), carbon dioxide (7.90, % Mole), methane (1.13, % Mole), nitrogen (45.58, % Mole) and other gases (9.42, % Mole). In this study, fermentation broth was prepared individually for yeast and bacteria based on syngas fermentation. However, by-product charcoal was also used as a nutrient of microorganisms for both experiments. Stored syngas (500 mL) was used as a carbon nutrient for the microorganisms which was collected from co-gasification of biomass (forest residue) and charcoal. A peristaltic

pump (Brand: OEM, power supply: AC220V 50/60HZ) was used to flow (1mL - 250mL/min) the syngas to the TFB and mixed with fermentation broth properly every 24h interval during the syngas fermentation process.

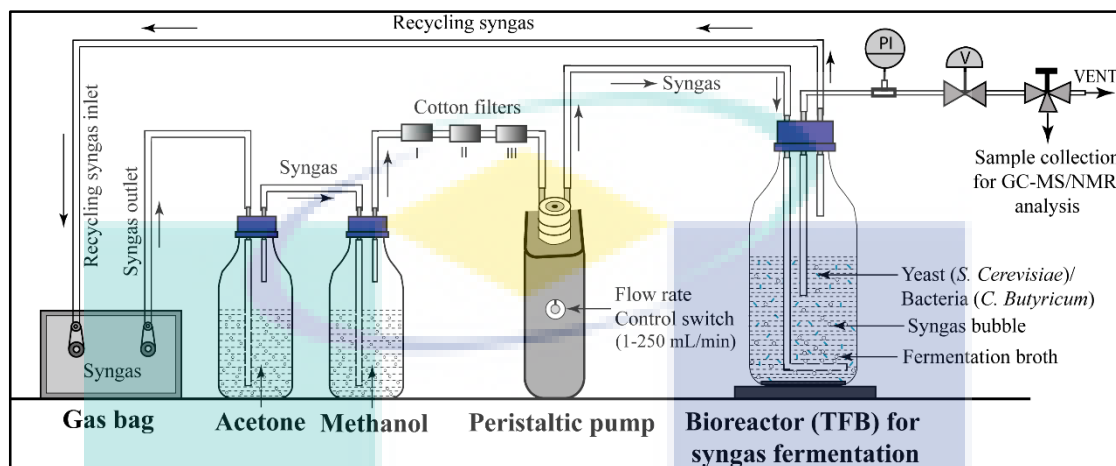


Figure 3.5 Experimental setup for bioethanol production through syngas fermentation using yeast and bacteria.

From the characterization results (XRF analysis), it was found that by-product charcoal contained some mineral solution and some trace elements. Therefore, by-product charcoal was also used for syngas fermentation. After mixing these, the medium was autoclaved at 121 °C for 20 min. Prior to run the experiment, syngas was passed through acetone and methanol for the filtration of tar compounds. The cotton filter was also used for the separation of fine particles. The effect of temperature, pH, colony forming unit (CFU), total organic carbon (TOC) and syngas impurity was investigated by observing microbial cell growth during syngas fermentation.

3.9.1 Syngas Fermentation Medium for *Saccharomyces Cerevisiae*

The fermentation medium (broth) was prepared for performing syngas fermentation using *S. cerevisiae*. A 500 mL impinger bottle was taken which was filled with 80% of fermentation broth and the remaining 20% was considered as working volume. The medium was prepared and included: (1) yeast extract (0.2 gm) (2) peptone (0.8 gm), (3) KH_2PO_4 (0.4 gm), (4) $\text{MnSO}_4 \cdot 7\text{H}_2\text{O}$ (0.2gm), (5) $(\text{NH}_4)_2\text{SO}_4$ (0.8 gm), (6) by-product charcoal (0.7 gm) and (6) DI water (400 mL). In this study, by-product charcoal was reused as a nutrient of *S. cerevisiae*. Then, pure syngas was passed through the TFB and *S. cerevisiae* was inoculated and connected with the biomass-based syngas bag. The pH was controlled within the ranges of 4.0-6.0. After that, the experiment was

run inside the shaking incubator. The temperature and rotational speed were controlled 37 °C and 200 rpm. The experiment was run for 16 days for the production of bioethanol.

3.9.2 Syngas Fermentation Medium for *Clostridium Butyricum*

The fermentation medium was prepared for *C. butyricum* based syngas fermentation. A 500 mL impinger bottle was taken which was filled with 80% of fermentation broth and the remaining 20% was considered as working volume. The fermentation medium was prepared by mixing with nutrient broth (10gm in 400 mL of DI water) and by-product charcoal. This by-product charcoal was reused as a nutrient of *C. butyricum*. Then, pure syngas was passed through the TFB and *C. butyricum* was inoculated and connected with the syngas bag. The pH was controlled within the ranges of 6.5-7.5. Subsequently, the experiment was run inside the shaking incubator. The temperature and rotational speed were maintained at 37 °C and 200 rpm, respectively. Similarly, this experiment was also run for 16 days for the production of bioethanol.

3.9.3 Syngas Fermentation Process for Bioethanol Production

Figure 3.6 represents the syngas fermentation process where *S. cerevisiae* and *C. butyricum* were used as the biocatalysts, and biomass-based syngas was used as the carbon source for microorganisms. Thereafter, syngas was passed through the fermentation broth medium through TFB. The shaking incubator was used to homogenize the mixture of syngas with *S. cerevisiae* or *C. butyricum*. The process for the production of bioethanol is shown as in the schematic diagram of Figure 3.6. The operating parameters for syngas fermentation were considered and the effect of temperature, feeding system of syngas, syngas impurity (treated and untreated syngas) effects on cell growth, the effect of total organic carbon and growth condition of *S. cerevisiae* and *C. butyricum* were investigated during the fermentation process. The syngas was recycled throughout the process to get the maximum production efficiency.

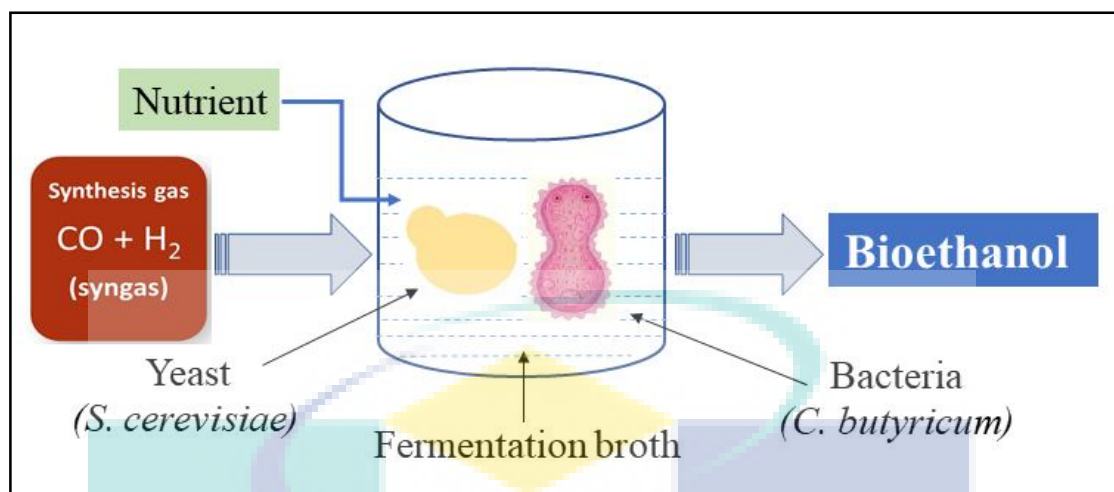


Figure 3.6 Process for the conversion of bioethanol from syngas.

3.9.4 Product Extraction and Analysis

The yield of bioethanol produced from the syngas fermentation was extracted from fermentation broth at the end of the process. In this study, the organic compounds were separated from the fermentation broth for further bioethanol detection using GC-MS and NMR analysis.

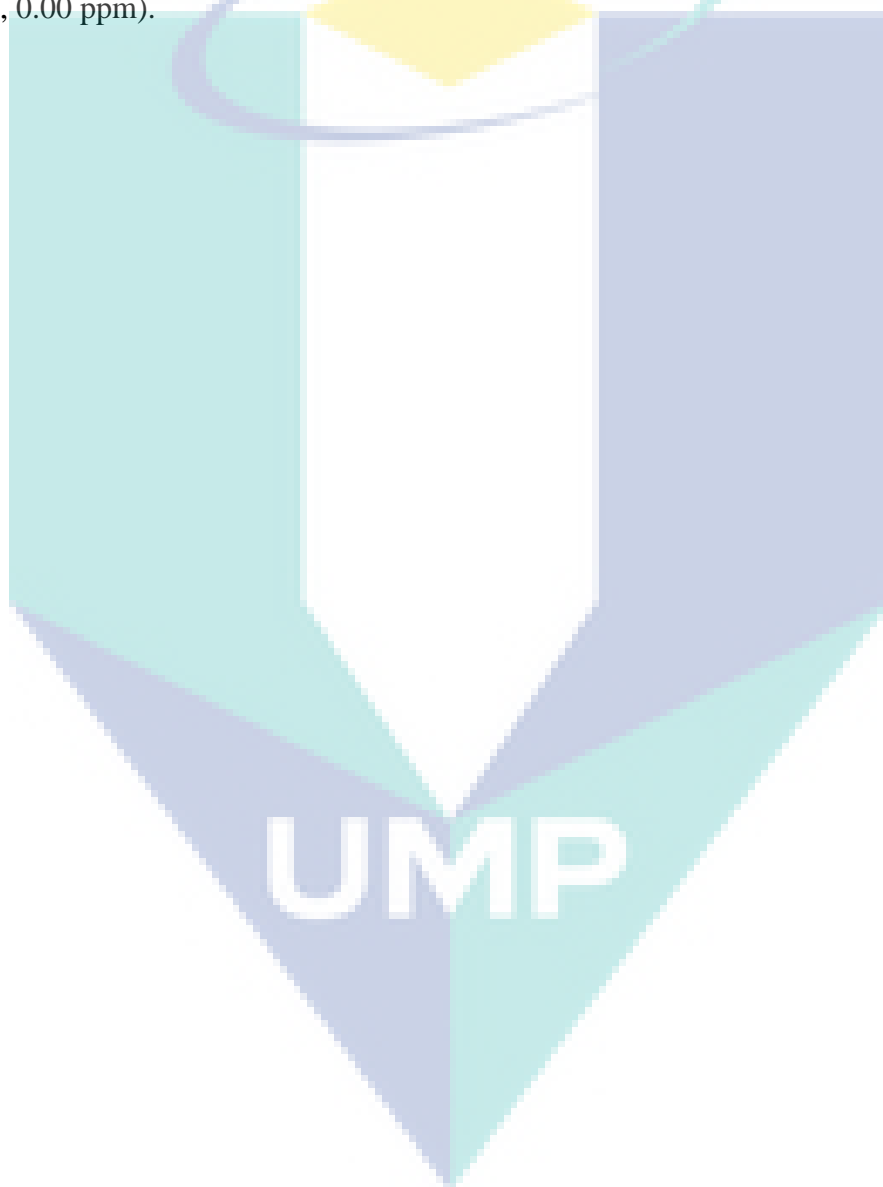
3.9.4.1 Liquid-liquid Extraction (LLE) using Solvent

The organic compounds were separated from the fermentation broth using liquid-liquid extraction. There were two solvents such as n-hexane (chromatogram pure grade, Sigma Chemicals, USA) and deuteriochloroform, CDCl_3 (Sigma-Aldrich) were used to extract bioethanol in an aqueous solution; a 5 ml of n-hexane or CDCl_3 were mixed with a 40 ml sample (fermentation broth), and then vortexed vigorously using a vortex mixer (Vortex-Genie 2, Scientific Industries Inc., USA) for 10 min. After phase separation, the solvent phase was transferred to a new tube for further analysis.

3.9.4.2 Bioethanol Detection and Analysis

In this product analysis, a 1 μL of extracted samples were used for both GC-MS and NMR (^1H) analysis. The bioethanol concentration was analyzed by GC-MS analyzer (Brand: Agilent, Model: 7890A). The initial and final temperatures were set as 70 $^\circ\text{C}$ and 325 $^\circ\text{C}$, respectively. The oven temperature was set as 325 $^\circ\text{C}$ and oven program was set as 100 $^\circ\text{C}$ for 2 min, then 5 $^\circ\text{C}/\text{min}$ to 120 $^\circ\text{C}$ for 0 min and 5 min (post run). The total run time was 6 min. and MS was operated in the scan mode mass ranges from 40 amu to

1000 amu. For the quantitative analysis, standard ethanol (99.99%) was also prepared to 1%, 2% and 3% (10 μ L, 20 μ L and 30 μ L in 1 mL n-hexane solution). Correspondingly, the MS fraction of extracted samples was matched with the standard ethanol (99.99%) and the ultimate bioethanol concentration was calculated. Moreover, for the final confirmation of bioethanol, NMR (^1H) analysis was also performed. In this analysis, ^1H NMR (500 MHz) spectra were recorded using BRUKER-500 spectrometer (Model: Bruker Ultra Shield Plus 500 MHz) and chemical shifts were stated relative to CDCl_3 (TMS, 0.00 ppm).



CHAPTER 4

RESULTS AND DISCUSSION

4.1 Feedstocks Characterization

The feedstock's (empty fruit bunch of palm oil, forest residue, coconut shell and charcoal) characterization results and its interpretation are presented in this chapter step by step. The analytical results of the feedstocks (lignocellulosic biomass and charcoal) were potential for syngas production through co-gasification. Subsequently, the yield of syngas and by-product of charcoal were suitable for syngas fermentation.

4.1.1 Proximate Analysis

In this study, proximate analytical results of lignocellulosic biomass (empty fruit bunch of palm oil, forest residue and coconut shell) and charcoal are shown in Table 4.1. In this table, it is shown that moisture content (MC) of all biomass samples are less than 10% (dry basis), which were potential for syngas production through a downdraft reactor reported by Yang and Chen (2015). The MC of charcoal showed higher value (6%) compared to the literature value (1.1%) that might be a reason for the higher humidity of the analytical day. Indeed, the drying process was needed for feedstocks to achieve maximum performance of co-gasification. The volatile matter (VM) of all feedstock samples was higher (57%-79.4%) than charcoal (26%-44%), observed in both experimental and literature value. In this study, CS contained the highest volatile matter of 61.5%, whereas EFB and FR had minor variations with CS. The higher VM containing biomasses were more efficient (easily ignited) than charcoal and favorable for syngas gas production (Loh, 2017; Singh et al., 2017). Hence, in this study, biomass ratios were higher (up to 60%) than charcoal (up to 40%) during the co-gasification process. On the contrary, biomasses contained less fixed carbon (FC) (<30%) than charcoal (~40%).

Higher FC of charcoal was the best mixture with biomass during co-gasification because of charcoal's longer combustion time that supported biomasses to release more bioenergy. On the other hand, ash content (AC) is an important parameter which has an adverse effect on fuel quality. Ash content in the EFB was seen to be maximum (11%) and minimum in CS (7%). In addition, higher AC stipulates reactor maintenance that increases the operational cost. The presence of more ash may cause blockage to the grate hole inside the reactor by clinker formation, and required higher maintenance cost. Although it acted as an absorbent of tar reported by Loh (2017).

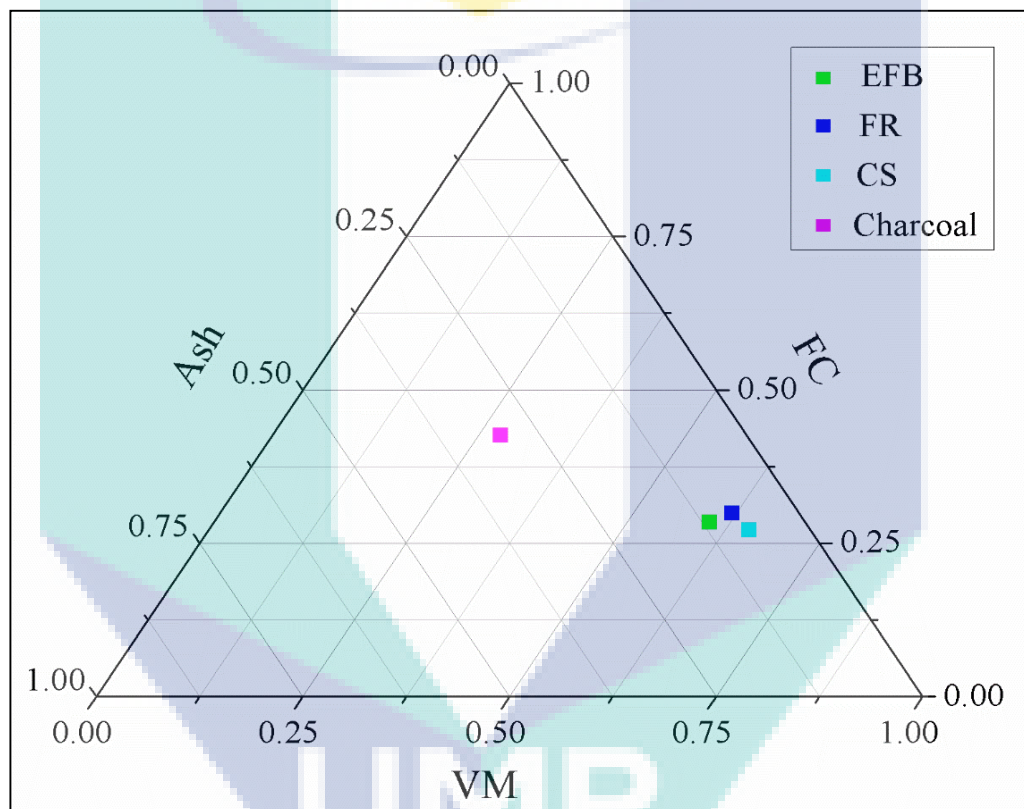


Figure 4.1 Ternary diagram based on VM, FC and Ash for EFB, FR, CS and Charcoal.

A ternary diagram was plotted (Figure 4.1) based on proximate analytical results (FC, VM and Ash) and revealed the phase behavior of these three components. The VM/FC ratio for EFB, FR, CS and charcoal are 2.11, 2.15, 2.41 and 0.65, respectively. The higher VM/FC ratio of the feedstock samples attributed for bioenergy production reported by Titirici, Antonietti, and Thomas (2006). On contrary, charcoal contained relatively low VM/FC ratio of 0.65 than biomasses (2.11-2.41). Hence, VM/FC ratios of lignocellulosic biomass were more suited than charcoal for the co-gasification process.

Accordingly, the charcoal became highly resistant to further decomposed during co-gasification with biomass.

Table 4.1 Proximate and ultimate analytical results of EFB, FR, CS and Charcoal compared to literature.

Properties		EFB		FR		CS		Charcoal	
		Exp.	Yoo et al. (2018)	Exp.	Ibarra-Gonzalez and Rong (2018)	Exp.	Prapakarn, Arjharn, Liplap, Prapakarn, and Hinsui (2017)	Exp.	Zhang Zhanrong et al. (2015)
Proximate analysis (wt.%) ^a	MC	5	9.63	6	19.0	6	5.84	6	1.1
	VM	57	64.95	59	79.4	61.5	76.69	26	44
	FC	27	19.48	27.5	19.5	25.5	15.24	40	21.1
	Ash	11	5.94	7.5	1.1	7	2.23	28	33.8
Ultimate analysis (wt.%) ^a	C	42.33	41.81	42.75	50.30	43.90	46.20	55.43	38.89
	H	5.28	5.73	4.67	5.70	4.63	5.42	1.05	4.00
	O ^b	50.84	37.36	47.76	41.7	50.14	45.23	42.42	23.14
	N	1.46	0.84	4.81	1.0	1.29	0.87	1.03	-
	S	0.08	-	0.01	0.2	0.04	0.05	0.06	0.17

^a Dry basis

^b By difference

Figure 4.2 represented the thermal degradation profile of all feedstocks and is investigated within the temperature ranges from 25 to 1000 °C. Three stages of biomass degradation in TGA curve were observed such as (i) insignificant mass reduction for evaporation of MC and light VM at ambient temperature (120 °C); (ii) significant mass loss at the temperature ranges from 120 °C to 400 °C, where organic compounds (cellulose and hemicellulose) were devolatilized; (iii) very slow mass loss above 400 °C caused by the degradation of lignin compounds (or other chemical compounds which have strong chemical bonds). Therefore, the nature of biomass degradation through thermogravimetric analysis agreed with the literature value (Chala, Lim, Sulaiman, & Liew, 2018). On the other hand, charcoal was degraded gradually within the temperature ranges of 80 °C-350 °C and 350 °C-950 °C. In spite of the fact that the sudden degradation of the same sample was observed in the temperature ranges from 800 °C to 960 °C.

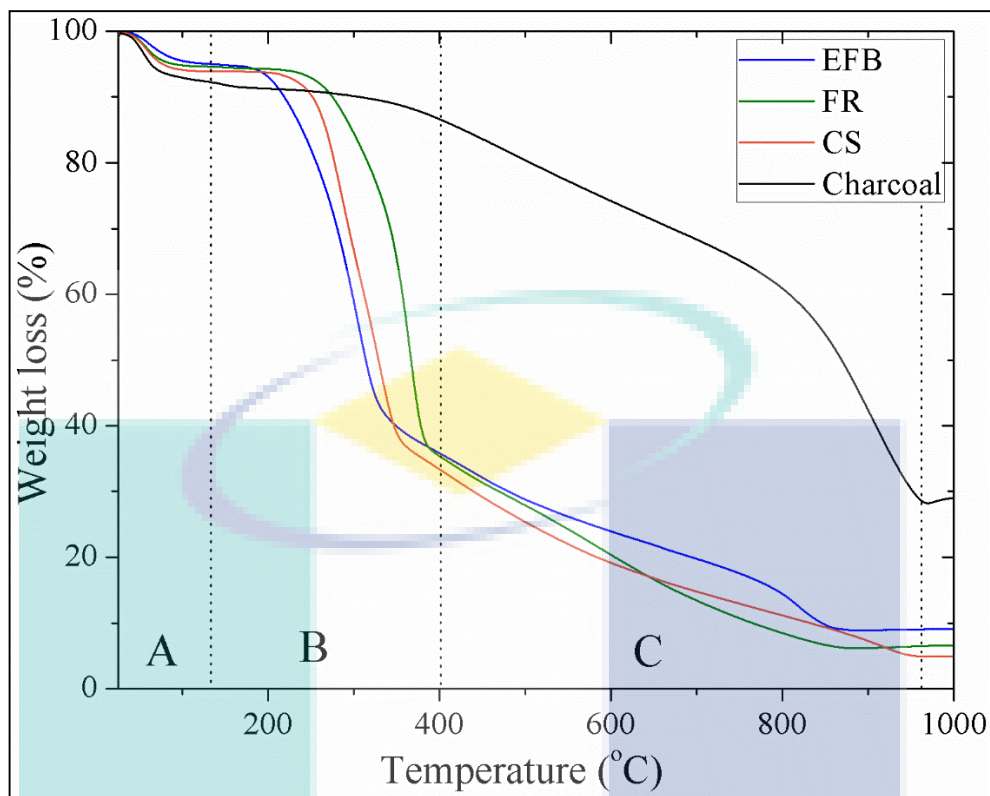


Figure 4.2 TGA Curves for EFB, FR, CS and Charcoal ('A' zone=Moisture content removal, 'B' zone=Cellulose and Hemicellulose decomposition and 'C' zone=Lignin decomposition).

From mass loss curves (Figure 4.2), it is shown that all biomass exhibit three main weight loss zones (A-zone, B-zone and C-zone), which correspond to dehydration, devolatilization and solid decomposition. Similar characteristics were also reported in the literature (Chala et al., 2018; Gogoi et al., 2018). It is also observed that cellulose and hemicellulose of all the biomass samples were decomposed within the temperature ranges from 120 °C to 400 °C effortlessly, with the weight loss of 0.07 (wt.%/°C) for CS at 220 °C, 0.05 (wt.%/°C) at 230 °C, 0.06 (wt.%/°C) at 250 °C for EFB and FR, respectively. When the temperature was higher than 400 °C, almost all cellulose and hemicellulose was pyrolyzed with minimum solid residue (~11 wt.%/°C). The lignin decomposition started for same biomass (EFB, FR and CS) were 0.42 (wt.%/°C) at 350 °C, 0.37 (wt.%/°C) at 400 °C and 0.37 (wt.%/°C) at 360 °C, respectively. The maximum temperature for lignin decomposition was 900 °C, where the weight loss of biomasses were 0.90 (wt.%/°C), 0.75 (wt.%/°C) and 0.93 (wt.%/°C) for EFB, FR and CS, respectively. However, most of the components of charcoal were decomposed at temperature of 960 °C of 0.92 (wt.%/°C). In this analysis, it is shown that lignin was the most complex part for biomass to be decomposed, and its decomposition occurred very slowly under the whole

temperature profile from ambient to 960 °C. Therefore, above the TGA curves, it was observed that three biomasses have a similar trend on cellulose, hemicellulose and lignin, but the burning behavior of these biomasses was quite different from charcoal.

From thermogravimetric (TG) analysis, it is concluded that lignocellulosic biomass and charcoal were potential for bioenergy (syngas) production through co-gasification. From this analysis, it was also confirmed that the required minimum temperature for biomass gasification using downdraft reactor was needed to 900 °C, and required temperature for co-gasification by adding charcoal was 960 °C for maximum energy efficiency.

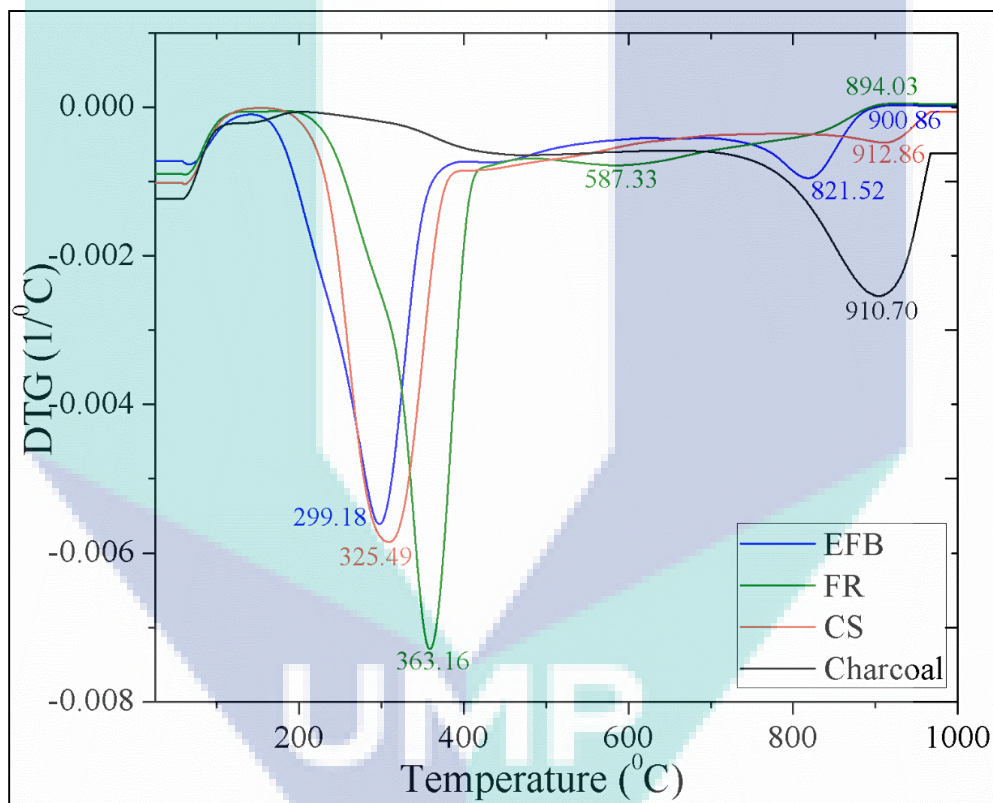


Figure 4.3 DTG curves for EFB, FR, CS and Charcoal at a heating rate of 10 °/min.

With increasing temperature, biomass (EFB, FR and CS,) and charcoal took place with an associated heat release (10°/min) shown in DTG curves (Figure 4.3). The heat flow occurred within the temperature of 25 °C to 1000 °C. Consequently, sharp peaks are shown in biomass curves at the temperature ranges from 200 °C to 400 °C and on charcoal, it was at 910.70 °C.

The peak profiles on DTG curves for EFB, FR and CS are comparatively similar trends, whereas charcoal it exhibits a different pattern. Major peaks were observed on

EFB, FR and CS samples at the temperature of 299.16 °C, 363.16 °C and 325.49 °C respectively, whereas peaks for charcoal was visible at the temperature of 910.70 °C. Another significant peak was also detected on EFB and CS biomass sample at the temperature of 821.52 °C and 912.86 °C, respectively, whereas FR showed a very minor peak at the temperature of 587.33 °C. On the contrary, charcoal exhibits a single peak on its whole DTG profile. A similar analysis was performed in the literature reported by Gogoi et al. (2018). The DTG analysis concluded major components were combusted due to the effect of heat on CS and EFB, whereas FR required higher heat. As a result, the main components burnt within the temperature ranges from 200 °C to 400 °C. The remaining components of three biomasses and charcoal were combusted within the temperature ranges from 750 °C to 960 °C. Therefore, the minimum required temperature for the complete combustion of all feedstocks suggested for co-gasification was at 960 °C.

4.1.2 Ultimate Analysis

The most remarkable results were obtained from the ultimate analysis (Table 4.1). In this analysis, it confirmed the existence of carbon (C) which is the main elemental contributor for bioenergy production. In biomass, it was less than 50%, and for the charcoal, it was more than 50%, in exception FR contained 50.03% literary. During the gasification process, this C was converted into CO and CO₂ reacting with oxygen where CO is the main component for syngas production (Cai et al., 2017). Moreover, EFB contained more hydrogen (H₂) percentage (5.28%) than FR (4.67%) and CS (4.63%) and similar trends were observed in the literature. In contrast to charcoal, it was only 1.05%. Therefore, biomass is the main source of hydrogen (H) that is converted into H₂ and H₂O. This H₂ is another main component for syngas production that was produced during co-gasification of biomass and charcoal at the temperature of around 900 °C, that is also reported by Al-Rahbi and Williams (2017). Other elements (N and S) of biomass are undesirable emissions in the form of NO_x and SO_x. The lower content of these elements in both experimental and literature suggested that this selected biomass were potential to be used for co-gasification with charcoal that is environmentally friendly (Loh, 2017).

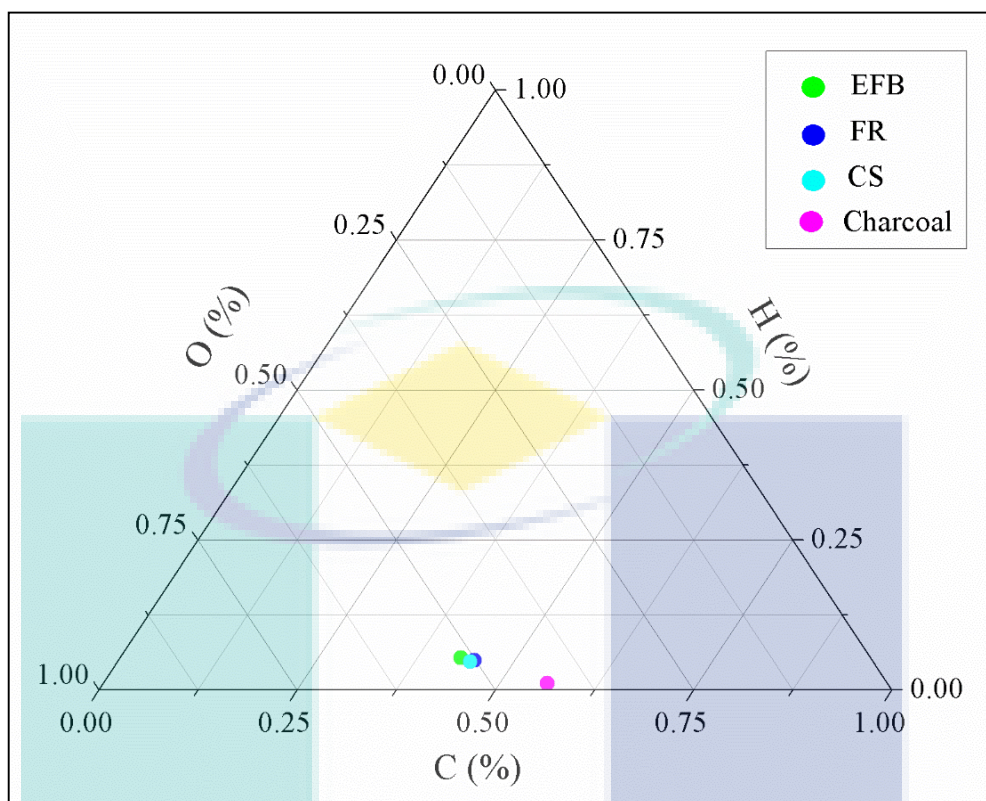


Figure 4.4 Ternary diagram of C, H and O for EFB, FR, CS and Charcoal.

The ternary diagram was created based on the ultimate analytical results of C, H and O as visualized in Figure 4.4. This diagram revealed these three elemental phase ratios for EFB, FR, CS and charcoal. The percentage of C, H and O of EFB, FR CS were almost similar and was plotted near the C boundary line. On the contrary, the charcoal touched the C boundary line because of its very low H content (Table 4.1). Therefore, biomasses generated more gaseous component than charcoal. However, charcoal supported the biomass for longer combustion time due to its higher C content compared to biomass. The fuel properties of biomass and charcoal were found to be a better interpretation by Van Krevelen diagram, where the hydrogen/carbon (H/C) molar ratio was plotted against the oxygen/carbon (O/C) molar ratio (Figure 4.5). Kang, Azargohar, Dalai, and Wang (2016) reported that biomass has a higher ratio of O/C and H/C compared to fossil fuel.

The H/C ratio for EFB, FR, CS and charcoal were 0.12, 0.11, 0.11 and 0.02, respectively and O/C ratio were 1.20, 1.12, 1.14 and 0.77, respectively (Figure 4.5). Therefore, in this study, the atomic ratios of O/C were more than H/C as shown in feedstock samples and these trends were consistent with the literature (Du, Chen, & Lucas, 2014). Moreover, EFB shows higher H/C and O/C ratio than other biomass (FR

and CS) and charcoal. Titirici et al. (2006) mentioned that this ratio is carbonized significantly by lowering the H/C and O/C ratio through the splitting of water during gasification. The advantages of raw feedstock samples include intensifying of bioenergy by reducing H/C and O/C ratios which were clearly visualized by this Van Krevelen diagram (Figure 4.5).

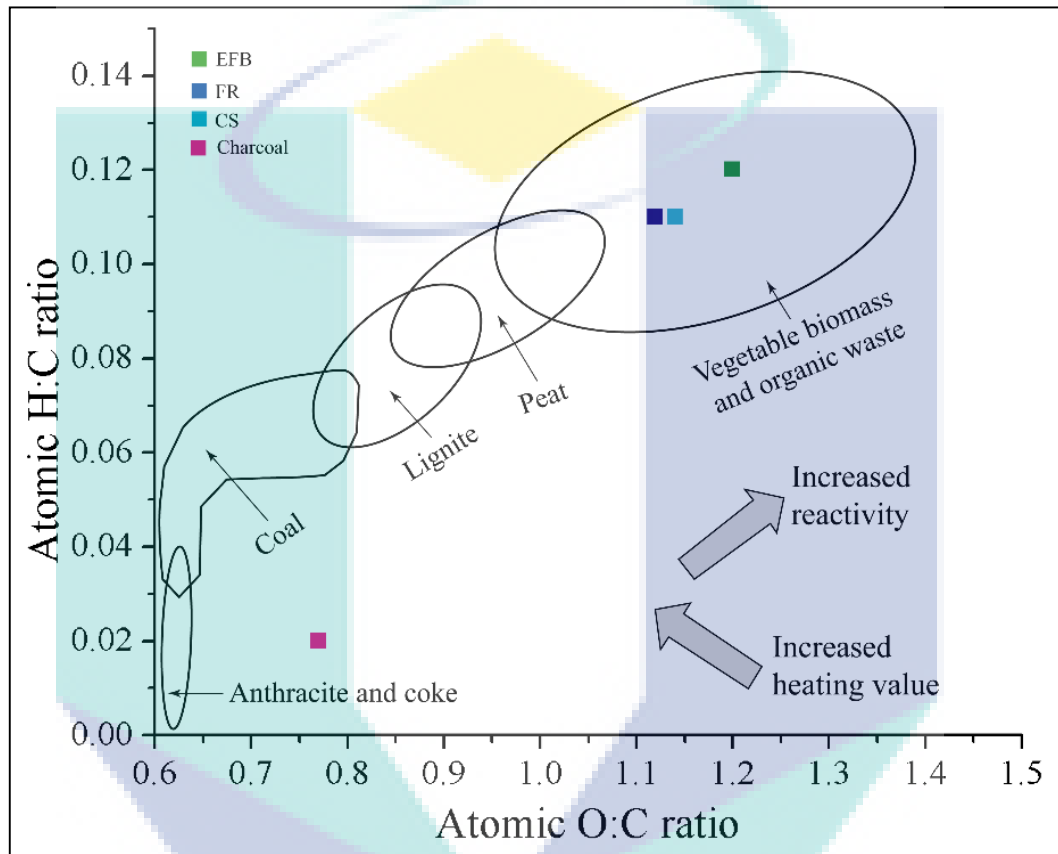


Figure 4.5 Van Krevelen diagram at the atomic ratio of H/C and O/C for EFB, FR, CS and Charcoal.

The heating value (HHV and LHV) of biomasses (EFB, FR, CS) and charcoal were calculated using Eq. 3.1 and Eq. 3.2 based on the proximate and ultimate analytical results (Table 4.1). Figure 4.6 represents the comparative HHV graph for all feedstocks (EFB, FR, CS and charcoal) with the literature (Ibarra-Gonzalez & Rong, 2018; Prapakarn et al., 2017; Yoo et al., 2018; Zhang Zhanrong et al., 2015). The HHV of biomasses (EFB, FR and CS) and charcoal were 15.62 (MJ/kg), 15.29 (MJ/kg), 15.45 (MJ/kg) and 16.07 (MJ/kg), respectively (Figure 4.6) and LHV were 14.43 (MJ/kg), 14.20 (MJ/kg), 14.37 (MJ/kg) and 15.72 (MJ/kg), respectively (Figure 4.7).

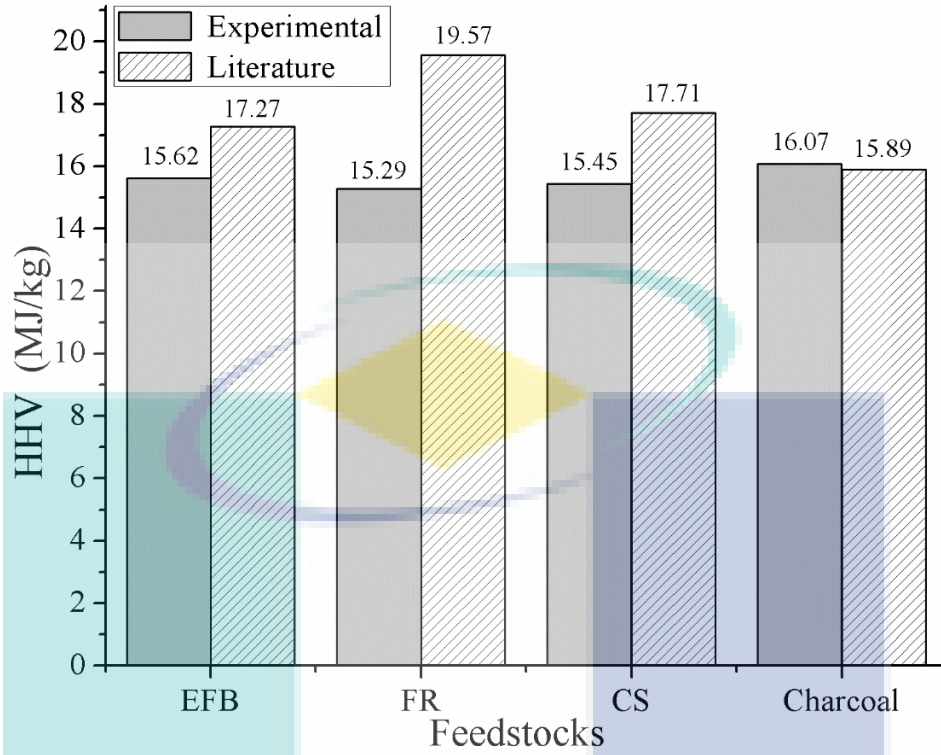


Figure 4.6 Higher heating value (MJ/kg) of feedstocks (EFB, FR, CS and Charcoal) compared with literature value.

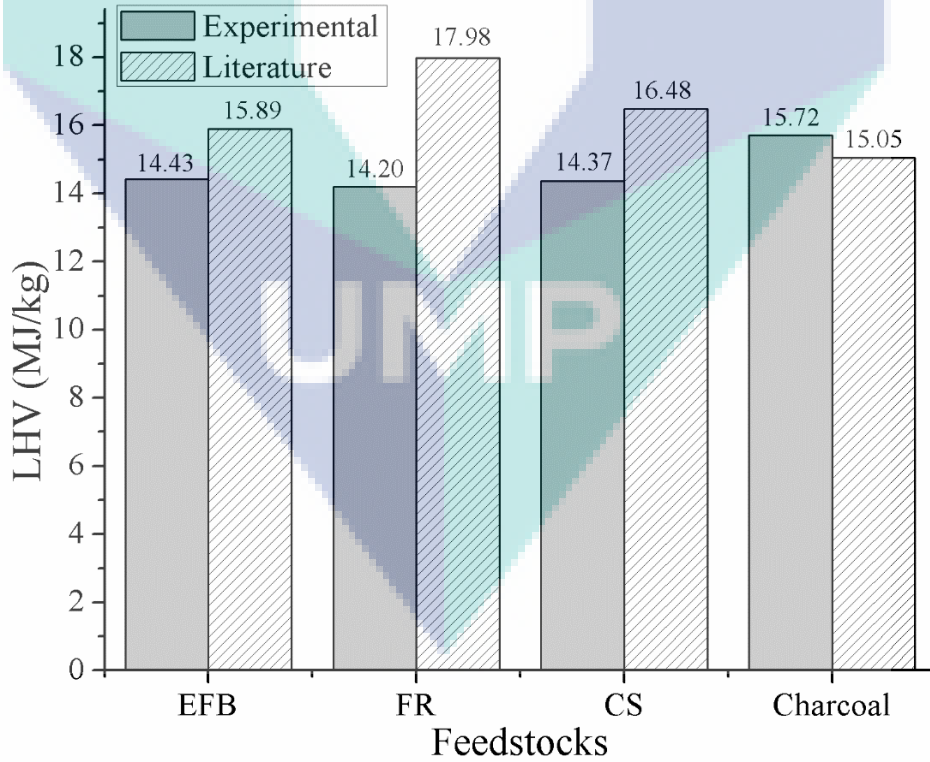


Figure 4.7 Lower heating value (MJ/kg) of feedstocks (EFB, FR, CS and Charcoal) compared with literature value.

In this analysis, it is clearly showed that EFB contained marginally higher HHV (MJ/kg) than FR and CS. In contrary, charcoal has maximum HHV (16.07 MJ/kg) than three biomasses. Similarly, EFB contained higher LHV (14.43 MJ/kg) than the other two biomasses (FR and CS), whereas charcoal contained highest LHV (15.72 MJ/kg). From the above two graphs (Figure 4.6 and Figure 4.7), it is observed that there was a minor difference between experimental and literature value. It might be a reason for different sources of samples and analytical variation. However, EFB contained higher HHV (15.62 MJ/kg) than FR and CS. On contrary, charcoal has maximum HHV (16.07 MJ/kg) than three biomass. From this calculation, it was decided that charcoal was also valorized by-product. Moreover, higher HHV and LHV of charcoal indicated that this by-product was valuable co-feedstocks that produced more energy when it was used with the biomass through the co-gasification process. Therefore, based on HHV and LHV analysis it is concluded that EFB, FR, CS and by-product charcoal were potential feedstocks that suited for co-gasification for the production of syngas.

4.1.3 X-ray Diffraction Analysis

The XRD patterns of feedstock samples (EFB of palm oil, forest residue, coconut shell and charcoal) are shown in Figure 4.8. The X-ray diffractogram showed the appearance of three sharp diffraction peaks of EFB sample at 2θ value of 44.03° , 64.36° and 77.48° representing (110), (200) and (211) planes, respectively (Figure 4.8). The interlayer distances of these crystal planes were 2.06 (Å), 1.45 (Å) and 1.23 (Å) with the corresponding peaks area of 27.26 (a.u.), 25.55 (a.u.) and 35.36 (a.u.), respectively. The broad diffractogram spectra peaks were detected in the forest residue (FR) at the 2θ value of 44.02° (110), 64.32° (200) and 77.43° (211) (Figure 4.8). The d-spacing of these crystal planes were 2.06 (Å), 1.45 (Å) and 1.23 (Å) with the correspond area of 36.25 (a.u.), 36.92 (a.u.) and 29.97 (a.u.), respectively. In the coconut shell, the significant peak positions exhibit at the 2θ value of 44.00° , 64.35° and 77.52° those denoting the correspond planes of (110), (200) and (211), respectively (Figure 4.8). The peaks area were 17.62 (a.u.), 25.76 (a.u.) and 25.45 (a.u.), respectively with matching interlayer crystal spaces were 2.06 (Å), 1.45 (Å) and 1.23 (Å) which were similar to other two biomass samples. On the other hand, X-ray diffractogram represents the peaks in the charcoal at the 2θ position of 29.39° , 44.01° , 64.36° and 77.49° that were corresponding to the presence of nanoparticles (Figure 4.8). The corresponding peaks area were 16.52

(a.u.), 24.58 (a.u.), 25.69 (a.u.) and 34.03 (a.u.), respectively with the interlayer crystal spacing were 3.04 (Å), 2.06 (Å), 1.45 (Å) and 1.23 (Å), respectively. The average crystal diameter of EFB, FR, CS and charcoal were 112.93 (nm), 124.98 (nm), 78.63 (nm) and 96.58 (nm), respectively.

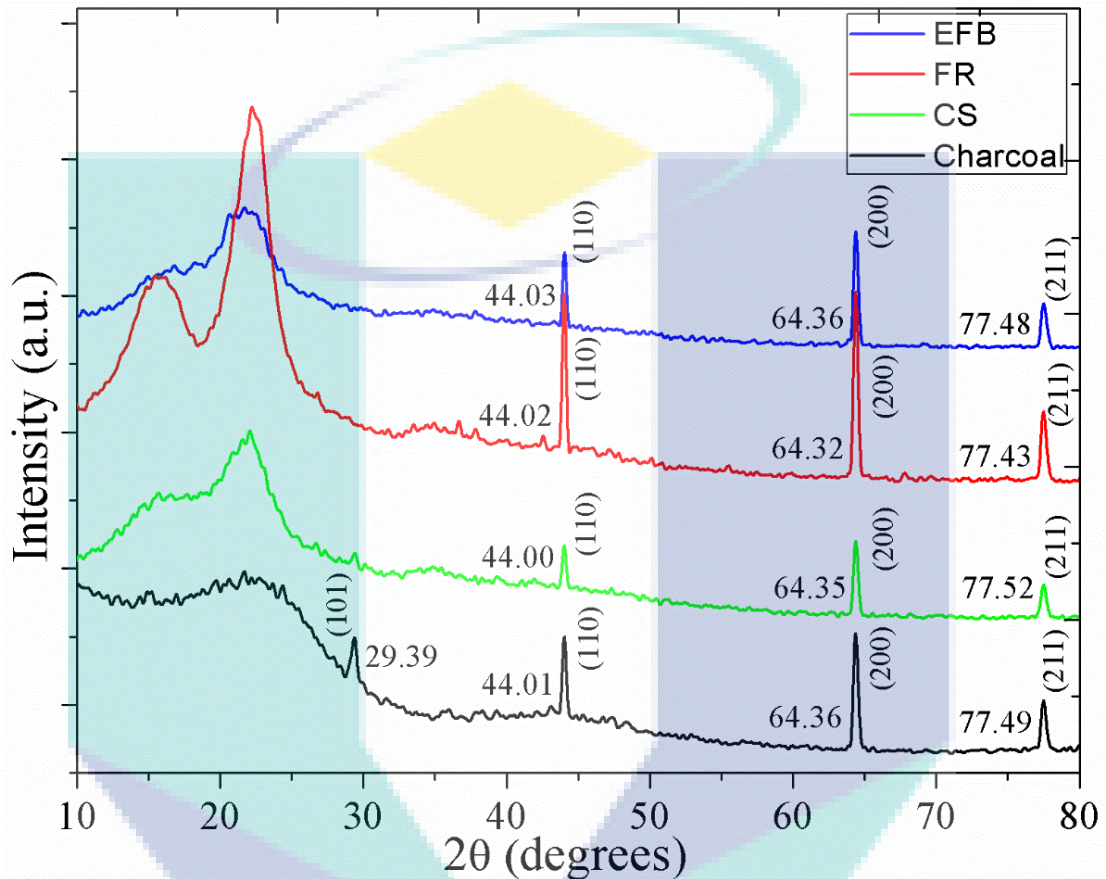


Figure 4.8 Comparison of X-ray diffraction spectra of feedstock samples (EFB, FR, CS and Charcoal).

The sharp high-intensity peaks indicated that the feedstock samples were in crystalline in nature. On the other hand, the wide range peaks in all biomass sample represented the amorphous in nature. The diffractogram of the cellulose showed the amorphous peaks which consistent with the results reported by Johar, Ahmad, and Dufresne (2012). The corresponding crystalline peaks of all feedstocks were observed within the 2θ value of 40° - 80° . A significant peak was observed in charcoal at 2θ value of 29.39° (Figure 4.8), whereas in this position there were no significant peak was observed in other samples. There were two additional amorphous peaks were detected in the forest residue sample with in the 2θ value of 10° - 25° . There were a limited number of sharp peaks were also detected by XRD in biomass samples than charcoal due to the

high amount of amorphous halo constituents on XRD patterns. The intensity of the amorphous halo peak increases with increasing temperature shown in the charcoal sample. Therefore, well-ordered charcoal crystalline structures appear to be more efficient with increasing gasification time when charcoal was blended with biomass during co-gasification. This characterization results are consistent with the literature value reported by Qin et al. (2017).

4.1.4 Scanning Electron Microscopy Analysis

The SEM images of lignocellulosic biomass and charcoal are shown in (Figure 4.9 and Figure 4.10). The pores and roughness of biomass samples were compared with charcoal (Figure 4.10b). In the SEM images (Figure 4.9 and Figure 4.10a), it is shown that the morphology of raw biomass changed during co-gasification. As a result, the rough surface was observed in by-product charcoal (Figure 4.10b). There were no significant pores detected in EFB (Figure 4.9a), forest residue (Figure 4.9b) and coconut shell (Figure 4.10a) SEM images. Moreover, the fiber like structure was observed in EFB and forest residue, whereas no clear fibres were identified on coconut shell images (Figure 4.10a). In contrary, small pores were investigated in the charcoal (Figure 4.10b), which was occurred as a result of thermal effects. As a result, there was the possibility of absorption of organic matter by these pores. Moreover, the addition of biomass causes an increase of inorganic and organic amorphous matter in the charcoal halo area when biomass and charcoal were co-gasified (Qin et al., 2017).

In Figure 4.10b, it was observed that charcoal surfaces contained vesicle and spherical pores. These pores were formed due to the release of volatile matters which melted as bursting bubbles and resulted as sphere-shaped pores on the surface. There were various types of pores were observed due to the variation of temperature acted on the charcoal surface during the co-gasification process. These morphological features are consistent with the literature reported by Yu et al. (2017).

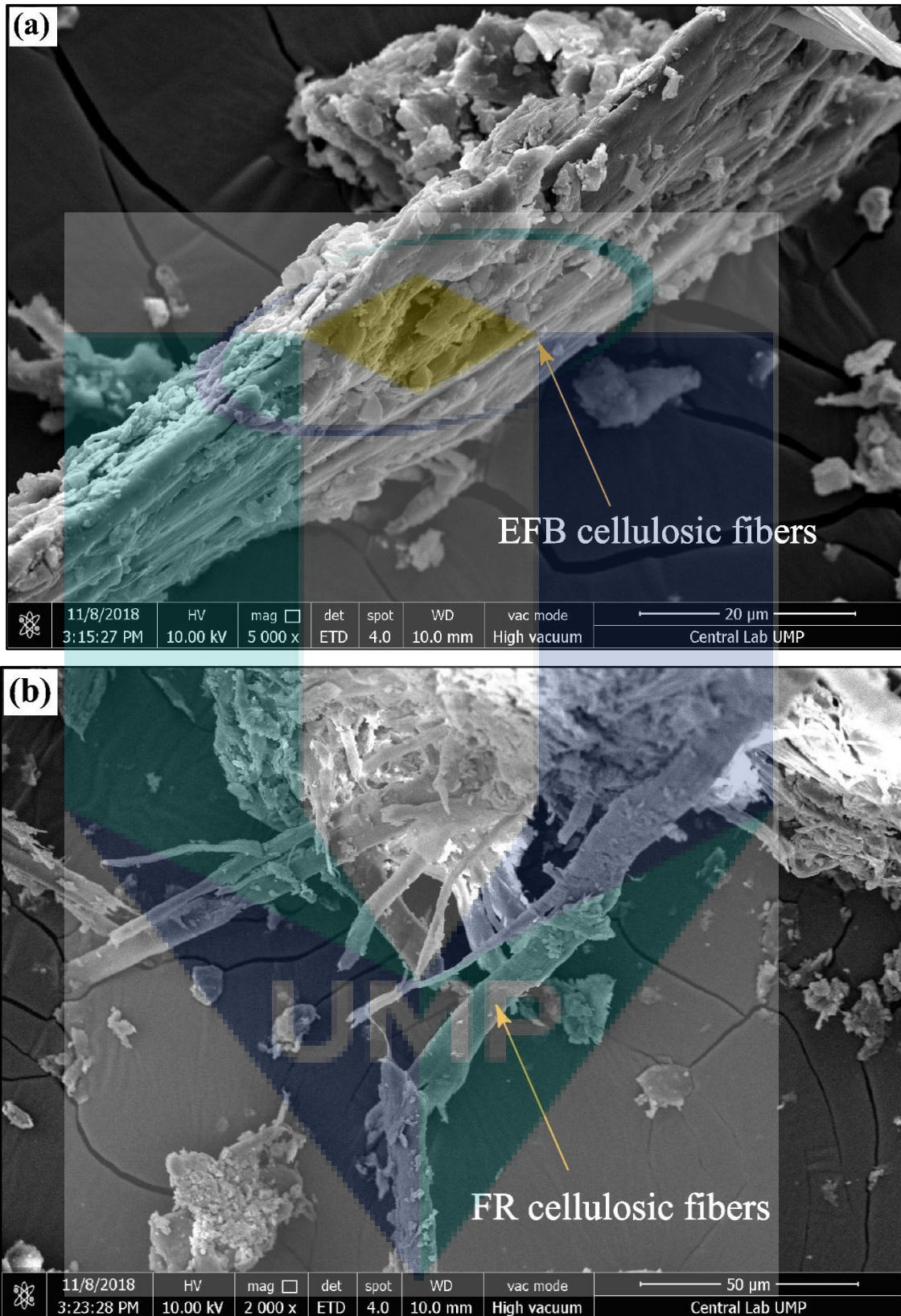


Figure 4.9 SEM images for feedstock samples: (a) EFB of palm oil (b) Forest residue.

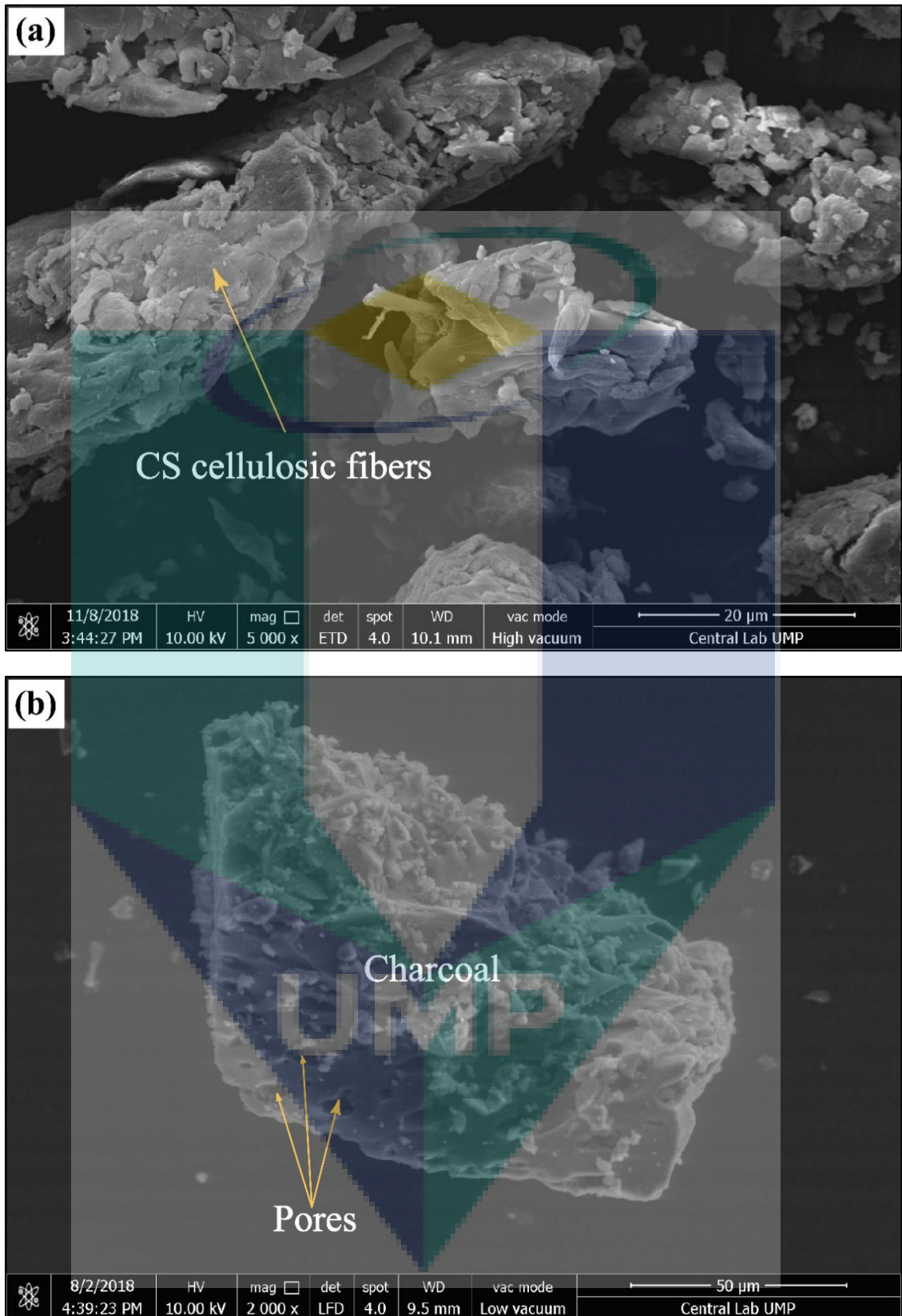


Figure 4.10 SEM images for feedstock samples: (a) Coconut shell and (b) Charcoal.

4.1.5 Field Emission Scanning Electron Microscopy and Energy-Dispersive X-ray Analysis

The FESEM analysis was performed for feedstocks characterization which supported the SEM results. In this analysis, Figure 4.11 represents the FESEM images with EDX for EFB of palm oil, forest residue, coconut shell and charcoal samples. These images represent the morphology and surface features more precisely. The EDX with the corresponding FESEM images denotes the elemental composition that was marked in Figure 4.11. From the morphological point of view, charcoal looked disordered features due to the thermal activities after the gasification which was highly porous (Kim et al., 2011). In contrary, biomasses of EFB, forest residue and coconut shell showed a smooth surface than charcoal (Figure 4.11d). The elemental weight percentage and atomic percentage are shown in Table 4.2.

Table 4.2 Elemental weight percentage and the atomic percentage of EFB, FR, CS and Charcoal.

Elements	FEFB of palm oil		Forest residue		Coconut shell		Charcoal	
	Weight (%)	Atomic (%)	Weight (%)	Atomic (%)	Weight (%)	Atomic (%)	Weight (%)	Atomic (%)
C	52.86	62.76	60.19	67.95	55.36	62.89	69.37	76.03
N	0.00	0.00	0.00	0.00	0.00	0.00	0.00	0.00
O	37.81	33.70	35.91	30.43	42.76	36.47	27.64	22.74
Na	-	-	-	-	-	-	0.21	0.12
Mg	0.48	0.28	-	-	-	-	0.00	0.00
Si	1.10	0.56	-	-	-	-	0.34	0.16
P	1.04	0.48	1.98	0.86	0.68	0.30	1.23	0.52
S	0.32	0.14	1.15	0.48	0.33	0.14	0.32	0.13
K	3.42	1.25	0.77	0.27	0.11	0.04	0.88	0.30
Ca	0.71	0.25	-	-	-	-	0.00	0.00
Fe	2.26	0.58	0.00	0.00	0.00	0.00	0.00	0.00
Cu	0.00	0.00	0.00	0.00	0.46	0.10	0.00	0.00
Zn	-	-	0.00	0.00	0.30	0.06	0.00	0.00
As	-	-	-	-	-	-	0.00	0.00

From the EDX analysis (Figure 4.11 and Table 4.2) of EFB of palm oil, forest residue, coconut shell and charcoal, it is shown that there were two major elements of carbon (C) and oxygen (O) was detected. The presence of C and O of the selected samples were agreed with the ultimate analytical results. In this analysis there were a trace amount

of S was also observed in the samples which indicated that these were environmentally friendly feedstocks. There were some trace of metals (Fe, Zn, Cu etc) were also found which were advantageous for microbial cell growth by using by-product charcoal as a nutrient during syngas fermentation (Asimakopoulos et al., 2018; Sikarwar et al., 2017).

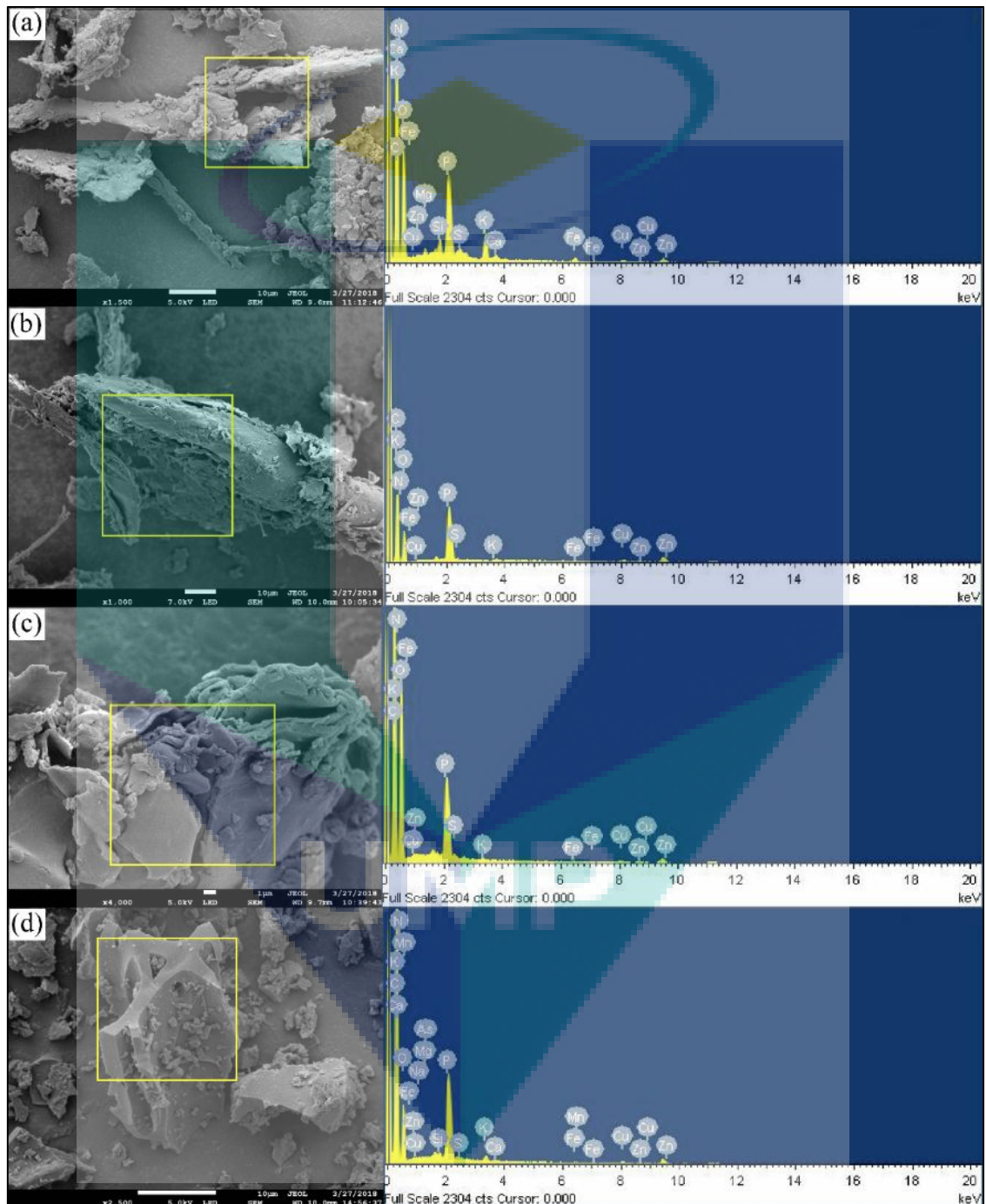


Figure 4.11 FESEM and EDX of feedstocks: (a) EFB of palm oil (b) Forest residue (c) Coconut shell (d) Charcoal.

4.1.6 Transmission Electron Microscopy Analysis

The TEM images for lignocellulosic biomass and charcoal samples are shown in Figure 4.12. The cellulosic structure and aggregated nanoparticles were observed in EFB of palm oil, forest residue, coconut sell and charcoal TEM images.

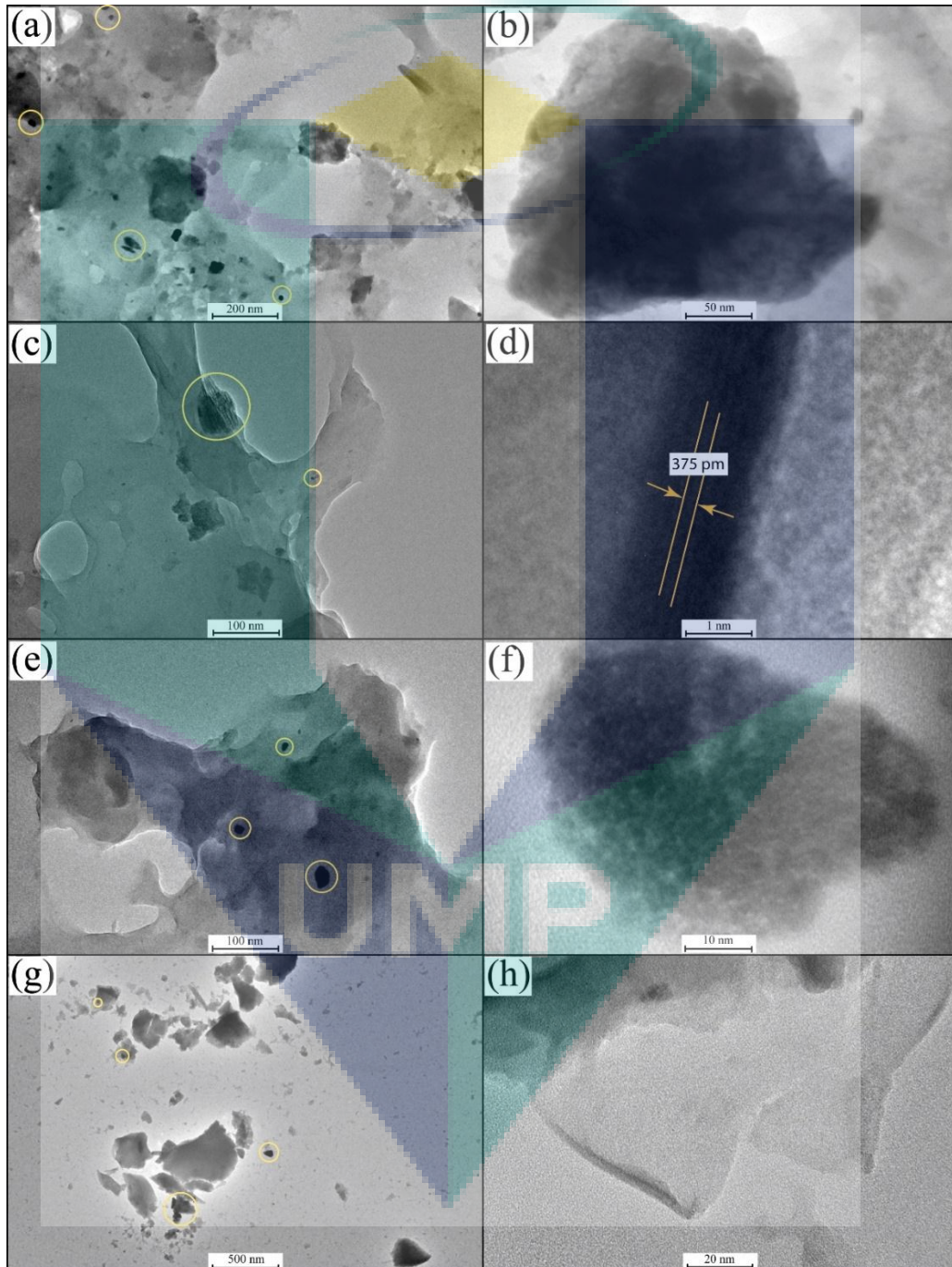


Figure 4.12 TEM analysis of feedstocks: (a-b) EFB of palm oil (c-d) Forest residue (e-f) Coconut shell (g-h) Charcoal.

The average spherical (avg. 18.80 nm) nanoparticles were detected that are aggregated within the porous cellulosic structure as shown in EFB TEM image (Figure 4.12a-b). The TEM images for forest residue confirmed the presence of nanoparticles (Figure 4.12c). The average dimension of the nanoparticles was 10-25 nm. The space between the two nanoparticles was 1.18 nm (Figure 4.12d). The average diameter of the nanoparticles in the coconut shell images was 10-25nm (avg.). These results agreed with the literature (Longhin et al., 2016) and XRD analysis. Therefore, distinct differences were observed in the shape and structures of charcoal might be due to the dominating materials presented in the charcoal. The dominant particles of charcoal were rounded spherical in shape with the diameter ranges from 68.74 nm to 125.54 nm. Therefore, the existence of cellulosic and nanoparticles was evidenced in this TEM analysis which is consistent with SEM and FESEM results.

4.1.7 Fourier Transform Infrared Analysis

The functional group of biomass and charcoal were investigated under certain pyrolysis condition using FTIR, and individual infrared spectra were shown in Figure 4.13. It is generally known that the distinctive components of biomass were cellulose, hemicellulose and lignin, consequently, their functional groups and spectral bands were also similarly reported by Meng, Zhou, Qin, Zhang, and Li (2013).

The most prominent peaks in the IR spectra for CS, EFB, FR and charcoal showed adsorption bands at 3437.11 cm^{-1} , 3461.85 cm^{-1} , 3437.09 cm^{-1} and 3435.04 cm^{-1} , respectively which were referred to as O-H stretching (Lin et al., 2016; Mohamad Ros et al., 2016). The CS, EFB and FR have the additional bands of 2918.58 cm^{-1} , 2924.48 cm^{-1} and 2922.33 respectively indicating C-H stretching, which is absent in charcoal. The insignificant band at 1734.28 cm^{-1} is attributed to the absorption of ester functional groups of hemicellulose (Singha & Guleria, 2015) is shown in only CS samples. The significant bands at 1638.46 cm^{-1} , 1637.43 cm^{-1} , 1638.04 cm^{-1} in three biomasses, and a relatively weak band at 1635.91 cm^{-1} in charcoal were due to the aromatic C=C vibrations in the lignin, which are evidenced that lignin exists in the biomass and charcoal (Sarkar & Rahman, 2017). In addition, bands at 1046.39 , 1045.03 , 1034.11 and 1077.03 cm^{-1} were also shown which indicated C-O stretching in the CS (most significant band), EFB (moderate band), FR (less significant band) and charcoal (very low significant band), respectively. In case of lignocellulosic biomass and charcoal, the intensity of hydroxyl

bands region decreased and additional bands (2918.58 to 2924.48 cm^{-1}) were observed in the three biomasses, whereas additional band was absent in charcoal.

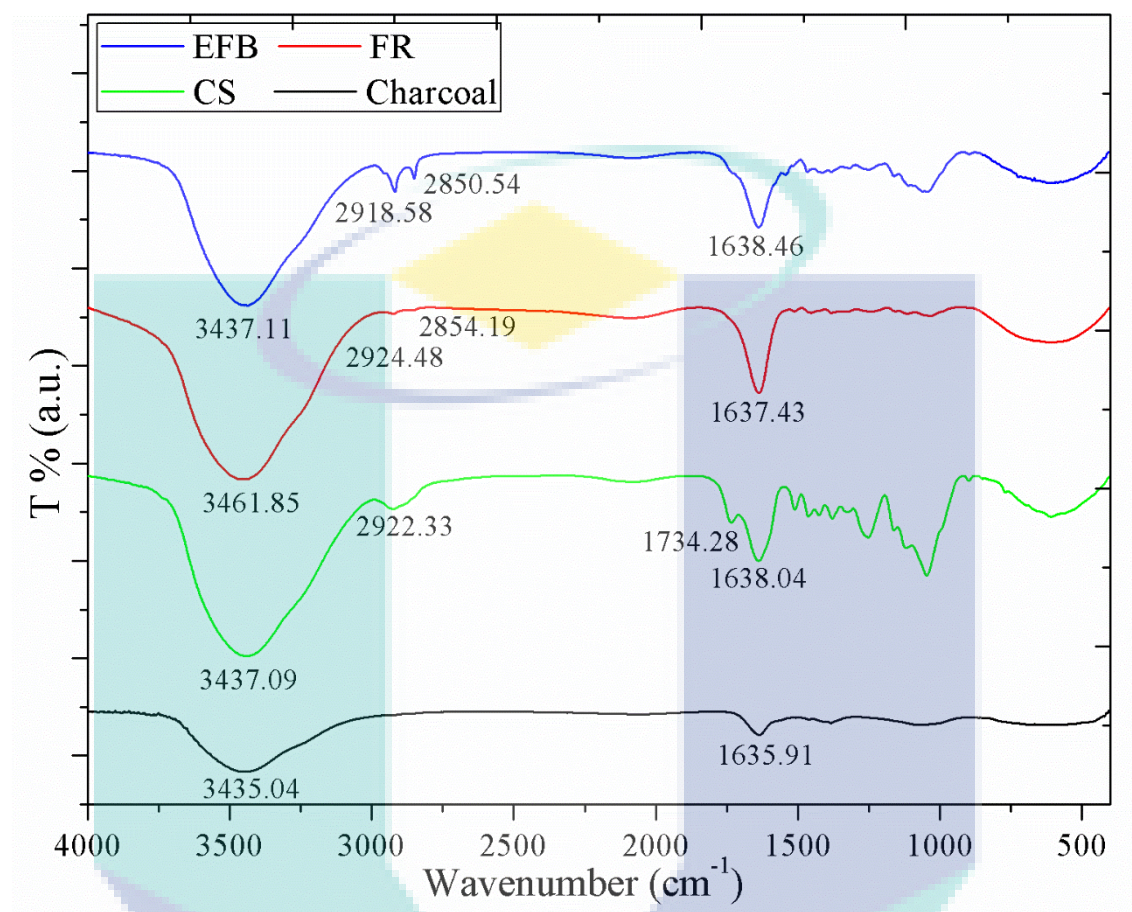


Figure 4.13 FTIR Spectrum of EFB, FR, CS and Charcoal.

Furthermore, biomass containing bands which are associated with the typical values of cellulose, hemicellulose or lignin, that have been interpreted based on the literature (Liu et al., 2006), whereas insignificant bands followed by the charcoal. Therefore, the selected biomass is most likely consisted of C-H, O-H and CH_2 stretching, whereas charcoal showed only OH due to the presence of moisture (Meng et al., 2013). Despite the structural differences between biomass and charcoal in the FTIR spectra, all biomass are to be processed by gasification or co-gasification with charcoal for the production of bioenergy.

4.1.8 X-ray Photoelectron Spectroscopy Analysis

Figure 4.14 represents the wide scan of XPS curves of EFB, FR, CS and charcoal. The detected elements that were associated with the corresponding binding energies are C1s, O1s, N1s, S2p. The carbonaceous materials were characterized by XPS to obtain

insights into the distribution of C and O functionalities in the biomass and charcoal. This characterization helps to understand about the precise chemical existence of elements including binding energy, type of bond and oxidation state in the feedstocks. The most significant peaks for C1s are shown in all samples which confirmed for the presence of carbon in all feedstocks that were the main elements for bioenergy production during co-gasification of biomass and charcoal.

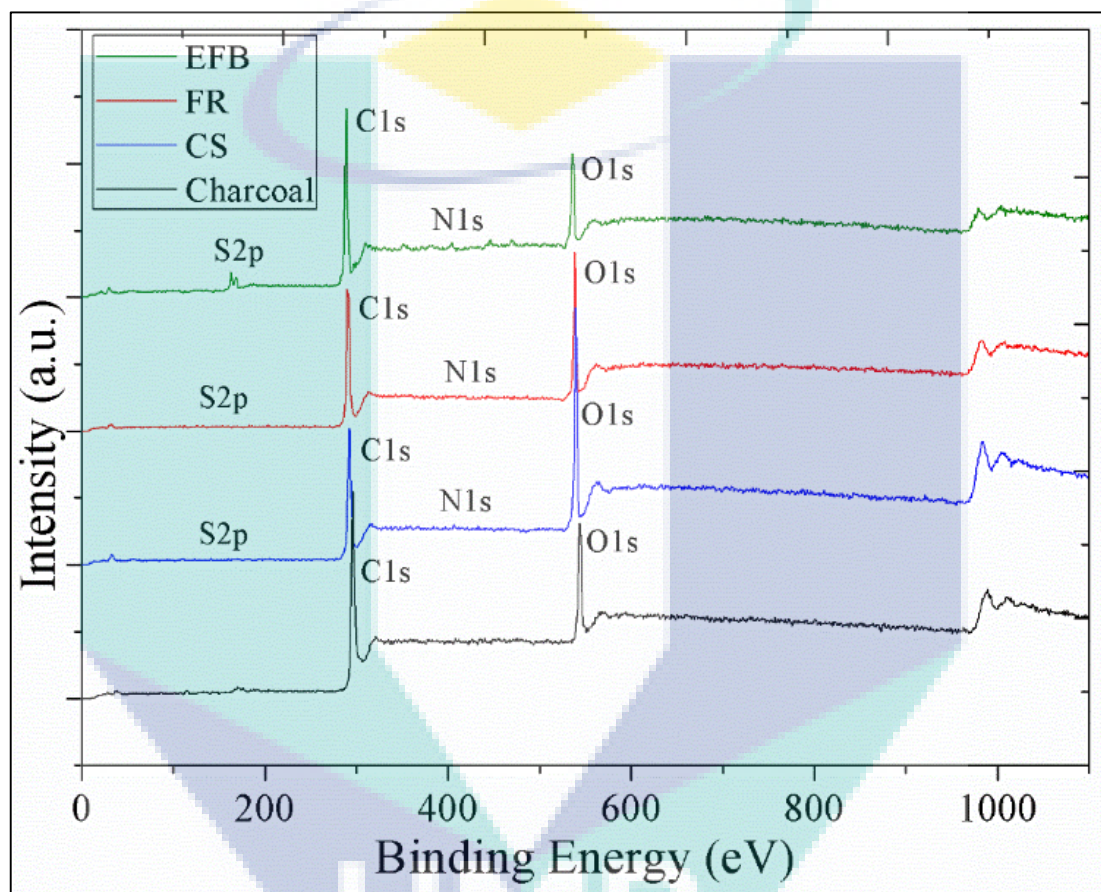


Figure 4.14 Wide scan XPS curves for EFB, FR, CS and Charcoal.

The C1s peaks in the EFB, FR, CS and charcoal samples are shown in Figure 4.15. The corresponding binding energies that are associated with functional groups are represented by this analysis.

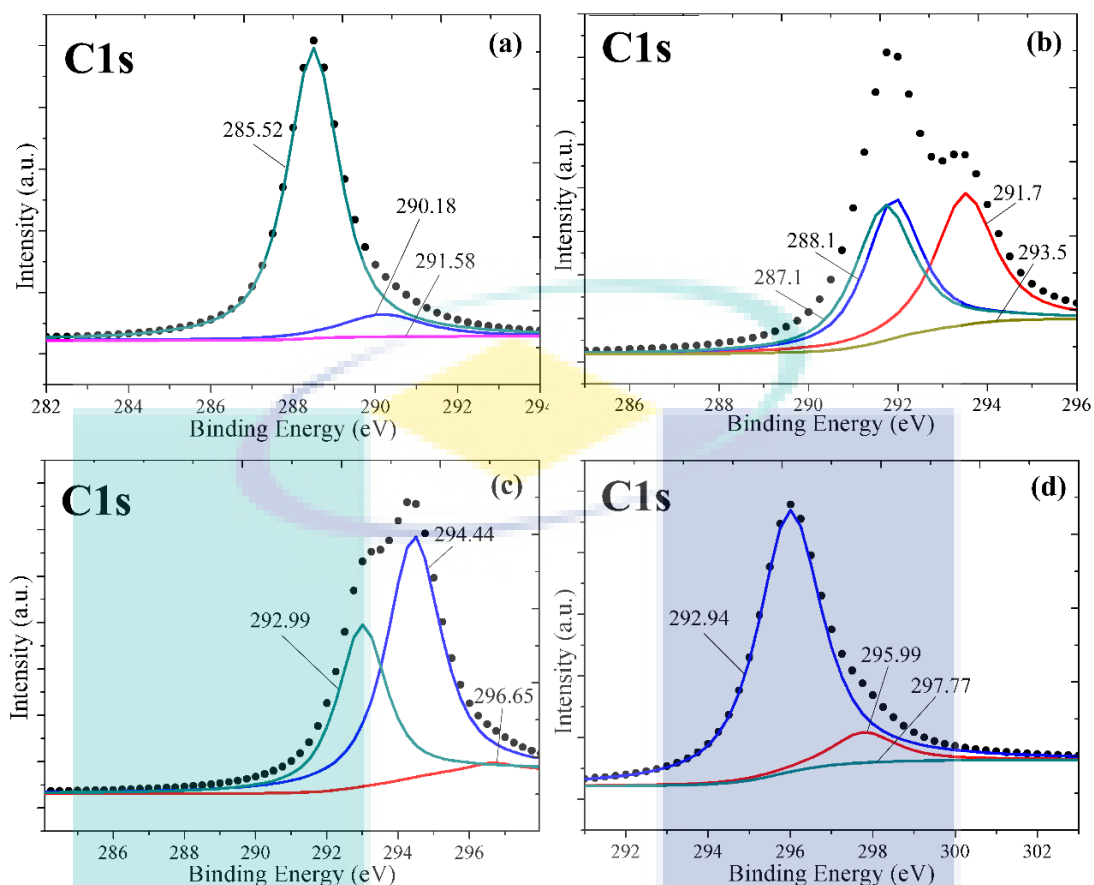


Figure 4.15 X-ray photoelectron spectroscopy (XPS) narrow scan of C1s : (a) EFB of palm oil, (b) Forest residue (FR), (c) Coconut shell (CS) and (d) by-product Charcoal.

The C1s peak in the EFB sample was deconvoluted into three different peaks, where binding energies of 285.52 eV, 290.18 eV and 291.58 eV (Figure 4.15a). The peak of C1s in the forest residue was represented by four individual peaks which corresponding to the binding energies of 287.1 eV, 288.1 eV, 291.7 eV and 293.5 eV (Figure 4.15b). The C1s peak in coconut shell sample was deconvoluted into three different peaks, where binding energies were 292.99 eV, 294.44 eV and 296.65 eV (Figure 4.15b). Deconvolution of the C1s peak of charcoal corresponds to different carbon-based functional groups as shown in Figure 4.15d. Presence of deconvoluted C1s peaks at three different binding energies of 292.94 eV, 295.99 eV and 297.77 eV supports the existence of C-C/C=C, C-O-C respectively. This result is consistent with the literature reported by Chia et al. 2014. The graphite (C=C) and aliphatic (C-C) are fitted together into a single peak due to the proximity of their binding energy. From elemental analysis (Table 4.1) it was evident that the total carbon content of EFB, FR, CS and charcoal is 42.33%, 42.75%, 43.90% and 55.43% respectively in the form of condensed aromatic rings and aliphatic groups. Figure 4.16 represents the O1s peaks in the EFB, FR, CS and charcoal samples.

The corresponding binding energies that are associated with functional groups are represented by this analysis.

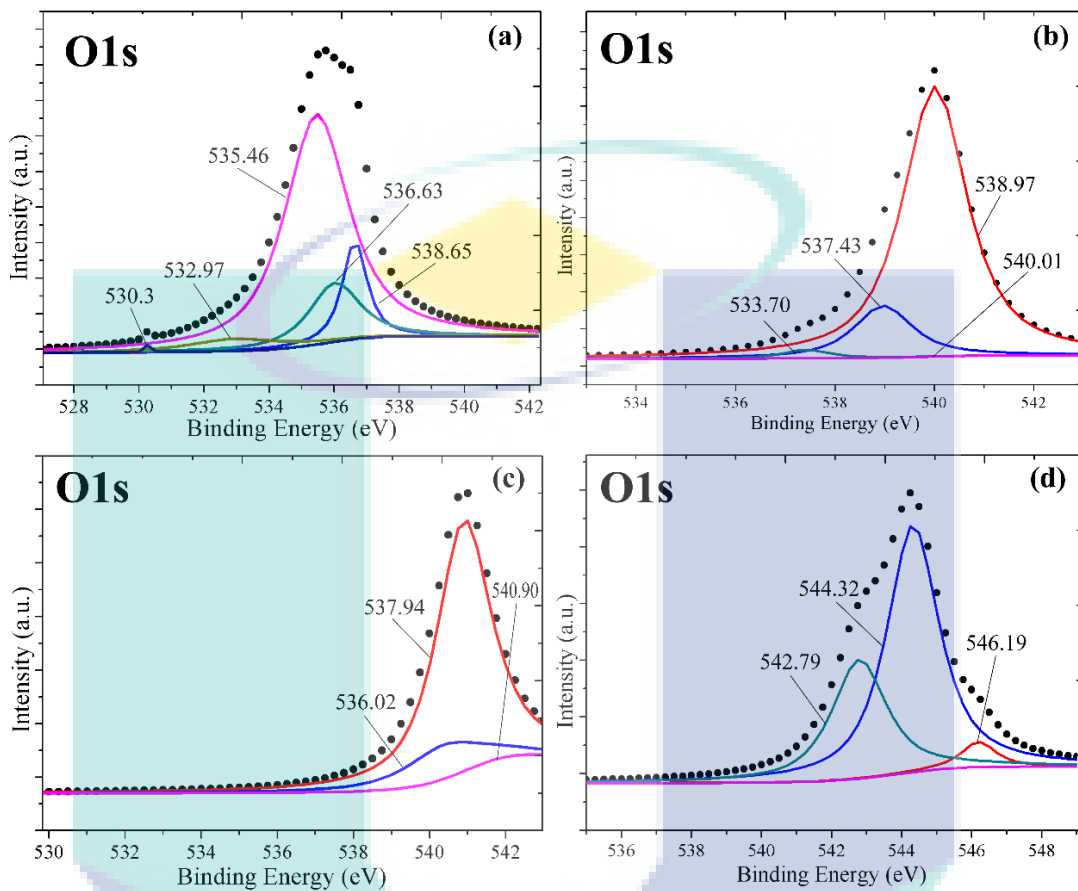


Figure 4.16 X-ray photoelectron spectroscopy (XPS) narrow scan of O1s : (a) EFB of palm oil, (b) Forest residue (FR), (c) Coconut shell (CS) and (d) by-product Charcoal.

There are five significant peaks were observed in EFB sample at the binding energies of 530.3 eV, 532.97 eV, 535.46 eV, 536.63 eV and 538.65 eV (Figure 4.16a) that were assigned to the O1s peaks (Wang, Geng, Li, & Zhang, 2015). In Figure 4.16b, there are four individual peaks were detected in the forest residue corresponding to the binding energies of 533.70 eV, 537.43 eV, 538.97 eV and 540.01 eV which were indicated to the O1s peaks. In the coconut shell sample (Figure 4.16c), three separate peaks were shown at the binding energy of 536.02, 537.94 and 540.90 eV as indicated to the O1s peaks. The detection of oxygenated functional groups for these three biomasses was consistent with the findings of proximate, ultimate and FTIR analytical results. On the other hand, there were three peaks were detected in the charcoal sample that was associated with the binding energies of 542.79 eV, 544.32 eV and 546.19 eV that were assigned to the O1s. The XPS narrow scans for N1s for EFB, FR and CS are shown in

Figure 4.17. There are several functional groups that were associated with N1s were investigated.

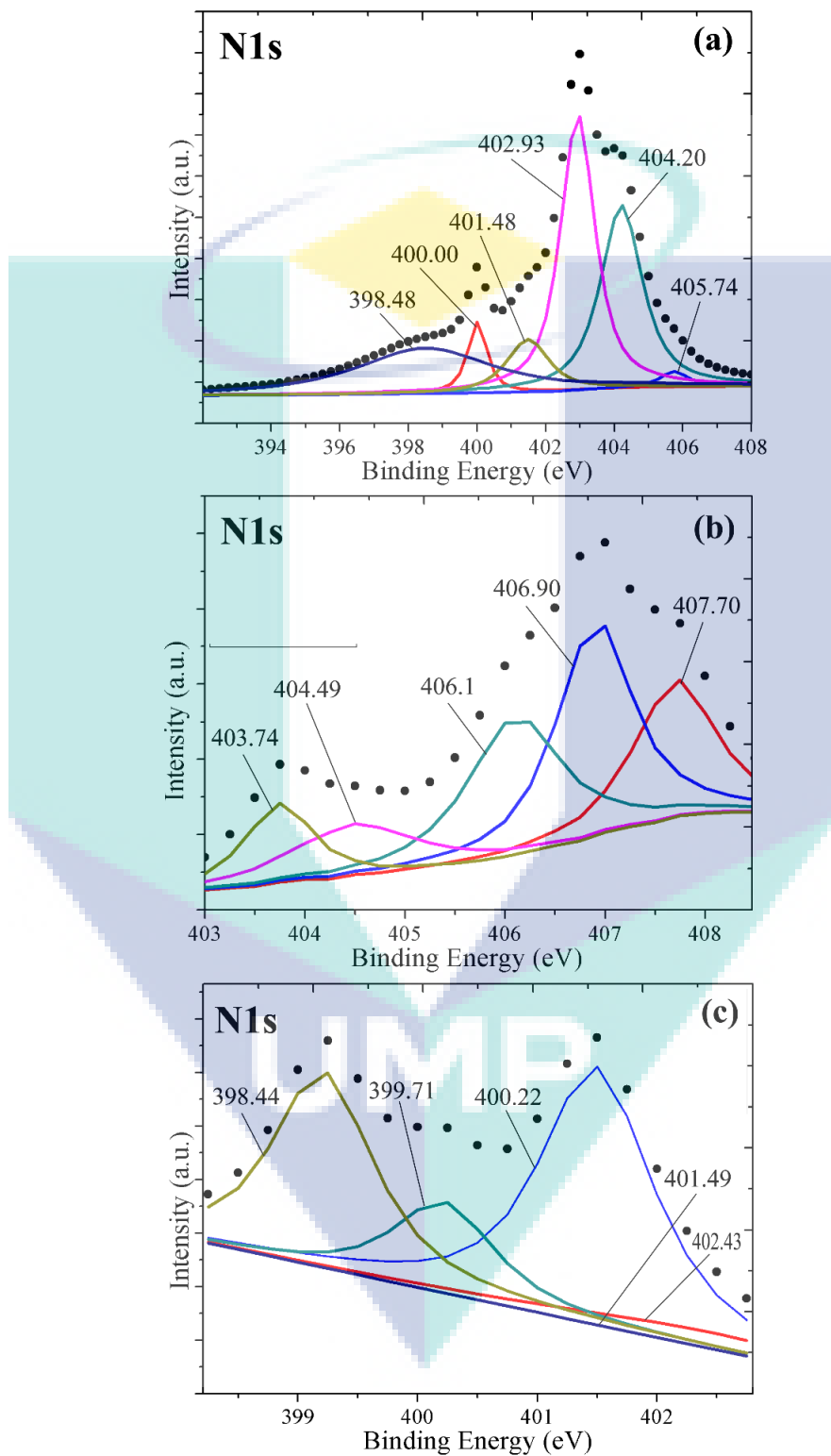


Figure 4.17 X-ray photoelectron spectroscopy (XPS) narrow scan of N1s : (a) EFB of palm oil, (b) Forest residue (FR) and (c) Coconut shell (CS).

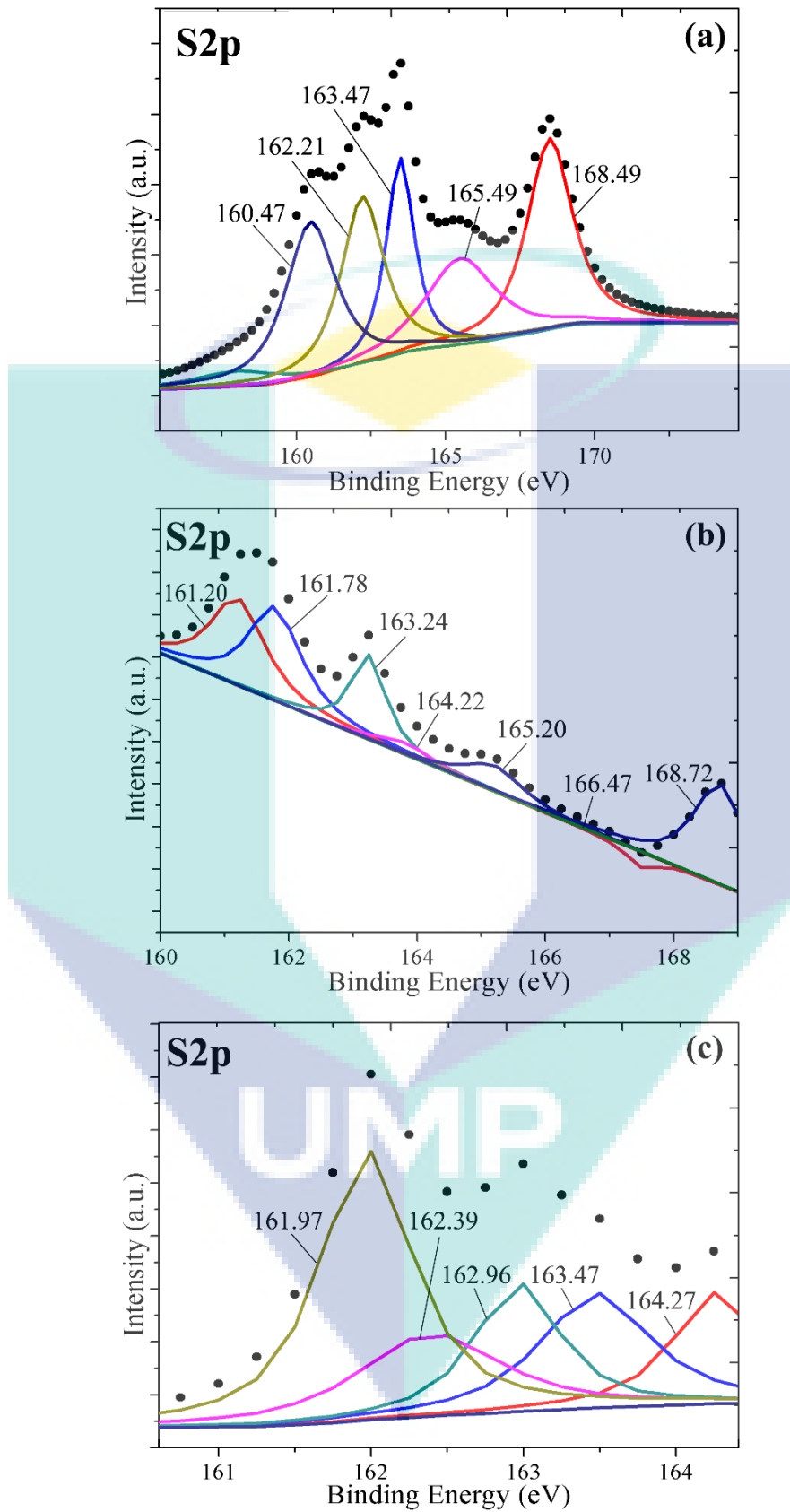


Figure 4.18 X-ray photoelectron spectroscopy (XPS) narrow scan of S_{2p} : (a) EFB of palm oil, (b) Forest residue (FR) and (c) Coconut shell (CS).

The spectrum of the EFB samples shows a peak at 398.48 eV, 400.00 eV, 401.48 eV, 402.93 eV, 404.20 eV and 405.74 eV corresponding to N1s species typically present in high-surface samples (Figure 4.17a). The peak spectrum identified at the binding energies of 403.74 eV, 404.49 eV, 406.1 eV, 406.9 eV and 407.7 eV corresponding to N1s species typically observed in the forest residue sample (Figure 4.17b). The spectrum of coconut shell represents peaks at 398.44 eV, 399.71 eV, 400.22 eV, 401.49 eV and 402.43 eV corresponding to N1s species typically exhibited by high-surface samples (Figure 4.17c). The XPS narrow scans for S2p for EFB, FR and CS are shown in Figure 4.18. There are several functional groups that were corresponding to S2p. The signal at 160.47 eV, 162.21 eV, 163.47 eV, 165.49 eV and 168.49 eV binding energy, is ascribed to S2p species in the sample (Figure 4.18a). The signal at 161.2 eV 161.78 eV, 163.24 eV, 164.22 eV, 165.2 eV, 166.47 eV and 168.72 eV binding energy, which is represented by S2p (Figure 4.18b). The signal at 161.97 eV, 162.39 eV, 162.96 eV, 163.47 eV and 164.27 eV binding energy, which is attributed to S2p species in the sample (Figure 4.18c). These curves are consistent with the literature value (Cai et al., 2014).

4.2 Simulation by Aspen Plus®

4.2.1 Model Flowsheet for Co-gasification Using Aspen Plus®

The Gibbs free energy flowsheet model was formed when the simulation was run using Aspen Plus® simulator based on the assumptions (Table 3.1) and characterization results (Table 4.1). This flowsheet-based model was used to investigate the composition variations due to the temperature and pressure variables. The co-gasification flowsheet model is shown in Figure 4.19.

The kinetics of drying, devolatilization, combustion and reduction were coupled with the gasification reactors on Aspen Plus® platform represented in Figure 4.19. The reactions were expressed by Gibbs equilibrium and reaction rate kinetics were used to determine the product gas. There were different types of Aspen Plus blocks were considered in this study. There was no steam considered in this system as a result of the native content of water in the feedstocks and inlet air. Figure 4.19 represents the main flowsheet of the model as it was taken from the Aspen Plus® (V8.6) screenshot.

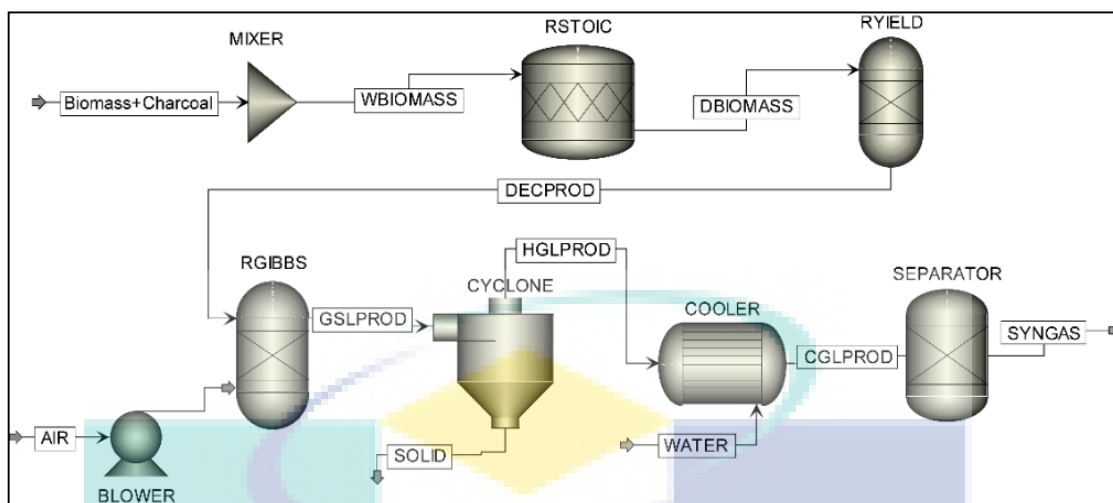


Figure 4.19 Aspen Plus® flowsheet simulation model for the co-gasification process using lignocellulosic biomass and charcoal for a pilot scale Downdraft Gasifier.

4.2.2 Mechanism of Simulation for Biomass and Charcoal Co-gasification Using Aspen Plus®

In this study, Figure 4.20 represents the mechanism of simulation for the co-gasification of lignocellulosic biomass (EFB, FR, CS) and charcoal in a pilot scale downdraft reactor. At the initial stage, feedstocks (biomass and charcoal) were mixed together and feed to the RSTOIC to eliminate its moisture content. The temperature for this block was considered as 120 °C (Figure 4.20). Pyrolysis process was completed for the conversion of non-conventional feedstock into conventional components within the reactor block of RYIELD and temperature was considered for this simulation as 400 °C. In this block, produced char was supposed to be 100% of carbon. The feedstocks were converted into different types of elements (C, H, O etc.) as shown in Figure 4.20. Subsequently, dry feedstock (elements) was moved down due to gravity and came in contact with air in the RGIBBS block corresponding to the oxidation zone. The amount of the char which was burnt in the oxidation zone to raise the temperature (RGIBBS block temperature 1050 °C) and decreased the temperature gradually in the reduction zone (RGIBBS block temperature 500 °C) of the feedstock bed, providing the required heat for the reaction. The aim of this block was to simulate the reaction between the feedstock and the gasifying agent (air) which was introduced into the reactor block. In this simulation, gasification temperature was considered at 500-1200 °C and the atmospheric air flow rate was 1-45 m³/h.

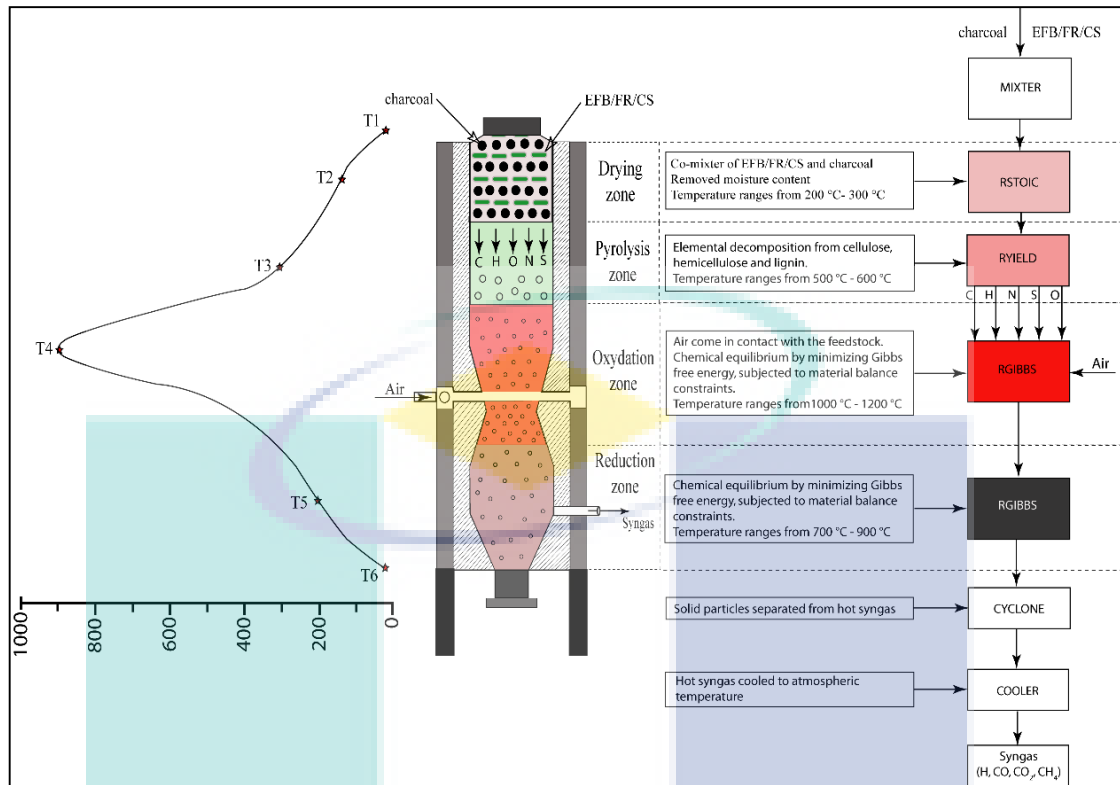


Figure 4.20 Simulation mechanisms for co-gasification of biomass (EFB of palm oil, forest residue (FR), coconut shell (CS)) and charcoal in a pilot scale downdraft reactor.

4.2.3 Simulation for Lignocellulosic Biomass and Charcoal Co-gasification

In this study, Figure 4.21 represents the biomass and charcoal co-gasification-based simulation considering the temperature ranges from 500° to 1200 °C and pressure ranges from 1bar to 45 bars. Based on this simulation, the main components of syngas (H₂, CO) with CO₂ and CH₄ were observed in the simulation (Figure 4.21) to establish the best-operating conditions for the production of syngas. The simulation result represents the syngas composition (H₂, CO, CO₂, CH₄) considering various pressure of 1 bar, 5 bars, 15 bars, 25 bars, 35 bars, 45 bars due to the effect of temperature (Figure 4.21). It can be seen that there was no significant change on the syngas when the pressure was 1 bar to 25 bars (Figure 4.21a-d). However, the significant curve was followed when the pressure increased at 35 bars and 45 bars (Figure 4.21) considering the syngas ratio (H₂:CO) up to the temperature of 1050 °C. The simulation curve revealed that the optimum temperature (T) and pressure (P) was 950-1050 °C and 30-35 bars, respectively for performing the co-gasification experiment. Moreover, the minimum required temperature was 950 °C for the decomposition of cellulose, hemicellulose and lignin which agreed with thermogravimetric analytical results (Figure 4.2). This result was also

consistent with the literature (Ramani, Allison, & Keller, 2004). The detailed procedure for simulation using Aspen Plus® are shown in Appendix B.

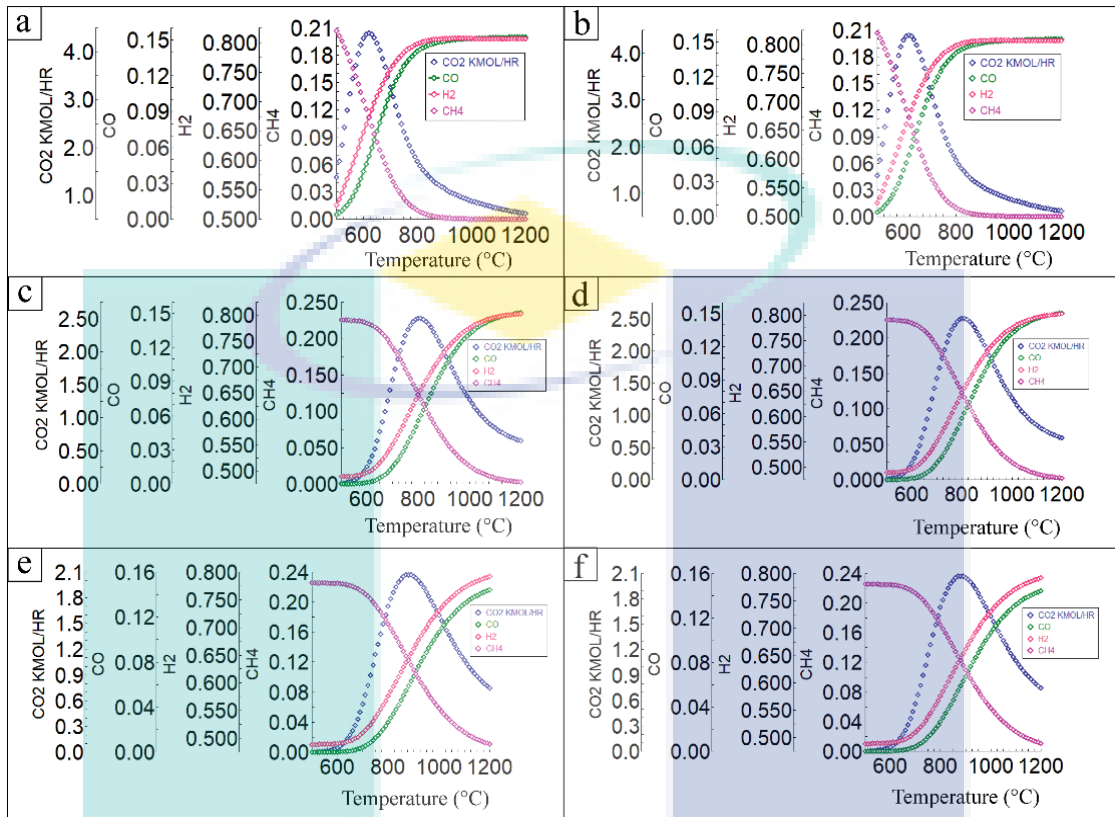


Figure 4.21 Aspen Plus® simulation based on the parameters of temperature (500-1200 °C) and pressure (1-45 bar): (a) 1 bar (b) 5 bars (c) 15 bars (d) 25 bars (e) 35 bars (f) 45 bars.

4.2.4 Experimental Validation with Simulation

The experimental results obtained from the experimental runs (EFB with charcoal, FR with charcoal and CS with charcoal) at the ratios of 100:00, 90:10, 80:20, 70:30 and 60:40 are compared with the simulation results (Aspen Plus® simulation based) in Table 4.3. The comparison throughout the gasification process revealed that the gasification efficiency was improved significantly with the rapid increase of temperature in the oxidation zone. During the gasification or co-gasification, various possible reactions occurred. When atmospheric air met with the elements in the oxidation zone, volatile compounds were produced with light gases that were pyrolyzed (Eq. 4.1) and formed charcoal (Eq. 4.2) which lead to having high CO concentrations during the transition stage and stable state.



The produced gases were available in the reactor during drying, pyrolysis and devolatilization processes, which implied the increased concentration of CO and H₂ (Eq. 4.3 and Eq. 4.4):



Table 4.3 Experimental results (syngas composition) were validated with simulation results at the temperature of 975°C and pressure 35 bar.

Feedstock ratios (Biomass:Charcoal)	Syngas composition	EFB and Charcoal		FR and Charcoal		CS and Charcoal	
		Exp.	Sim.	Exp.	Sim.	Exp.	Sim.
100:00	H ₂	3.91	3.87	9.88	9.50	7.07	7.02
	CO	5.70	5.50	20.90	20.10	13.04	13.00
	CO ₂	20.60	19.56	8.41	8.50	5.66	5.48
	CH ₄	0.35	0.34	1.08	0.95	1.12	1.00
90:10	H ₂	4.01	3.99	11.40	11.30	7.68	7.60
	CO	5.81	5.78	21.51	21.03	14.04	14.01
	CO ₂	17.42	16.98	8.29	8.15	5.52	5.51
	CH ₄	0.34	0.33	1.09	0.90	1.13	0.98
80:20	H ₂	4.30	4.28	11.81	11.67	8.04	8.01
	CO	6.02	5.89	21.67	21.56	14.64	14.62
	CO ₂	15.13	15.04	8.23	8.13	5.49	5.40
	CH ₄	0.36	0.29	1.11	0.85	1.16	0.96
70:30	H ₂	4.66	4.58	13.05	13.02	8.43	8.42
	CO	6.22	6.10	22.93	22.80	15.38	15.31
	CO ₂	14.08	14.03	7.90	7.50	5.38	5.32
	CH ₄	0.37	0.29	1.13	0.84	1.16	0.95
60:40	H ₂	4.70	4.54	13.07	13.03	8.50	8.42
	CO	6.30	6.10	22.96	22.87	15.40	15.35
	CO ₂	12.67	12.46	7.91	7.80	5.41	5.31
	CH ₄	0.37	0.28	1.14	0.84	1.15	0.95

Possible reactions that occurred that limits the quantity of CO₂ produced by partial CO oxidation were that the Boundard heterogenous reaction (Eq. 2.2 and Eq. 2.4). It was evident (Adeyemi, Janajreh, Arink, & Ghenai, 2017; Ali et al., 2017) that the high heating rate and energy-transfer conditions favored for downdraft gasification based reactors. A small fraction into the process, at bed temperatures of 975 °C promoted other reactions, such as gasification (Eq. 2.7) and methanation (Eq. 2.6) heterogenous reactions as well as shift the homogeneous reactions (Eq. 2.10) and reformed methane-vapor (Eq. 4.5) and ultimately syngas composition stability of the produced gas was reached.



4.2.5 Economic Analysis Using Aspen Plus®

An economic analysis was performed in this study using Aspen Plus® simulator as shown in Figure 4.22. For the sake of optimized temperature and pressure for co-gasification of lignocellulosic biomass with charcoal in a downdraft reactor, it is of persistence to reduce the syngas production cost, reducing feedstock cost, enhancing the gasification rate and finally to validate its suitability for commercialization.

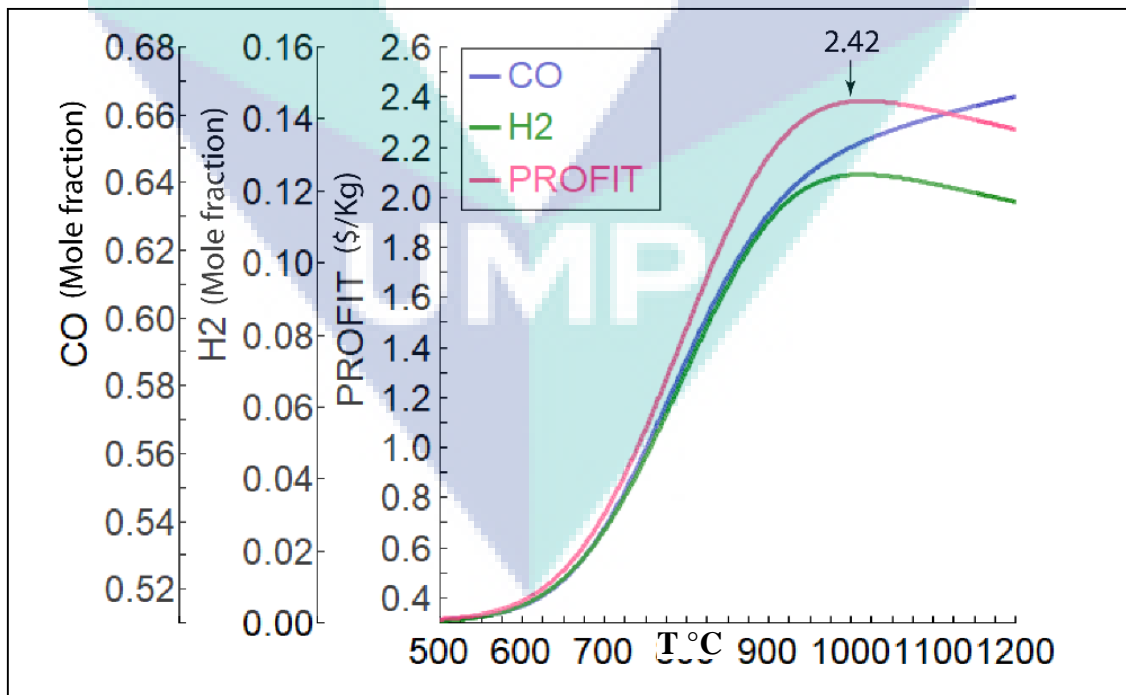


Figure 4.22 Economic analysis of product syngas using Aspen Plus® simulator.

The economic analysis depends on several factors, mainly the capital costs of the equipment (i.e. downdraft reactor, air blower, cyclone separator, heat exchanger, civil works and suitable local distribution network) and maintenance cost. The feedstocks price was also another variable factor that influences the syngas cost. In this study, Aspen Plus simulator was used to evaluate the optimum profit using FORTRAN CODE considering produced syngas of CO and H₂. The pressure and temperature were set for the evaluation were 35 bar and 975 °C, respectively. The prices of the CO and H₂ were assumed to be \$0.6 and \$16, respectively. The economic evaluation result is shown in Figure 4.23. At this figure indicated that the profit of syngas at the temperature of 875°C, 975°C and 1075 °C were \$2.2129, \$2.4203 and \$2.3739, respectively. Therefore, this study suggested for the experiment of co-gasification at the pressure of ~35 bar, maximum profit for syngas production that was generated at the temperature of ~975 °C.

4.3 Syngas Production Through Co-gasification

In this study, three different co-gasification processes were performed for syngas production using a pilot scale downdraft reactor. The co-gasification performance of empty fruit bunch of palm oil with charcoal, forest residue with charcoal and coconut shell with charcoal are discussed and compared to each other. The co-product of tar and by-product charcoal were characterized.

4.3.1 Co-gasification of EFB of Palm Oil and Charcoal

The co-gasification experiment was performed using EFB with charcoal (0-40%). The optimized temperature and pressure were used which were taken from the simulation results using Aspen Plus® simulator based on the feedstocks characterization results. The experimental results revealed that the concentration of H₂ and CO increased from 3.91-4.70 mole% and 5.70-6.30 mole% respectively, but the CO₂ concentration decreased from 20.6 to 12.67 mole% with increasing temperature (800-1000 °C) and pressure (25-35 bar). The product gas from co-gasification with charcoal has higher H₂ and CO concentrations in comparison with the EFB gasification. Hence, co-gasification of the feedstock has a significant potential to overcome the problem of disrupted feedstock supply in gasification. The yield of syngas concentration and gasification performance are discussed based on various parameters.

4.3.1.1 Temperature Profile on Co-gasification of EFB of Palm Oil and Charcoal

In this co-gasification study, temperatures profile was represented where EFB and charcoal were used as the feedstocks. The co-gasification temperature profile was also compared with EFB (100%) gasification (Table 4.4). The temperature profile with respect to time in various reactor zones (drying, pyrolysis, oxidation and reduction) are shown in Figure 4.23.

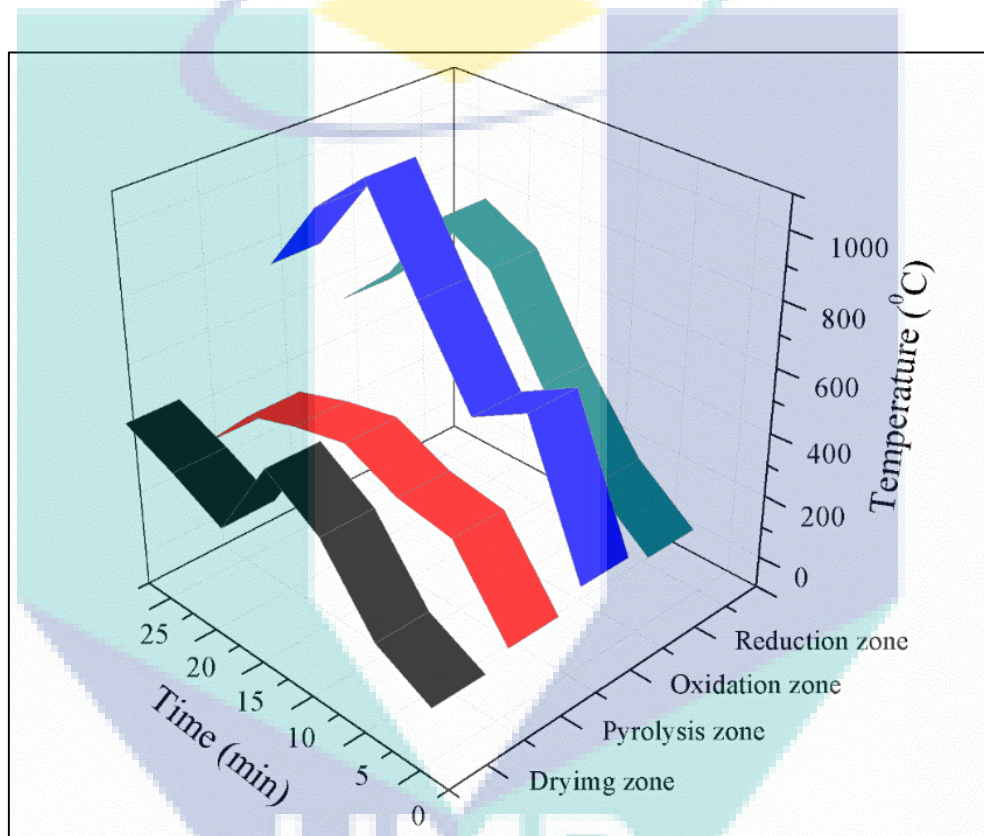


Figure 4.23 Temperature profile of various downdraft reactor zones (drying zone, pyrolysis zone, oxidation zone and reduction zone) with time during the co-gasification of EFB (70%) and charcoal (30%).

This is one of the most significant parameters for co-gasification that affected the product of syngas. The temperature in the drying, pyrolysis, oxidation and reduction zone during co-gasification of EFB and charcoal were recorded in the ranges of 200 - 400 °C, 400 - 600 °C, 700 - 1200 °C, and 700 - 1000 °C, respectively and zonewise temperatures agreed with the literature (Cai, Wang, Wang, & Kuang, 2016). The investigated average temperature was recorded by data logger from four individual reactor zones and the temperature difference between theoretical and experimental are shown in Table 4.4.

The average experimental temperature in the pyrolysis zone (T_3) was lower than the theoretical temperature, and in the oxidation zone (T_4) was also lower than the theoretical value, whereas the average experimental temperature for drying zone (T_2) and reduction zone (T_5), were obviously higher than the theoretical value of EFB gasification and EFB with charcoal co-gasification. Particularly, the average experimental temperature for T_2 was remarkably too much higher than the theoretical temperature.

Table 4.4 Comparison between experimental and theoretical temperature during the gasification of EFB and co-gasification of EFB with Charcoal.

Parameters	Gasification of EFB (100%)				Co-gasification of EFB (70%) with charcoal (30%)			
	Drying Zone (T_2)	Pyrolysis Zone (T_3)	Oxidation Zone (T_4)	Reduction Zone (T_5)	Drying zone (T_2)	Pyrolysis Zone (T_3)	Oxidation Zone (T_4)	Reduction Zone (T_5)
Experimental temperature (°C)	350	410	792	870	380	518	1000	975
Theoretical temperature (°C)	250	550	1100	800	250	550	1100	800
Temperature difference (°C)	100	-140	-308	70	130	-32	-100	-175
Absolute temperature (%)	40.00	25.45	28.00	8.75	52.00	5.82	9.09	21.88

From the comparative study of average theoretical and experimental temperature (Table 4.4), it is observed that the gasification and co-gasification for oxidizing temperature were lower than 28.00% and 9.09%, respectively. The plausible reason for this phenomenon was due to the hot flue gases produced from various gasification reactions with a high temperature in the drying and pyrolysis zone.

4.3.1.2 Effect of EFB of Palm Oil and Charcoal Mixture on Syngas Composition

The syngas composition was observed with various mixture of EFB and charcoal (100:0, 90:10, 80:20, 70:30 and 60:40). The product syngas was investigated and as shown in Figure 4.24. The syngas (H_2 and CO) composition during co-gasification of EFB with charcoal was higher in percentage than the EFB (100%) gasification.

In this study, it was clearly shown that the concentration of H_2 and CO were significantly increased by increasing the mixture of charcoal with EFB. The increase of H_2 with EFB was attributed to higher reactivity during gasification. With an increase of charcoal from 0-30%, the concentration of H_2 and CO increased from 3.91-4.66% and

5.70-6.22%, respectively (Figure 4.24). After that, up to 40% of charcoal, this composition increased slightly (4.70% and 6.30%). In contrary, the concentration of CO₂ decreased with increasing the charcoal ration (Figure 4.24). However, the CH₄ concentration (0.35-0.37%) was insignificantly affected by various ratios of EFB and charcoal. The CH₄ concentration agreed with the literature as reported by Kumabe, Hanaoka, Fujimoto, Minowa, and Sakanishi (2007).

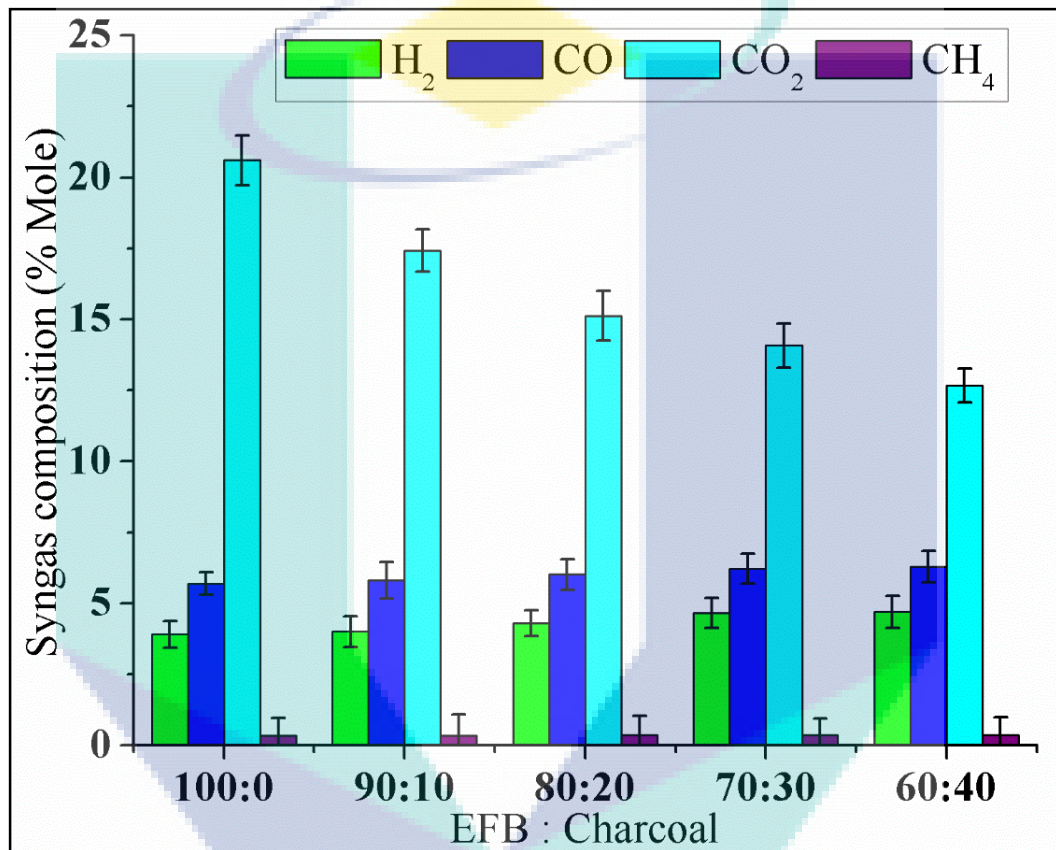


Figure 4.24 Syngas composition with various ratios of EFB of palm oil and Charcoal (100:0; 90:10; 80:20; 70:30 and 60:40).

The increase of H₂ composition occurred due to the increase of temperature on both oxidation and reduction zone. It was happened due to the synergistic effect between EFB and charcoal. As the CH₄ concentration insignificantly occurred in the producer gas, it might happen due to limited methanation reaction (Eq. 2.6). The produced syngas composition was consistent with the literature (Fermoso et al., 2009; Prasertcharoensuk, Hernandez, Bull, & Phan, 2018).

4.3.1.3 Effect of EFB of Palm Oil and Charcoal Mixture on H₂ and CO Yield

The H₂ and CO yield were investigated throughout the various mixture of charcoal (0-40%) with EFB based co-gasification process. The effect of EFB and charcoal mixture on the H₂ and CO yield is shown in Figure 4.25.

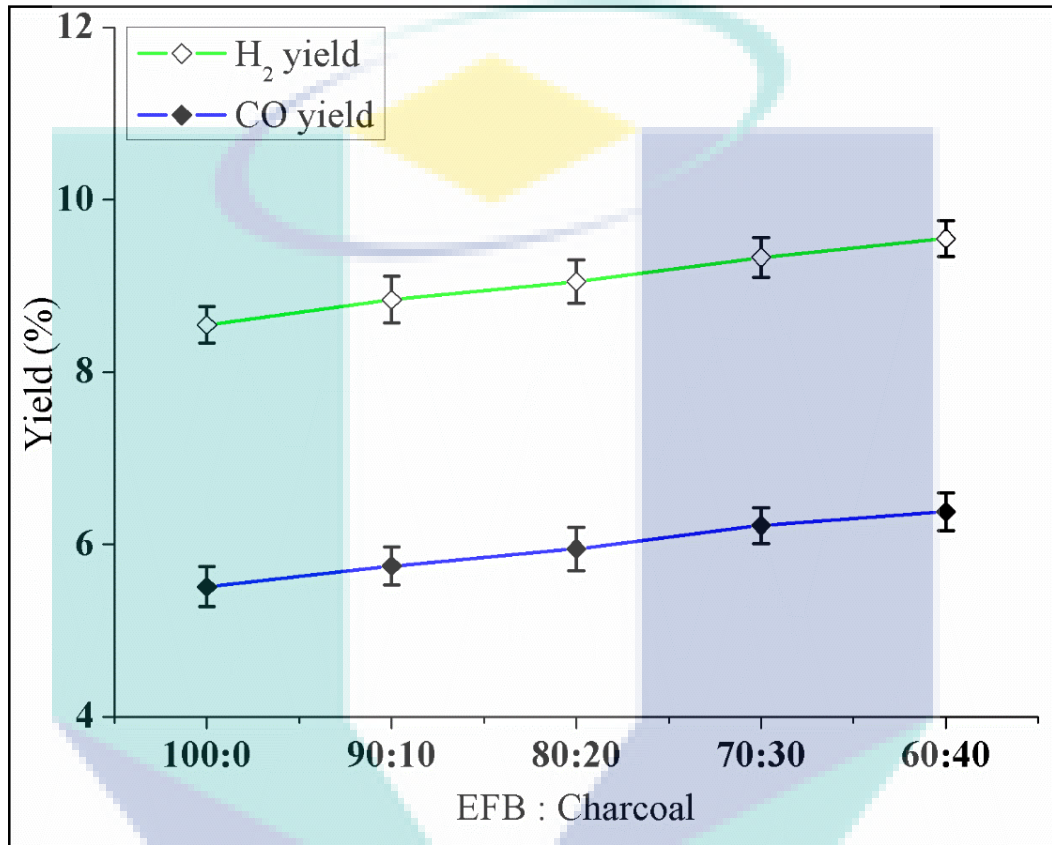


Figure 4.25 H₂ and CO yield (%) of syngas produced from co-gasification of EFB of and Charcoal with various ratios (100:0; 90:10; 80:20; 70:30 and 60:40).

In this analysis, it is exhibited that H₂ and CO concentration increased from 8.55-9.33% and 5.51-6.22%, respectively with increased in percentage of charcoal 0-30% with EFB. Subsequently, up to 40% of charcoal, these concentrations increased considerably by 9.55% and 6.38%, respectively. Therefore, there is a significant effect on the H₂ and CO concentration by adding the charcoal mixture on EFB.

4.3.1.4 Effect of EFB of Palm Oil and Charcoal Mixture on Syngas Ratio

The syngas (H₂ and CO) ratio was investigated with co-gasification mixture of EFB and charcoal throughout the process. The scenario of the syngas ratio is shown in Figure 4.26. In this study, it was observed that the syngas ratios for the mixture of EFB

and charcoal of 100:0, 90:10, 80:20, 70:30 and 60:40 were 1.41, 1.45, 1.48, 1.50 and 1.55, respectively (Figure 4.26). The syngas ratio was relatively identical when the charcoal ratio was 30% to 40%. Therefore, an optimum mixture of EFB and charcoal was 70% and 30%, respectively for the proper utilization of lignocellulosic biomass of EFB.

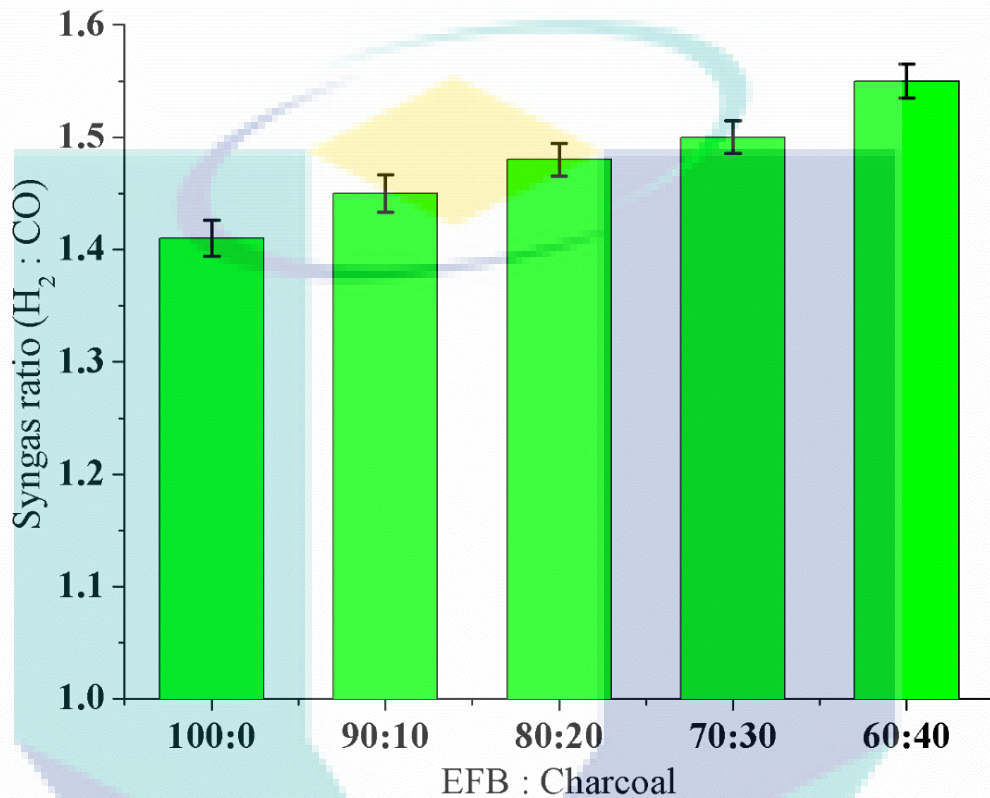


Figure 4.26 Syngas ratio (H₂:CO) during the co-gasification of EFB of palm oil and Charcoal with various ratios (100:0; 90:10; 80:20; 70:30 and 60:40).

4.3.1.5 Effect of Syngas Flame Before and After Particle Purification

The raw and clean syngas-based flame is shown in Figure 4.27. The experimental setup was investigated the syngas flame before and after particle clean-up through cyclone separator. The investigated syngas flame was long continuous and yellow to blue in colour which consistent with the literature (Rathod & Bhale, 2014). There was a remarkable change occurred on the quality of syngas flame after passing through the cyclone separator. This indicated that mixture of particular syngas reduced the quality of syngas. The yellow circle (a) contained some particle impurities whereas yellow circle (b) not contained any particles. There is a particles separator (cyclone separator) installed to purify the syngas where produced gases pass through it. As a result, the flame colour was not changed significantly only changed its quality when it purified by particles

separator (Figure 4.27). Therefore, purified syngas exhibits acceptable and quality syngas that was indicated by syngas flame which was more effective for energy conversion than raw syngas (Rathod, Shete, & Bhale, 2016).

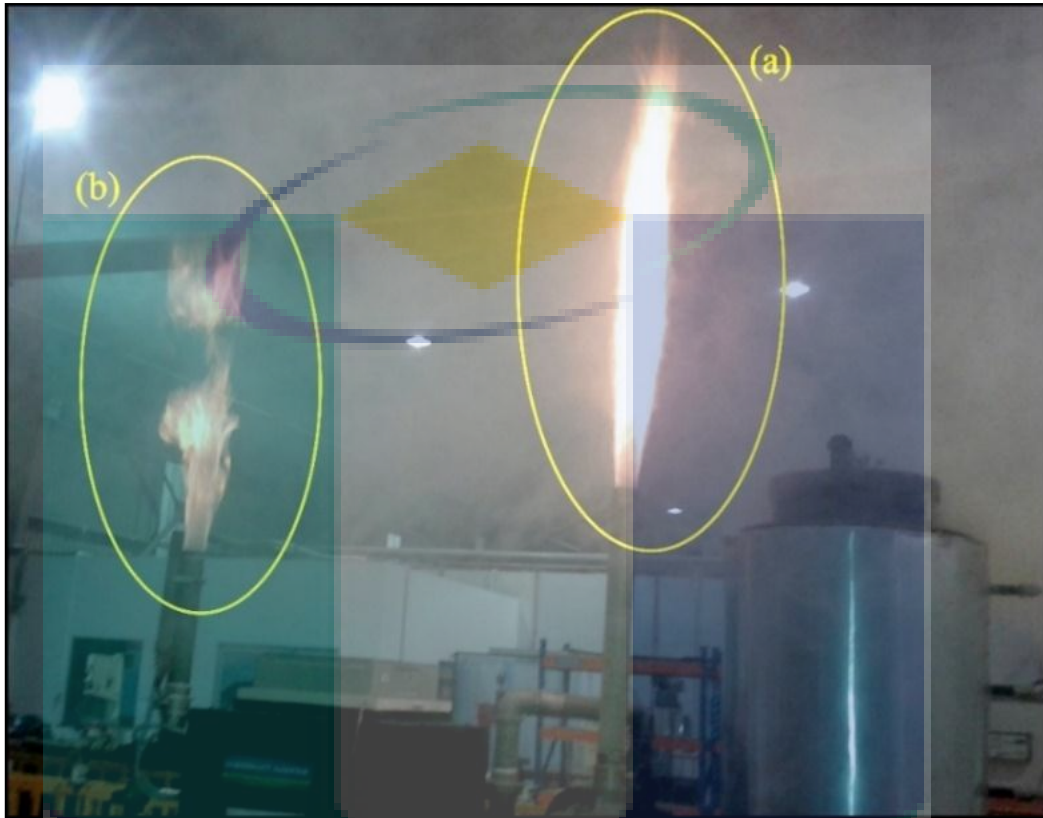


Figure 4.27 The syngas flame appearance of raw syngas (a) purified based syngas (b) during the co-gasification of EFB (70%) and Charcoal (30%).

4.3.1.6 Effect of EFB of Palm Oil and Charcoal Mixture on Exergy Efficiency

The exergy efficiency for syngas produced from the co-gasification of EFB and charcoal considering various feedstock ratios (100:0; 90:10; 80:20; 70:30 and 60:40) are shown in Figure 4.28. In this analysis, it was clearly shown that the exergy efficiency was increased with increasing the mixture of charcoal with EFB. The overall exergy efficiency depends on the initial moisture content of the feedstocks. The fuel mixture exergy with chemical and physical mixture exergy affect on the total exergy efficiency. The exergy efficiencies were varied from 46.46% to 68.99% when EFB/charcoal ratio was changed from 0 to 40%. This was happened due to the increase of physical and chemical exergy in producer syngas. Moreover, the effect on reactor temperature depends on the physical exergy of the producer gas. Therefore, the value of LHV, MC and β was found to be proportional to the overall exergy.

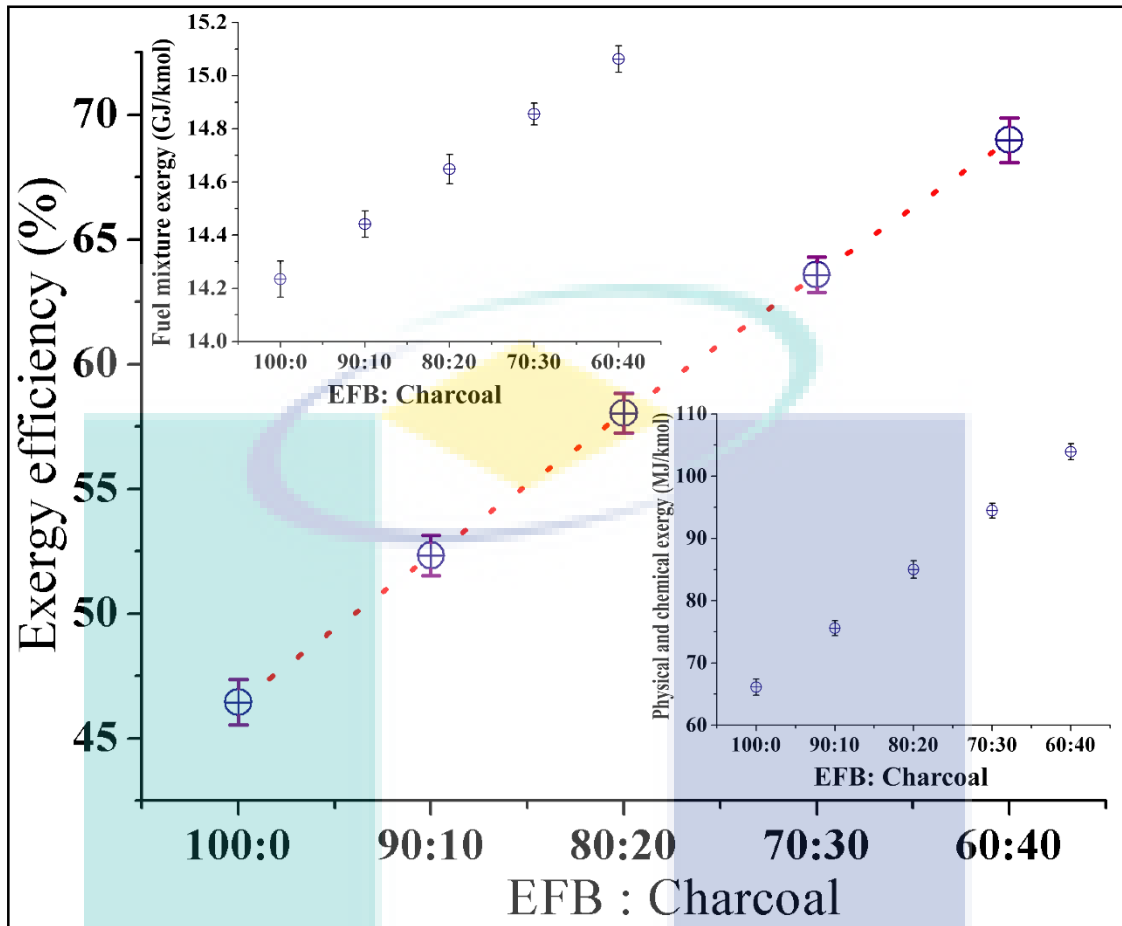


Figure 4.28 Exergy efficiency during the co-gasification of EFB of palm oil and charcoal with various ratios (100:0; 90:10; 80:20; 70:30 and 60:40).

4.3.1.7 Effect of EFB of Palm Oil and Charcoal Mixture on Syngas Heating Value

The heating value of product syngas is represented by the following Figure 4.29. The LHV and HHV for produced syngas for the EFB and charcoal ratio of 0-40% are 1.27-1.43 MJ/kg and 1.36-1.54 MJ/kg, respectively which is consistent with the literature value (Hagos, Aziz, & Sulaiman, 2013; Ng et al., 2017). Furthermore, the results revealed that the LHV for the EFB was lower than charcoal and the ratio of EFB and charcoal increased with increasing the heating value of EFB and charcoal. Correspondingly, the moisture content of the feedstocks decreased when the EFB and charcoal ratios changed from 0 to 40%. However, β value decreased with increasing ratio of EFB and charcoal ratios.

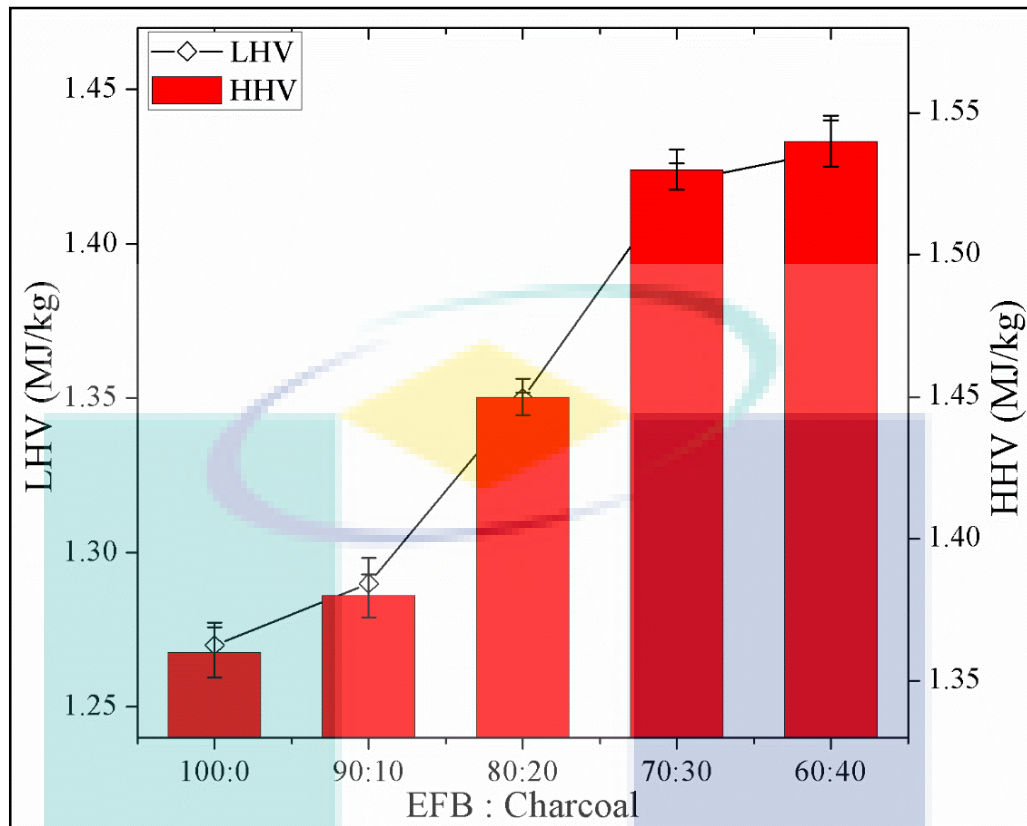


Figure 4.29 HHV (a) and LHV (b) of Syngas during the co-gasification of EFB of palm oil and Charcoal with various ratios (100:0; 90:10; 80:20; 70:30 and 60:40).

4.3.2 Co-gasification of Forest Residue and Charcoal

The experiments were performed with a mixture of forest residue and charcoal with a ratio of 100:0, 90:10, 80:20, 70:30 and 60:40. The yield of syngas comprises of combustible (H_2 , CO , CH_4) and non-combustible (CO_2 , N_2) gases. Co-gasification-based produced syngas was reported by some researchers (Kalita & Baruah, 2018; Ng et al., 2017; Patel et al., 2017; Ramos et al., 2018) where the carbonaceous materials of forest residue and charcoal was gasified with a controlled amount of gasifying medium at high temperature ($>900\text{ }^\circ\text{C}$). The concentration variation of the downdraft reactor showed that the CO concentration increased with increasing charcoal (up to 40%) with forest residue. On contrary, an opposite trend for the case of CO_2 concentration was observed with increasing charcoal. The optimal yield of syngas ($H_2:CO$) ratio was found to be 1.14 after the forest residue:charcoal mixture of 70:30 and 60:40 w/w for maximizing the benefits of the gasification process. The yield of syngas concentration and gasification performance are discussed below on the basis of various parameters.

4.3.2.1 Temperature Profile on Co-gasification of Forest Residue and Charcoal

In this co-gasification study, temperatures profile was recorded where forest residue and charcoal were used as the feedstocks. The graphical representation of drying, pyrolysis, oxidation and reduction zone is shown in Figure 4.30. In the pyrolysis stage (relatively low temperature), it's cellulose, hemicellulose or lignin is converted into char. At the same time, it reduces organic materials through the depolymerization process. In this profile, it is clearly shown that the highest temperature (~1044 °C) comprised in the oxidation zone where feedstocks were decomposed (Table 4.5). The atmospheric air was contacted and reacted with the decomposed feedstocks.

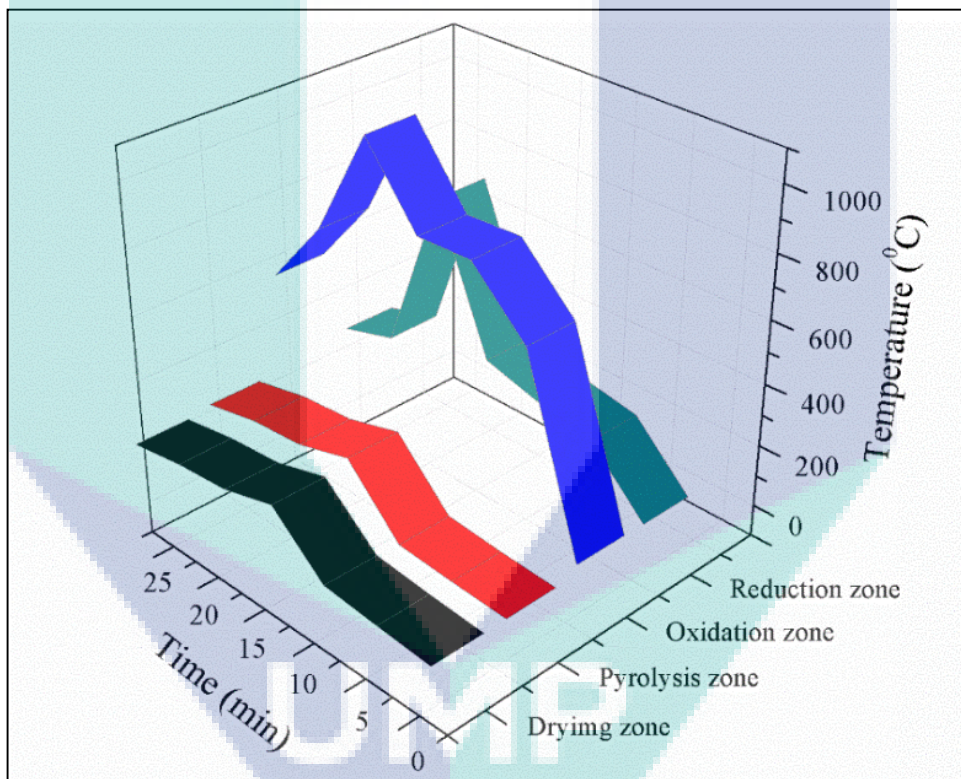


Figure 4.30 Temperature profile of various downdraft reactor zones (drying zone, pyrolysis zone, oxidation zone and reduction zone) with time during the co-gasification of FR (70%) and Charcoal (30%).

The average experimental temperature in the drying zone (T_2), pyrolysis zone (T_3), oxidation zone (T_4) and reduction zone (T_5) was comparatively lower than the theoretical temperature. On contrary, during co-gasification the average experimental value in the drying zone is relatively higher. Particularly, the average experimental temperature for T_2 was remarkably too much higher than the theoretical temperature. From the comparative study of average theoretical and experimental temperature (Table

4.5), it is observed that the gasification and co-gasification for oxidizing temperature were lower than 25.09% and 5.09%, respectively. The possible reason for this trend was similar to EFB and charcoal based co-gasification.

Table 4.5 Comparison between experimental and theoretical temperature during the gasification of FR (100%) and co-gasification of FR (70%) with Charcoal (30%).

Parameters	Gasification of FR (100%)				Co-gasification of FR (70%) with charcoal (30%)			
	Drying Zone (T ₂)	Pyrolysis Zone (T ₃)	Oxidation Zone (T ₄)	Reduction Zone (T ₅)	Drying zone (T ₂)	Pyrolysis Zone (T ₃)	Oxidation Zone (T ₄)	Reduction Zone (T ₅)
Experimental temperature (°C)	222	310	824	531	275	470	1044	765
Theoretical temperature (°C)	250	550	1100	800	250	550	1100	800
Temperature difference (°C)	-28	-240	-276	-269	25	-80	-56	-35
Absolute temperature (%)	11.20	43.64	25.09	33.63	10.00	14.55	5.09	4.38

Combustion process occurred and various reactions happened in this zone and temperature reached to around 1044 °C. Several types of gases occurred in this zone and transferred to the reduction zone which reduced the amount of oxygen. Accordingly, gases were converted to other gases like CO, H₂, CH₄ and CO₂. In this zone the temperature goes down to 765 °C.

4.3.2.2 Effect of Forest Residue and Charcoal Mixtures on Syngas Composition

The syngas composition was observed with various mixture of forest residue and charcoal (100:0, 90:10, 80:20, 70:30 and 60:40). In this ratio, product syngas compositions were investigated (Figure 4.31). The syngas composition during co-gasification of forest residue and charcoal was a higher percentage than the biomass (FR, 100 %) gasification.

From this study, it was revealed that the concentration of H₂ and CO increased significantly due to increasing mixture of charcoal with FR. The increase of H₂ with forest residue was attributed to higher reactivity during gasification. During this study, it was also observed that with an increase of charcoal from 0-30%, the concentration of H₂ and CO increased from 9.88-13.05% and 20.09-22.93%, respectively (Figure 4.31). Subsequently, up to 40% of charcoal, H₂ and CO composition were increased marginally

(13.06% and 22.96%). On the other hand, the composition of CO₂ decreased with increasing the charcoal ratio. However, the CH₄ composition was slowly affected by various ratios of FR and charcoal. The CH₄ concentration agreed with the literature (Kumabe et al., 2007) and EFB and charcoal based co-gasification

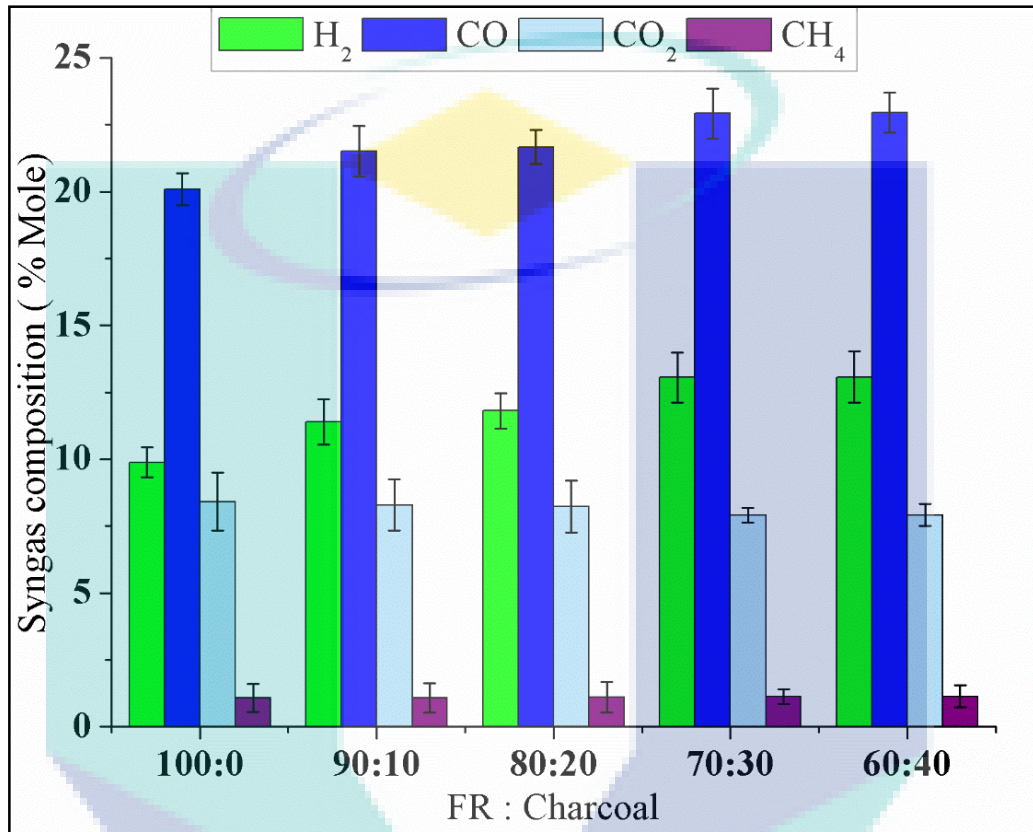


Figure 4.31 Syngas composition with various ratios of FR and Charcoal (100:0; 90:10; 80:20; 70:30 and 60:40).

The increase of H₂ concentration occurred due to an increase of temperature on both oxidation and reduction zone. It also happened due to the synergistic effect between forest residue and charcoal. As the CH₄ concentration insignificantly occurred in the producer gas, it might be happened due to limited methanation reaction (Eq. 2.6). The produced syngas concentration agreed with the literature value (Fermoso et al., 2009; Prasertcharoensuk et al., 2018).

4.3.2.3 Effect of Forest Residue and Charcoal Mixture on H₂ and CO Yield

The effect of FR and charcoal mixture on the H₂ and CO yield is expressed in Figure 4.32. In this observation, FR and charcoal ratios were considered as 100:0; 90:10; 80:20; 70:30 and 60:40, respectively.

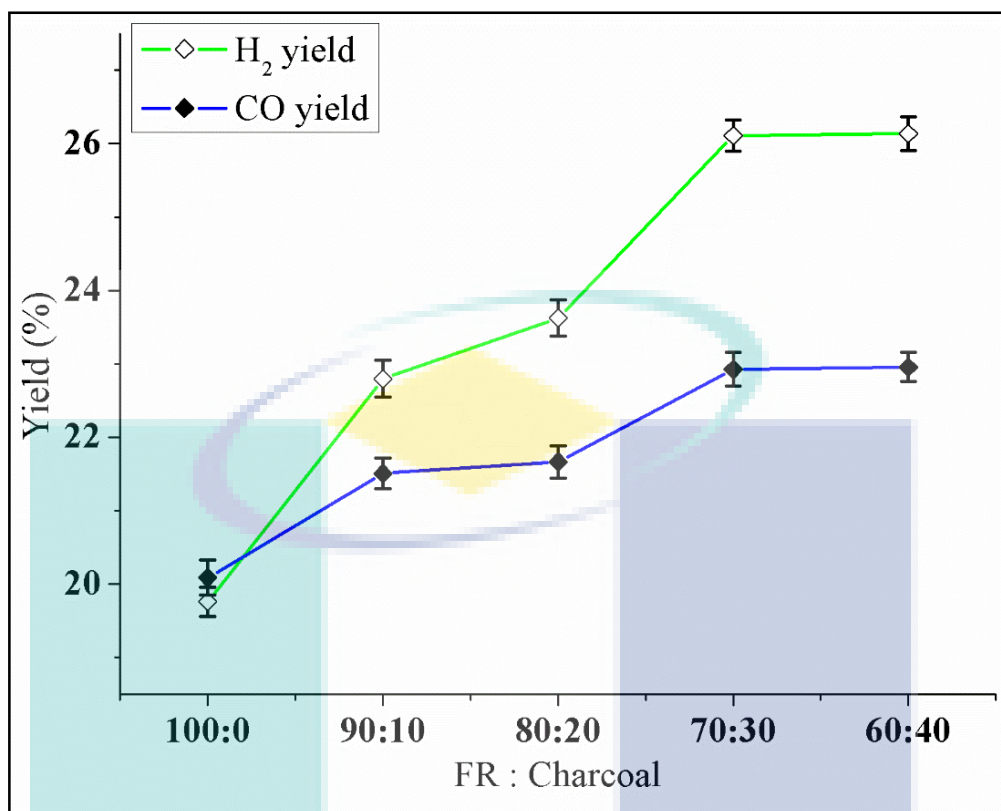


Figure 4.32 H₂ and CO yield (%) of syngas produced from co-gasification of FR and Charcoal with various ratios (100:0; 90:10; 80:20; 70:30 and 60:40).

In this analysis, it is shown that H₂ and CO concentration increased from 19.78-26.14% and 20.09-22.96%, respectively with the increased percentage of charcoal 0-30% with forest residue. Subsequently, up to 40% of charcoal, these concentrations increased considerably by 26.14% and 22.96%, respectively. Thus, a significant effect on the H₂ and CO concentration by adding charcoal mixture (0 to 40%) on FR feedstock was observed.

4.3.2.4 Effect of Forest Residue and Charcoal Mixture on Syngas Ratio

The syngas (H₂ and CO) ratio was investigated with the co-gasification mixture of FR and charcoal throughout the process. The scenario of the syngas ratio is shown in Figure 4.33. In this study, it was observed that the syngas ratios for the mixture of forest residue and charcoal of 100:0, 90:10, 80:20, 70:30 and 60:40 were 0.98, 1.06, 1.09, 1.14 and 1.14, respectively (Figure 4.33). The syngas ratio was relatively identical when charcoal ratio was 30% to 40%. Therefore, the best mixture of FR and charcoal was considered as 70% and 30%, respectively for suitable utilization of lignocellulosic biomass of FR.

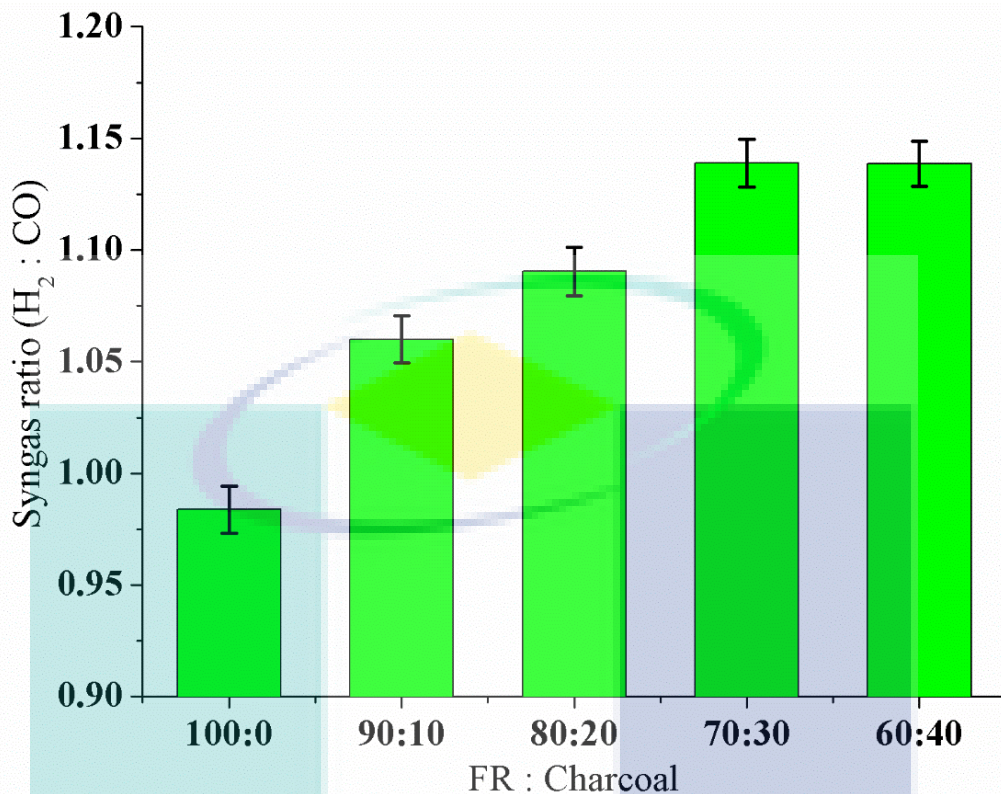


Figure 4.33 Syngas ratio (H₂:CO) during the co-gasification of FR and Charcoal with various ratios (100:0; 90:10; 80:20; 70:30 and 60:40).

4.3.2.5 Effect of Syngas Flame Before and After Particle Purification

The raw and clean syngas-based flame is visualized in Figure 4.34 that was obtained from the forest residue and charcoal co-gasification. The syngas flame was found to be intermittent and yellow as shown in the literature (Rathod & Bhale, 2014). A significant change was investigated on the flame after passing through the cyclone separator. It was revealed that the particulate compositions within the syngas decreased the quality of syngas. The yellow circle (a) contained some particles and yellow circle (b) particles free syngas flame. Therefore, the flame colour was not changed significantly, only changed its quality when it was passed through the cyclone separator. From this analysis, it was suggested that particle free syngas was collected after purification system.



Figure 4.34 The flame appearance of raw and purified syngas during the co-gasification of FR (70%) and Charcoal (30%).

4.3.2.6 Effect of Forest Residue and Charcoal Mixture on Exergy Efficiency

The exergy efficiency for syngas produced from co-gasification of forest residue and charcoal considering various feedstock ratios (100:0; 90:10; 80:20; 70:30 and 60:40) are shown in Figure 4.35. In this analysis, it was clearly shown that the exergy efficiency increased with increasing mixture of charcoal with forest residue. The overall exergy efficiency depends on the initial moisture content of the feedstocks. The exergy efficiencies varied from 38.90% to 62.14% when forest residue/charcoal ratio was changed from 0 to 40%. The increasing exergy efficiency by adding charcoal from 0 to 40% was observed as 23.24%. This happened due to increased of physical and chemical exergy in producer syngas. Moreover, the effect on reactor temperature depends on the physical exergy of the producer gas. Therefore, the value of LHV, MC and β was found to be proportional to the overall exergy and this results are consistent with EFB and charcoal based co-gasification. The detailed exergy calculations are shown in Appendix A.

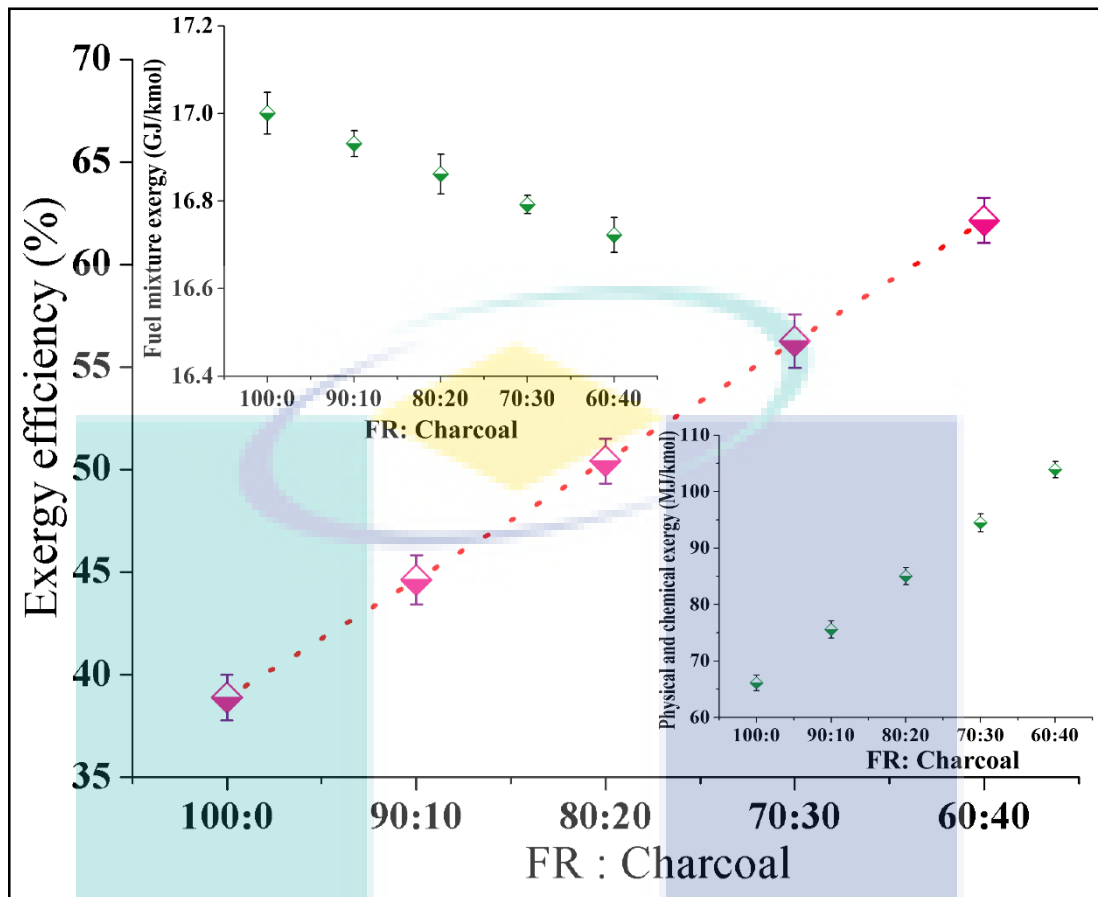


Figure 4.35 Exergy efficiency during the co-gasification of FR and Charcoal with various ratios (100:0; 90:10; 80:20; 70:30 and 60:40).

4.3.2.7 Effect of Forest Residue and Charcoal Mixture on Syngas Heating Value

The heating value of product syngas is represented by Figure 4.36. The LHV and HHV of produced syngas for the forest residue and charcoal ratio of 0-40% are 3.98-4.71 MJ/kg and 4.23-5.02 MJ/kg, respectively which are consistent with the literature value (Hagos et al., 2013; Ng et al., 2017). Furthermore, the results revealed that the LHV for the forest residue was lower than charcoal and the ratio of forest residue and charcoal increased with increasing the heating value of forest residue and charcoal. Correspondingly, the moisture content of the feedstocks decreased when the forest residue and charcoal ratios changed from 0 to 40%. However, β value decreased with increasing ratio of forest residue and charcoal ratios.

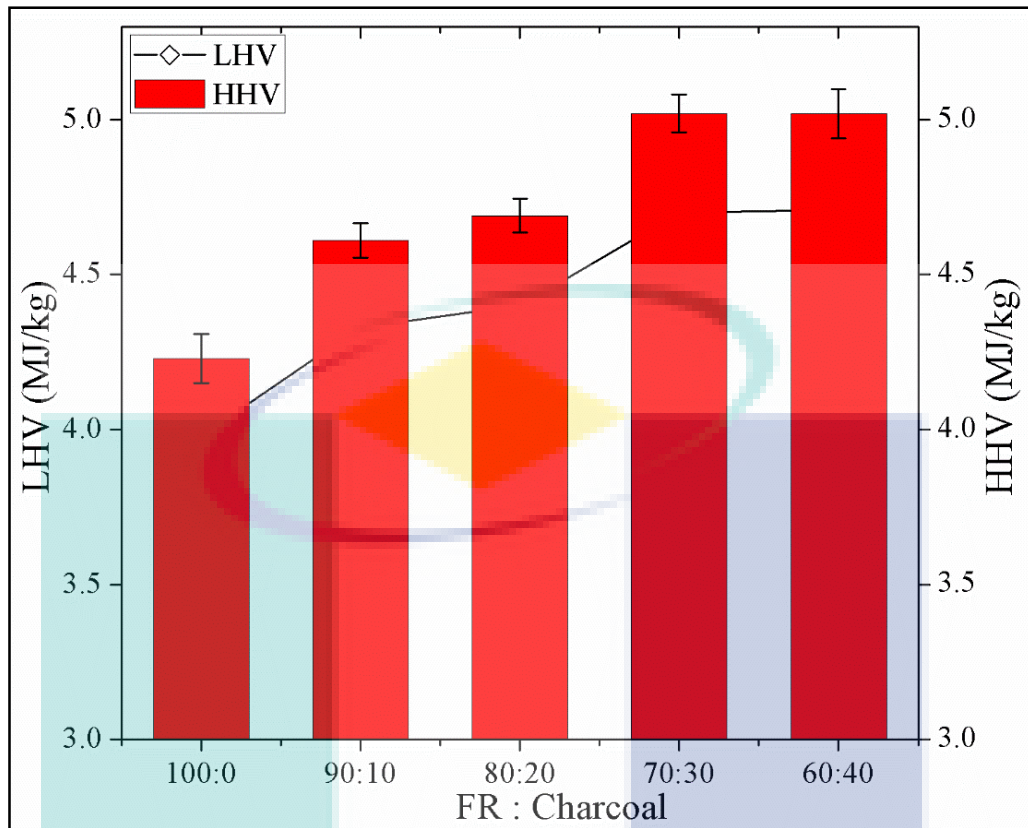


Figure 4.36 HHV (a) and LHV (b) of Syngas during the co-gasification of FR and Charcoal with various ratios (100:0; 90:10; 80:20; 70:30 and 60:40).

4.3.3 Co-gasification of Coconut Shell and Charcoal

The co-gasification experiments were completed with a mixture of coconut shell and charcoal with the blending ratio of 100:0, 90:10, 80:20, 70:30 and 60:40. The controlling parameter of temperature and pressure were used to verify the production of gas during the gasification process with air. The higher contents of cellulose and hemicellulose than lignin in the sample were found to gasify better, as evident from structural analysis. The gasifier produces a combustible gas with H₂, CO, CO₂ and CH₄ concentrations of 8.44, 15.38, 5.38 and 1.62 mol.% respectively, at a total flow of air of 30 m³ h⁻¹. The results revealed that 30 wt.% charcoal in the feedstock was effectively gasified to generate syngas comprising over 30 mol.% of syngas with a lower heating value of 3.27 MJ/Nm³.

4.3.3.1 Temperature Profile on Co-gasification of Coconut Shell and Charcoal

The temperature profile in the drying, pyrolysis, oxidation and reduction zone during the co-gasification of coconut shell (70%) and charcoal (30%) were recorded and

shown in Figure 4.37. In the drying and pyrolysis stage, the trends of temperature profile were relatively similar. The average temperatures in this zone were less than 500 °C (relatively low temperature). In these zones, the moisture content was eliminated, and cellulose, hemicellulose or lignin is converted into gases and char. At the same time, it reduces organic materials through the depolymerization process.

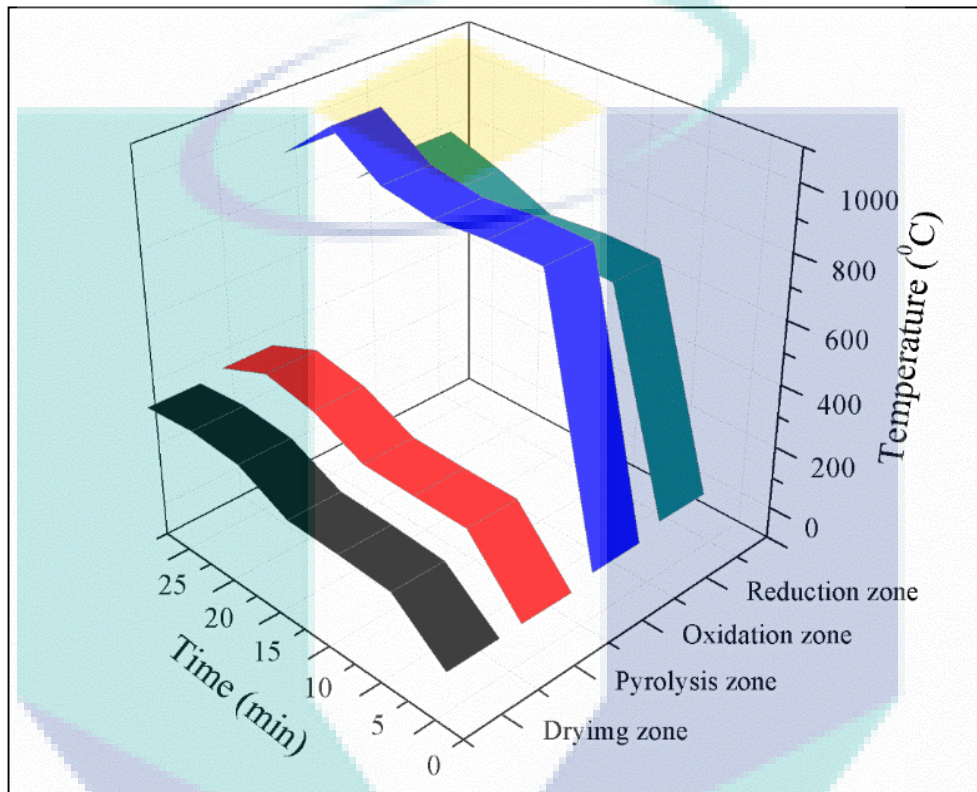


Figure 4.37 Temperature profile of various downdraft reactor zones (drying zone, pyrolysis zone, oxidation zone and reduction zone) with time during the co-gasification of CS (70%) and Charcoal (30%).

In this temperature profile, it was shown that the highest temperature contained in the oxidation zone where atmospheric air assisted for the combustion process and at the same time decomposed feedstocks were converted into gases. Various reactions occurred in this zone and temperature reached to around 1000 °C. Various gases also occurred in this zone and after that these gases were transferred to the reduction zone which reduced the amount of oxygen. Consequently, gases were converted into other gases like CO, H₂, CH₄ and CO₂. In this zone, the temperature fell down less than 900 °C.

Table 4.6 Comparison between experimental and theoretical temperature during the gasification of CS (100%) and co-gasification of CS (70%) with Charcoal (30%).

Parameters	Gasification of CS (100%)				Co-gasification of CS (70%) with Charcoal (30%)			
	Drying Zone (T ₂)	Pyrolysis Zone (T ₃)	Oxidation Zone (T ₄)	Reduction Zone (T ₅)	Drying zone (T ₂)	Pyrolysis Zone (T ₃)	Oxidation Zone (T ₄)	Reduction Zone (T ₅)
Experimental temperature (°C)	275	320	972	613	295	481	1000	788
Theoretical temperature (°C)	250	550	1100	800	250	550	1100	800
Temperature difference (°C)	25	-230	-128	-187	45	-69	-100	-12
Absolute temperature (%)	10.00	41.82	11.64	23.38	18.00	12.55	9.09	1.50

The average experimental temperature in the pyrolysis zone (T₃), oxidation zone (T₄) and reduction zone (T₅) were lower than the theoretical temperature, whereas the average experimental temperature for drying zone (T₂) was comparatively higher than the theoretical value for the CS gasification and CS with charcoal co-gasification. From the comparative study of average theoretical and experimental temperature (Table 4.6), it is observed that the gasification and co-gasification for oxidizing temperature were lower than 11.64% and 9.09%, respectively. As a result, this happened due to hot flue gases produced from various gasification reactions with a high temperature in the drying zone and this trend was followed the EFB and FR with charcoal based co-gasification.

4.3.3.2 Effect of Coconut Shell and Charcoal Mixture on Syngas Composition

The syngas composition was observed considering the mixture of CS and charcoal with aratio of 100:0, 90:10, 80:20, 70:30 and 60:40that is shown in Figure 4.38. The mole percentage of H₂ and CO increased gradually by increasing the mixture of charcoal with CS. In this analysis, it was observed that due to increasing ratios of charcoal (0-30%), the composition of H₂ and CO increased from 7.07-8.43% and 13.04-15.38%, respectively. On the other hand, the concentration of CO₂ decreased with increasing the charcoal ratio with CS. Moreover, there are no remarkable effects observed on CH₄ composition. Similar trend is followed for CH₄ concentration that is consistent with the literature (Kumabe et al., 2007).

The increasing trend for H₂ and CO (%) within the reactor occurred due to the change of temperature in both oxidation and reduction zone. It occurred because of the synergistic effect between CS and charcoal. As a result, limited methanation reactions and CH₄ concentration insignificantly occurred in the producer gas (Fermoso et al., 2009).

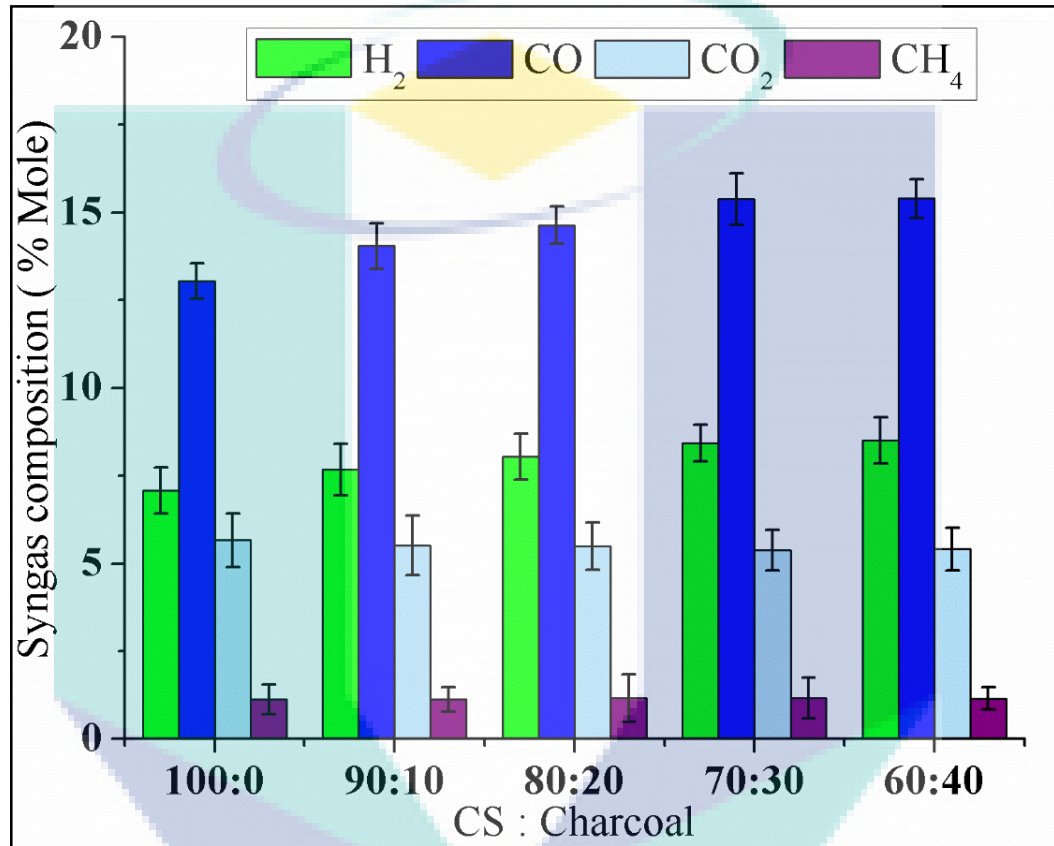


Figure 4.38 Syngas composition with various ratios of CS and Charcoal (100:0; 90:10; 80:20, 70:30 and 60:40).

4.3.3.3 Effect of Coconut Shell and Charcoal Mixture on H₂ and CO Yield

The effect of CS and charcoal mixture on various ratios (100:0; 90:10; 80:20, 70:30 and 60:40) were observed on the H₂ and CO yield in this analysis are shown in Figure 4.39. In this analysis, it is shown that H₂ and CO concentration increased from 14.13-16.87% and 13.04-15.38%, respectively with an increased percentage of charcoal 0-30% with CS. Subsequently, up to 40% of charcoal, these concentrations increased slightly to 16.90% and 15.41%, respectively. From this study, it is clearly showed that a significant effect on the H₂ and CO concentration by adding the mixture of charcoal (0 to 40%) on CS.

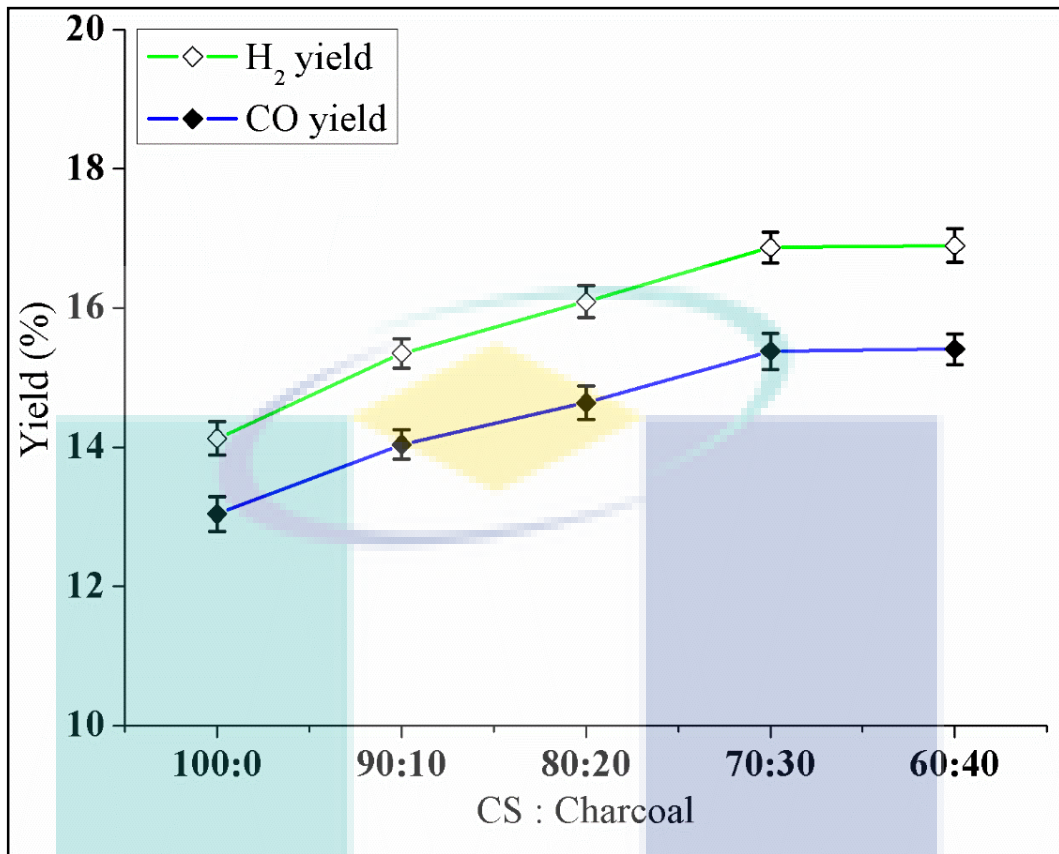


Figure 4.39 Syngas ratio (H₂:CO) during the co-gasification of CS and Charcoal at various ratios (100:0; 90:10; 80:20, 70:30 and 60:40).

4.3.3.4 Effect of Coconut Shell and Charcoal Mixture on Syngas Ratio

The syngas (H₂ and CO) ratio was observed with co-gasification mixture of CS and charcoal during the co-gasification process. The scenario of syngas ratio is represented in Figure 4.40. In this analysis, it was shown that the syngas ratios for the mixture of CS with charcoal of 100:0, 90:10, 80:20, 70:30 and 60:40 were 1.04, 1.08, 1.09, 1.10 and 1.11, respectively (Figure 4.40). The syngas ratio was relatively similar when charcoal ratio was 30% to 40%. Therefore, the best mixture of CS and charcoal was considered as 70% and 30%, respectively for suitable utilization of lignocellulosic biomass of FR. This results followed the other two co-gasification of EFB with charcoal and FR with charcoal.

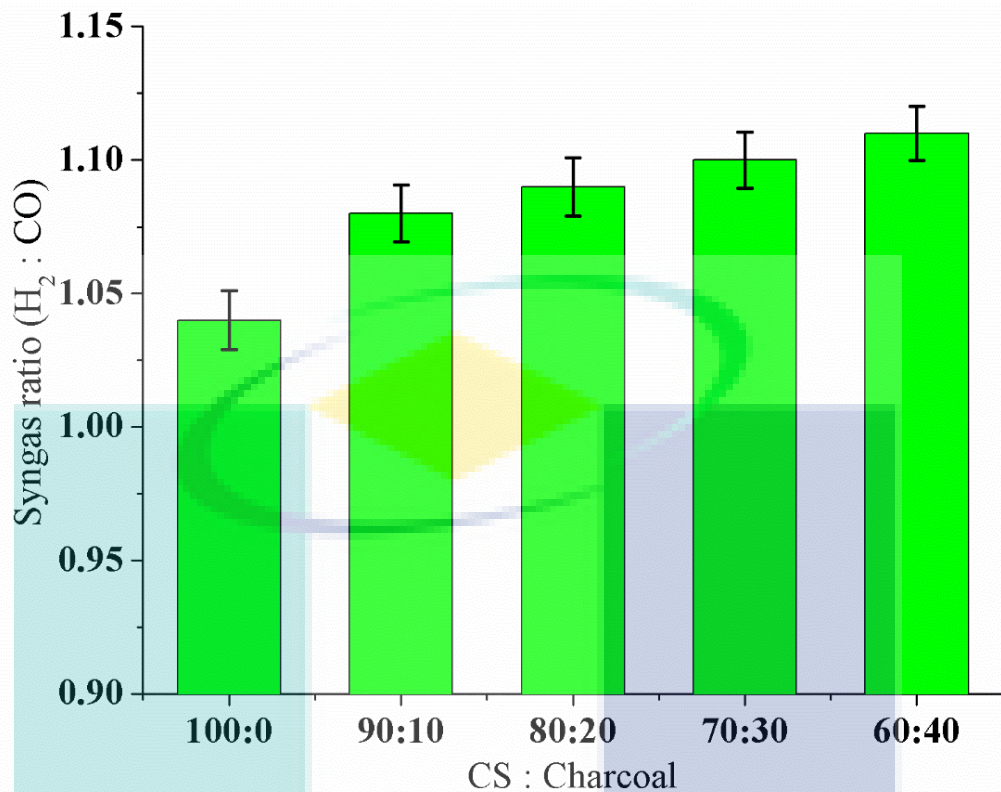


Figure 4.40 Syngas ratio (H₂:CO) during the co-gasification of CS and Charcoal with various ratios (100:0; 90:10; 80:20; 70:30 and 60:40).

4.3.3.5 Effect of Syngas Flame Before and After Particle Purification

The raw and particles free syngas flame is shown in Figure 4.41. The experimental setup was to investigate the flame colour and quality before and after particle clean-up through cyclone separator. The investigated syngas flame was yellow to bluish in colour which consistent with EFB with charcoal and FR with charcoal based syngas flame. This syngas flame was also agreed with the literature reported by Rathod and Bhale (2014). There was a change investigated on syngas flame quality after passing through the cyclone separator. This indicated that particulate reduced the quality of syngas. The yellow circle (a) contained some particles and yellow circle (b) did not contain any particles. These two outlet pipes were connected to a particles separator where produced gases passed through it. Therefore, syngas flame quality changed significantly that was observed during co-gasification.

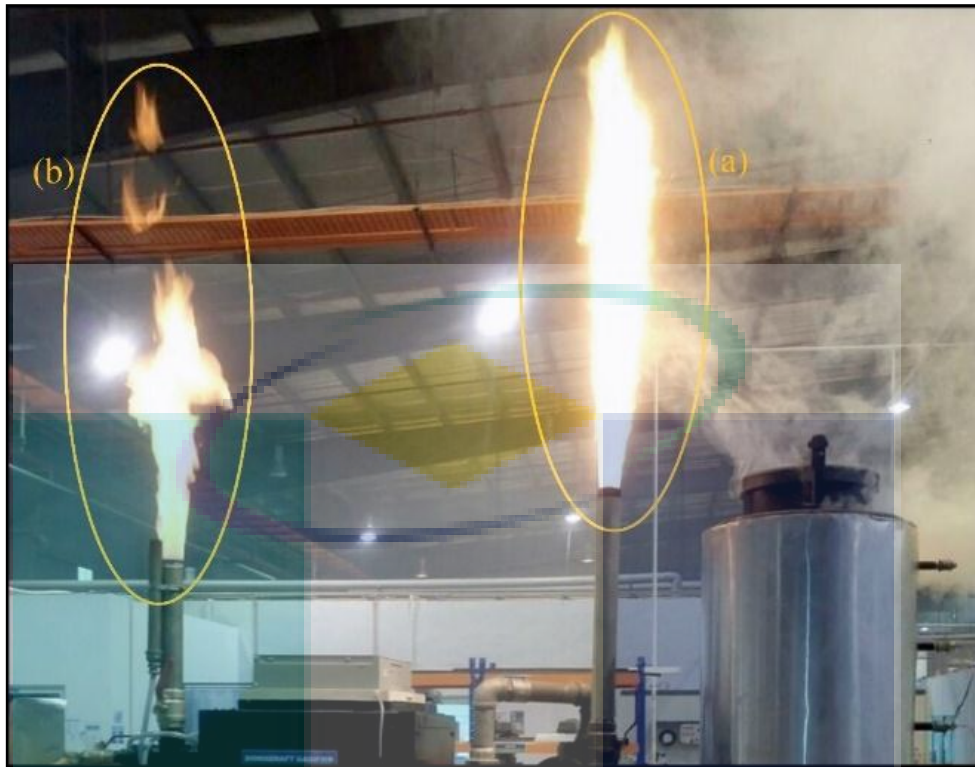


Figure 4.41 The syngas flame appearance of raw (a) and purified (b) based syngas during the co-gasification of CS (70%) and Charcoal (30%).

4.3.3.6 Effect of Coconut Shell and Charcoal Mixture on Exergy Efficiency

The exergy efficiency of syngas produced from the co-gasification of coconut shell and charcoal considering various ratios (100:0; 90:10; 80:20, 70:30 and 60:40) are shown in Figure 4.42. From this analysis, it is shown that exergy efficiency increasing with increasing the mixture of charcoal with CS. The exergy efficiencies varied from 38.95% to 62.19% when charcoal with CS was changed from 0% to 40%. It occurred because of the increasing nature of physical and chemical exergy in the syngas. As a result, the effect on reactor temperature depends on the physical exergy of the producer gas. Similar trends of exergy efficiency were consistent in the CS and charcoal based co-gasification.

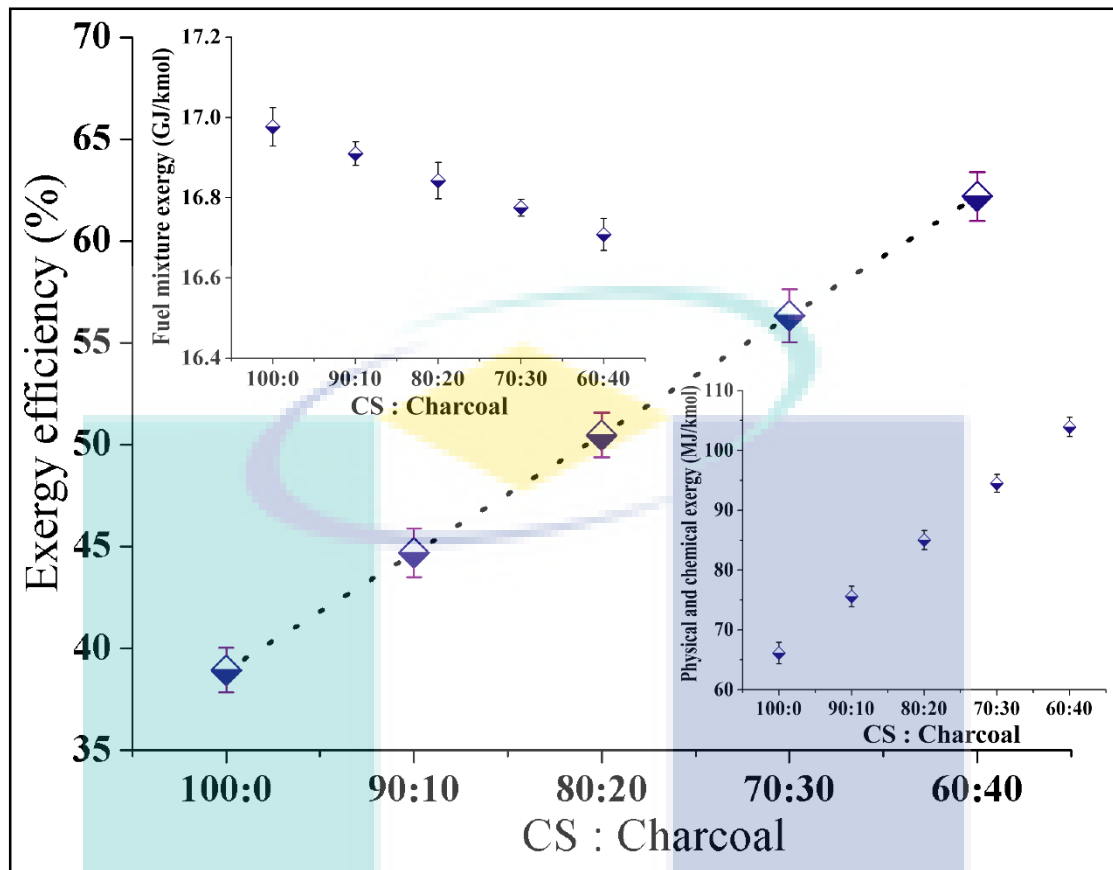


Figure 4.42 Exergy efficiency for co-gasification of CS and Charcoal with the ratios of 100:0, 90:10, 80:20, 70:30 and 60:40.

4.3.3.7 Effect of Coconut Shell and Charcoal Mixture on Syngas Heating Value

The CS and charcoal co-gasification-based heating value of product syngas are shown in Figure 4.43. The LHV and HHV for produced syngas for the CS and charcoal ratio of 0-40% are 2.81-3.27 MJ/kg and 3.00-3.49 MJ/kg, respectively which consistent with the literature value (Hagos et al., 2013; Ng et al., 2017). Furthermore, the results revealed that the LHV of the CS was lower than charcoal and the ratio of CS and charcoal increased with increasing heating value of CS and charcoal. Correspondingly, the moisture content of the feedstocks decreased when the CS and charcoal ratios changed from 0 to 40%. However, β value decreased with increasing the ratio of forest residue and charcoal ratios.

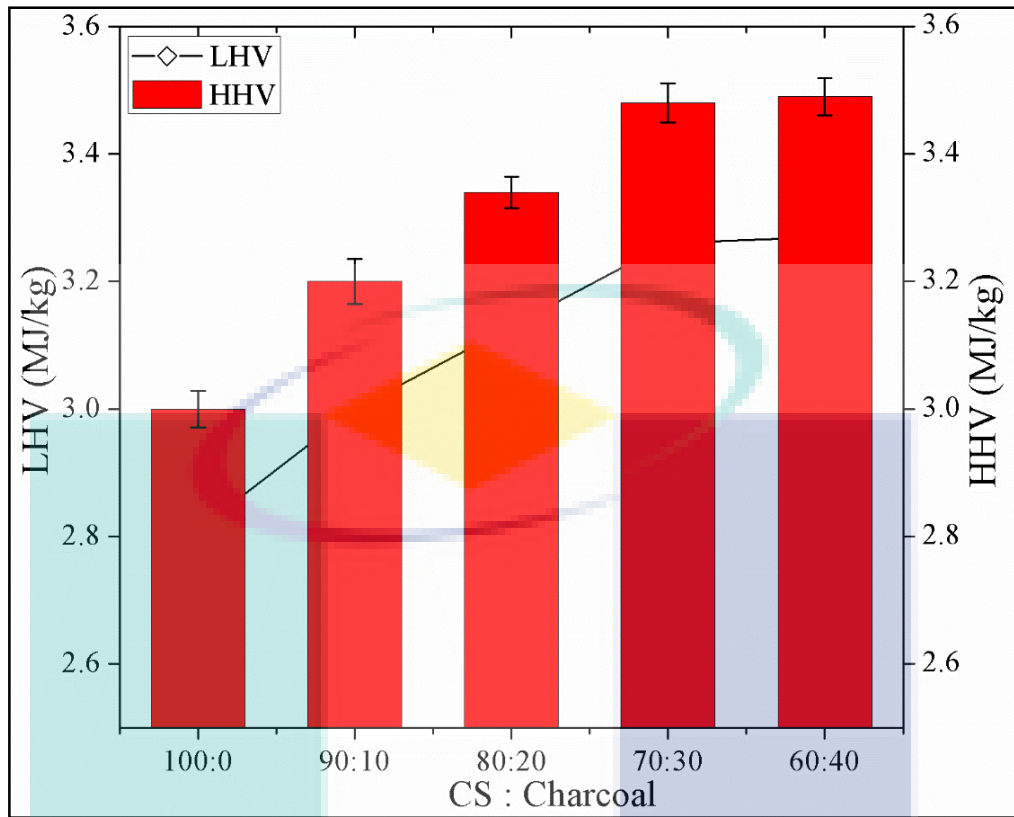


Figure 4.43 HHV (a) and LHV (b) of Syngas during the co-gasification of CS and Charcoal with various ratios (100:0; 90:10; 80:20, 70:30 and 60:40).

4.3.4 Co-product Analysis

Tar is one of the most important co-product produced from the co-gasification of biomass and charcoal. It is the mixture of several organic compounds having low or no water solubility characteristics. Generally, the presence of tar compounds affected the quality of syngas. The concentration of tar in the syngas depended on the type of feedstock, moisture content and reactor design (Rakesh & Dasappa, 2018; Valderrama Rios et al., 2018).

4.3.4.1 Tar Separation from Syngas

In this study, co-product tar was separated from raw syngas that was produced from coconut shell and charcoal-based co-gasification. The raw syngas passed through the acetone and tar sample collection process are shown in the schematic diagram (Figure 4.44).

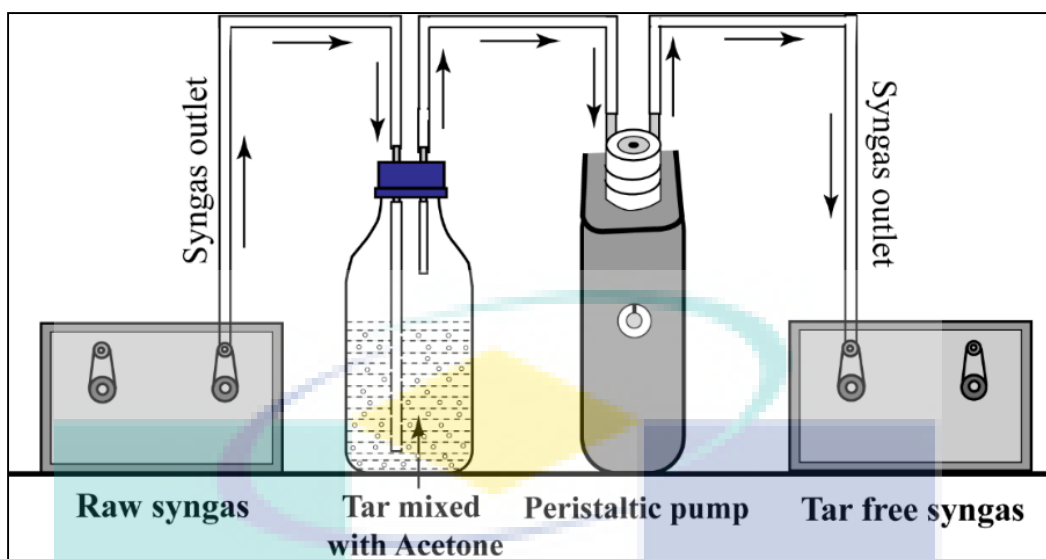


Figure 4.44 Tar separation process from raw syngas (collected from co-gasification of CS and Charcoal).

During the separation process, tar compounds were diluted when it passed through the impinger bottle that was filled with acetone. The peristaltic pump was fixed to the system to suck the raw syngas. Subsequently, tar samples were collected that was diluted with acetone. The color of the tar is thick dark liquid and high molecular weighted hydrocarbons were characterized by FTIR, SEM with EDX, GC-MS and NMR analysis.

4.3.4.2 Identification of Tar Compounds

The surface morphology and elemental composition of tar samples are shown in Figure 4.45. SEM image of the tar represents a smooth surface with minor pitting. This was occurred on the tar surface due to the release of volatile gases under pressure during the co-gasification of CS and charcoal. The major elements on tar that were identified by EDX analysis were carbon (81.76%) and oxygen (17.89%). The other elements were aluminum (0.17%), potassium (0.10%) and trace amounts of sodium, sulfur and calcium (Figure 4.45). The null amount of sulfur (0.00%) showed that it effects the environment due to pollution considering SO_x formation during the co-gasification of CS and charcoal using downdraft gasifier. Figure 4.46 represents the various peak of organic compounds of co-product tar produced from the co-gasification of CS and charcoal. Table 4.7 shows the list of tar compounds that were identified by GC-MS analysis. The main compounds are numbered in Figure 4.46 and each compound has the same number shown in Table 4.7. From this analysis, it is observed that the major identified compounds were phenolic that cover the maximum peak area (57.20%). The other significant peaks were also

identified that are shown in Figure 4.46 at the retention time of 10.824 (min), 11.441 (min), 19.305 (min), 19.502 (min) which denotes the corresponding compounds of Phenol, 3-methyl-, 2-methoxy- and Catechol (Table 4.7). Moreover, other significant compounds were also identified in the tar samples as Butyrolactone, 2-Ethylbutylamine, 2-Chloro-5,5-dimethyl-1-phenyl-3-h exen-1-ol, Acetaldehyde, 1-Hexen-3-yne, 2,5,5-trimethyl-, 5-Acetyl-2-furanmethanol, 1,3,5-Cyclooctatriene, Phenol, 4-ethyl-2-methoxy-, 1,2-Benzenediol, 4-methyl-. Some other minor peaks were also observed in Figure 4.46. The results are consistent with the literature (Pallozzi et al., 2018; Tsai, Lee, & Chang, 2006).

Table 4.7 Main chemical compounds of co-product tar produced from the co-gasification of CS and Charcoal.

Peak No	R.T. (min)	Compound name	% Area
1	4.710	Butyrolactone	1.53
2	6.606	Phenol	57.20
3	8.375	2-Ethylbutylamine	2.42
4	9.635	2-Chloro-5,5-dimethyl-1-phenyl-3-h exen-1-ol	2.99
5	10.824	Phenol, 3-methyl-	5.42
6	11.441	Phenol, 2-methoxy-	4.61
7	12.039	Acetaldehyde	1.05
8	15.615	1,1-Difluoro-2-methyl-2-methoxycyclopropane	0.85
9	16.970	1-Hexen-3-yne, 2,5,5-trimethyl-	1.58
10	18.185	Naphthalene	1.20
11	18.707	Creosol	2.41
12	19.305	Catechol	6.17
13	19.502	Catechol	4.02
14	24.477	5-Acetyl-2-furanmethanol	1.29
15	25.069	1,3,5-Cyclooctatriene	1.58
16	26.443	Phenol, 4-ethyl-2-methoxy-	2.10
17	26.799	1,3,5,7-Cyclooctatetraene	0.34
18	28.192	1,2-Benzenediol, 4-methyl-	2.70
19	29.268	2-Pentanone	0.54

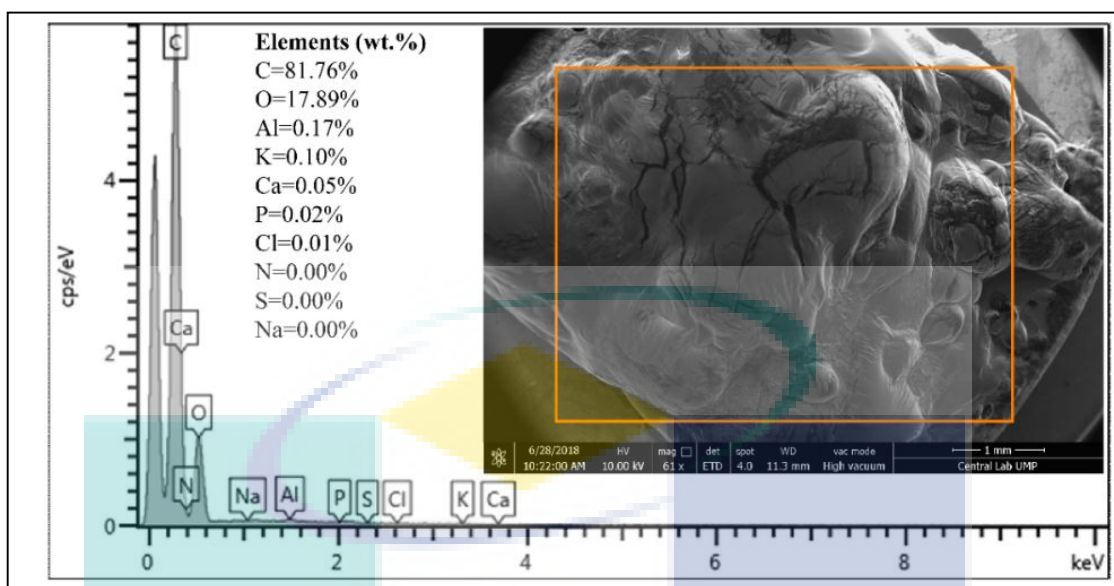


Figure 4.45 SEM image with EDX of raw co-product tar produced from co-gasification of CS and Charcoal in the downdraft reactor.

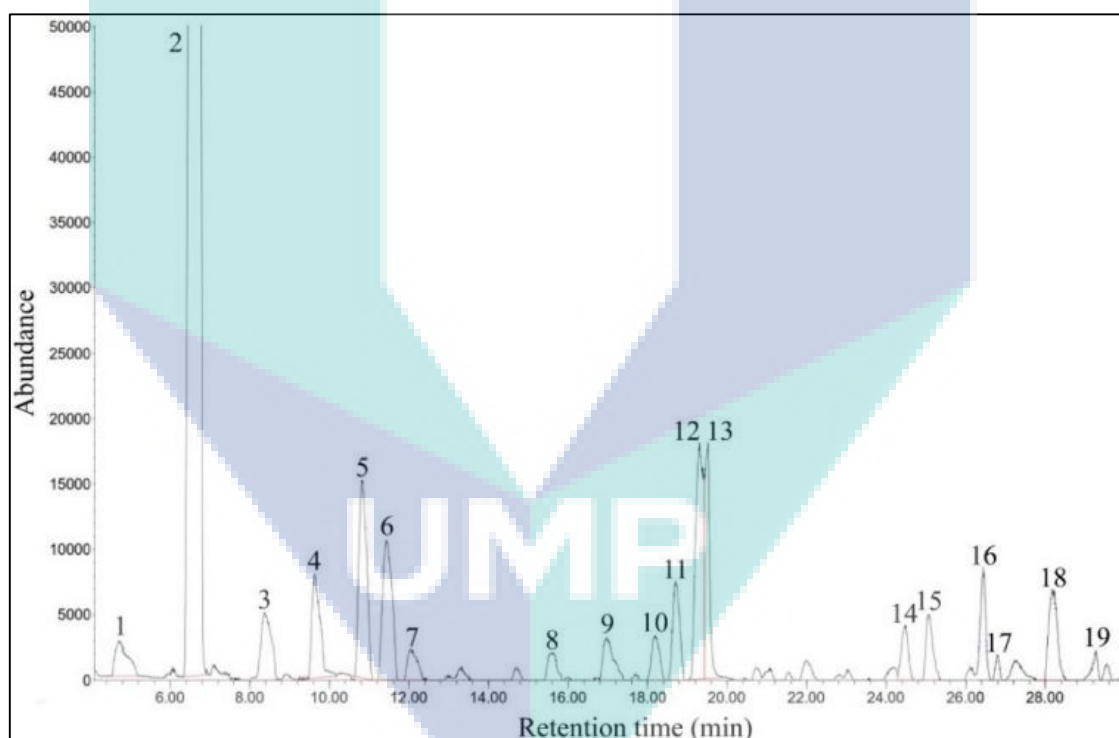


Figure 4.46 GC-MS chromatogram of co-product tar produced from the co-gasification of CS and Charcoal.

The normalized integration spectra of ^{13}C NMR and ^1H NMR for the co-gasification-based co-product of tar are shown in Table 4.8. In the ^{13}C NMR spectra analysis of tar represents 100-157 ppm (aromatic region), indicated various types of carbon to -OH in phenolic compounds. Similar spectra were also observed in the literature (Michel et al., 2011; Wang, Jin, Liu, Zhu, & Hu, 2013). Observing the spectra of aromatic

hydrogen from ^1H NMR (Table 4.8), it is shown that the co-product tars are rich in aromatic hydrogen. The detection of tar compounds by GC-MS analysis agreed on this study to identify the main peaks in ^{13}C and ^1H NMR analysis. Due to the effect of little concentration on chemical shifts makes the quantitative analysis of the spectra difficult. However, several signals can be assigned and were related to the main peaks observed by GC-MS analysis: Phenols, Butyrolactone, 2-Chloro-5, 5-dimethyl-1-phenyl-3-h exen-1-ol, 2-Ethylbutylamine and Naphthalene. Undeniably, both ^{13}C NMR and ^1H NMR analyses agreed the results obtained in GC-MS. The ^{13}C and ^1H NMR analytical peak curves are attached in the Appendix C.

Table 4.8 ^{13}C NMR and ^1H NMR data of co-product tar compounds generated from co-gasification of CS and Charcoal.

Peaks	^{13}C NMR (δ_{C} ppm)	^1H NMR (δ_{H} ppm)
1	55.695	0.658
2	115.203	1.069
3	118.360	2.720
4	119.199	3.607
5	119.788	5.037
6	129.334	5.071
7	131.798	6.568
8	137.741	6.583
9	148.664	6.598
10	155.079	6.613
11	157.464	6.704
12	166.676	6.958
13	-	7.683
14	-	7.700
15	-	8.147
16	-	8.495

From the above analysis, various types of organic compounds were found in the co-product tar. The main components of the tar were phenols, Butyrolactone, 2-Chloro-5, 5-dimethyl-1-phenyl-3-h exen-1-ol, 2-Ethylbutylamine and Naphthalene in the biomass as shown in Table 4.7 and Table 4.8. A conclusion has been reached by several researchers (Al-Rahbi & Williams, 2017; Pallozzi et al., 2018; Tsai et al., 2006; Xu et al., 2016) that the water phase exists in oxygenated organic components was separated during the co-gasification process. Therefore, it is suggested that the water phase are needed to be remove from the component to produce clean and sustainable energy.

4.3.4.3 Effect of Thermal Cracking on Tar

The thermal effect on co-product of tar sample was observed at the temperature of 700 °C, 800 °C, 900 °C and 1000 °C (Figure 4.47 and Figure 4.48)

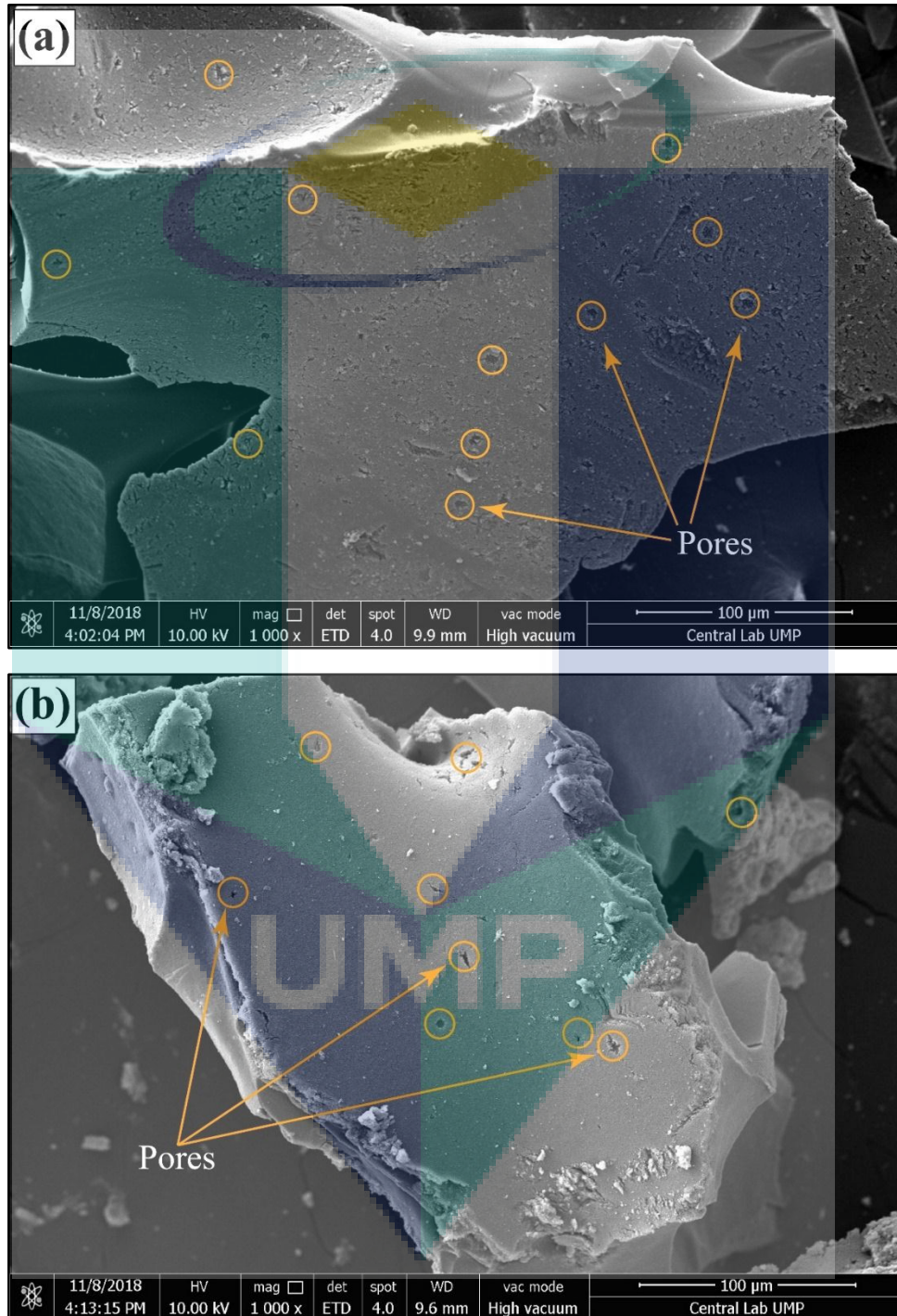


Figure 4.47 SEM images of tar samples after thermal treatment: (a) at 700 °C (b) at 800 °C.

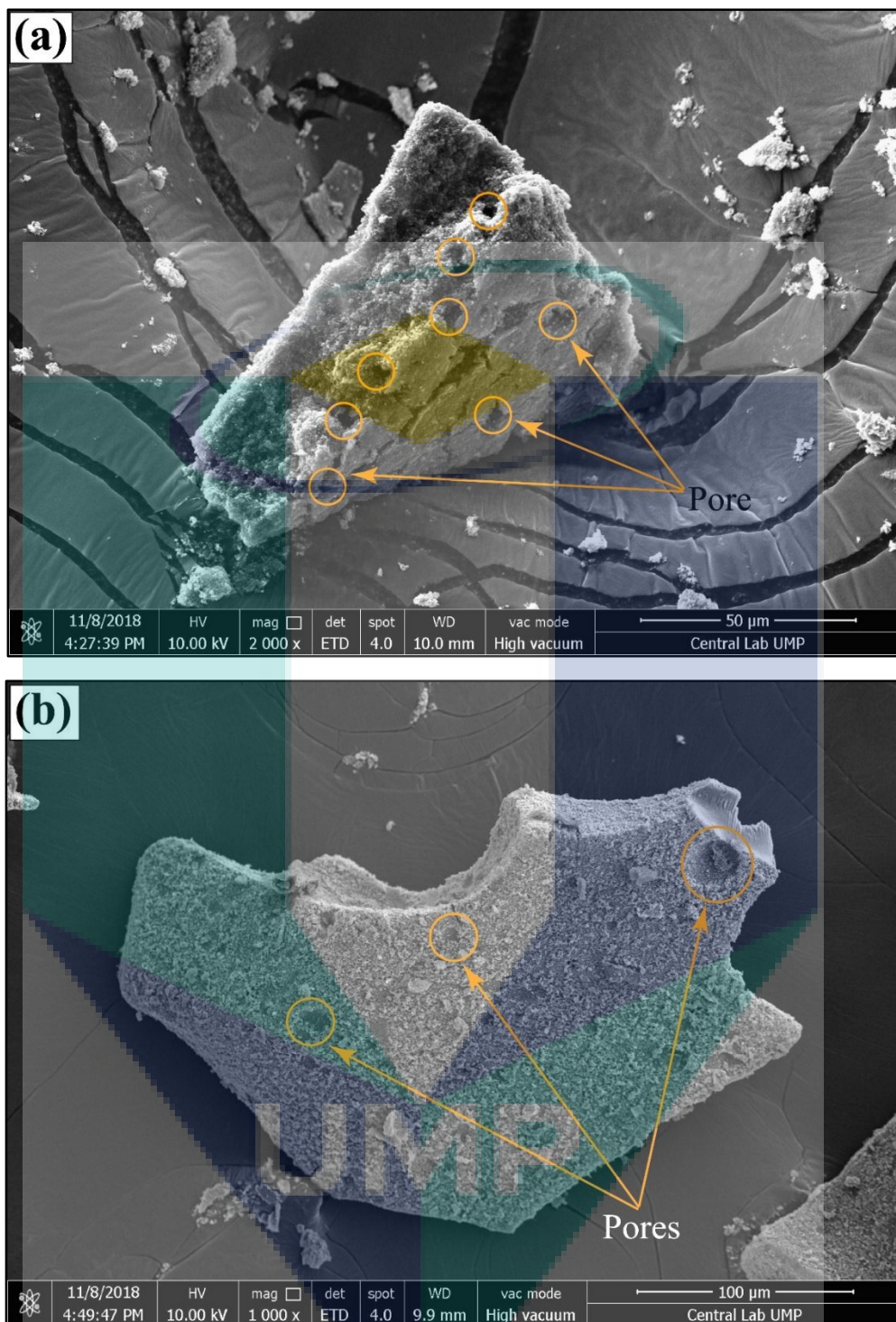


Figure 4.48 SEM images of tar samples after thermal treatment: (a) at 900 °C (b) at 1000 °C.

The morphological changes occurred due to thermal effect and surface of the tar observed significantly. The SEM image of tar shows that the roughness of tar surface increases significantly with increasing of temperature. The morphological changes were compared with the raw tar sample as shown in Figure 4.45. Figure 4.49(a) represents the

FTIR spectra of raw tar sample obtained from the co-gasification process (CS and Charcoal). The raw FTIR spectra were compared with the thermal-cracked tar samples considering the temperatures of 700 °C, 800 °C, 900 °C and 1000 °C.

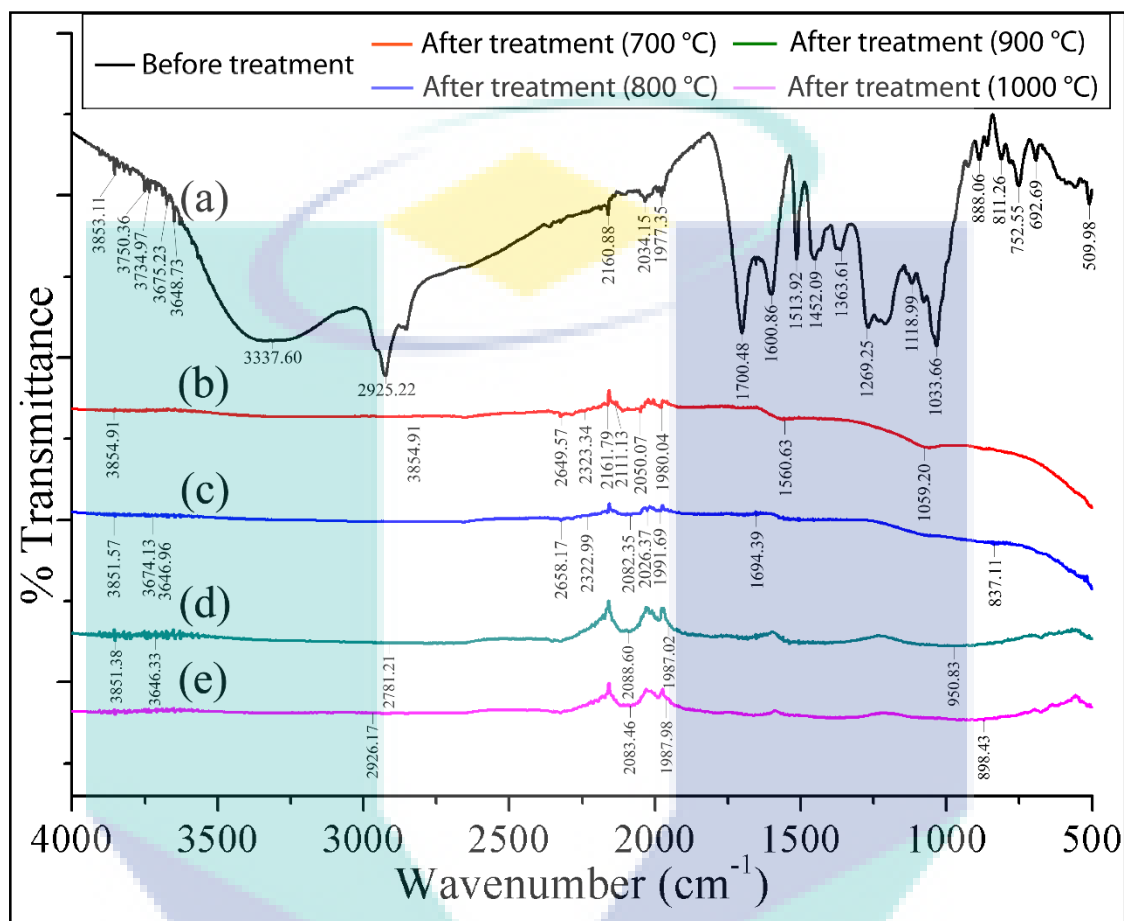


Figure 4.49 FTIR spectra of tar sample obtained from the co-gasification process: (a) before thermal treatment (b) thermal treatment at 700 °C (c) thermal treatment at 800 °C (d) thermal treatment at 900 °C and (e) thermal treatment at 1000 °C.

The spectral band for raw tar sample at 3337.60 cm^{-1} represents OH stretching. The bands located in 2925.22 cm^{-1} corresponding to the distribution of aliphatic CH_2 groups. A smaller band at 1452.09 cm^{-1} was investigated for the symmetric bending of CH_2 . The bands at 1363.61 cm^{-1} matched to the distribution of aliphatic CH_3 groups. Moreover, C=C ring stretching bands at 1600.86 cm^{-1} and 1513.92 cm^{-1} is also present in tar sample. In the presence of phenol, it is known that this band is strongly exalted. These bands are consistent with the literature value reported by Michel et al. (2011). In addition, the infrared spectra show the presence of phenolic compounds (Figure 4.49). According to this analysis, same functional groups were found in all experiments.

Therefore, from these analyses, it is clearly shown that due to thermal effect (700 °C to 1000 °C) high molecular compounds (functional groups) were reduced. In conclusion, it is suggested that syngas could be tar free by applying the thermal cracking technique. These results are also consistent with the SEM images analysis.

4.3.5 By-product Analysis

The most important by-product of biomass and charcoal co-gasification are charcoal. The characterization results are already mentioned in the characterization results section. To give the valorization of this by-product charcoal, selected biomass (EFB, CS and CS) are the best mixture to achieved yield. The by-product charcoal was characterized using XRF analysis to know the detailed elements and oxide groups (Figure 4.50).

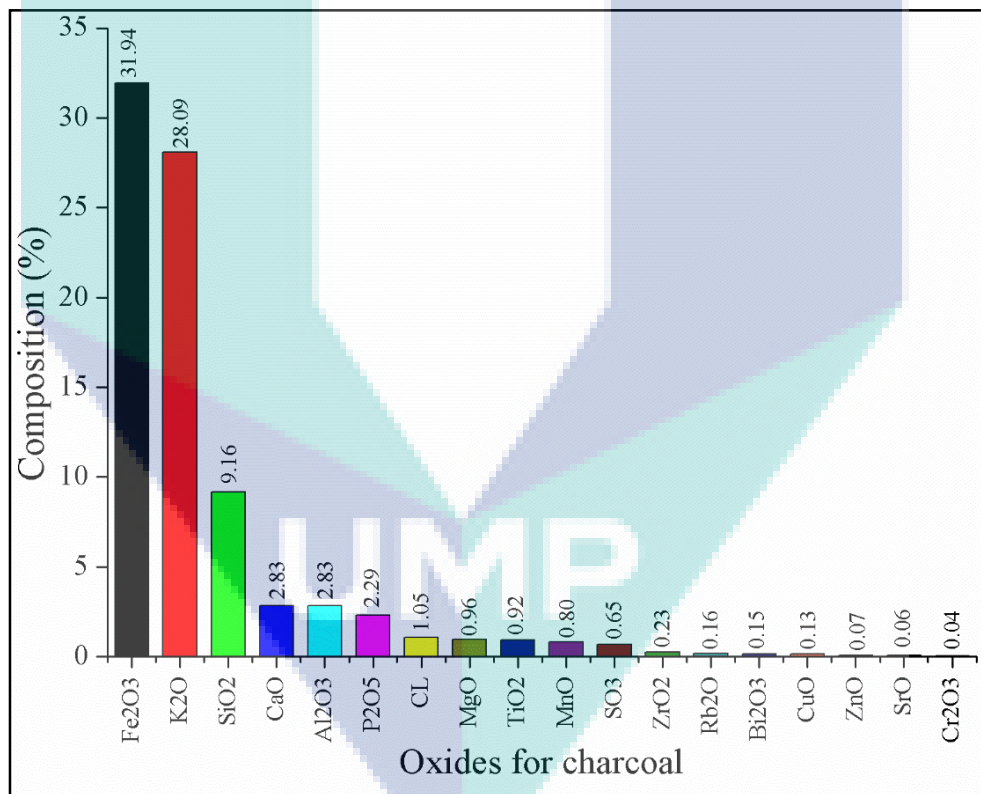


Figure 4.50 Oxides of by-product of charcoal produced from co-gasification of biomass and charcoal.

The aims of this characterization were feasible for syngas fermentation process which was the nutrient for biocatalysts (yeast and bacteria). In this study, forest residue and charcoal co-gasification-based charcoal were characterized using XRF. Various oxides of charcoal are shown in Figure 4.50. In this analysis (Figure 4.50), it was also

observed that major oxides were detected in the charcoal. The major oxides were Fe_2O_3 (31.94%), K_2O (28.09%), SiO_2 (9.16%), CaO (2.83%), Al_2O_3 (2.83%), P_2O_5 (2.29%). The other oxides were MgO , TiO_2 , MnO , SO_3 , ZrO_2 , CuO , ZnO that were less than 1%.

4.3.6 Comparative Study on Co-gasification

In this study, there were three different co-gasification processes (EFB with charcoal, forest residue with charcoal and coconut shell with charcoal) were compared to each other. The comparative study was investigated based on syngas concentration, cold gas efficiency, carbon conversion efficiency and heating value of syngas focused on its bioenergy potential.

4.3.6.1 Syngas (H_2 , CO , CO_2 and CH_4) Concentration

Figure 4.51 represents a comparative study of syngas concentration on the co-gasification of EFB with charcoal, FR with charcoal and CS with charcoal. The produced syngas comprises of combustible gases of H_2 , CO , CH_4 and non-combustible gases of CO_2 , N_2 compounds. The carbonaceous materials of EFB of palm oil, forest residue, coconut shell and charcoal with the controlled amount of gasifying medium of between $25\text{--}35 \text{ Nm}^3\text{h}^{-1}$ at higher temperature ranges from $950 \text{ }^\circ\text{C}$ to $1050 \text{ }^\circ\text{C}$ converted gaseous fuel of syngas (H_2 , CO , CO_2 and CH_4). Previous study and literature agreed with the syngas concentration obtained (Kalita & Baruah, 2018; Ng et al., 2017; Patel et al., 2017; Ramos et al., 2018).

In this comparative study, it is shown that the highest H_2 concentration was produced in FR and charcoal based co-gasification. The lowest H_2 concentration was formed in EFB and charcoal based co-gasification. On the other hand, CS and charcoal based H_2 production was higher than EFB based co-gasification and lower than FR based co-gasification. The trend of CO concentration was relatively the same as that of H_2 concentration of all co-gasification. Very interesting concentration of CO_2 was observed in the CS based co-gasification, whereas the other two co-gasification produced more CO_2 than CS and charcoal based co-gasification. The CH_4 concentration was almost similar in FR and CS based co-gasification. In contrary, EFB based co-gasification produced a relatively low concentration of CH_4 . The variation of this concentration was due to the feedstock's size, moisture content, composition, density and reaction temperature.

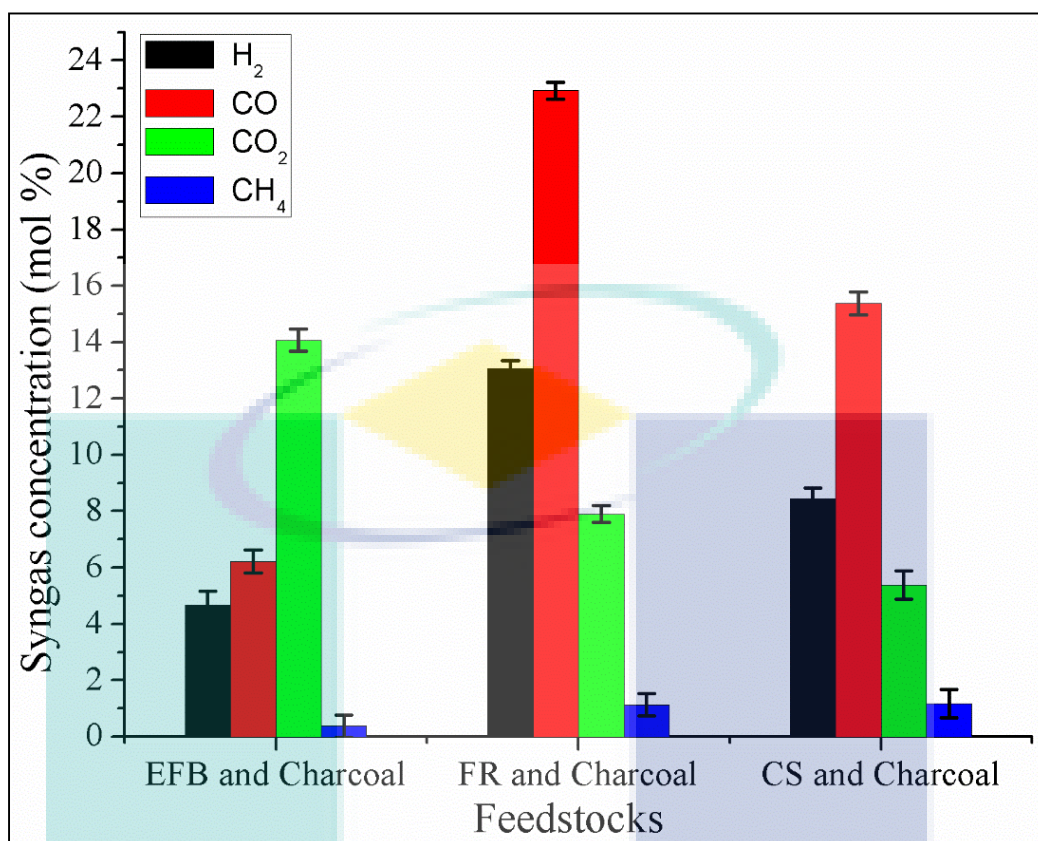


Figure 4.51 Comparative study on syngas concentration on the co-gasification of EFB with charcoal, FR with charcoal and CS with charcoal (70:30).

4.3.6.2 Cold Gas Efficiency and Carbon Conversion efficiency

The cold gas efficiency was compared with three different co-gasification processes of EFB with charcoal, FR with charcoal and CS with charcoal with biomass and charcoal ratio of (70:30) is shown in Figure 4.52. The highest cold gas efficiency was observed in FR with charcoal-based co-gasification. On the other hand, the lowest cold gas efficiency was found in EFB based co-gasification. The comparatively low cold gas efficiency was observed in CS based co-gasification with respect to FR based co-gasification. The comparative study on carbon conversion efficiency is shown in the following graphical representation (Figure 4.53).

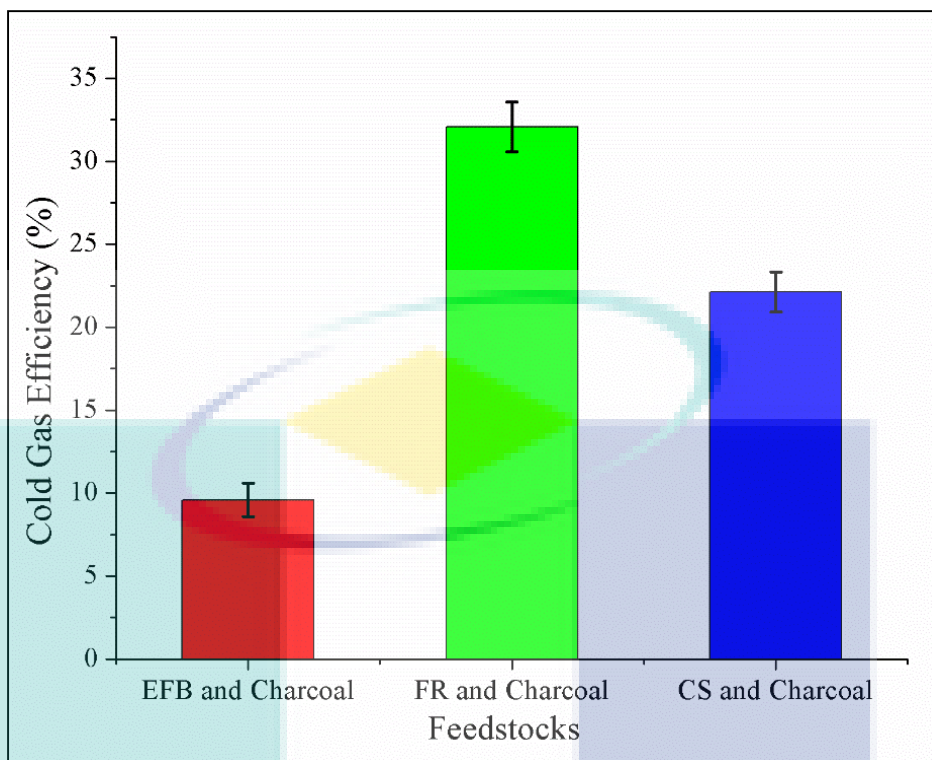


Figure 4.52 Comparative study on cold gas efficiency on the co-gasification of EFB with charcoal, FR with charcoal and CS with charcoal (70:30).

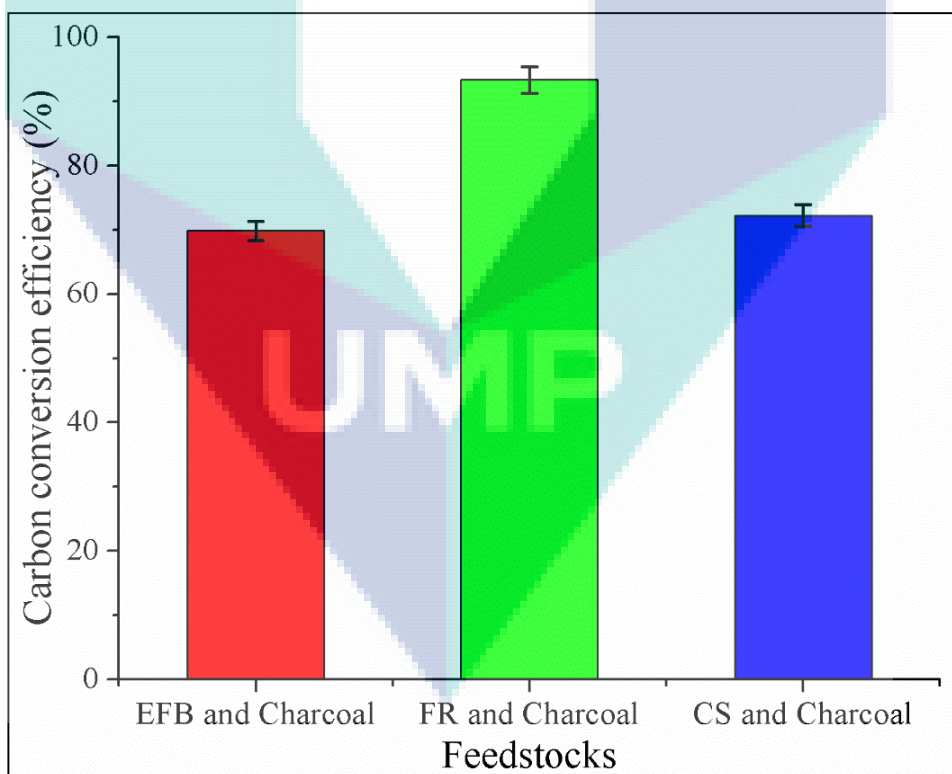


Figure 4.53 Comparative carbon conversion efficiency on the co-gasification of EFB with charcoal, FR with charcoal and CS with charcoal (70:30).

In this analysis, it is shown that the highest carbon conversion efficiency was found during the FR and charcoal co-gasification of 93.34%. The carbon conversion efficiency was relatively the same in the co-gasification of EFB with charcoal and CS with charcoal of about 69.89% and 72.25%, respectively. This results agreed with the literature reported by Valdés et al. (2015).

4.3.6.3 Heating Value of Syngas

The HHV and LHV were calculated using Eq. 3.3 and Eq. 3.4 from produced syngas and were compared with each co-gasification as shown in Figure 4.54. In this comparative study, it was shown that the heating value (HHV and LHV) of the produced syngas was higher in FR and charcoal-based co-gasification (5.02 MJ/Nm^3 , 4.70 N/m^3) than EFB with charcoal co-gasification (1.53 MJ/Nm^3 , 1.42 N/m^3) and CS with charcoal-based co-gasification (3.48 MJ/Nm^3 , 3.27 N/m^3). These results are in good agreement with the previous study and literature value (Shahbaz et al., 2017).

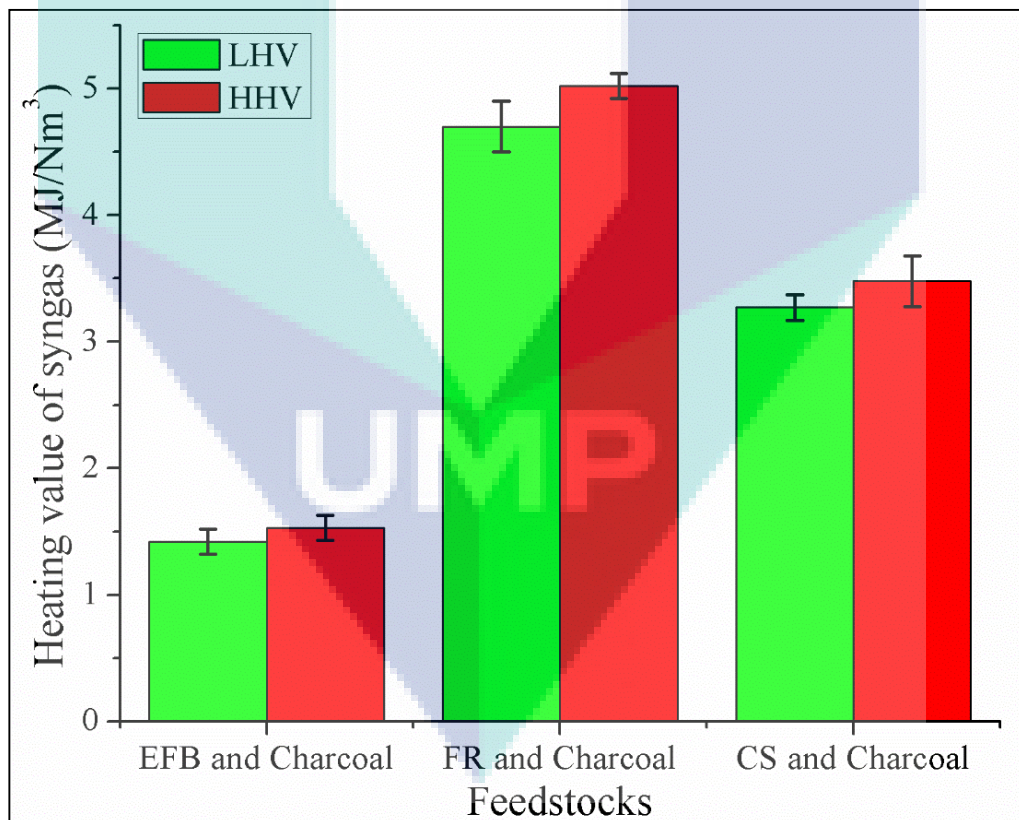


Figure 4.54 Comparative study on the heating value of syngas on the co-gasification of EFB with charcoal, FR with charcoal and CS with charcoal (70:30).

4.4 Bioethanol Production Through Syngas Fermentation

Biofuel production through syngas fermentation using biocatalysts (*S. cerevisiae* and *C. butyricum*) in a tar free bioreactor has been performed. The cell growth of *S. cerevisiae* and *C. butyricum* were cultured for syngas fermentation. The optimized parameters for syngas fermentation were investigated. Finally, bioethanol was separated and analyzed by GC-MS and NMR (^1H) analysis.

4.4.1 Biocatalysts Preparation and Characterization

4.4.1.1 *Saccharomyces Cerevisiae*

The freshly cultured *S. cerevisiae* was prepared for syngas fermentation is as shown in Figure 4.55. In this figure, it is revealed that the fresh cell growth was cultured both in slant and petri dish. This type of microorganism has the ability to take nutrients and maintained some limiting conditions for the production of bioethanol.

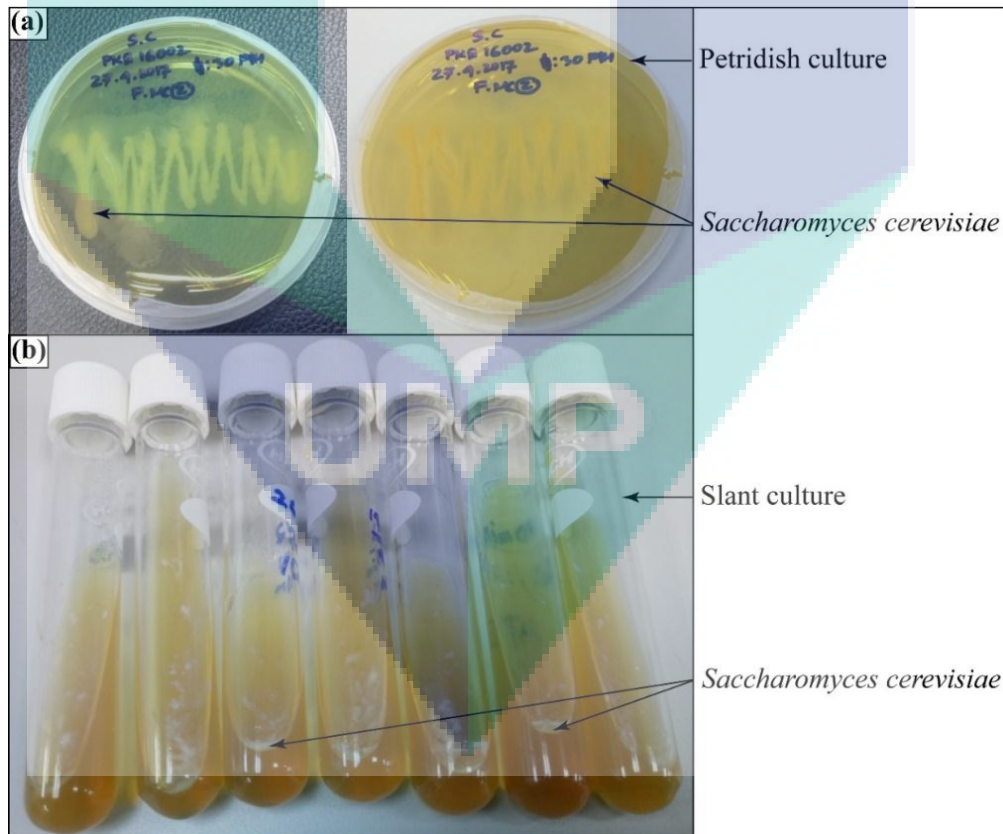


Figure 4.55 Growth Culture of *S. cerevisiae* in Petridish and Slant.

The newly cultured *S. cerevisiae* was characterized for the confirmation of the specific types of microbes. Figure 4.56 represents the *S. Cerevisiae* which was taken from FESEM analysis.

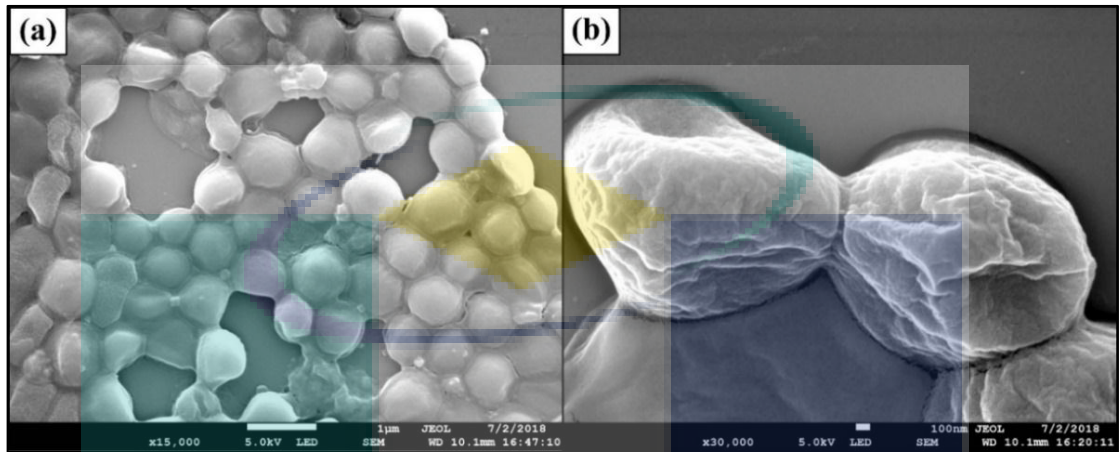


Figure 4.56 FESEM images of *S. cerevisiae*: (a) group of the colony (b) single colony.

From this morphological analysis of *S. cerevisiae*, it is shown that the surface of the cell body is smooth and the shape of the body was spherical. The FESEM images of *S. cerevisiae* colony is consistent with the literature reported by Zhao, Lin, and Chen (2018). Therefore, this freshly cultured *S. cerevisiae* was capable for the syngas fermentation and suited for the production of bioethanol.

4.4.1.2 *Clostridium Butyricum*

The liquid medium prepared and the cell cultured was used for further syngas fermentation is shown in Figure 4.57. The *C. butyricum* cell growth was freshly cultured under the incubator maintained at an optimized parameter of temperature (37 °C). The changes in medium colour after inoculum of *C. butyricum* is clearly shown in Figure 4.57. For the confirmation of *C. butyricum* FESEM analysis was performed which is shown in Figure 4.58. This FESEM images indicated that the *C. butyricum* was cultured effectively and suited for further syngas fermentation. The morphological characteristics of *C. butyricum* was also consistent with the literature reported by Li, Tian, and Dong (2019).

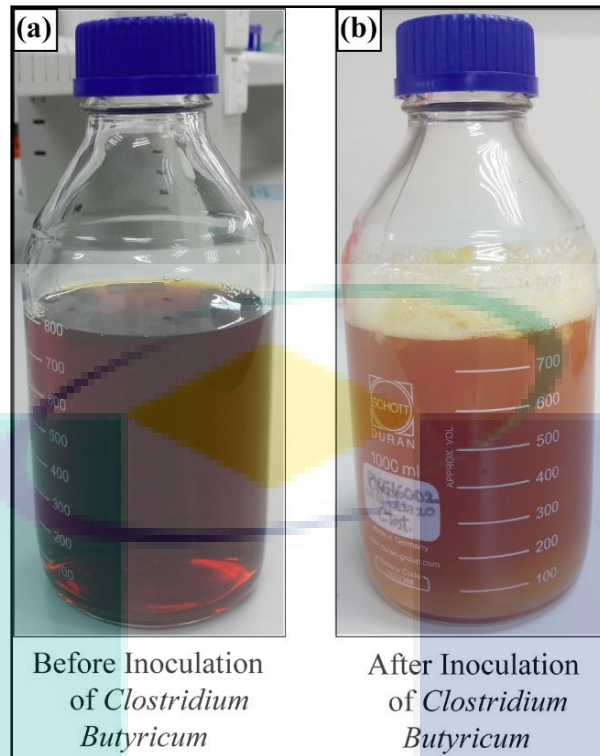


Figure 4.57 Growth Culture of *C. butyricum*: (a) before inoculation (b) after inoculation at 37 °C for 24 h.

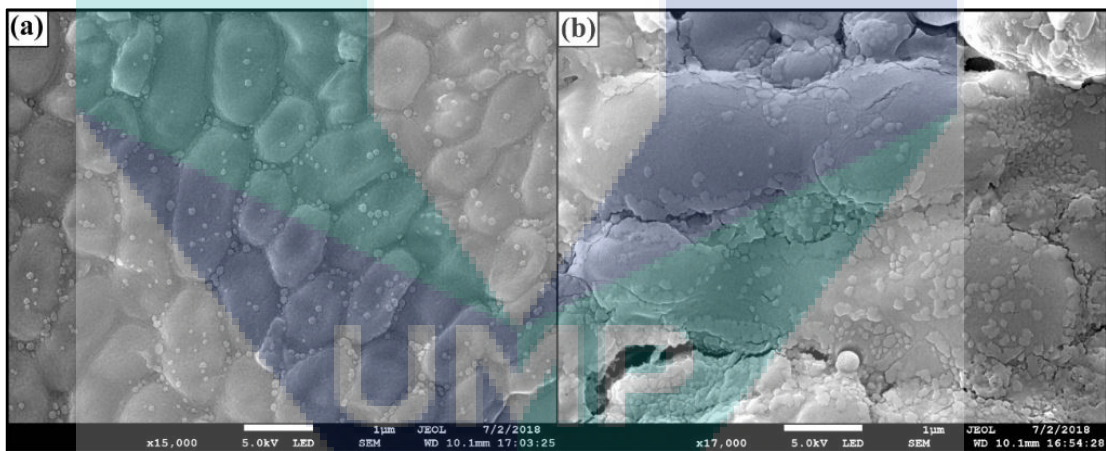


Figure 4.58 FESEM images of *C. butyricum*: (a) group of the colony (b) single colony.

4.4.2 Effect of Syngas Fermentation

The syngas fermentation processes were carried out using both *S. cerevisiae* and *C. butyricum* in a TFB reactor. The following effects were investigated throughout the syngas fermentation processes.

4.4.2.1 Effect of Treated and Untreated Syngas on Microbial Cell Growth

The treated and untreated syngas effect on the growth of *S. cerevisiae* and *C. butyricum* were observed throughout the syngas fermentation process are shown in Figure 4.59 and Figure 4.60. The syngas fermentation run for 16 days and the microbial colony was counted every 24h interval. The untreated syngas and treated syngas were used in this experiment.

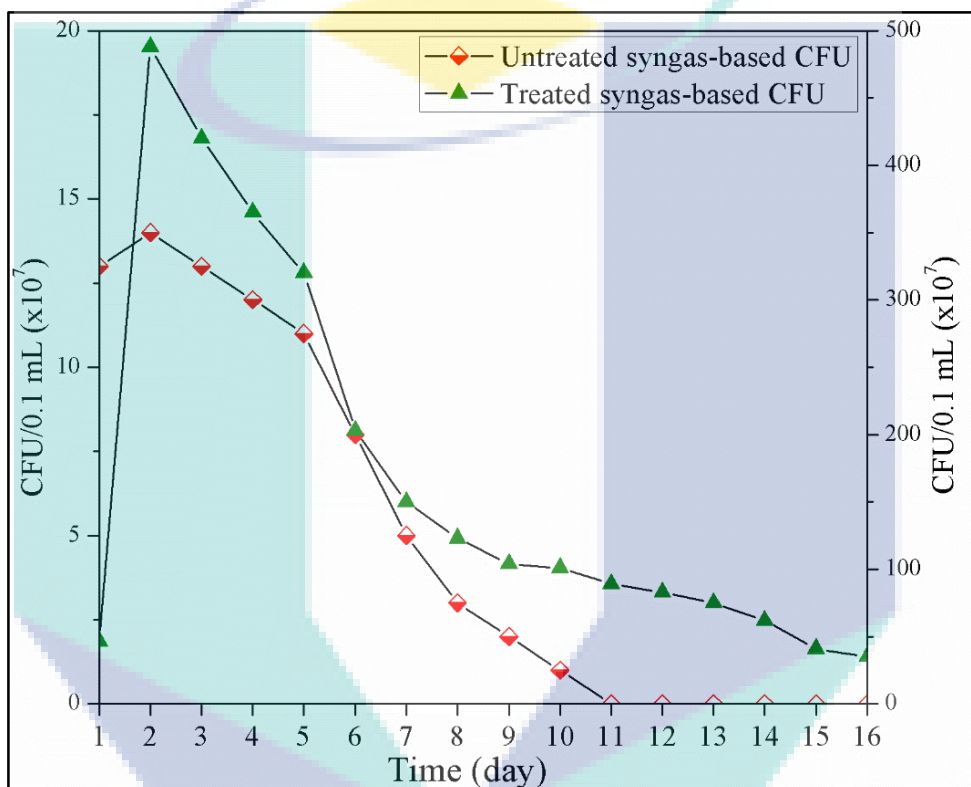


Figure 4.59 Effect of treated and untreated syngas on CFU during *S. cerevisiae* based syngas fermentation.

In this study, it is shown that there was a significant effect on untreated syngas-based fermentation. Initially, the colony of *S. cerevisiae* and *C. butyricum* increased slightly (Figure 4.59 and Figure 4.60). After 2 (two) days it was found that the cell growth trends decreased suddenly. Subsequently, the growth of the cell rapidly decreased until 10th day. After that, no microbial cells were observed in the fermentation broth. Therefore, considering this analysis syngas fermentation was performed by using tar free bioreactor (TFB). The facilities of this bioreactor were high molecular weight tar compounds and particles that were purified of untreated syngas before introduced in the fermentation broth. The effect of CFU on the cell growth of *S. cerevisiae* and *C. butyricum* is shown

in Figure 4.59 and Figure 4.60. The most remarkable trends observed for both experiments when treated syngas was used.

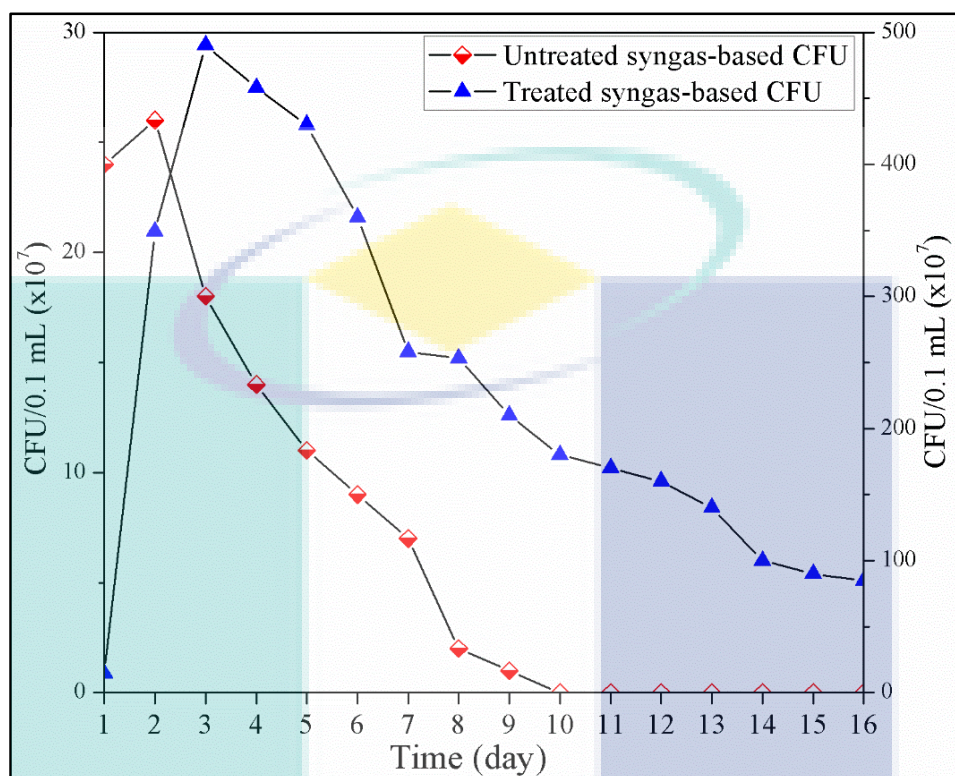


Figure 4.60 Effect of treated and untreated syngas on CFU during *C. butyricum* syngas fermentation.

The maximum growth of *S. cerevisiae* was investigated at 2nd day and *C. butyricum* was observed on 3rd day which was around 15 times higher microbial colony than untreated based syngas fermentation (Figure 4.59 and Figure 4.60). The reducing trend in microbial cell growth was similar in both species. However, the cell growth rate was abruptly increased at 1st and 2nd day during syngas fermentation which indicated significant log phase. Subsequently, the microbial growth was slowly decreased until 16th days. Therefore, maximum microbial growth was responsible for bioethanol production using treated syngas. Similar effect was also found in the literature as reported by Xu et al. (2011).

4.4.2.2 Effect of Temperature on Microbial Cell Growth

The temperature effect was investigated on the microbial cell growth during syngas fermentation. The graphical representation in Figure 4.61 shows that the maximum microbial growth was at a temperature of 37 °C. Therefore, based on the

optimum temperature, the whole fermentation was performed at 37 °C for achieving the maximum yield of bioethanol.

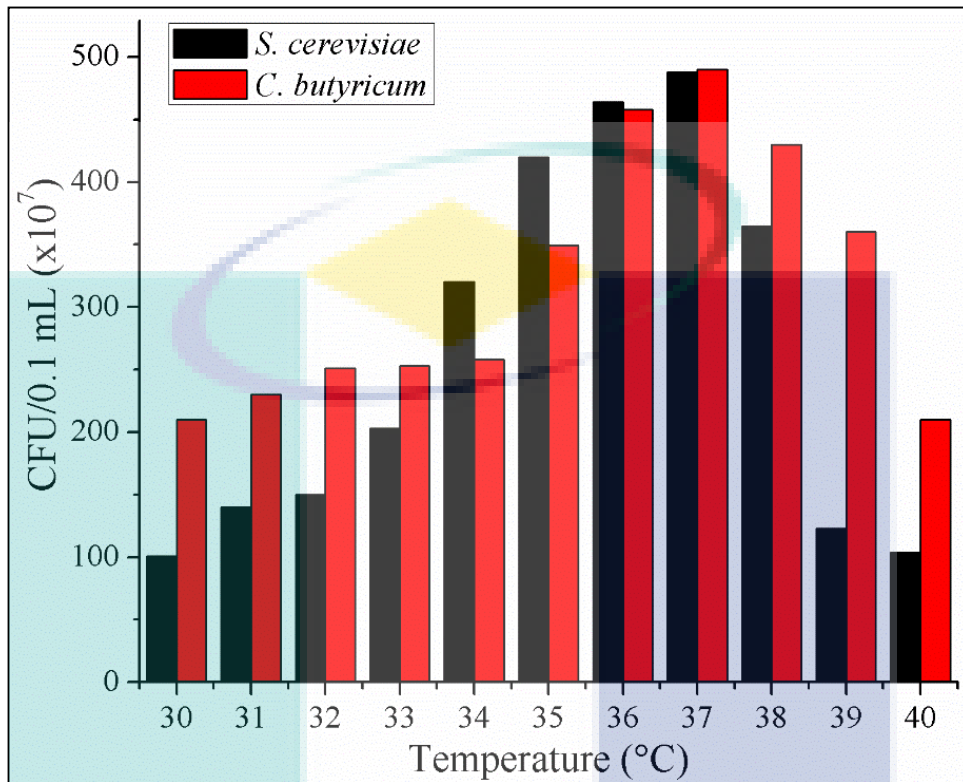


Figure 4.61 Temperature effect on syngas fermentation.

4.4.2.3 Effect of pH on Microbial Cell Growth

The effect of pH on the whole fermentation process for both microbial syngas fermentation was observed. The initial pH set for *S. cerevisiae* and *C. butyricum* was 6.7 and 5.4 respectively. Figure 4.62 shows that pH was reduced around 5.6 and 4.4 respectively at the end of the process (16th day). In both cases, the pH level was reduced from the initial value. After 10th day, the pH level was gradually decreased and no significant changes were observed on the pH value. In the literature, it was reported that the ability of acetic acid generation was reduced when the pH value was around 4.5 and bioethanol concentration was not increased when pH decreased to 4.5 (Asimakopoulos et al., 2018).

The cell growth process occurred in an optimum growth at the pH value of 5.0 to 7.0 and carbon source from syngas was transferred to a cell, bioethanol or another organic acid as it was identified in this process. The growing cell tends to use liquid carbon source (charcoal mixed with fermentation broth) and a gas phases carbon sources such as syngas

or CO, CH₄ and CO₂. Moreover, the initial medium of pH had significant effects on the metabolism process of *S. cerevisiae* and *C. butyricum*. More acidic pH level lead to slower growth rates and lower bioethanol yields (Asimakopoulos et al., 2018). Thus, pH is one of the most important factors for bioethanol production.

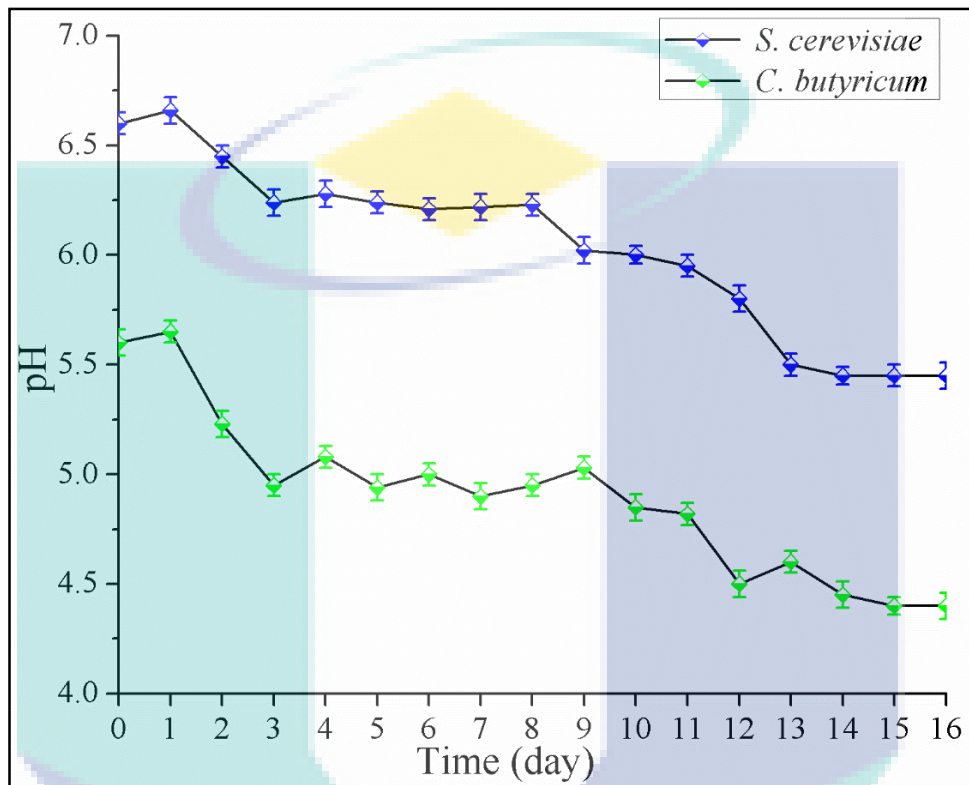


Figure 4.62 Effect of pH on syngas fermentation.

4.4.2.4 Effect of Time (day) on Total Organic Carbon (TOC)

The total organic carbon (TOC) was also monitored and analytical results are shown in Figure 4.63. The organic carbon content reduced from the initial to the final stage of the experiment. The syngas and charcoal were the main sources of carbon for both *S. cerevisiae* and *C. butyricum* based on syngas fermentation. These microbes were taken as carbon sources gradually throughout the whole process. It is indicated that microbes received carbon from syngas slowly until the 16th day.

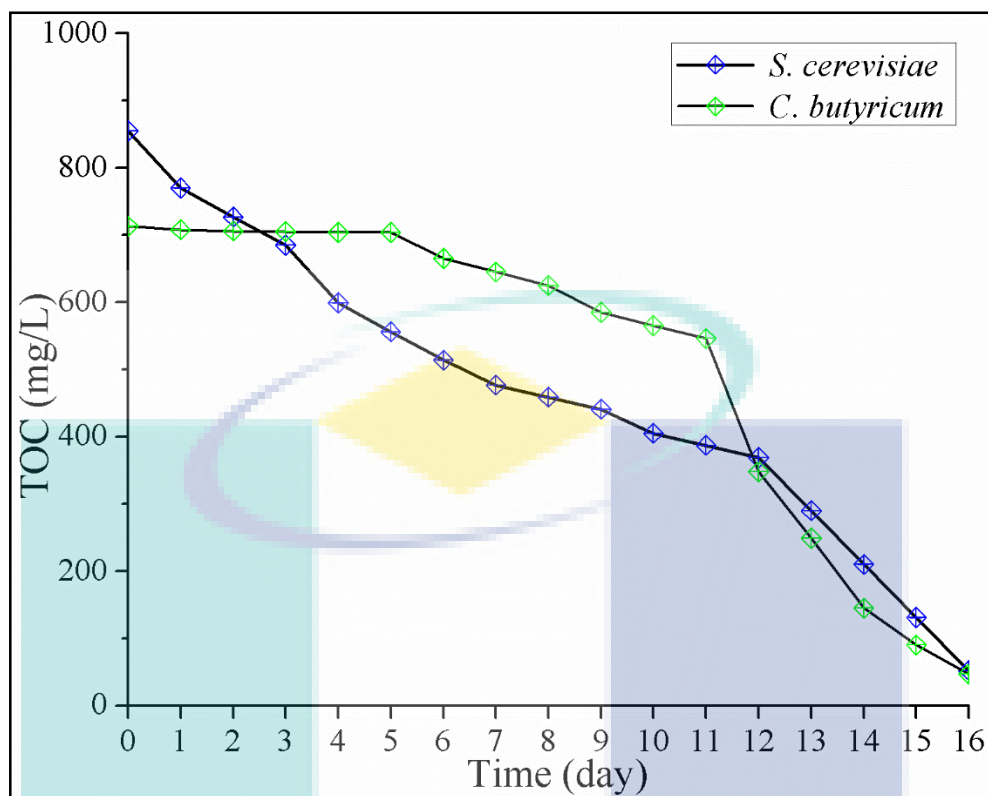


Figure 4.63 Effect of TOC on syngas fermentation.

During syngas fermentation, it was observed that the microbes died due to the reduction of carbon sources slowly. Thus, during their lifetime bioethanol was produced which was detected by GC-MS and NMR (^1H) analysis (Figure 4.65 and Figure 4.66).

4.4.2.5 Effect of Fermentation on Syngas Composition

The effect of syngas composition on syngas fermentation was observed in Figure 4.64. The syngas composition for fermentation was H_2 -13.05%, CO -22.92%, CO_2 -7.9% and CH_4 -1.13% that was derived from FR (70%) and charcoal (30%) based co-gasification. From both *S. cerevisiae* and *C. butyricum* based syngas fermentation, it is clearly shown that most of the carbon from CO , CO_2 and CH_4 were mixed with fermentation broth, and microbes taken that carbon enormously. At the end of the fermentation, the rest of the gases were analyzed and found except the CO_2 , the other two gases were dissolved completely (Figure 4.64, Appendix E). From this analysis, it also indicated that both microbes successfully taken the carbon nutrient from the syngas and produced bioethanol which was detected by GC-MS and NMR analysis (Figure 4.65 and Figure 4.66).

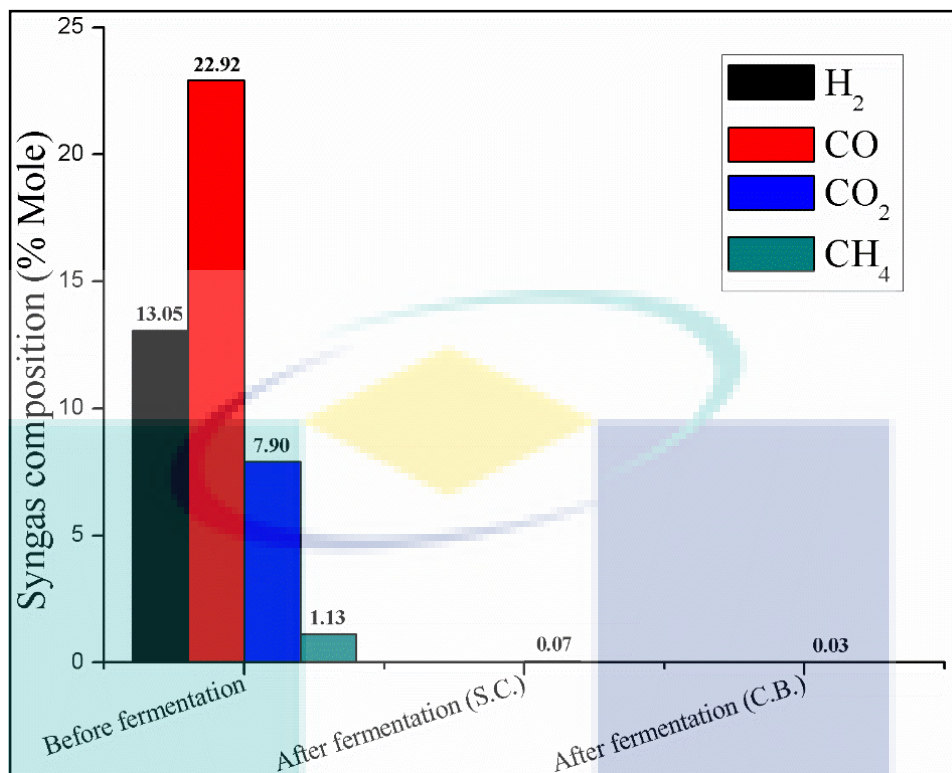


Figure 4.64 Effect of syngas composition before and after syngas fermentation.

4.4.3 Bioethanol Production and Analysis

Bioethanol was produced from *Saccharomyces cerevisiae* and *Clostridium butyricum*-based syngas fermentation considering optimized parameters. At the end of the fermentation process, bioethanol was separated from the fermentation broth and analyzed by NMR (¹H) and GC-MS study. The formation of bioethanol was confirmed by NMR (¹H) and yield was calculated by GC-MS analysis.

The formation of bioethanol was detected by ¹H NMR spectrum when syngas was fermented by *S. cerevisiae* and *C. butyricum*. From this analysis, it is clearly shown that bioethanol gives a triplet signal at 1.28 ppm, which referred to the methyl group (-CH₃) along with the neighbouring methylene group (-CH₂-) (Figure 4.65a and Table 4.9). A quartet signal indicated the presence of methylene group (-CH₂-) and the peaks position of this signal at 3.75 ppm further confirmed the methylene group is connected with an oxygen atom. Additionally, a singlet peak appeared at 2.19 with one proton integral value which revealed that the presence of the hydroxyl group in the ethanol molecule. Similarly, *C. butyricum* bacteria also participated the fermentation of syngas and the formation of bioethanol was characterized by ¹H NMR analysis (Figure 4.66a and Table 4.9) and these

results are consistent with the literature reported by Zuriarrain, Zuriarrain, Villar, and Berregi (2015).

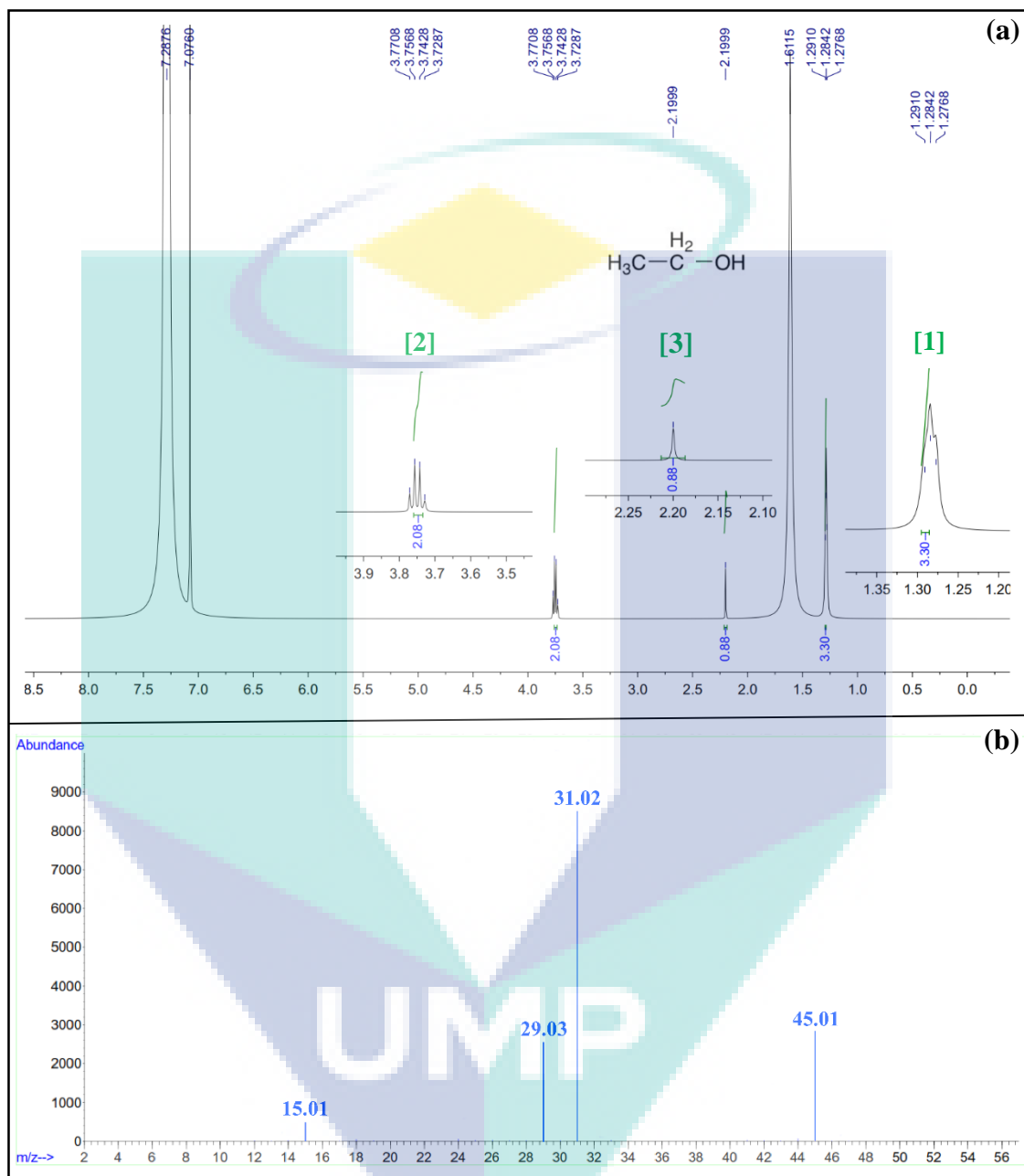


Figure 4.65 Syngas fermentation using *Saccharomyces Cerevisiae* : (a) ¹H NMR, 500 MHz (CDCl₃): δ = 3.75 (q, J = 7.00 Hz, 2H [CH₂]), 2.19 (s, 1H [OH]), 1.28 (t, J = 3.70 Hz, 3H [CH₃]). (b) *S. cerevisiae*-based bioethanol MS fraction (15.01:29.03:31.02:45.01).

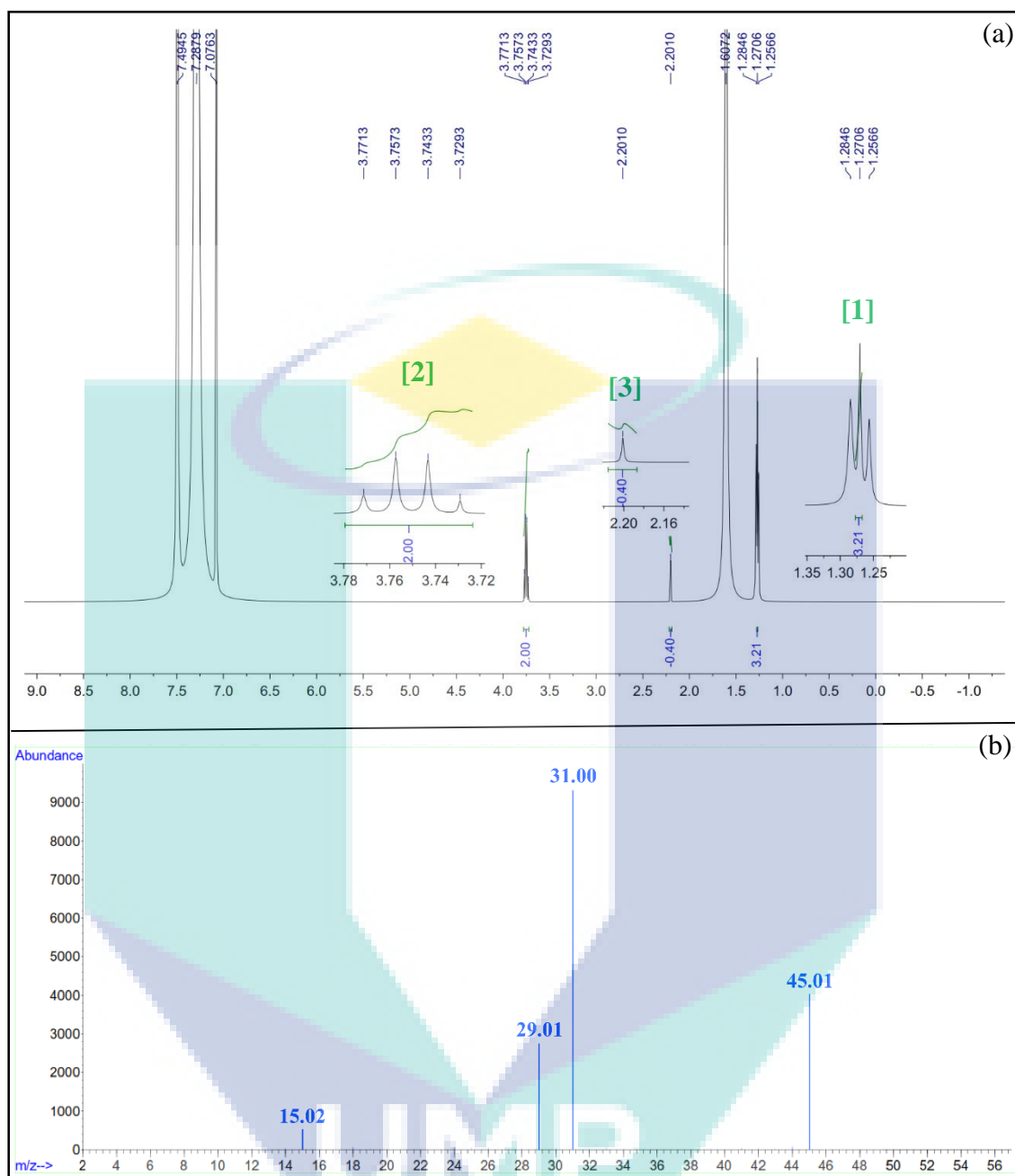


Figure 4.66 Syngas fermentation using *Clostridium Butyricum*: (a) ¹H NMR, 500 MHz (CDCl₃): δ = 3.75 (q, J = 7.00 Hz, 2H [CH₂]), 2.20 (s, 1H [OH]), 1.27 (t, J = 7.00 Hz, 3H [CH₃]). (b) *C. butyricum*-based bioethanol MS fraction (15.02:29.01:31.00:45.01).

Table 4.9 ^1H NMR data of bioethanol generated from biocatalysts (*S. cerevisiae* and *C. butyricum*) based syngas fermentation.

Syngas fermentation	Peaks	^1H NMR (δ_{H} ppm)
<i>S. cerevisiae</i> based syngas fermentation	1	1.28 (t, CH ₃)
	2	3.75 (q, OCH ₂)
	3	2.19 (s, OH)
<i>C. butyricum</i> based syngas fermentation	1	1.27 (t, CH ₃)
	2	3.75 (q, OCH ₂)
	3	2.20 (s, OH)

For the further confirmation of the formation of bioethanol molecule GC-MS analysis of both samples has been performed. From this analysis, it was observed that the MS fraction of *S. cerevisiae*-based bioethanol was 15.01:29.03:31.02:45.01 (Figure 4.66b) and MS fraction of *C. Butyricum* -based bioethanol was 15.02:29.01:31.00:45.01 (Figure 4.67b) which were similar as the standard MS fraction of 15:29:31:45 (Appendix D).

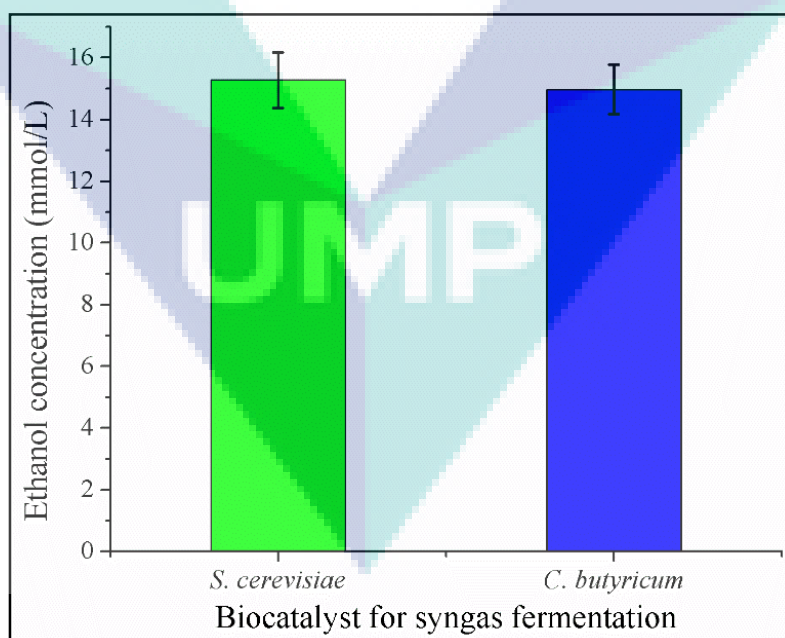


Figure 4.67 Bioethanol concentration from syngas fermentation using *S. cerevisiae* and *C. butyricum*.

The GC-MS results for both samples are shown in Figure 4.65b and Figure 4.66b. According to the literature, the MS for ethanol is 45. In this study, the obtained MS value from GC-MS analysis was 45.01 for both samples. From the fragmentation data, it is shown that MS 31 is corresponding to $[\text{CH}_2\text{-OH}]^+$. The fragmentation of 31 is indicated that $[\text{CH}_2\text{OH}]^+$ was changed to the more stable cation of $[\text{CH}_3=\text{O}]$. The MS of 15 is corresponding to $[\text{CH}_3]^+$. In addition, the MS of 29 is corresponding to $[\text{CH}_3\text{CH}_2]^+$.

From the above discussion, it is concluded that both biocatalysts generated bioethanol from biomass-based syngas. Moreover, charcoal as by-product contributed and assisted microbes for syngas fermentation. The concentration of bioethanol production using yeast (*S. cerevisiae*) and bacteria (*C. butyricum*) was 15.28 mmol/L and 14.97 mmol/L, respectively as shown in Figure 4.67. From the above analysis, it is confirmed that bioethanol was produced through syngas fermentation using *S. cerevisiae* and *C. butyricum*. Therefore, biomass-based syngas suited for bioethanol production.



UMP

CHAPTER 5

CONCLUSION AND RECOMMENDATIONS

5.1 Conclusion

The co-gasification of lignocellulosic biomass (EFB, FR and CS) and charcoal with the blending ratio of 100:0, 90:10, 80:20, 70:30 and 60:40 was investigated in a downdraft gasifier (DG) for the production of syngas. Then lignocellulosic biomass-based syngas was fermented in a TFB bioreactor for the production of bioethanol. This integrated hybrid process was performed based on the physical and chemical characterization of feedstocks and biocatalysts, and the parametric optimization for the experimental run. The simulation results were found to be in good agreement with the experimental results. From the feedstock characterization results, it is revealed that higher volatile matter containing lignocellulosic biomass of EFB, FR and CS were more competent than by-product charcoal for syngas production. Therefore, the required temperature for the co-gasification of biomass and charcoal were 960 °C for performing the maximum heating value. From the ultimate analytical results, it is determined that biomass generated more gaseous compounds (H_2 , CO , CO_2 , CH_4 , etc.) than charcoal. Conversely, charcoal supported biomass for longer combustion time due to its higher carbon content compared to biomass. Moreover, charcoal has maximum HHV (16.07 MJ/kg) than three biomass (15.29-15.62 MJ/kg). As a result, charcoal was valorized by-product and potential co-feedstock that suited for co-gasification with biomass for the production of syngas. The obtained simulation results by Aspen Plus® indicated that more bioenergy can be produced by adding charcoal with the biomass (EFB, FR and CS). From the economic analysis using Aspen Plus®, it is shown that maximum profit for syngas production was produced at temperature of 950 °C to 1050 °C and pressure of 25-35 Nm^3h^{-1} .

From co-gasification experimental results, it is shown that temperature in the oxidation and reduction zone increased gradually with increasing time and it decreased with the reduction of feedstocks. The main components of producer syngas (H_2 and CO) increased its concentration with increasing charcoal ratio and biomass. However, the concentration of CH_4 was relatively unchanged with increasing charcoal ratio to biomass. Moreover, the remarkable syngas ratio ($H_2:CO$) was observed as 1.50 when EFB and charcoal ratio was 70:30, 1.14 when the FR and charcoal ratio was 70:30 and 1.10 when the CS and charcoal ratio was 70:30. Meanwhile, the highest cold gas efficiency was observed in FR with charcoal-based co-gasification. On the other hand, the lowest cold gas efficiency was found in EFB based co-gasification. Correspondingly, the highest carbon conversion efficiency was found during the forest residue and charcoal co-gasification of 93.34%. In addition, the carbon conversion efficiency was relatively same in the co-gasification of EFB with charcoal and coconut shell with charcoal of about 69.89% and 72.25%, respectively. Ultimately, the highest overall exergy efficiency was achieved to be 69.04% from 46.66% by the addition of charcoal to biomass (forest residue) as the percentage of charcoal increased up to 30-40%. On the other hand, co-product of tar was reduced from syngas through thermal treatment (700 °C to 1000 °C). Moreover, by-product charcoal was one of the important gasifying materials that enhanced the co-gasification process and it comprised major oxides of Fe_2O_3 (31.94%), K_2O (28.09%), SiO_2 (9.16%), CaO (2.83%), Al_2O_3 (2.83%) and P_2O_5 (2.29%). The other oxides were MgO , TiO_2 , MnO , SO_3 , ZrO_2 , CuO , ZnO that were less than 1%. From comparative of co-gasification study of three different lignocellulosic biomass with a charcoal based on syngas concentration, cold gas efficiency, carbon conversion efficiency and heating value of syngas was found that FR with charcoal-based syngas is the highest bioenergy value compared to other two co-gasification-based syngas.

The yield of bioethanol produced from *S. cerevisiae* and *C. butyricum* based syngas fermentation considering optimized parameters. The produced bioethanol was detected by NMR (1H) spectra analysis and yield concentration was calculated by GC-MS analysis. This bioethanol gives triplet signal at 1.27 ppm -1.28 ppm, corresponding to the protons from methyle group, CH_3- , and a multiplet signal at 3.75 ppm, produced by the methylene group, $-CH_2-$ for both experiments. The concentration of bioethanol production using yeast (*S. cerevisiae*) and bacteria (*C. butyricum*) was 15.28 mmol/L and 14.97 mmol/L, respectively. Therefore, lignocellulosic biomass of EFB, FR, CS and

charcoal is the potential source of renewable bioenergy in the form of syngas and bioethanol for the fulfillment the future energy demand.

5.2 Recommendations

The co-gasification of lignocellulosic biomass of EFB, FR and CS with by-product charcoal is now a mature technology. Subsequently, the biomass-based syngas fermentation for the production of bioethanol is currently being promising and advance technique. However, there are some recommendations that are summarised below which will be helpful for future research-

- (a) Existing downdraft gasifier is needed to be modified by adding the tar sampling system. Moreover, thermocouples are needed to connect with software-based data logger where temperature profile would be recorded digitally.
- (b) The on-line gas analyzer can be attached with the downdraft gasifier. Thus, the kinetic study would be more specific for further research.
- (c) The concentration of bioethanol was relatively low compared to other fermentation process and therefore to enhance the bioethanol production further advanced research can be conducted.

The logo for UIMP (Universiti Malaysia Perlis) is a large, stylized 'V' shape. The left side of the 'V' is light blue, the right side is light green, and the bottom point is a darker blue. The letters 'UIMP' are written in white, bold, sans-serif font across the bottom of the 'V'.

REFERENCES

- Abdoulmoumine, N., Adhikari, S., Kulkarni, A., & Chattanathan, S. (2015). A review on biomass gasification syngas cleanup. *Applied Energy*, 155, 294-307. doi:<http://dx.doi.org/10.1016/j.apenergy.2015.05.095>
- Abubackar, H. N., Veiga, M. C., & Kennes, C. (2018). Production of acids and alcohols from syngas in a two-stage continuous fermentation process. *Bioresource Technology*, 253, 227-234. doi:10.1016/j.biortech.2018.01.026
- Acharya, B., Roy, P., & Dutta, A. (2014). Review of syngas fermentation processes for bioethanol. *Biofuels*, 5(5), 551-564.
- Adeyemi, I., Janajreh, I., Arink, T., & Ghenai, C. (2017). Gasification behavior of coal and woody biomass: Validation and parametrical study. *Applied Energy*, 185, 1007-1018.
- Adhikari, S., Abdoulmoumine, N., Nam, H., & Oyedeji, O. (2017). 16 - Biomass gasification producer gas cleanup. In *Bioenergy Systems for the Future* (pp. 541-557): Woodhead Publishing.
- Ahmad, A. A., Zawawi, N. A., Kasim, F. H., Inayat, A., & Khasri, A. (2016). Assessing the gasification performance of biomass: A review on biomass gasification process conditions, optimization and economic evaluation. *Renewable and Sustainable Energy Reviews*, 53, 1333-1347. doi:<http://doi.org/10.1016/j.rser.2015.09.030>
- Akhtar, M. N. (2016). Biofuel: A Stepping Stone towards Sustainable Development. *International Journal of Research in BioSciences*, 5(3), 1-12.
- Al-Rahbi, A. S., & Williams, P. T. (2017). Hydrogen-rich syngas production and tar removal from biomass gasification using sacrificial tyre pyrolysis char. *Applied Energy*, 190, 501-509. doi:<https://doi.org/10.1016/j.apenergy.2016.12.099>
- Alfenore, S., & Molina-Jouve, C. (2016). Current status and future prospects of conversion of lignocellulosic resources to biofuels using yeasts and bacteria. *Process Biochemistry*, 51(11), 1747-1756.
- Ali, D. A., Gadalla, M. A., Abdelaziz, O. Y., Hulteberg, C. P., & Ashour, F. H. (2017). Co-gasification of coal and biomass wastes in an entrained flow gasifier: Modelling, simulation and integration opportunities. *Journal of Natural Gas Science and Engineering*, 37, 126-137.
- Alzate, C. A. C., Toro, J. C. S., & Peña, Á. G. (2018). Fermentation, thermochemical and catalytic processes in the transformation of biomass through efficient biorefineries. *Catalysis today*, 302, 61-72.
- Anex, R. P., Aden, A., Kazi, F. K., Fortman, J., Swanson, R. M., Wright, M. M., . . . Dutta, A. (2010). Techno-economic comparison of biomass-to-transportation

fuels via pyrolysis, gasification, and biochemical pathways. *Fuel*, 89, S29-S35. doi:<https://doi.org/10.1016/j.fuel.2010.07.015>

- Anil, M., Rupesh, S., Muraleedharan, C., & Arun, P. (2016). Performance Evaluation of Fluidised Bed Biomass Gasifier Using CFD. *Energy Procedia*, 90, 154-162. doi:<https://doi.org/10.1016/j.egypro.2016.11.180>
- Anukam, A., Mamphweli, S., Reddy, P., Meyer, E., & Okoh, O. (2016). Pre-processing of sugarcane bagasse for gasification in a downdraft biomass gasifier system: A comprehensive review. *Renewable and Sustainable Energy Reviews*, 66, 775-801. doi:<https://doi.org/10.1016/j.rser.2016.08.046>
- Arevalo-Gallegos, A., Ahmad, Z., Asgher, M., Parra-Saldivar, R., & Iqbal, H. M. (2017). Lignocellulose: A sustainable material to produce value-added products with a zero waste approach—A review. *International journal of biological macromolecules*, 99, 308-318.
- Asimakopoulos, K., Gavala, H. N., & Skiadas, I. V. (2018). Reactor systems for syngas fermentation processes: A review. *Chemical Engineering Journal*, 348, 732-744. doi:<https://doi.org/10.1016/j.cej.2018.05.003>
- Atia, A. (2016). Modeling and simulation of coupling enhanced Oil/Gas recovery with CO₂ injection.
- Atnaw, S. M., Kueh, S. C., & Sulaiman, S. A. (2014). Study on tar generated from downdraft gasification of oil palm fronds. *The Scientific World Journal*, 2014.
- Atnaw, S. M., Sulaiman, S. A., Singh, L., Wahid, Z. A., Che, C. K. M. F. B., & Yahya, K. (2017). Modeling and Parametric Study for Maximizing Heating Value of Gasification Syngas. *BioResources*, 12(2), 2548-2564.
- Atnaw, S. M., Sulaiman, S. A., & Yusup, S. (2011). A simulation study of downdraft gasification of oil-palm fronds using ASPEN PLUS. *Journal of Applied Sciences*, 11(11), 1913-1920.
- Atnaw, S. M., Sulaiman, S. A., & Yusup, S. (2013). Syngas production from downdraft gasification of oil palm fronds. *Energy*, 61, 491-501. doi:<http://dx.doi.org/10.1016/j.energy.2013.09.039>
- Atnaw, S. M., Sulaiman, S. A., & Yusup, S. (2017). Biomass Gasification. In *Waste Biomass Management—A Holistic Approach* (pp. 159-185): Springer.
- Aydin, E. S., Yucel, O., & Sadikoglu, H. (2018). Numerical Investigation of Fixed-Bed Downdraft Woody Biomass Gasification. In *Exergetic, Energetic and Environmental Dimensions* (pp. 323-339): Elsevier.
- Baharuddin, A. S., Sulaiman, A., Kim, D. H., Mokhtar, M. N., Hassan, M. A., Wakisaka, M., . . . Nishida, H. (2013). Selective component degradation of oil palm empty fruit bunches (OPEFB) using high-pressure steam. *Biomass and Bioenergy*, 55(Supplement C), 268-275. doi:<https://doi.org/10.1016/j.biombioe.2013.02.013>

- Bahng, M.-K., Mukarakate, C., Robichaud, D. J., & Nimlos, M. R. (2009). Current technologies for analysis of biomass thermochemical processing: A review. *Analytica Chimica Acta*, 651(2), 117-138. doi:<https://doi.org/10.1016/j.aca.2009.08.016>
- Baidya, T., Cattolica, R. J., & Seiser, R. (2018). High performance Ni-Fe-Mg catalyst for tar removal in producer gas. *Applied Catalysis A: General*, 558, 131-139. doi:<https://doi.org/10.1016/j.apcata.2018.03.026>
- Baruah, D., & Baruah, D. C. (2014). Modeling of biomass gasification: A review. *Renewable and Sustainable Energy Reviews*, 39, 806-815. doi:<http://dx.doi.org/10.1016/j.rser.2014.07.129>
- Basu, P. (2010). *Biomass gasification and pyrolysis: practical design and theory*: Academic press.
- Basu, P. (2018). *Biomass gasification, pyrolysis and torrefaction: practical design and theory*: Academic press.
- Beagle, E., Wang, Y., Bell, D., & Belmont, E. (2018). Co-gasification of pine and oak biochar with sub-bituminous coal in carbon dioxide. *Bioresource Technology*, 251, 31-39. doi:<https://doi.org/10.1016/j.biortech.2017.12.027>
- Bhaskar, T., Bhavya, B., Singh, R., Naik, D. V., Kumar, A., & Goyal, H. B. (2011). Chapter 3 - Thermochemical Conversion of Biomass to Biofuels A2 - Pandey, Ashok. In C. Larroche, S. C. Ricke, C.-G. Dussap, & E. Gnansounou (Eds.), *Biofuels* (pp. 51-77). Amsterdam: Academic Press.
- Birol, F. (2017). Key world energy statistics. In: IEA Publications, International Energy Agency, rue de la Federation, Paris, France.
- Brown, T. R., Thilakaratne, R., Brown, R. C., & Hu, G. (2013). Techno-economic analysis of biomass to transportation fuels and electricity via fast pyrolysis and hydroprocessing. *Fuel*, 106, 463-469. doi:<https://doi.org/10.1016/j.fuel.2012.11.029>
- Buruiana, C.-T., Vizireanu, C., Garrote, G., & Parajó, J. C. (2014). Bioethanol production from hydrothermally pretreated and delignified corn stover by fed-batch simultaneous saccharification and fermentation. *Energy & Fuels*, 28(2), 1158-1165.
- Cai, J., He, Y., Yu, X., Banks, S. W., Yang, Y., Zhang, X., . . . Bridgwater, A. V. (2017). Review of physicochemical properties and analytical characterization of lignocellulosic biomass. *Renewable and Sustainable Energy Reviews*, 76, 309-322. doi:<https://doi.org/10.1016/j.rser.2017.03.072>
- Cai, J., Wang, S., Wang, Q., & Kuang, C. (2016). The characteristics of biomass gasification in multistage heating and gradient chain gasifier. *International journal of hydrogen energy*, 41(35), 15674-15681. doi:<https://doi.org/10.1016/j.ijhydene.2016.04.128>

- Cai, Y., Yang, X., Liang, T., Dai, L., Ma, L., Huang, G., . . . Xu, M. (2014). Easy incorporation of single-walled carbon nanotubes into two-dimensional MoS₂ for high-performance hydrogen evolution. *Nanotechnology*, 25(46), 465401.
- Capuano, L. (2018). International Energy Outlook 2018 (IEO2018). Available from: https://www.eia.gov/outlooks/ieo/executive_summary.php.
- Casolari, A. (2018). Microbial death. In *Physiological models in microbiology* (pp. 1-44): CRC press.
- Catalán-Martínez, D., Domínguez, M. E., & Serra, J. M. (2018). Liquid fuels from biomass: An energy self-sustained process integrating H₂ recovery and liquid refining. *Fuel*, 212(Supplement C), 353-363. doi:<https://doi.org/10.1016/j.fuel.2017.10.014>
- Chala, G. T., Lim, Y. P., Sulaiman, S. A., & Liew, C. L. (2018). *Thermogravimetric analysis of empty fruit bunch*. Paper presented at the MATEC Web of Conferences.
- Channiwala, S. A., & Parikh, P. P. (2002). A unified correlation for estimating HHV of solid, liquid and gaseous fuels. *Fuel*, 81(8), 1051-1063. doi:[http://dx.doi.org/10.1016/S0016-2361\(01\)00131-4](http://dx.doi.org/10.1016/S0016-2361(01)00131-4)
- Chaurasia, A. (2018). Modeling of downdraft gasification process: Studies on particle geometries in thermally thick regime. *Energy*, 142, 991-1009. doi:<https://doi.org/10.1016/j.energy.2017.10.093>
- Che, D., Li, S., Yang, W., Jia, J., & Zheng, N. (2012). Application of Numerical Simulation on Biomass Gasification. *Energy Procedia*, 17, 49-54. doi:<https://doi.org/10.1016/j.egypro.2012.02.061>
- Chen, F., Srinivasa Reddy, M. S., Temple, S., Jackson, L., Shadle, G., & Dixon, R. A. (2006). Multi-site genetic modulation of monolignol biosynthesis suggests new routes for formation of syringyl lignin and wallbound ferulic acid in alfalfa (*Medicago sativa* L.). *Plant Journal*, 48(1), 113-124. doi:10.1111/j.1365-313X.2006.02857.x
- Chen, H. (2014). Chemical composition and structure of natural lignocellulose. In *Biotechnology of lignocellulose* (pp. 25-71): Springer.
- Chen, J., & Henson, M. A. (2016). In silico metabolic engineering of *Clostridium ljungdahlii* for synthesis gas fermentation. *Metabolic engineering*, 38, 389-400. doi:<https://doi.org/10.1016/j.ymben.2016.10.002>
- Claypool, J. T., & Simmons, C. W. (2016). Hybrid thermochemical/biological processing: The economic hurdles and opportunities for biofuel production from bio-oil. *Renewable Energy*, 96, 450-457. doi:<http://dx.doi.org/10.1016/j.renene.2016.04.095>

- Clews, R. J. (2016). Chapter 7 - Petroleum Refining. In R. J. Clews (Ed.), *Project Finance for the International Petroleum Industry* (pp. 119-136). San Diego: Academic Press.
- Collet, C., Ng, J. Y., & Aston, D. N. (2018). Multiple reactor system for continuous gas fermentation. In: Google Patents.
- Dalena, F., Senatore, A., Tursi, A., & Basile, A. (2017). 17 - Bioenergy production from second- and third-generation feedstocks. In *Bioenergy Systems for the Future* (pp. 559-599): Woodhead Publishing.
- Darmawan, A., Hardi, F., Yoshikawa, K., Aziz, M., & Tokimatsu, K. (2017). Enhanced process Integration of entrained flow gasification and combined cycle: modeling and simulation using Aspen Plus. *Energy Procedia*, *105*, 303-308.
- Davis, R., Molloy, S., Quigley, B., Nikodinovic-Runic, J., Solano, F., O'Connor, K. E. J. A. m., & biotechnology. (2018). Biocatalytic versatility of engineered and wild-type tyrosinase from *R. solanacearum* for the synthesis of 4-halocatechols. 1-11.
- De, S., Agarwal, A. K., Moholkar, V., & Thallada, B. (2018). Coal and Biomass Gasification. *Energy, Environment, and Sustainability*.
- Derman, E., Abdulla, R., Marbawi, H., & Sabullah, M. K. (2018). Oil palm empty fruit bunches as a promising feedstock for bioethanol production in Malaysia. *Renewable Energy*, *129*, 285-298. doi:<https://doi.org/10.1016/j.renene.2018.06.003>
- Devarapalli, M., Atiyeh, H. K., Phillips, J. R., Lewis, R. S., & Huhnke, R. L. (2016). Ethanol production during semi-continuous syngas fermentation in a trickle bed reactor using *Clostridium ragsdalei*. *Bioresource Technology*, *209*, 56-65. doi:<https://doi.org/10.1016/j.biortech.2016.02.086>
- Drzyzga, O., Revelles, O., Durante-Rodriguez, G., Diaz, E., Garcia, J. L., & Prieto, A. (2015). New challenges for syngas fermentation: towards production of biopolymers. *Journal of Chemical Technology and Biotechnology*, *90*(10), 1735-1751. doi:10.1002/jctb.4721
- Du, S.-W., Chen, W.-H., & Lucas, J. A. (2014). Pretreatment of biomass by torrefaction and carbonization for coal blend used in pulverized coal injection. *Bioresource Technology*, *161*, 333-339. doi:<https://doi.org/10.1016/j.biortech.2014.03.090>
- Edrisi, S. A., & Abhilash, P. (2016). Exploring marginal and degraded lands for biomass and bioenergy production: an Indian scenario. *Renewable and Sustainable Energy Reviews*, *54*, 1537-1551.
- Ellabban, O., Abu-Rub, H., & Blaabjerg, F. (2014). Renewable energy resources: Current status, future prospects and their enabling technology. *Renewable and Sustainable Energy Reviews*, *39*, 748-764.

- Emami-Taba, L., Irfan, M. F., Wan Daud, W. M. A., & Chakrabarti, M. H. (2013). Fuel blending effects on the co-gasification of coal and biomass – A review. *Biomass and Bioenergy*, 57, 249-263. doi:<http://dx.doi.org/10.1016/j.biombioe.2013.02.043>
- Fermoso, J., Arias, B., Plaza, M. G., Pevida, C., Rubiera, F., Pis, J. J., . . . Casero, P. (2009). High-pressure co-gasification of coal with biomass and petroleum coke. *Fuel Processing Technology*, 90(7), 926-932. doi:<https://doi.org/10.1016/j.fuproc.2009.02.006>
- Foo, J. L., Susanto, A. V., Keasling, J. D., Leong, S. S. J., Chang, M. W. J. B., & bioengineering. (2017). Whole - cell biocatalytic and de novo production of alkanes from free fatty acids in *Saccharomyces cerevisiae*. 114(1), 232-237.
- Furuoka, F. (2017). Renewable electricity consumption and economic development: New findings from the Baltic countries. *Renewable and Sustainable Energy Reviews*, 71, 450-463. doi:<https://doi.org/10.1016/j.rser.2016.12.074>
- Gaikwad, V., Panghal, A., Jadhav, S., Sharma, P., Bagal, A., Jadhav, A., & Chhikara, N. (2018). Designing of Fermenter and its utilization in food industries.
- Gao, X., Zhang, Y., Li, B., & Yu, X. (2016). Model development for biomass gasification in an entrained flow gasifier using intrinsic reaction rate submodel. *Energy Conversion and Management*, 108, 120-131.
- Gaurav, N., Sivasankari, S., Kiran, G. S., Ninawe, A., & Selvin, J. (2017). Utilization of bioresources for sustainable biofuels: A Review. *Renewable and Sustainable Energy Reviews*, 73, 205-214. doi:<https://doi.org/10.1016/j.rser.2017.01.070>
- Gírio, F. M., Fonseca, C., Carvalheiro, F., Duarte, L. C., Marques, S., & Bogel-Lukasik, R. (2010). Hemicelluloses for fuel ethanol: A review. *Bioresource Technology*, 101(13), 4775-4800. doi:[10.1016/j.biortech.2010.01.088](https://doi.org/10.1016/j.biortech.2010.01.088)
- Gogoi, M., Konwar, K., Bhuyan, N., Borah, R. C., Kalita, A. C., Nath, H. P., & Saikia, N. (2018). Assessments of pyrolysis kinetics and mechanisms of biomass residues using thermogravimetry. *Bioresource Technology Reports*, 4, 40-49. doi:<https://doi.org/10.1016/j.biteb.2018.08.016>
- Guan, G., Kaewpanha, M., Hao, X., & Abudula, A. (2016). Catalytic steam reforming of biomass tar: Prospects and challenges. *Renewable and Sustainable Energy Reviews*, 58, 450-461. doi:<http://dx.doi.org/10.1016/j.rser.2015.12.316>
- Guangul, F. M., Sulaiman, S. A., & Ramli, A. (2012). Gasifier selection, design and gasification of oil palm fronds with preheated and unheated gasifying air. *Bioresource Technology*, 126, 224-232. doi:<https://doi.org/10.1016/j.biortech.2012.09.018>
- Gupta, J. G., De, S., Gautam, A., Dhar, A., & Pandey, A. (2018). Introduction to Sustainable Energy, Transportation Technologies, and Policy. In A. Gautam, S. De, A. Dhar, J. G. Gupta, & A. Pandey (Eds.), *Sustainable Energy and*

Transportation : Technologies and Policy (pp. 3-7). Singapore: Springer Singapore.

- Hagos, F. Y., Aziz, A. R. A., & Sulaiman, S. A. (2013). Study of syngas combustion parameters effect on internal combustion engine. *Asian Journal of Scientific Research*, 6(2), 187-196.
- Haq, F., Ali, H., Shuaib, M., Badshah, M., Hassan, S. W., Munis, M. F. H., & Chaudhary, H. J. (2016). Recent progress in bioethanol production from lignocellulosic materials: A review. *International Journal of Green Energy*, 13(14), 1413-1441.
- Hassan, H., Lim, J., & Hameed, B. (2016). Recent progress on biomass co-pyrolysis conversion into high-quality bio-oil. *Bioresource Technology*.
- Heiskanen, H., Virkajärvi, I., & Viikari, L. (2007). The effect of syngas composition on the growth and product formation of *Butyribacterium methylotrophicum*. *Enzyme and Microbial Technology*, 41(3), 362-367.
- Henstra, A. M., Sipma, J., Rinzema, A., & Stams, A. J. M. (2007). Microbiology of synthesis gas fermentation for biofuel production. *Current Opinion in Biotechnology*, 18(3), 200-206. doi:<https://doi.org/10.1016/j.copbio.2007.03.008>
- Hoffmeister, S., Gerdorf, M., Bengelsdorf, F. R., Linder, S., Flüchter, S., Öztürk, H., . . . Bahl, H. (2016). Acetone production with metabolically engineered strains of *Acetobacterium woodii*. *Metabolic engineering*, 36, 37-47.
- Holland, D. J. (2015). 18 - Applications of tomography in bubble column and trickle bed reactors A2 - Wang, Mi. In *Industrial Tomography* (pp. 477-507): Woodhead Publishing.
- Hossain, N., Zaini, J. H., & Mahlia, T. (2017). A Review of Bioethanol Production from Plant-based Waste Biomass by Yeast Fermentation. *INTERNATIONAL JOURNAL OF TECHNOLOGY*, 8(1), 5-18.
- Hu, M., Laghari, M., Cui, B., Xiao, B., Zhang, B., & Guo, D. (2018). Catalytic cracking of biomass tar over char supported nickel catalyst. *Energy*, 145, 228-237. doi:<https://doi.org/10.1016/j.energy.2017.12.096>
- Ibarra-Gonzalez, P., & Rong, B.-G. (2018). A review of the current state of biofuels production from lignocellulosic biomass using thermochemical conversion routes. *Chinese Journal of Chemical Engineering*.
- Inayat, A., Ahmad, M. M., Mutalib, M. A., & Yusup, S. (2010). Effect of process parameters on hydrogen production and efficiency in biomass gasification using modelling approach. *Journal of Applied Sciences(Faisalabad)*, 10(24), 3183-3190.
- Inderwildi, O. R., & King, D. A. (2009). Quo vadis biofuels? *Energy Environ. Sci.*, 2(4), 343-346.

- Isikgor, F. H., & Becer, C. R. (2015). Lignocellulosic biomass: a sustainable platform for the production of bio-based chemicals and polymers. *Polymer Chemistry*, 6(25), 4497-4559. doi:10.1039/c5py00263j
- Islam, M. A., Yousuf, A., Karim, A., Pirozzi, D., Khan, M. R., & Wahid, Z. A. (2018). Bioremediation of palm oil mill effluent and lipid production by *Lipomyces starkeyi*: A combined approach. *Journal of Cleaner Production*, 172, 1779-1787. doi:https://doi.org/10.1016/j.jclepro.2017.12.012
- Ismail, H. Y., Abbas, A., Azizi, F., & Zeaiter, J. (2017). Pyrolysis of waste tires: A modeling and parameter estimation study using Aspen Plus®. *Waste Management*, 60, 482-493.
- Janda, K., & Tan, T. (2017). Overview of Sustainable Energy in Central Europe and East Asia.
- Jin, E., & Sutherland, J. W. (2018). An integrated sustainability model for a bioenergy system: Forest residues for electricity generation. *Biomass and Bioenergy*, 119, 10-21. doi:https://doi.org/10.1016/j.biombioe.2018.09.005
- Johar, N., Ahmad, I., & Dufresne, A. (2012). Extraction, preparation and characterization of cellulose fibres and nanocrystals from rice husk. *Industrial Crops and Products*, 37(1), 93-99.
- Kalita, P., & Baruah, D. (2018). Investigation of Biomass Gasifier Product Gas Composition and its Characterization. In *Coal and Biomass Gasification* (pp. 115-149): Springer.
- Kaman, S. P. D., Tan, I. A. W., & Lim, L. L. P. (2017). Palm oil mill effluent treatment using coconut shell – based activated carbon: Adsorption equilibrium and isotherm. *MATEC Web Conf.*, 87, 03009. Retrieved from https://doi.org/10.1051/mateconf/20178703009
- Kamble, A. D., Saxena, V. K., Chavan, P. D., & Mendhe, V. A. (2018). Co-gasification of coal and biomass an emerging clean energy technology: Status and prospects of development in Indian context. *International Journal of Mining Science and Technology*. doi:https://doi.org/10.1016/j.ijmst.2018.03.011
- Kanchanasuta, S., Prommeenate, P., Boonapatcharone, N., & Pisutpaisal, N. (2017). Stability of *Clostridium butyricum* in biohydrogen production from non-sterile food waste. *International journal of hydrogen energy*, 42(5), 3454-3465. doi:https://doi.org/10.1016/j.ijhydene.2016.09.111
- Kang, K., Azargohar, R., Dalai, A. K., & Wang, H. (2016). Hydrogen production from lignin, cellulose and waste biomass via supercritical water gasification: Catalyst activity and process optimization study. *Energy Conversion and Management*, 117, 528-537. doi:https://doi.org/10.1016/j.enconman.2016.03.008

- Kaushal, P., & Tyagi, R. (2017a). Advanced simulation of biomass gasification in a fluidized bed reactor using ASPEN PLUS. *Renewable Energy*, *101*, 629-636. doi:<https://doi.org/10.1016/j.renene.2016.09.011>
- Kaushal, P., & Tyagi, R. (2017b). Advanced simulation of biomass gasification in a fluidized bed reactor using ASPEN PLUS. *Renewable Energy*, *101*(Supplement C), 629-636. doi:<https://doi.org/10.1016/j.renene.2016.09.011>
- Keche, A. J., Gaddale, A. P. R., Tated, R. G. J. C. T., & Policy, E. (2015). Simulation of biomass gasification in downdraft gasifier for different biomass fuels using ASPEN PLUS. *17*(2), 465-473.
- Kennes, D., Abubackar, H. N., Diaz, M., Veiga, M. C., & Kennes, C. (2016). Bioethanol production from biomass: carbohydrate vs syngas fermentation. *Journal of Chemical Technology & Biotechnology*, *91*(2), 304-317. doi:10.1002/jctb.4842
- Khatun, F., Monir, M. M. U., Arham, S. N., & Wahid, Z. (2016). Implementation of Carbon Dioxide Gas Injection Method for Gas Recovery at Rashidpur Gas Field, Bangladesh. *INTERNATIONAL JOURNAL OF ENGINEERING TECHNOLOGY AND SCIENCES (IJETS)*, *5*(1), 52-61.
- Kim, K. H., Eom, I. Y., Lee, S. M., Choi, D., Yeo, H., Choi, I.-G., & Choi, J. W. (2011). Investigation of physicochemical properties of biooils produced from yellow poplar wood (*Liriodendron tulipifera*) at various temperatures and residence times. *Journal of Analytical and Applied Pyrolysis*, *92*(1), 2-9. doi:<https://doi.org/10.1016/j.jaap.2011.04.002>
- Kim, Y.-K., Park, S. E., Lee, H., & Yun, J. Y. (2014). Enhancement of bioethanol production in syngas fermentation with *Clostridium ljungdahlii* using nanoparticles. *Bioresource Technology*, *159*, 446-450.
- Konur, O. (2018). *Bioenergy and Biofuels*: CRC Press.
- Kuba, M., & Hofbauer, H. (2018). Experimental parametric study on product gas and tar composition in dual fluid bed gasification of woody biomass. *Biomass and Bioenergy*, *115*, 35-44. doi:<https://doi.org/10.1016/j.biombioe.2018.04.007>
- Kumabe, K., Hanaoka, T., Fujimoto, S., Minowa, T., & Sakanishi, K. (2007). Co-gasification of woody biomass and coal with air and steam. *Fuel*, *86*(5), 684-689.
- Kumar, U., & Paul, M. C. (2019). CFD modelling of biomass gasification with a volatile break-up approach. *Chemical Engineering Science*, *195*, 413-422. doi:<https://doi.org/10.1016/j.ces.2018.09.038>
- Kundu, K., Chatterjee, A., Bhattacharyya, T., Roy, M., & Kaur, A. (2018). Thermochemical Conversion of Biomass to Bioenergy: A Review. In A. P. Singh, R. A. Agarwal, A. K. Agarwal, A. Dhar, & M. K. Shukla (Eds.), *Prospects of Alternative Transportation Fuels* (pp. 235-268). Singapore: Springer Singapore.

- Kuo, P.-C., Chen, H.-T., & Wu, W. (2014). Heat Integration of Biomass Co-firing in Coal Power Plant. *Energy Procedia*, 61, 1756-1759. doi:<https://doi.org/10.1016/j.egypro.2014.12.205>
- Kurniawan, R., & Managi, S. (2018). Coal consumption, urbanization, and trade openness linkage in Indonesia. *Energy Policy*, 121, 576-583. doi:<https://doi.org/10.1016/j.enpol.2018.07.023>
- Ladisch, M. R., Mosier, N. S., Youngmi, K. I. M., Ximenes, E., & Hogsett, D. (2010). Converting cellulose to biofuels. *Chemical Engineering Progress*, 106(3), 56-63. Retrieved from <https://www.scopus.com/inward/record.uri?eid=2-s2.0-77950199195&partnerID=40&md5=98a34793da78529e418475784876e345>
- Lagoa-Costa, B., Abubackar, H. N., Fernández-Romasanta, M., Kennes, C., & Veiga, M. C. (2017). Integrated bioconversion of syngas into bioethanol and biopolymers. *Bioresource Technology*, 239, 244-249.
- Lauri, P., Havlik, P., Kindermann, G., Forsell, N., Bottcher, H., & Obersteiner, M. (2014). Woody biomass energy potential in 2050. *Energy Policy*, 66, 19-31. doi:10.1016/j.enpol.2013.11.033
- Lee, S., Speight, J. G., & Loyalka, S. K. (2014). *Handbook of alternative fuel technologies*: crc Press.
- Lewis, R. S., Tanner, R. S., & Huhnke, R. L. (2007). Indirect or direct fermentation of biomass to fuel alcohol. In: Google Patents.
- Li, H.-d., Tian, X.-l., & Dong, S.-l. (2019). Growth performance, non-specific immunity, intestinal histology and disease resistance of *Litopenaeus vannamei* fed on a diet supplemented with live cells of *Clostridium butyricum*. *Aquaculture*, 498, 470-481. doi:<https://doi.org/10.1016/j.aquaculture.2018.09.003>
- Liao, J. C., Mi, L., Pontrelli, S., & Luo, S. (2016). Fuelling the future: microbial engineering for the production of sustainable biofuels. *Nat Rev Micro*, 14(5), 288-304. doi:10.1038/nrmicro.2016.32
- Liew, F., Henstra, A. M., Köpke, M., Winzer, K., Simpson, S. D., & Minton, N. P. (2017). Metabolic engineering of *Clostridium autoethanogenum* for selective alcohol production. *Metabolic engineering*, 40, 104-114. doi:<https://doi.org/10.1016/j.ymben.2017.01.007>
- Limayem, A., & Ricke, S. C. (2012). Lignocellulosic biomass for bioethanol production: Current perspectives, potential issues and future prospects. *Progress in Energy and Combustion Science*, 38(4), 449-467. doi:<https://doi.org/10.1016/j.pecs.2012.03.002>
- Lin, G., Yang, H., Wang, X., Mei, Y., Li, P., Shao, J., & Chen, H. (2016). The moisture sorption characteristics and modelling of agricultural biomass. *Biosystems Engineering*, 150, 191-200. doi:<https://doi.org/10.1016/j.biosystemseng.2016.08.006>

- Lin, Y., Zhang, W., Li, C., Sakakibara, K., Tanaka, S., & Kong, H. (2012). Factors affecting ethanol fermentation using *Saccharomyces cerevisiae* BY4742. *Biomass and Bioenergy*, 47, 395-401. doi:<https://doi.org/10.1016/j.biombioe.2012.09.019>
- Liu, C.-F., Ren, J.-L., Xu, F., Liu, J.-J., Sun, J.-X., & Sun, R.-C. (2006). Isolation and characterization of cellulose obtained from ultrasonic irradiated sugarcane bagasse. *Journal of agricultural and food chemistry*, 54(16), 5742-5748.
- Loh, S. K. (2017). The potential of the Malaysian oil palm biomass as a renewable energy source. *Energy Conversion and Management*, 141, 285-298. doi:<https://doi.org/10.1016/j.enconman.2016.08.081>
- Longhin, E., Gualtieri, M., Capasso, L., Bengalli, R., Mollerup, S., Holme, J. A., . . . Camatini, M. (2016). Physico-chemical properties and biological effects of diesel and biomass particles. *Environmental Pollution*, 215, 366-375. doi:<https://doi.org/10.1016/j.envpol.2016.05.015>
- Lü, J., Sheahan, C., & Fu, P. (2011). Metabolic engineering of algae for fourth generation biofuels production. *Energy & Environmental Science*, 4(7), 2451-2466.
- Malek, A. A., Hasanuzzaman, M., Rahim, N. A., & Al Turki, Y. A. (2017). Techno-economic analysis and environmental impact assessment of a 10 MW biomass-based power plant in Malaysia. *Journal of Cleaner Production*, 141, 502-513.
- Mansfield, A. B., & Wooldridge, M. S. (2015). The effect of impurities on syngas combustion. *Combustion and Flame*, 162(5), 2286-2295. doi:<https://doi.org/10.1016/j.combustflame.2015.01.026>
- Mathieu, P., & Dubuisson, R. (2002). Performance analysis of a biomass gasifier. *Energy Conversion and Management*, 43(9-12), 1291-1299.
- Matsushika, A., Inoue, H., Kodaki, T., & Sawayama, S. (2009). Ethanol production from xylose in engineered *Saccharomyces cerevisiae* strains: current state and perspectives. *Applied Microbiology and Biotechnology*, 84(1), 37-53.
- Mehrpooya, M., Khalili, M., & Sharifzadeh, M. M. M. (2018). Model development and energy and exergy analysis of the biomass gasification process (Based on the various biomass sources). *Renewable and Sustainable Energy Reviews*, 91, 869-887. doi:<https://doi.org/10.1016/j.rser.2018.04.076>
- Meng, A., Zhou, H., Qin, L., Zhang, Y., & Li, Q. (2013). Quantitative and kinetic TG-FTIR investigation on three kinds of biomass pyrolysis. *Journal of Analytical and Applied Pyrolysis*, 104, 28-37. doi:<https://doi.org/10.1016/j.jaap.2013.09.013>
- Michel, R., Rapagnà, S., Burg, P., Mazziotti di Celso, G., Courson, C., Zimny, T., & Gruber, R. (2011). Steam gasification of *Miscanthus X Giganteus* with olivine as catalyst production of syngas and analysis of tars (IR, NMR and GC/MS). *Biomass and Bioenergy*, 35(7), 2650-2658. doi:<https://doi.org/10.1016/j.biombioe.2011.02.054>

- Mikulcic, H., Klemeš, J. J., Vujanovic, M., Urbaniec, K., & Duic, N. (2016). Reducing greenhouse gasses emissions by fostering the deployment of alternative raw materials and energy sources in the cleaner cement manufacturing process. *Journal of Cleaner Production*, *30*, 1e14.
- Moghadam, R. A., Yusup, S., Uemura, Y., Chin, B. L. F., Lam, H. L., & Al Shoaibi, A. (2014). Syngas production from palm kernel shell and polyethylene waste blend in fluidized bed catalytic steam co-gasification process. *Energy*, *75*, 40-44. doi:https://doi.org/10.1016/j.energy.2014.04.062
- Mohamad Ros, S. H., Islam, M. S., Rahman, M. L., Rashid, S. S., Chowdhury, Z. Z., Ali, M. E., & Sarkar, S. M. (2016). *Highly Active and Reusable Kenaf Cellulose Supported Bio-Poly(hydroxamic acid) Functionalized Copper Catalysts for C–N Bond Formation Reactions* (Vol. 12).
- Mohd Azhar, S. H., Abdulla, R., Jambo, S. A., Marbawi, H., Gansau, J. A., Mohd Faik, A. A., & Rodrigues, K. F. (2017). Yeasts in sustainable bioethanol production: A review. *Biochemistry and Biophysics Reports*, *10*, 52-61. doi:https://doi.org/10.1016/j.bbrep.2017.03.003
- Molino, A., Chianese, S., & Musmarra, D. (2016). Biomass gasification technology: The state of the art overview. *Journal of Energy Chemistry*, *25*(1), 10-25.
- Molino, A., Larocca, V., Chianese, S., & Musmarra, D. (2018). Biofuels production by biomass gasification: A review. *Energies*, *11*(4), 811.
- Molitor, B., Marcellin, E., & Angenent, L. T. (2017). Overcoming the energetic limitations of syngas fermentation. *Current Opinion in Chemical Biology*, *41*, 84-92. doi:https://doi.org/10.1016/j.cbpa.2017.10.003
- Monir, M. U., Abd Aziz, A., Kristanti, R. A., & Yousuf, A. (2018a). Co-gasification of empty fruit bunch in a downdraft reactor: A pilot scale approach. *Bioresource Technology Reports*, *1*, 39-49. doi:https://doi.org/10.1016/j.biteb.2018.02.001
- Monir, M. U., Abd Aziz, A., Kristanti, R. A., & Yousuf, A. (2018b). Gasification of lignocellulosic biomass to produce syngas in a 50 kW downdraft reactor. *Biomass and Bioenergy*, *119*, 335-345. doi:https://doi.org/10.1016/j.biombioe.2018.10.006
- Monir, M. U., Abd Aziz, A., Kristanti, R. A., & Yousuf, A. (2018c). Syngas Production from Co-gasification of Forest Residue and Charcoal in a Pilot Scale Downdraft Reactor. *Waste and Biomass Valorization*. doi:10.1007/s12649-018-0513-5
- Monir, M. U., Yousuf, A., Aziz, A. A., & At Naw, S. M. (2017). Enhancing Co-Gasification of Coconut Shell by Reusing Char. *Indian Journal of Science and Technology*, *10*(6), 1-4. doi:10.17485/ijst/2017/v10i6/111217
- Moon, J., Jo, W., Jeong, S., Bang, B., Choi, Y., Hwang, J., & Lee, U. (2017). Gas cleaning with molten tin for hydrogen sulfide and tar in producer gas generated from

biomass gasification. *Energy*, 130, 318-326.
doi:<https://doi.org/10.1016/j.energy.2017.04.121>

- Morero, B., Groppelli, E. S., & Campanella, E. A. (2017). Evaluation of biogas upgrading technologies using a response surface methodology for process simulation. *Journal of Cleaner Production*, 141, 978-988.
- Moriarty, P., & Honnery, D. (2019). 6 - Global renewable energy resources and use in 2050. In T. M. Letcher (Ed.), *Managing Global Warming* (pp. 221-235): Academic Press.
- Mujah, D. (2016). Compressive strength and chloride resistance of grout containing ground palm oil fuel ash. *Journal of Cleaner Production*, 112, Part 1, 712-722. doi:<http://dx.doi.org/10.1016/j.jclepro.2015.07.066>
- Munasinghe, P. C., & Khanal, S. K. (2011a). Biomass-derived syngas fermentation into biofuels. *Biofuels*, 101(13), 79-98.
- Munasinghe, P. C., & Khanal, S. K. (2011b). Chapter 4 - Biomass-derived Syngas Fermentation into Biofuels A2 - Pandey, Ashok. In C. Larroche, S. C. Ricke, C.-G. Dussap, & E. Gnansounou (Eds.), *Biofuels* (pp. 79-98). Amsterdam: Academic Press.
- Naik, S. N., Goud, V. V., Rout, P. K., & Dalai, A. K. (2010). Production of first and second generation biofuels: a comprehensive review. *Renewable and Sustainable Energy Reviews*, 14(2), 578-597.
- Ng, W. C., You, S., Ling, R., Gin, K. Y.-H., Dai, Y., & Wang, C.-H. (2017). Co-gasification of woody biomass and chicken manure: Syngas production, biochar reutilization, and cost-benefit analysis. *Energy*, 139(Supplement C), 732-742. doi:<https://doi.org/10.1016/j.energy.2017.07.165>
- Nigam, P. S., & Singh, A. (2011). Production of liquid biofuels from renewable resources. *Progress in Energy and Combustion Science*, 37(1), 52-68.
- Nikoo, M. B., & Mahinpey, N. (2008). Simulation of biomass gasification in fluidized bed reactor using ASPEN PLUS. *Biomass and Bioenergy*, 32(12), 1245-1254. doi:<http://dx.doi.org/10.1016/j.biombioe.2008.02.020>
- Nwokolo, N., Mamphweli, S., & Makaka, G. (2016). An investigation into heat recovery from the surface of a cyclone dust collector attached to a downdraft biomass gasifier. *Applied Thermal Engineering*, 98(Supplement C), 1158-1164. doi:<https://doi.org/10.1016/j.applthermaleng.2016.01.014>
- Oakey, J. (2015). *Fuel Flexible Energy Generation: Solid, Liquid and Gaseous Fuels*: Woodhead Publishing.
- Oh, G., Ra, H. W., Yoon, S. M., Mun, T. Y., Seo, M. W., Lee, J. G., & Yoon, S. J. (2018). Gasification of coal water mixture in an entrained-flow gasifier: Effect of air and

oxygen mixing ratio. *Applied Thermal Engineering*, 129(Supplement C), 657-664. doi:<https://doi.org/10.1016/j.applthermaleng.2017.10.055>

- Osman, N., Othman, H. T., Karim, R. A., & Mazlan, M. A. F. (2014). Biomass in Malaysia: Forestry-based residues. *Int J Biomass Renew*, 3, 7-14.
- Oumer, A. N., Hasan, M. M., Baheta, A. T., Mamat, R., & Abdullah, A. A. (2018). Bio-based liquid fuels as a source of renewable energy: A review. *Renewable and Sustainable Energy Reviews*, 88, 82-98. doi:<https://doi.org/10.1016/j.rser.2018.02.022>
- Ozturk, M., Saba, N., Altay, V., Iqbal, R., Hakeem, K. R., Jawaid, M., & Ibrahim, F. H. (2017). Biomass and bioenergy: An overview of the development potential in Turkey and Malaysia. *Renewable and Sustainable Energy Reviews*, 79, 1285-1302. doi:<https://doi.org/10.1016/j.rser.2017.05.111>
- Paiman, M., Hamzah, N., Idris, S., Rahman, N., & Ismail, K. (2018). *Synergistic Effect of Co-utilization of Coal and Biomass Char: An Overview*. Paper presented at the IOP Conference Series: Materials Science and Engineering.
- Pallozzi, V., Di Carlo, A., Bocci, E., & Carlini, M. (2018). Combined gas conditioning and cleaning for reduction of tars in biomass gasification. *Biomass and Bioenergy*, 109, 85-90. doi:<https://doi.org/10.1016/j.biombioe.2017.12.023>
- Pambudi, N. A., Itaoka, K., Chapman, A., & Dinh, N. Biomass energy in Japan: Current status and future potential.
- Patel, V. R., Patel, D., Varia, N., & Patel, R. N. (2017). Co-gasification of lignite and waste wood in a pilot-scale (10 kW_e) downdraft gasifier. *Energy*, 119, 834-844. doi:<https://doi.org/10.1016/j.energy.2016.11.057>
- Patra, T. K., & Sheth, P. N. (2015). Biomass gasification models for downdraft gasifier: A state-of-the-art review. *Renewable and Sustainable Energy Reviews*, 50, 583-593.
- Peters, J. F., Banks, S. W., Bridgwater, A. V., & Dufour, J. (2017). A kinetic reaction model for biomass pyrolysis processes in ASPEN Plus. *Applied Energy*, 188, 595-603.
- Phillips, J. R., Huhnke, R. L., & Atiyeh, H. K. (2017). Syngas fermentation: a microbial conversion process of gaseous substrates to various products. *Fermentation*, 3(2), 28.
- Prapakarn, S., Arjharn, W., Liplap, P., Prapakarn, N., & Hinsui, T. (2017). Effect of Steam on the Energy and Activated Carbon Production of A Pilot-Scale Downdraft Steam Co-Gasification. *Oriental Journal of Chemistry*, 33(5), 2443-2451.

- Prasertcharoensuk, P., Hernandez, D. A., Bull, S. J., & Phan, A. N. (2018). Optimisation of a throat downdraft gasifier for hydrogen production. *Biomass and Bioenergy*, *116*, 216-226. doi:<https://doi.org/10.1016/j.biombioe.2018.06.019>
- Prins, M. J., & Ptasiński, K. J. (2005). Energy and exergy analyses of the oxidation and gasification of carbon. *Energy*, *30*(7), 982-1002. doi:<https://doi.org/10.1016/j.energy.2004.08.010>
- Qin, Y.-h., Han, Q.-q., Zhao, Z.-b., Du, Z.-y., Feng, J., Li, W.-y., . . . Vassileva, C. G. (2017). Impact of biomass addition on organic structure and mineral matter of char during coal-biomass co-gasification under CO₂ atmosphere. *Fuel*, *202*, 556-562. doi:<https://doi.org/10.1016/j.fuel.2017.04.072>
- Rakesh, N., & Dasappa, S. (2018). A critical assessment of tar generated during biomass gasification - Formation, evaluation, issues and mitigation strategies. *Renewable and Sustainable Energy Reviews*, *91*, 1045-1064. doi:<https://doi.org/10.1016/j.rser.2018.04.017>
- Ramani, S., Allison, J. D., & Keller, A. E. (2004). Controlling syngas H₂: CO ratio by controlling feed hydrocarbon composition. In: Google Patents.
- Ramos, A., Monteiro, E., Silva, V., & Rouboa, A. (2018). Co-gasification and recent developments on waste-to-energy conversion: A review. *Renewable and Sustainable Energy Reviews*, *81*, 380-398.
- Rastogi, M., & Shrivastava, S. (2017). Recent advances in second generation bioethanol production: An insight to pretreatment, saccharification and fermentation processes. *Renewable and Sustainable Energy Reviews*, *80*, 330-340.
- Rathod, V., & Bhale, P. V. (2014). Experimental Investigation on Biogas Reforming for Syngas Production over an Alumina based Nickel Catalyst. *Energy Procedia*, *54*, 236-245. doi:<https://doi.org/10.1016/j.egypro.2014.07.267>
- Rathod, V. P., Shete, J., & Bhale, P. V. (2016). Experimental investigation on biogas reforming to hydrogen rich syngas production using solar energy. *International journal of hydrogen energy*, *41*(1), 132-138. doi:<https://doi.org/10.1016/j.ijhydene.2015.09.158>
- Rauch, R., Hrbek, J., & Hofbauer, H. (2014). Biomass gasification for synthesis gas production and applications of the syngas. *Wiley Interdisciplinary Reviews: Energy and Environment*, *3*(4), 343-362.
- Reddy, B. R., & Vinu, R. (2018). Feedstock Characterization for Pyrolysis and Gasification. In *Coal and Biomass Gasification* (pp. 3-36): Springer.
- Richardson, Y., Drobek, M., Julbe, A., Blin, J., & Pinta, F. (2015). Biomass gasification to produce syngas. *Recent Advances in Thermo-chemical Conversion of Biomass*.
- Roy, D., & Ghosh, S. (2017). Energy and exergy analyses of an integrated biomass gasification combined cycle employing solid oxide fuel cell and organic Rankine

cycle. *Clean Technologies and Environmental Policy*, 19(6), 1693-1709.
doi:10.1007/s10098-017-1358-5

- Ruiz, B., Girón, R. P., Suárez-Ruiz, I., & Fuente, E. (2017). From fly ash of forest biomass combustion (FBC) to micro-mesoporous silica adsorbent materials. *Process Safety and Environmental Protection*, 105, 164-174.
doi:https://doi.org/10.1016/j.psep.2016.11.005
- Sadhukhan, J., Martinez-Hernandez, E., Murphy, R. J., Ng, D. K. S., Hassim, M. H., Siew Ng, K., . . . Andiappan, V. (2018). Role of bioenergy, biorefinery and bioeconomy in sustainable development: Strategic pathways for Malaysia. *Renewable and Sustainable Energy Reviews*, 81, 1966-1987.
doi:https://doi.org/10.1016/j.rser.2017.06.007
- Sadhukhan, J., Ng, K. S., & Hernandez, E. M. (2014). *Biorefineries and chemical processes: design, integration and sustainability analysis*: John Wiley & Sons.
- Sadhwani, N., Adhikari, S., Eden, M. R., & Li, P. (2018). Aspen plus simulation to predict steady state performance of biomass - CO₂ gasification in a fluidized bed gasifier. *Biofuels, Bioproducts and Biorefining*, 12(3), 379-389.
- Sakai, S., Nakashimada, Y., Yoshimoto, H., Watanabe, S., Okada, H., & Nishio, N. (2004). Ethanol production from H₂ and CO₂ by a newly isolated thermophilic bacterium, *Moorella* sp. HUC22-1. *Biotechnology letters*, 26(20), 1607-1612.
- Samiran, N. A., Jaafar, M. N. M., Ng, J.-H., Lam, S. S., & Chong, C. T. (2016). Progress in biomass gasification technique – With focus on Malaysian palm biomass for syngas production. *Renewable and Sustainable Energy Reviews*, 62, 1047-1062.
doi:https://doi.org/10.1016/j.rser.2016.04.049
- Sansaniwal, S. K., Pal, K., Rosen, M. A., & Tyagi, S. K. (2017). Recent advances in the development of biomass gasification technology: A comprehensive review. *Renewable and Sustainable Energy Reviews*, 72, 363-384.
doi:https://doi.org/10.1016/j.rser.2017.01.038
- Saravanakumar, K., Senthilraja, P., & Kathiresan, K. (2013). Bioethanol production by mangrove-derived marine yeast, *Sacchromyces cerevisiae*. *Journal of King Saud University - Science*, 25(2), 121-127.
doi:https://doi.org/10.1016/j.jksus.2012.12.005
- Sarkar, S. M., & Rahman, M. L. (2017). Cellulose supported poly(amidoxime) copper complex for Click reaction. *Journal of Cleaner Production*, 141, 683-692.
doi:https://doi.org/10.1016/j.jclepro.2016.09.153
- Sarrai, A., Hanini, S., Merzouk, N., Tassalit, D., Szabó, T., Hernádi, K., & Nagy, L. (2016). Using central composite experimental design to optimize the degradation of tylosin from aqueous solution by photo-fenton reaction. *Materials*, 9(6), 428.
- Saw, W. L., & Pang, S. (2013). Co-gasification of blended lignite and wood pellets in a 100kW dual fluidised bed steam gasifier: The influence of lignite ratio on

- producer gas composition and tar content. *Fuel*, 112, 117-124. doi:<https://doi.org/10.1016/j.fuel.2013.05.019>
- Sayed, E. T., & Abdelkareem, M. A. (2017). Yeast as a Biocatalyst in Microbial Fuel Cell. In *Old Yeasts-New Questions: InTech*.
- Searle, S., & Malins, C. (2015). A reassessment of global bioenergy potential in 2050. *Gcb Bioenergy*, 7(2), 328-336.
- Serrano-Ruiz, J. C. (2017). Biomass Conversion Technologies: Catalytic Conversion Technologies. In M. Rabaçal, A. F. Ferreira, C. A. M. Silva, & M. Costa (Eds.), *Biorefineries: Targeting Energy, High Value Products and Waste Valorisation* (pp. 113-121). Cham: Springer International Publishing.
- Shahbaz, M., Yusup, S., Inayat, D. A., Ammar, M., Patrick, D. O., Pratama, A., & Naqvi, S. R. (2017). Syngas production from steam gasification of Palm kernel shell with subsequent CO₂ Capturing using CaO sorbent: An Aspen plus modelling. *Energy & Fuels*. doi:10.1021/acs.energyfuels.7b02670
- Shankar, S., & Shikha. (2017). Renewable and Nonrenewable Energy Resources: Bioenergy and Biofuels. In R. L. Singh (Ed.), *Principles and Applications of Environmental Biotechnology for a Sustainable Future* (pp. 293-314). Singapore: Springer Singapore.
- Sharma, M., Attanoor, S., & Dasappa, S. (2015). Investigation into co-gasifying Indian coal and biomass in a down draft gasifier—Experiments and analysis. *Fuel Processing Technology*, 138, 435-444.
- Shayan, E., Zare, V., & Mirzaee, I. (2018). Hydrogen production from biomass gasification; a theoretical comparison of using different gasification agents. *Energy Conversion and Management*, 159, 30-41. doi:<https://doi.org/10.1016/j.enconman.2017.12.096>
- Shen, Y., Brown, R., & Wen, Z. (2014a). Enhancing mass transfer and ethanol production in syngas fermentation of *Clostridium carboxidivorans* P7 through a monolithic biofilm reactor. *Applied Energy*, 136, 68-76. doi:<https://doi.org/10.1016/j.apenergy.2014.08.117>
- Shen, Y., Brown, R., & Wen, Z. (2014b). Syngas fermentation of *Clostridium carboxidivoran* P7 in a hollow fiber membrane biofilm reactor: Evaluating the mass transfer coefficient and ethanol production performance. *Biochemical Engineering Journal*, 85, 21-29.
- Shen, Y., Brown, R. C., & Wen, Z. (2017). Syngas fermentation by *Clostridium carboxidivorans* P7 in a horizontal rotating packed bed biofilm reactor with enhanced ethanol production. *Applied Energy*, 187, 585-594. doi:<https://doi.org/10.1016/j.apenergy.2016.11.084>

- Shone, C. M., & Jothi, T. J. S. (2016). Preparation of gasification feedstock from leafy biomass. *Environmental Science and Pollution Research*, 23(10), 9364-9372. doi:10.1007/s11356-015-5167-2
- Sikarwar, V. S., Zhao, M., Clough, P., Yao, J., Zhong, X., Memon, M. Z., . . . Fennell, P. S. (2016). An overview of advances in biomass gasification. *Energy & Environmental Science*, 9(10), 2939-2977. doi:10.1039/C6EE00935B
- Sikarwar, V. S., Zhao, M., Fennell, P. S., Shah, N., & Anthony, E. J. (2017). Progress in biofuel production from gasification. *Progress in Energy and Combustion Science*, 61, 189-248. doi:<https://doi.org/10.1016/j.pecs.2017.04.001>
- Singh, V. C. J., & Sekhar, S. J. (2016). Performance studies on a downdraft biomass gasifier with blends of coconut shell and rubber seed shell as feedstock. *Applied Thermal Engineering*, 97, 22-27. doi:<https://doi.org/10.1016/j.applthermaleng.2015.09.099>
- Singh, Y. D., Mahanta, P., & Bora, U. (2017). Comprehensive characterization of lignocellulosic biomass through proximate, ultimate and compositional analysis for bioenergy production. *Renewable Energy*, 103, 490-500.
- Singha, A. S., & Guleria, A. (2015). Utility of chemically modified agricultural waste okra biomass for removal of toxic heavy metal ions from aqueous solution. *Engineering in Agriculture, Environment and Food*, 8(1), 52-60. doi:<https://doi.org/10.1016/j.eaef.2014.08.001>
- Smith, M. W., Pecha, B., Helms, G., Scudiero, L., & Garcia-Perez, M. (2017). Chemical and morphological evaluation of chars produced from primary biomass constituents: Cellulose, xylan, and lignin. *Biomass and Bioenergy*, 104, 17-35. doi:<https://doi.org/10.1016/j.biombioe.2017.05.015>
- Speight, J. G. (2011). *The biofuels handbook*: Royal Society of Chemistry.
- Stitt, E. H. (2002). Alternative multiphase reactors for fine chemicals: A world beyond stirred tanks? *Chemical Engineering Journal*, 90(1), 47-60. doi:[https://doi.org/10.1016/S1385-8947\(02\)00067-0](https://doi.org/10.1016/S1385-8947(02)00067-0)
- Sun, X., Atiyeh, H. K., Kumar, A., & Zhang, H. (2018). Enhanced ethanol production by *Clostridium ragsdalei* from syngas by incorporating biochar in the fermentation medium. *Bioresource Technology*, 247, 291-301. doi:<https://doi.org/10.1016/j.biortech.2017.09.060>
- Sun, X., Atiyeh, H. K., Kumar, A., Zhang, H., & Tanner, R. S. J. B. t. (2018). Biochar enhanced ethanol and butanol production by *Clostridium carboxidivorans* from syngas. 265, 128-138.
- Susastriawan, A., & Saptoadi, H. (2017). Small-scale downdraft gasifiers for biomass gasification: A review. *Renewable and Sustainable Energy Reviews*, 76, 989-1003.

- Suzuki, K., Tsuji, N., Shirai, Y., Hassan, M. A., & Osaki, M. (2017). Evaluation of biomass energy potential towards achieving sustainability in biomass energy utilization in Sabah, Malaysia. *Biomass and Bioenergy*, 97, 149-154. doi:http://dx.doi.org/10.1016/j.biombioe.2016.12.023
- Tian, L., Papanek, B., Olson, D. G., Rydzak, T., Holwerda, E. K., Zheng, T., . . . Giannone, R. J. (2016). Simultaneous achievement of high ethanol yield and titer in *Clostridium thermocellum*. *Biotechnology for biofuels*, 9(1), 116.
- Titirici, M.-M., Antonietti, M., & Thomas, A. (2006). A generalized synthesis of metal oxide hollow spheres using a hydrothermal approach. *Chemistry of Materials*, 18(16), 3808-3812.
- Toklu, E. (2017). Biomass energy potential and utilization in Turkey. *Renewable Energy*, 107, 235-244. doi:https://doi.org/10.1016/j.renene.2017.02.008
- Tsai, W. T., Lee, M. K., & Chang, Y. M. (2006). Fast pyrolysis of rice straw, sugarcane bagasse and coconut shell in an induction-heating reactor. *Journal of Analytical and Applied Pyrolysis*, 76(1), 230-237. doi:https://doi.org/10.1016/j.jaap.2005.11.007
- Tsuchida, Y., Tsukagoshi, N., & Ueyama, M. (2017). Growth method for microbe and bioethanol production method. In: Google Patents.
- Unyaphan, S., Tarnpradab, T., Takahashi, F., & Yoshikawa, K. (2017). Improvement of tar removal performance of oil scrubber by producing syngas microbubbles. *Applied Energy*, 205, 802-812. doi:https://doi.org/10.1016/j.apenergy.2017.08.071
- Valderrama Rios, M. L., González, A. M., Lora, E. E. S., & Almazán del Olmo, O. A. (2018). Reduction of tar generated during biomass gasification: A review. *Biomass and Bioenergy*, 108, 345-370. doi:https://doi.org/10.1016/j.biombioe.2017.12.002
- Valdés, C. F., Marrugo, G., Chejne, F., Montoya, J. I., & Gómez, C. A. (2015). Pilot-scale fluidized-bed co-gasification of palm kernel shell with sub-bituminous coal. *Energy & Fuels*, 29(9), 5894-5901.
- Vassilev, S. V., Vassileva, C. G., & Vassilev, V. S. (2015). Advantages and disadvantages of composition and properties of biomass in comparison with coal: An overview. *Fuel*, 158, 330-350. doi:http://dx.doi.org/10.1016/j.fuel.2015.05.050
- Vinícius de Melo Pereira, G., Soccol, V. T., Brar, S. K., Neto, E., & Soccol, C. R. (2017). Microbial ecology and starter culture technology in coffee processing. *Critical reviews in food science nutrition*, 57(13), 2775-2788.
- Wang, D., Geng, Z., Li, B., & Zhang, C. (2015). High performance electrode materials for electric double-layer capacitors based on biomass-derived activated carbons. *Electrochimica Acta*, 173(Supplement C), 377-384. doi:https://doi.org/10.1016/j.electacta.2015.05.080

- Wang, P., Jin, L., Liu, J., Zhu, S., & Hu, H. (2013). Analysis of coal tar derived from pyrolysis at different atmospheres. *Fuel*, *104*, 14-21. doi:<https://doi.org/10.1016/j.fuel.2010.06.041>
- Wang, S., Dai, G., Yang, H., & Luo, Z. (2017). Lignocellulosic biomass pyrolysis mechanism: A state-of-the-art review. *Progress in Energy and Combustion Science*, *62*, 33-86. doi:<https://doi.org/10.1016/j.pecs.2017.05.004>
- Wang, S. R., Dai, G. X., Yang, H. P., & Luo, Z. Y. (2017). Lignocellulosic biomass pyrolysis mechanism: A state-of-the-art review. *Progress in Energy and Combustion Science*, *62*, 33-86. doi:[10.1016/j.pecs.2017.05.004](https://doi.org/10.1016/j.pecs.2017.05.004)
- Wei, L. (2005). Experimental study on the effects of operational parameters of a downdraft gasifier. *Masters Abstracts International*, *47*(01).
- Widjaya, E. R., Chen, G., Bowtell, L., & Hills, C. (2018). Gasification of non-woody biomass: A literature review. *Renewable and Sustainable Energy Reviews*, *89*, 184-193. doi:<https://doi.org/10.1016/j.rser.2018.03.023>
- Wyman, C. E. (2018). Ethanol production from lignocellulosic biomass: overview. In *Handbook on Bioethanol* (pp. 1-18): Routledge.
- Xu, D., Tree, D. R., & Lewis, R. S. (2011). The effects of syngas impurities on syngas fermentation to liquid fuels. *Biomass and Bioenergy*, *35*(7), 2690-2696. doi:<https://doi.org/10.1016/j.biombioe.2011.03.005>
- Xu, H., Liang, C., Yuan, Z., Xu, J., Hua, Q., & Guo, Y. (2017). A study of CO/syngas bioconversion by *Clostridium autoethanogenum* with a flexible gas-cultivation system. *Enzyme and Microbial Technology*, *101*, 24-29.
- Xu, N., Kim, S. S., Li, A., Grace, J. R., Lim, C. J., & Boyd, T. (2016). Investigation of the influence of tar-containing syngas from biomass gasification on dense Pd and Pd-Ru membranes. *Powder Technology*, *290*, 132-140.
- Yang, H., & Chen, H. (2015). 11 - Biomass gasification for synthetic liquid fuel production A2 - Luque, Rafael. In J. G. Speight (Ed.), *Gasification for Synthetic Fuel Production* (pp. 241-275): Woodhead Publishing.
- Yi, Q., Qi, F., Cheng, G., Zhang, Y., Xiao, B., Hu, Z., . . . Xu, S. (2013). Thermogravimetric analysis of co-combustion of biomass and biochar. *Journal of Thermal Analysis and Calorimetry*, *112*(3), 1475-1479. doi:[10.1007/s10973-012-2744-1](https://doi.org/10.1007/s10973-012-2744-1)
- Yoo, H.-M., Lee, J.-S., Yang, W.-S., Choi, H. S., Jang, H.-N., & Seo, Y.-C. (2018). Co-gasification characteristics of palm oil by-products and coals for syngas production. *Korean Journal of Chemical Engineering*, *35*(3), 654-661. doi:[10.1007/s11814-017-0312-x](https://doi.org/10.1007/s11814-017-0312-x)

- Yu, J., Paterson, N., Blamey, J., & Millan, M. (2017). Cellulose, xylan and lignin interactions during pyrolysis of lignocellulosic biomass. *Fuel*, *191*, 140-149. doi:<https://doi.org/10.1016/j.fuel.2016.11.057>
- Zhang, J., Choi, Y. S., Yoo, C. G., Kim, T. H., Brown, R. C., & Shanks, B. H. (2015). Cellulose–hemicellulose and cellulose–lignin interactions during fast pyrolysis. *ACS Sustainable Chemistry & Engineering*, *3*(2), 293-301.
- Zhang, J., Taylor, S., & Wang, Y. (2016). Effects of end products on fermentation profiles in *Clostridium carboxidivorans* P7 for syngas fermentation. *Bioresource Technology*, *218*, 1055-1063. doi:<http://dx.doi.org/10.1016/j.biortech.2016.07.071>
- Zhang, Y., Zhao, Y., Gao, X., Li, B., & Huang, J. (2015). Energy and exergy analyses of syngas produced from rice husk gasification in an entrained flow reactor. *Journal of Cleaner Production*, *95*, 273-280. doi:<https://doi.org/10.1016/j.jclepro.2015.02.053>
- Zhang, Y., & Zheng, Y. (2016). Co-gasification of coal and biomass in a fixed bed reactor with separate and mixed bed configurations. *Fuel*, *183*, 132-138. doi:<http://dx.doi.org/10.1016/j.fuel.2016.06.066>
- Zhang, Z., Macquarrie, D. J., Budarin, V. L., Hunt, A. J., Gronnow, M. J., Fan, J., . . . Matharu, A. S. (2015). Low-temperature microwave-assisted pyrolysis of waste office paper and the application of bio-oil as an AI adhesive. *Green Chemistry*, *17*(1), 260-270.
- Zhang, Z., Pang, S., & Levi, T. (2017). Influence of AAEM species in coal and biomass on steam co-gasification of chars of blended coal and biomass. *Renewable Energy*, *101*, 356-363.
- Zhao, J., Lin, M., & Chen, G. (2018). Facile recycling of *Escherichia coli* and *Saccharomyces cerevisiae* cells from suspensions using magnetic modification method and mechanism analysis. *Colloids and Surfaces B: Biointerfaces*, *169*, 1-9. doi:<https://doi.org/10.1016/j.colsurfb.2018.05.006>
- Zhou, C., Rosén, C., & Engvall, K. (2016). Biomass oxygen/steam gasification in a pressurized bubbling fluidized bed: Agglomeration behavior. *Applied Energy*, *172*, 230-250. doi:<http://dx.doi.org/10.1016/j.apenergy.2016.03.106>
- Zuriarrain, A., Zuriarrain, J., Villar, M., & Berregi, I. (2015). Quantitative determination of ethanol in cider by ¹H NMR spectrometry. *Food Control*, *50*, 758-762. doi:<https://doi.org/10.1016/j.foodcont.2014.10.024>

LIST OF PUBLICATIONS

No.	Title	Authors	Journal/ Conference	Type of Article	Objective covered	Status
Articles						
1.	Gasification of lignocellulosic biomass to produce syngas in a 50kW downdraft reactor	Minhaj Uddin Monir , Azrina Abd Aziz, Risky Ayu Kristanti and Abu Yousuf	Biomass and Bioenergy	Journal (Elsevier, ISI and Scopus Indexed, IF: 3.358)	Objectives 1 and 2	Published (2018)
2.	Syngas production from co-gasification of forest residue and charcoal in a pilot scale downdraft reactor	Minhaj Uddin Monir , Azrina Abd Aziz, Risky Ayu Kristanti and Abu Yousuf	Waste and Biomass Valorization	Journal (SpringerLink, ISI and Scopus Indexed, IF: 1.874)	Objectives 1 and 2	Published (2018)
3.	Co-gasification of empty fruit bunch in a downdraft reactor: A pilot scale approach.	Minhaj Uddin Monir , Azrina Abd Aziz, Risky Ayu Kristanti and Abu Yousuf	Bioresource Technology Reports	Journal (Elsevier, Peer review)	Objectives 1 and 2	Published (2018)
4.	Enhancing Co-Gasification of Coconut Shell by Reusing Char	Monir, M. U. , Yousuf, A., Aziz, A. A., and Atnaw	Indian Journal of Science and Technology	Journal (Scopus Indexed)	Objective 2	Published (2017)
5.	Application of Electroporation Technique in Biofuel Processing	Yousuf, A., Khan, M. R., Islam, A., Monir, M. U. , Ab Wahid, Z., and Pirozzi, D	MATEC Web of Conferences	Conference cited by Scopus	Objective 3 (Related)	Published (2017)
6.	Social business models for empowering the biogas technology.	Yousuf, A., Sultana, S., Monir, M. U. , Karim, A., and Rahmaddulla, S. R. B.	Energy Sources, Part B: Economics, Planning, and Policy	Journal (Taylor & Francis, ISI and Scopus Indexed, IF: 0.976)	Objective 2 (Related)	Published (2017)
7.	Implementation of Carbon Dioxide Gas Injection Method for Gas Recovery at Rashidpur Gas Field, Bangladesh	Khatun, Fatema and Minhaj Uddin Monir and Arham, S. M. Nafefun and Zulari sam, A. W.	International Journal of Engineering Technology And Sciences (IJETS)	Journal	Objective 2 (Related)	Published (2016)
8.	Syngas fermentation to bioethanol	Minhaj Uddin Monir , Abu Yousuf and Azrina Abd Aziz	Lignocellulosic biomass to Liquid biofuels	Book Chapter Elsevier. (Academic Press).	Objective 3	Under Production (2019)
9.	Thermal effect on co-product tar produced with syngas through co-gasification of coconut shell and charcoal	Minhaj Uddin Monir , Fatema Khatun, U. R. Ramzilah and Azrina Abd Aziz	Energy Security and Chemical Engineering Congress (ESChE) 2019	IOP Conference (Scopus Indexed)	Objective 2 (Related)	Accepted
10.	Hydrogen-rich syngas fermentation for bioethanol production using <i>Sacharomyces Cerevisia</i>	Minhaj Uddin Monir , Azrina Abd Aziz, Abu Yousuf and Md. Zahangir Alam	International Journal of Hydrogen Energy	Journal (ISI and Scopus Indexed)	Objective 3	Under Review

No.	Title	Authors	Journal/ Conference	Type of Article	Objective covered	Status
11	Recovery Mechanism of Entrapped Oil by Applying Hybrid Enhanced Oil Recovery (HEOR) Technique: A Review	Minhaj Uddin Monir , Fatema Khatun, Abu Yousuf and Azrina Abd Aziz1	Arabian Journal of Geosciences	Journal (ISI and Scopus Indexed)	Objective 2 (Related)	Under Review
12	Co-product Tar Reduction from Syngas Produced from the Co-gasification of Coconut shell and Charcoal: A Study on the Effect of Temperature	Minhaj Uddin Monir , Fatema Khatun, U. R. Ramzilah and Azrina Abd Aziz	International Journal of Hydrogen Energy	Journal (ISI and Scopus Indexed)	Objective 2 (Related)	In Preparation
13	Lignocellulosic Biomass Conversion to Syngas Through Co-gasification Approach	Minhaj Uddin Monir , Azrina Abd Aziz, Fatema Khatun and Nadzirah Mohd Mokhtar	Biomass Conversion to Fuel and Chemicals	Book Chapter CRC Press Taylor & Francis Group	Objective 3	In Preparation
14	Bioethanol production through syngas fermentation in a tar free bioreactor using <i>Clostridium Butyricum</i>	Minhaj Uddin Monir , Azrina Abd Aziz and Abu Yousuf	Bioresource Technology	Journal (ISI and Scopus Indexed)	Objective 3	In Preparation
Conference Abstract						
1.	New Strategy For Enhancing Co-Gasification Process By Reusing Tar/Char	Monir, M. U., Yousuf, A., Aziz, A. A., and At Naw, S. M.	International Conference on Fluids and Chemical Engineering (FluidsChE 2017)	Conference	Objective 2	Published (4-6 April 2017, Sabah, Malaysia)
2.	Liquid biofuel production from lignocellulosic biomass through syngas fermentation	Monir, M. U., Yousuf, A., and Aziz, A. A	5th World Convention on Recycling and Waste Management	Conference	Objective 3	Published (September 11- 12, 2017, Singapore)
3.	Lipid extraction from microbial cell by electroporation technique and its influence on direct transesterification for biodiesel synthesis	Yousuf, A., Khan, M. R., Karim, A., Islam, A., Monir, M. U., Sultana, S., and Pirozzi, D.	World Academy of Science, Engineering and Technology, International Journal of Energy and Power Engineering	Conference	Objective 3 (Related)	Published (2017)



Research paper

Gasification of lignocellulosic biomass to produce syngas in a 50 kW downdraft reactor

Minhaj Uddin Monir^{a,b}, Azrina Abd Aziz^{a,*}, Risky Ayu Kristanti^a, Abu Yousuf^c

^a Faculty of Engineering Technology, Universiti Malaysia Pahang, 26300, Gambang, Malaysia

^b Department of Petroleum and Mining Engineering, Jessore University of Science and Technology, Jessore, 7408, Bangladesh

^c Department of Chemical Engineering and Polymer Science, Shahjalal University of Science and Technology, Sylhet, 3114, Bangladesh

ARTICLE INFO

Keywords:

Co-gasification
Coconut shell
Charcoal
Downdraft reactor
Syngas

ABSTRACT

Lignocellulosic biomass gasification shows a pronounced prospective to replace fossil fuels. In this study, the gasification of coconut shell with charcoal using a 50 kW downdraft reactor was investigated. The controlling parameter of temperature and pressure were used to verify the production of gas during the gasification process with air. The higher contents of cellulose and hemicellulose than lignin in the sample were found to gasify better, as evident from structural analysis. The gasifier produces a combustible gas with a H₂, CO, CO₂ and CH₄ concentrations of 8.44, 15.38, 5.38 and 1.62 mol.% respectively, at a total flow of air of 30 m³ h⁻¹. The results revealed that 30 wt% charcoal in the feedstock was effectively gasified to generate syngas comprising over 30 mol.% of syngas with a lower heating value of 3.27 MJ/Nm³. Thus, the co-gasification of lignocellulosic biomass with charcoal may contribute to affordable and environmentally friendly syngas energy.

1. Introduction

Worldwide energy demand is increasing exponentially due to the rising trend of global population, industrial expansion, rapid urbanization, economic growth which results the gradual depletion of fossil-based fuels like oil, gas and coal [1–3]. Lignocellulosic biomass is an alternative, promising and fastest-growing renewable energy sources to produce bioenergy [4,5]. This type of biomass absorbs and stored energy from the sunlight in the form of chemical energy through photosynthesis process. These biomasses contain 40 to 50 wt% of cellulose, 25 to 35 wt% of hemicellulose and 16 to 33 wt% of lignin [6]. Generally, biomass consists of chemical bonds of C–C, C–O and some other elements of nitrogen (N) and sulfur (S) [7]. Bioenergy containing biomass is converted into energy through thermochemical conversion of combustion, pyrolysis and gasification [4]. Gasification is the thermochemical partial oxidation process that converted biomass into synthetic gas (syngas) using a reactor and further processing it is used for electricity or transporting fuel purposes [8]. Generally, there are four types of reactors (downdraft, updraft, fluidized bed and entrained bed) are used for syngas production through this conversion process.

Biomass gasification through downdraft reactor is most widely used due to its high conversion efficiency of the producer syngas [9]. The choice of reactor depends on feedstock type, size, moisture content, and gasification agents (steam/oxygen/air) [10]. Downdraft reactor has

four separate thermochemical conversion zones. These zones are drying, pyrolysis, oxidation and reduction, included from top to bottom, respectively, while reduction zone is responsible for syngas production. This type of reactor produces less amount of tar, and reduction zone plays a vital role for the maximum conversion of tar and high quality syngas [11]. Syngas consists of H₂, CO, CO₂, CH₄, N₂ and some other compounds like C₂H₄, C₂H₆, NH₃, H₂S, and tar [9,12]. The production of syngas is affected by some important factors such as reactor type, fuel type, gasification medium (steam or air) and operational conditions (temperature, pressure) whereas fuel type has the most significant impact. The previous work stated that the co-gasification rate in a downdraft reactor was increased gradually due to the addition of char (charcoal) with coconut shell [13].

The co-gasification process was performed for the reduction of tar content in the produced syngas by blending of biomass with coal [14]. Some researchers reported the co-gasification process using fossil-based fuel (coal) and lignocellulosic biomass considering the environmental and gasification enhancement point of view [15–19]. Furthermore, coal-based energy is treated as a dirty energy due to the presence of sulfur, contrarily lignocellulosic biomass and biomass-based charcoal contain least amount of sulfur. In addition, exploitation, processing and transportation cost of coal is relatively high [20,21]. Collard and Blin [22] reported that conversion of biomass-based feedstock (cellulose, hemicelluloses and lignin) through thermochemical process followed

* Corresponding author.

E-mail address: azrinaaziz@ump.edu.my (A. Abd Aziz).

<https://doi.org/10.1016/j.biombioe.2018.10.006>

Received 20 March 2018; Received in revised form 28 September 2018; Accepted 3 October 2018
0961-9534/ © 2018 Elsevier Ltd. All rights reserved.



Syngas Production from Co-gasification of Forest Residue and Charcoal in a Pilot Scale Downdraft Reactor

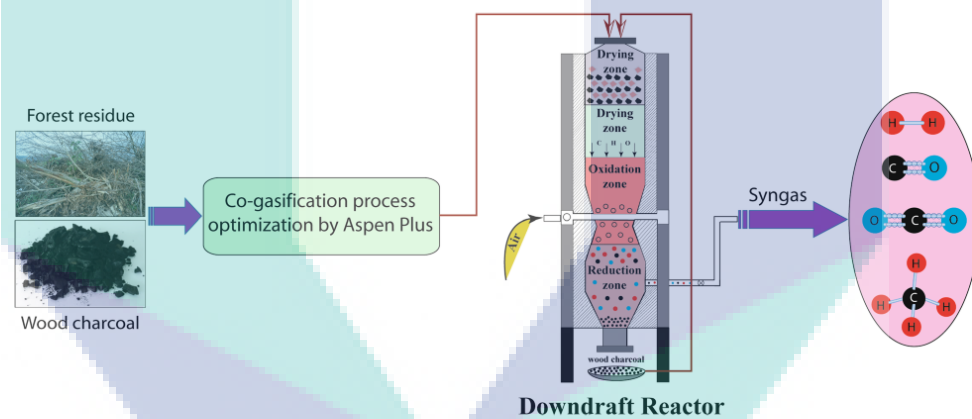
Minhaj Uddin Monir^{1,2} · Azrina Abd Aziz¹ · Risky Ayu Kristanti¹ · Abu Yousuf³

Received: 18 April 2018 / Accepted: 1 November 2018
© Springer Nature B.V. 2018

Abstract

A study on the co-gasification of forest residue and wood charcoal was executed on pilot-scale 50 kWth downdraft gasification reactor. The reactor parameters (i.e. temperature, pressure) were evaluated on various parameters namely heating value, syngas yield, exergy, feedstock consumption rate and produced syngas composition. To facilitate the optimization of the exergy efficiency of gasification systems, a comprehensive fixed-bed gasification model has been established using an Aspen Plus (V8.6) simulator to predict the product rate of syngas. The model is applicable for efficient analysis of fixed-bed biomass gasification under variable operating conditions, such as syngas ratio, moisture content of feedstock, and air inlet location. The concentration variation of the downdraft reactor showed that the CO concentration increased with increasing wood charcoal (up to 40%) with forest residue. In contrary, an opposite trend for the case CO₂ concentration was observed with increasing the wood charcoal in the reactor. The optimal yield of syngas (H₂:CO) ratio was found to be 1.14 after the FR:WC mixture of 70:30 and 60:40 w/w for maximizing the benefits of the gasification process.

Graphical Abstract



Keywords Co-gasification · Forest residue · Wood charcoal · Downdraft reactor · Syngas · Exergy efficiency

✉ Azrina Abd Aziz
azrinaaziz@ump.edu.my

Extended author information available on the last page of the article

Published online: 09 November 2018



Co-gasification of empty fruit bunch in a downdraft reactor: A pilot scale approach

Minhaj Uddin Monir^{a,b}, Azrina Abd Aziz^{a,*}, Risky Ayu Kristanti^a, Abu Yousuf^c

^a Faculty of Engineering Technology, Universiti Malaysia Pahang, 26300 Gambang, Malaysia

^b Department of Petroleum and Mining Engineering, Jessore University of Science and Technology, Jessore 7408, Bangladesh

^c Department of Chemical Engineering and Polymer Science, Shahjalal University of Science and Technology, Sylhet 3114, Bangladesh



ARTICLE INFO

Article history:

Received 30 December 2017

Received in revised form 3 February 2018

Accepted 4 February 2018

Available online 10 February 2018

Keywords:

Co-gasification

Downdraft reactor

EFB

Charcoal

Aspen plus

ABSTRACT

Biomass gasification shows great potential to displace fossil fuels. This paper states the steady state simulation for the gasification of palm oil empty fruit bunch (EFB) in pilot plant downdraft reactor and modelled using Aspen Plus®. The biomass was characterized to evaluate the degree of feedstock's structural order. The effect of reactor temperature and pressure on syngas production of downdraft gasification of EFB at the constant steam flow rate of 186.37 mol/h were investigated. The results revealed the concentration of hydrogen and CO increased from 12 to 17.5 mol% and 55–60.6 mol% respectively, but the CO₂ concentration decreased from 30 to 19.4 mol% with increasing temperature (875–975 °C) and pressure (25–35 bar). The results indicated that the product gas from co-gasification with charcoal has higher H₂ and CO concentrations in comparison with the EFB gasification. Therefore, co-gasification of the feedstock has a significant potential to overcome the problem of disrupted feedstock supply in gasification.

© 2018 Elsevier Ltd. All rights reserved.

1. Introduction

Energy consumption increases exponentially with the rapid increments of the global population, urbanization and industrial expansion. World's energy is facing a critical situation due to the depletion of limited fossil fuels. >80% of the world's energy demand is covered by non-renewable energy resources (oil, gas, coal etc.), whereas renewable energy resources cover only 10–15% (Singh and Sekhar, 2016). In terms of environmental consideration, biomass contains the negligible amount of sulfur (S), produce fewer ash particles and generate the least amount of air emissions in comparison with fossil fuels (coal treats as a dirty energy and oil creates adverse environmental impact) (Cai et al., 2017). Therefore, biomass combustion does not contribute to sulfur dioxide (SO₂) emissions, which may cause acid rain. In addition, continuous development of the technological exploitation and discovery of new reserves of oil and gas cannot meet the energy demand, and thus a gap exists between the demand and the supply of fuel resources. Consequently, due to increasing demand of energy, more attention has been paid to develop new renewable energy sources. Suzuki et al. (2017) reported on the biomass energy utilization from the lignocellulosic biomasses of empty fruit bunches (EFB). In this aspect, this biomass based syngas production could be the suitable alternative for non-renewable energy sources in future for Malaysia.

Lignocellulosic biomasses are composed of three main macromolecules: cellulose (40–50 wt%), hemicellulose (25–35 wt%) and lignin (16–33 wt%) that could be converted to energy by thermochemically (Cai et al., 2017). The main elemental composition of biomasses are carbon (C), hydrogen (H) and oxygen (O) molecules that are bonded together and broken by combustion or decomposition (Chen et al., 2016). Energy from gasification involves some repeated processes which are drying, pyrolysis, oxidation and reduction. Products are obtained in three stages: low molecular weight liquid, gas fuel and solid residue (Sikarwar et al., 2016). Different types of gasifiers (reactors) are generally used for syngas production; such as fixed bed gasifier (downdraft and updraft), fluidized bed gasifier (circulating and bubbling) and entrained flow gasifier (Oakey, 2015). The choice of the reactor is usually depended on the feedstock type, size, moisture content and end product with the interaction system of steam/oxygen/air (Sansaniwal et al., 2017). The simulation modelling is very useful since it provides precise analysis of a process without performing experimental study. Suitable selection of simulation model helped to find the optimized process that can reduce time and expenses involved in experimental studies (Buyya and Murshed, 2002). Aspen plus simulator is a software tool used for the simulation of gasification process, combustion and coal gasification along with the integrated coal/biomass gasification to predict the syngas, synthetic natural gas (SNG) and power production (Shahbaz et al., 2017).

At present, Malaysia is the world's largest producer and exporter of palm oil and produces about 47% of the world's supply of palm oil

* Corresponding author.

E-mail address: azrinaaziz@ump.edu.my (A. Abd Aziz).

Enhancing Co-Gasification of Coconut Shell by Reusing Char

Minhaj Uddin Monir, Abu Yousuf*, Azrina Abd Aziz and Samson Mekbib Atnaw

Faculty of Engineering Technology, Universiti Malaysia Pahang, 26300, Gambang, Malaysia; ayousufcep@yahoo.com

Abstract

Objectives: This paper aims to investigate the influence of char reuse in the gasification process. **Methods:** Co-gasification of biomass (coconut shell) and char was carried out in a downdraft gasifier. Char was produced as a by-product in biomass gasification process which contains a huge amount of concentrated carbon. The simulation was run for the different ratios of coconut shell and char (100:0, 90:10, 80:20 and 70:30) by ASPEN PLUS process simulator software to find out a suitable ratio. **Findings:** The calculated energy is 23703.45 Kcal, 24207.78 Kcal, 24964.28 Kcal and 25468.60 Kcal, where the char ratio is 0%, 10%, 20% and 30%, respectively. Based on the simulation result, gasification was accomplished by adding 30% of char with coconut shell biomass. The simulated and experiment results proved that more energy can be produced by increasing the char ratio. **Application:** Many countries started to find out an alternative source of energy instead of non-renewable energy resources, especially from biomass. Co-gasification of the coconut shell with suitable char ratios is the best alternatives to meet up the world's future energy demand.

Keywords: ASPEN PLUS Simulator, Biomass, Char, Co-Gasification, Syngas

1. Introduction

In this century, energy is the most important political issue for ongoing fuel and economic crisis globally. It is the key components for the development of any country¹. World economy is still depends on the non-renewable energy sources (natural gas, oil and coal), which are exhaustible, geographically concentrated, limited to reserve, increasingly expensive and very polluting². Therefore, energy generation from renewable sources has attracted the attention of investor and energy scientists. The most abundant renewable energy resource is biomass, which is mainly carbon based. It also contains mixture of organic molecules encompassed with hydrogen, oxygen, nitrogen and small number of other elements. It is mainly derived from biological origins, such as agricultural residue (rice straw, wheat straw, coconut shell, empty fruit bunch of palm oil, etc.), forest residues, municipal solid wastes, etc.³⁻⁵. Biomass gasification is a promising technique for energy production as syngas afterward that can be converted to synthetic hydrocarbon^{6,9}. Nevertheless, co-gasification of




char and biomass is a favorable approach to provide both environmental and economic benefits, including significant reduction in CO₂ emission, less waste disposal, and low fuel cost¹⁰. Co-gasification of coconut shell (biomass) with adding char provides an opportunity to enhance the gasification process. This gas consists of CO, H₂, CH₄, aliphatic hydrocarbon, benzene, toluene and tars (besides carbon dioxide and water)^{3,9}. In this gasification process, some by-product such as char, tar, particle, ash are also produce⁴, which are mostly useless as well as they make troublesome to the cleanness of syngas. Therefore, the aim of this study is to utilise by-product materials (mainly char) for further gasification.

2. Experimental Design and Procedure

The experiment of biomass (coconut shell) and char co-gasification has been done by Downdraft Gasifier (DG). The reactor of the experimental DG contains four sep-

*Author for correspondence

Social business models for empowering the biogas technology

Abu Yousuf ^a, Sharmin Sultana ^b, Minhaj Uddin Monir ^a, Ahasanul Karim^a,
and Syed Radzi Bin Rahmaddulla^c

^aFaculty of Engineering Technology, University Malaysia Pahang, Kuantan, Malaysia; ^bFaculty of Industrial Science and Technology, University Malaysia Pahang, Kuantan, Malaysia; ^cFaculty of Industrial Management, University Malaysia Pahang, Kuantan, Malaysia

ABSTRACT

Biogas is such type of renewable energy which provides clean energy, reduces environmental pollution and greenhouse gas caused by the biological wastes, creates job opportunity for skilled and unskilled persons, and offers new income sources for investors. However, mostly practiced small-scale or family-size biogas plant becomes unsuccessful due to the lack of financial attractiveness. Therefore, it is essential to design a proper financial mode of operation to sustain this technology. The policy makers, investors, and researchers should develop a viable financial mechanism to attract the investors by offering loan with flexible conditions, restructure the subsidies skim, and liberalize the gas grid management and involvement of the end users in biogas project. The engagement of social business concept can stimulate the sustainability of the biogas technology and make it financially gorgeous. This study proposed a number of social business plans and described microeconomic evaluation systems to calculate their commercial viability to improve the survival of biogas technology.


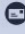
KEYWORDS

Biogas technology;
economic evaluation;
economic viability;
investment in biogas
technology; social business
models

1. Introduction

The global megatrends such as climate change, depletion of fossil fuel, greenhouse gas effect, and global warming are driving the increased adoption of renewable energy sources. The price volatility, supply issues, and environmental hazards of fossil fuel production are about to accelerate the pace in the investments of nonfossil fuels production. Particularly, biogas bears the potential to bring a basic change in the energy supply of rural households in developing countries. Biogas technology offers environmental, health, and socioeconomic benefits for farmers, localities, and even at a national level. Furthermore, it bears the potential to facilitate an independent economic development of the area when applied as social business. Though biogas technology is easy, accessible, and applicable to both developed and developing countries compared to other biofuels like biodiesel, bioethanol, and biohydrogen, its dissemination is still limited by economic factors (Yousuf et al., 2016). Even top-rated biogas producer countries (USA, Germany, Austria, Greece, China, India, and Sweden) are also providing governmental and nongovernmental subsidies (Tsagarakis and Papadogiannis, 2006; Börjesson and Mattiasson, 2008; Bond and Templeton, 2011; Emmann et al., 2013).

In the least developed countries, biogas technology is mainly using by small-scale farmers, when these farmers have enough livestock for running a small-scale biogas plant (Buysman and Mol, 2013). Major constraints of the biogas technology are related to lack of financial attractiveness, although highly subsidized, and to the conditions to be met by households: they require a minimum amount of cattle, access to water, and a financial contribution to construction cost. Unfortunately,

CONTACT Abu Yousuf  ayousufcep@yahoo.com  Faculty of Engineering Technology, University Malaysia Pahang, Kuantan, 26300 Malaysia.

Color versions of one or more of the figures in the article can be found online at www.tandfonline.com/uesb.

© 2017 Taylor & Francis Group, LLC

Application of Electroporation Technique in Biofuel Processing

Abu Yousuf^{1,*}, Maksudur Rahman Khan², Amirul Islam², MdMinhaj Uddin Monir¹, Zularisam Ab Wahid¹, and Domenico Pirozzi³

¹Faculty of Engineering Technology, University Malaysia Pahang, Malaysia

²Faculty of Chemical and Natural Resources Engineering, University Malaysia Pahang, Malaysia

³Department of Chemical Engineering, Materials and Industrial Production, University Naples Federico II, Italy

Abstract. Biofuels production is mostly oriented with fermentation process, which requires fermentable sugar as nutrient for microbial growth. Lignocellulosic biomass (LCB) represents the most attractive, low-cost feedstock for biofuel production, it is now arousing great interest. The cellulose that is embedded in the lignin matrix has an insoluble, highly-crystalline structure, so it is difficult to hydrolyze into fermentable sugar or cell protein. On the other hand, microbial lipid has been studying as substitute of plant oils or animal fat to produce biodiesel. It is still a great challenge to extract maximum lipid from microbial cells (yeast, fungi, algae) investing minimum energy. Electroporation (EP) of LCB results a significant increase in cell conductivity and permeability caused due to the application of an external electric field. EP is required to alter the size and structure of the biomass, to reduce the cellulose crystallinity, and increase their porosity as well as chemical composition, so that the hydrolysis of the carbohydrate fraction to monomeric sugars can be achieved rapidly and with greater yields. Furthermore, EP has a great potential to disrupt the microbial cell walls within few seconds to bring out the intracellular materials (lipid) to the solution. Therefore, this study aims to describe the challenges and prospect of application of EP technique in biofuels processing.

1 Introduction

Biofuel (biodiesel, bioethanol, biogas, bio-H₂) is a promising alternative to conventional fossil fuels since it does not have the same environmental impact associated with fossil fuels. Lignocellulosic biomass is considered as a reliable renewable source for the production of biodiesel, bioethanol, biogas and bio-H₂[1-3]. The conversion of lignocellulosic biomass to biofuels requires the following common steps: hydrolysis of cellulose and hemicellulose, sugar fermentation, lignin residue separation and finally recovery and purification of biofuels in order to fulfill fuel specifications. The

*Corresponding Author: ayousufcep@yahoo.com, ayousuf@ump.edu.my

5th World Convention on

RECYCLING AND WASTE MANAGEMENT

September 11- 12, 2017 Singapore

Liquid biofuel production from lignocellulosic biomass through syngas fermentationMinhaj Uddin Monir, Abu Yousuf and Azrina Abd Aziz
University Malaysia Pahang, Malaysia

Statement of the Problem: Energy demand is increasing globally due to the revolutionized economic and population growth, energy-dependent lifestyles and trending to minimize the greenhouse gas emission. Non-renewable energy resources (oil, gas, coal, etc.) cover ~80%, whereas biomass (renewable) covers only 10-15%, although it is available. However, biomass with byproduct char co-gasification and further biofuel production through syngas fermentation has very limited studied previously. The aim of this study is to produce liquid biofuels from lignocellulosic biomass through syngas fermentation.

Methodology & Theoretical Orientation: Empty fruit bunch (EFB) of palm oil, coconut shell (CS) and forest residues (FR) were used as feedstock for the production of syngas which are massively available in Malaysia. Co-gasification process was carried out in a downdraft gasifier (DG) with different biomass and char ratios. An Aspen Plus simulator (V8.6) was used for optimizing gasifier operational conditions.

Findings: At the initial stage, clean syngas was produced through the co-gasification of biomass and byproduct char. In the final stage, produced syngas (CO, H₂, etc.) was stored and fermented using microorganisms to synthesize bioethanol.

Conclusion & Significance: Produced syngas and bioethanol are the alternative energy from biomass (CS, EFB and FR) that will fulfill the future world energy demand and also reduce the dependency on fossil fuel.

mayyoung780@gmail.com

Notes:

RENEWABLE ENERGY AND BIOFUELS

NEW STRATEGY FOR ENHANCING CO-GASIFICATION PROCESS BY REUSING TAR/CHAR
FCE060

Minhaj Uddin Monir^{1,2}, Abu Yousuf^{1*}, Azrina Binti ABD Aziz¹ and Samson Mekbib Ataw¹

¹Faculty of Engineering Technology, University Malaysia Pahang, Gambang, Malaysia.

²Department of Petroleum and Mining Engineering, Jessore University of Science and Technology, Jessore, Bangladesh

*Corresponding author: ayousufcep@yahoo.com, ayousuf@ump.edu.my

Abstract

Energy demand is exponentially increased globally, and both developed or developing countries are giving emphasis on renewable energy sources to be used for clean energy production due to its CO neutrality. Co-gasification of lignocellulosic biomass (empty fruit bunch, forest waste, etc.) and various types of carbon contain materials (petroleum coke, coal, etc.) is one of the reliable and environmentally accepted options for synthetic hydrocarbon production. This process takes place within the reactor (Fixed bed, fluidized bed, etc.) under certain temperatures and pressures. Syngas is produced at the initial stage of this process and later synthetic hydrocarbon is formed by Fischer-Tropsch reaction. Co-gasification process also produces significant amount of by-product materials such as ash, tar and char. By-products tar or char contains huge amount of concentrated carbons, which may be treat as a suitable catalyst. The aim of this research is to reuse tar/char for enhancing co-gasification process.

Key words: Biomass, coal, co-gasification, tar/char, catalyst.

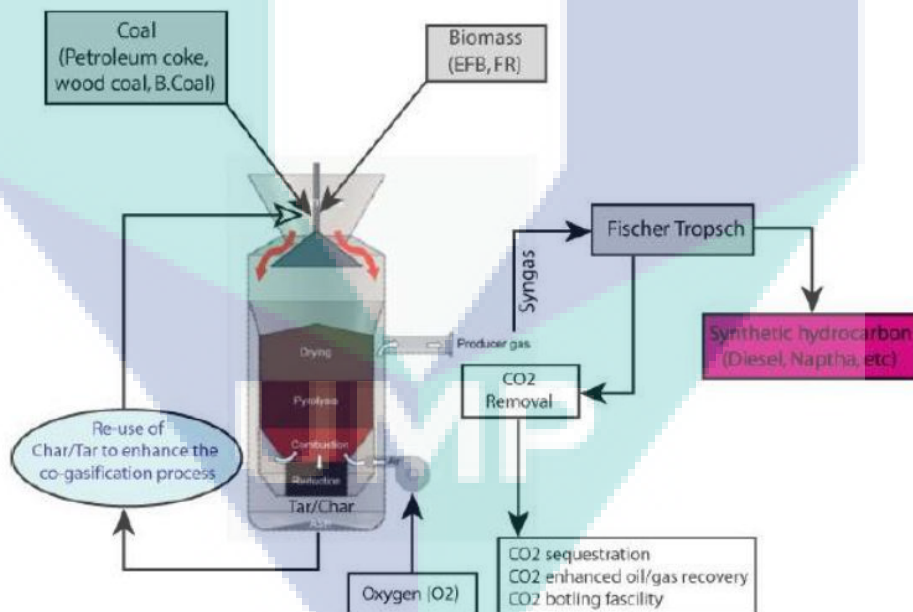


Fig. 1: Schematic diagram by re-using tar/char to enhance co-gasification process.

Lipid Extraction from Microbial Cell by Electroporation Technique and Its Influence on Direct Transesterification for Biodiesel Synthesis

Authors : Abu Yousuf, Maksudur Rahman Khan, Ahasanul Karim, Amirul Islam, Minhaj Uddin Monir, Sharmin Sultana, Domenico Pirozzi

Abstract : Traditional biodiesel feedstock like edible oils or plant oils, animal fats and cooking waste oil have been replaced by microbial oil in recent research of biodiesel synthesis. The well-known community of microbial oil producers includes microalgae, oleaginous yeast and seaweeds. Conventional transesterification of microbial oil to produce biodiesel is lethargic, energy consuming, cost-ineffective and environmentally unhealthy. This process follows several steps such as microbial biomass drying, cell disruption, oil extraction, solvent recovery, oil separation and transesterification. Therefore, direct transesterification of biodiesel synthesis has been studying for last few years. It combines all the steps in a single reactor and it eliminates the steps of biomass drying, oil extraction and separation from solvent. Apparently, it seems to be cost-effective and faster process but number of difficulties need to be solved to make it large scale applicable. The main challenges are microbial cell disruption in bulk volume and make faster the esterification reaction, because water contents of the medium sluggish the reaction rate. Several methods have been proposed but none of them is up to the level to implement in large scale. It is still a great challenge to extract maximum lipid from microbial cells (yeast, fungi, algae) investing minimum energy. Electroporation technique results a significant increase in cell conductivity and permeability caused due to the application of an external electric field. Electroporation is required to alter the size and structure of the cells to increase their porosity as well as to disrupt the microbial cell walls within few seconds to leak out the intracellular lipid to the solution. Therefore, incorporation of electroporation techniques contributed in direct transesterification of microbial lipids by increasing the efficiency of biodiesel production rate.

Keywords : biodiesel, electroporation, microbial lipids, transesterification

Open Science Index, Vol:10, No., 2016 waset.org/abstracts/58319



UMP

APPENDIX A EXERGY EFFICIENCY CALCULATION

Calculation of physical exergy (ϵ_{ph}):

Physical exergy can be calculated by using the following equation:

$$\epsilon_{ph} = (h - h_0) - T_0(s - s_0) \quad (i)$$

Where, ϵ_{ph} = Physical exergy (KJ/Kmol.)

h and s = Enthalpy and entropy at any temperature (T) and pressure (P);

h_0 and s_0 = Enthalpy and entropy at dead state ($T_0 = 298.15$ K, $P_0 = 1$ atm).

Calculation:

Produced gases are CO_2 , CO , H_2 , CH_4 , N_2 .

So, using the equation (i),

Physical exergy for $\text{CO}_2 = 18.47$ (KJ/Kmol.)

Physical exergy for $\text{CO} = 32.68$ (KJ/Kmol.)

Physical exergy for $\text{H}_2 = 6065.08$ (KJ/Kmol.)

Physical exergy for $\text{CH}_4 = 165.87$ (KJ/Kmol.)

Physical exergy for $\text{N}_2 = 32.40$ (KJ/Kmol.)

Thus, total physical exergy = (Physical exergy for CO_2) + (Physical exergy for CO) + (Physical exergy for H_2) + (Physical exergy for CH_4) + (Physical exergy for N_2)

Thus, Total physical exergy for produced gases = 6314.49 (KJ/Kmol.).

Calculation of chemical exergy (ϵ_{ph}):

$$\epsilon_{ch,m} = \sum_i x_i \epsilon_{ch,i} + RT_0 \sum_i x_i \ln x_i \quad (ii)$$

Where, ϵ_{ph} = chemical exergy (KJ/Kmol.)

x_i = Mole fraction of i^{th} species;

R = Universal gas constant;

$\epsilon_{ch,i}$ = Standard chemical exergy of i^{th} species in KJ/kmol.

Calculation:

Table 1: Parameters and value for the calculation of chemical exergy of produced gases of CO₂, CO, H₂, CH₄, N₂.

Produced gases	Mole fraction	Chemical exergy (Standard)	I _n value	R value	T ₀ value (°C)
CO ₂	0.14	19870	-1.966112856	0.008314	25
CO	0.27	275100	-1.30933332		
H ₂	0.01	236100	-4.605170186		
CH ₄	0.01	831650	-4.605170186		
N ₂	0.58	720	-0.544727175		

Thus, using the equation (ii), total chemical exergy values for produced gases are, 88153.68 (KJ/Kmol.).

So, Total exergy is the sum of physical and chemical exergy that are expressed as Eq. iii.

$$Ex = Ex_{phy} + Ex_{chem} \quad (iii)$$

So, $Ex = 6314.49$ (KJ/Kmol.) + 88153.68 (KJ/Kmol.)

= 94468.18 (KJ/Kmol.).

Hence, overall exergy is 94468.18 (KJ/Kmol.) for the mixture of forest residue and charcoal at the ratio of 70:30.

Calculation of fuel mixture exergy (ϵ_{fm}):

$$\epsilon_{fm}=(LHV_{fm}+2442 \times W_{fm})\beta \quad (\text{iv})$$

Where, ϵ_{fm} =Fuel mixture exergy ($\frac{\text{KJ}}{\text{Kmol}}$)

LHV_{fm} =Lower heating value of fuel (forest residue and charcoal) mixture;

W_{fm} =Mass fraction of moisture in the fuel (forest residue and charcoal) mixture.

$$\beta = \frac{1.0438 + 0.1882 \frac{H}{C} - 0.2509 \frac{O}{C} \left[1 + 0.7256 \frac{H}{C} \right] + 0.0383 \frac{N}{C}}{1 - 0.3035 \frac{O}{C}} \quad (\text{v})$$

Where, C=mass fraction of carbon in the fuel mixture (forest residue and charcoal) (%)

H=mass fraction of hydrogen in the fuel mixture (forest residue and charcoal) (%)

O=mass fraction of oxygen in the fuel mixture (forest residue and charcoal) (%)

N=mass fraction of nitrogen in the fuel mixture (forest residue and charcoal) (%)

Table 2: Calculation of β and ϵ_{fm} value for forest residue and charcoal using Eq. iv and Eq. v.

Feedstocks (Fuels)	C	H	O	N	LHV	W_{fm}	Calculation of β value using Eq. v	Calculation of ϵ_{fm} value using Eq. iv
Forest residue	42.75	4.67	47.76	4.81	14.20	6	1.16	14170.62
Charcoal	55.43	1.05	42.42	1.03	15.72	6	1.11	16371.51

Calculation of exergy efficiency (η_{ex}):

For the calculation of exergy efficiency, following equation are used,

$$\eta_{ex} = \frac{Ex_{prod}}{Ex_{feedstocks} + Ex_{agent}} \quad (vii)$$

Atmospheric air was used as a gasifying agent and injected to the reactor system at the atmospheric condition. As a result, for the calculation of exergy efficiency, the gasifying agent was neglected (Prins & Ptasiński, 2005). So, exergy efficiency (η_{ex})= 63.69% for the co-gasification of forest residue and charcoal with the ratio of 70:30. Correspondingly, the physical and chemical exergy, fuel mixture exergy and exergy efficiency with the various ratios of forest residue and charcoal are shown in Table 3.

Table 3: Results of physical and chemical exergy, fuel mixture exergy and exergy efficiency with the various ratios of forest residue and charcoal.

Forest Residue and Charcoal ratio	Physical and chemical exergy (MJ/Kmol.)	Fuel mixture exergy (GJ/Kmol.)	Exergy efficiency (%)
100:00	66.13	17.00	38.90
90:10	75.57	16.93	44.64
80:20	85.02	16.86	50.42
70:30	94.47	16.79	56.26
60:40	103.91	16.72	62.14

Similarly, exergy efficiency for EFB with charcoal and CS with charcoal were calculated.

APPENDIX B

PROCEDURE FOR SIMULATION USING ASPEN PLUS®

The real image procedure for the simulated parameters of temperature and pressure using Aspen Plus simulator has been given below:

- (a) Installed and opened Aspen Plus® (V.8.6) simulator (University Malaysia Pahang has the facilities for simulation using Aspen Plus V.8.6)
- (b) File⇒New⇒Chemical Processes⇒Chemicals with metric units (C, bar, Kmol/hr, Gcal/hr, Cum/hr); Property methods: NRTL; Flow basis for input: Mole; Stream report composition: Mole flow) ⇒Create
- (c) Selected compounds (Compounds ID) as per simulation needed (CO, H₂, CO₂, CH₄, H₂O, Air) from Aspen Plus software database.
- (d) Methods⇒Specifications⇒Select base methods (NRTL with ideal gas and Henry's Law) [This method was selected from the methods assistant: Specific process type⇒type of process or application (Chemical) ⇒appropriate as NRTL/WILSON/UNIQUAC) ⇒Selected NRTL]
- (e) Simulation⇒Created process flowsheet (Fig. 3) as per our research. [Process flow sheet was used as per Aspen Plus block and stream (Fig. 3 and Table 3)]
- (f) Aspen Plus block and stream (Fig. 3 and Table 3) temperature and pressure were set and selected as per experimental Downdraft Gasifier temperature (°C) and pressure (bar): drying zone, pyrolysis zone, oxidation zone and reduction zone. The considered pressure was set as 1 bar to 45 bar (R1, R2, R3, R4, R5 and R6) (capacity of the air flow rate of the air blower was up to 60 m³/h).
- (g) Total flowrate for the selected feedstock (forest residue and wood charcoal) composition (calculated from the result of elemental analysis and total weight of the feedstock)
- (h) Selected mole fraction of the selected compounds.
- (i) Once inlet and outlet value (Temperature, pressure and flowrate) input completed then click the Reinitialised button
- (j) Then run the simulation
- (k) Sensitivity analysis: Select Model Analysis Tools ⇒ Sensitivity⇒New⇒S1⇒ok
- (l) Vary⇒variable No.1 (Manipulated variable type⇒Block-Var; Variable⇒Temp; Overall range (Lower value: 500 °C; upper value: 1200 °C)
- (m) Define⇒Flowsheet variable name (CO, H₂, CO₂ and CH₄) [Every variable needed to select the category: Blocks or Streams]

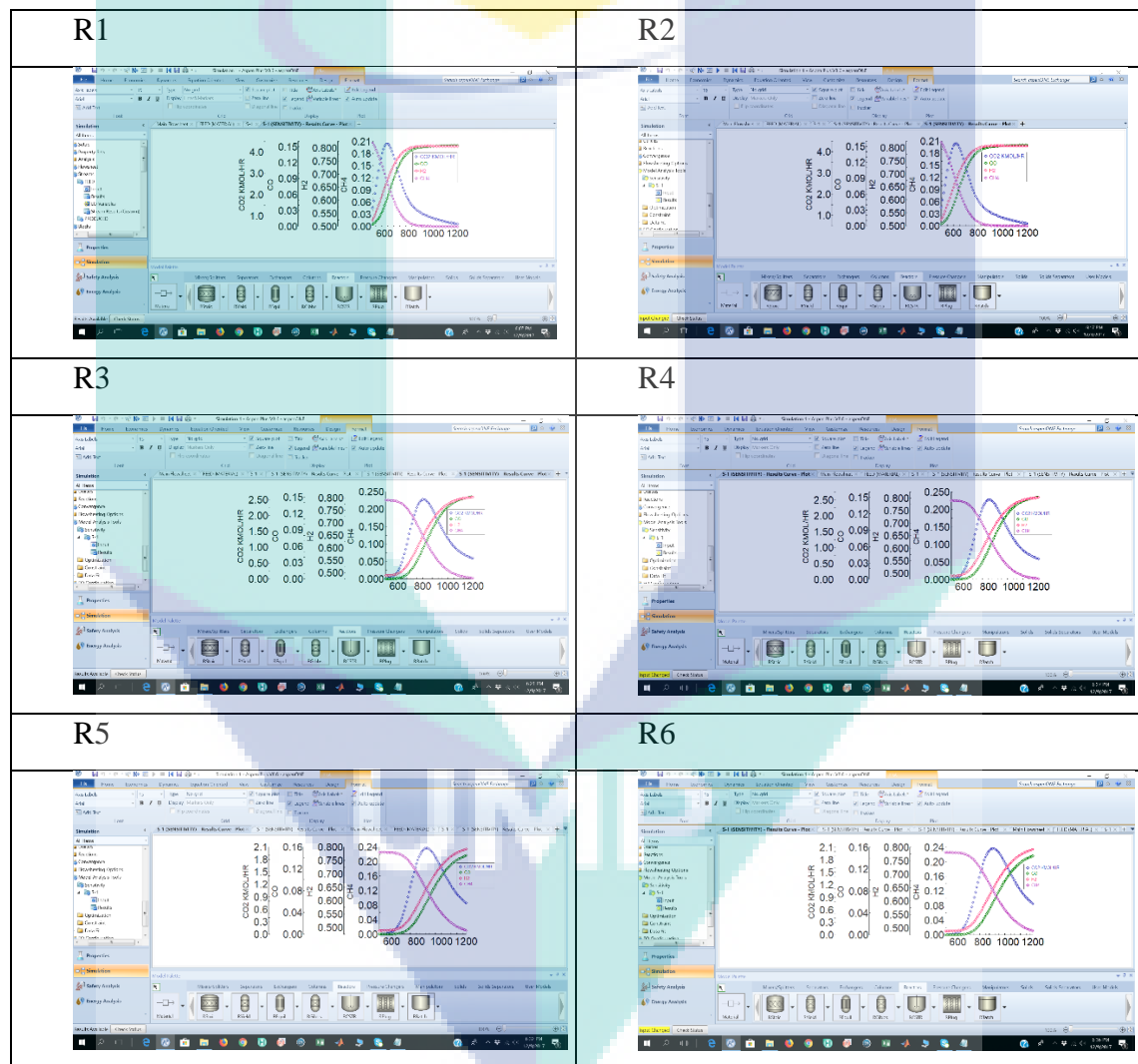
(n) Reference type \Rightarrow Mole flow \Rightarrow Streams (CO , H_2 , CO_2 and CH_4) [individually selected as per this simulation]

(o) Tabulate \Rightarrow Fill variable \Rightarrow automatically generated variable or expression.

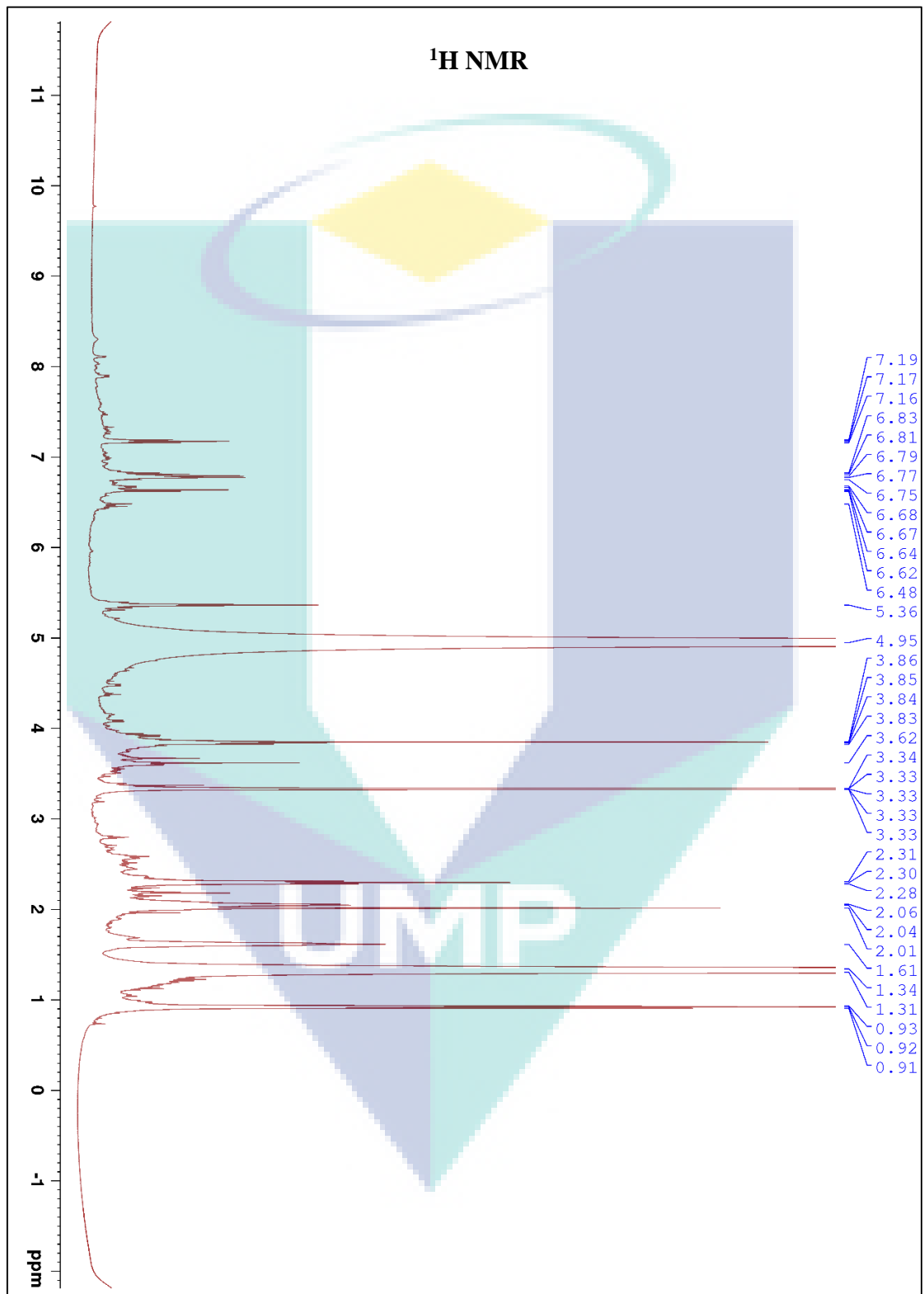
(p) Once all input data were completed then again run the simulation

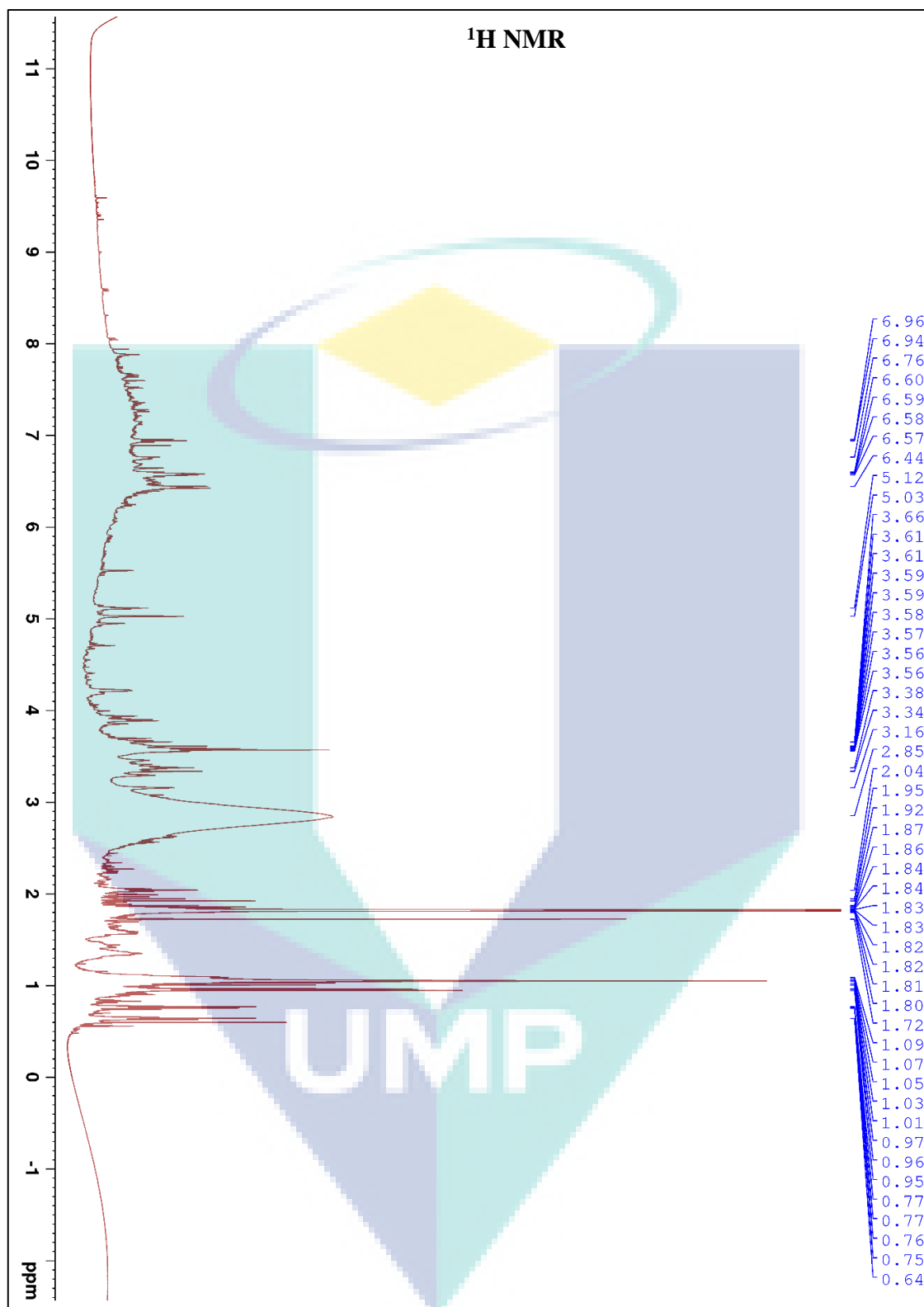
(q) Result curve appeared \Rightarrow selected targeted compounds as per research output \Rightarrow ok

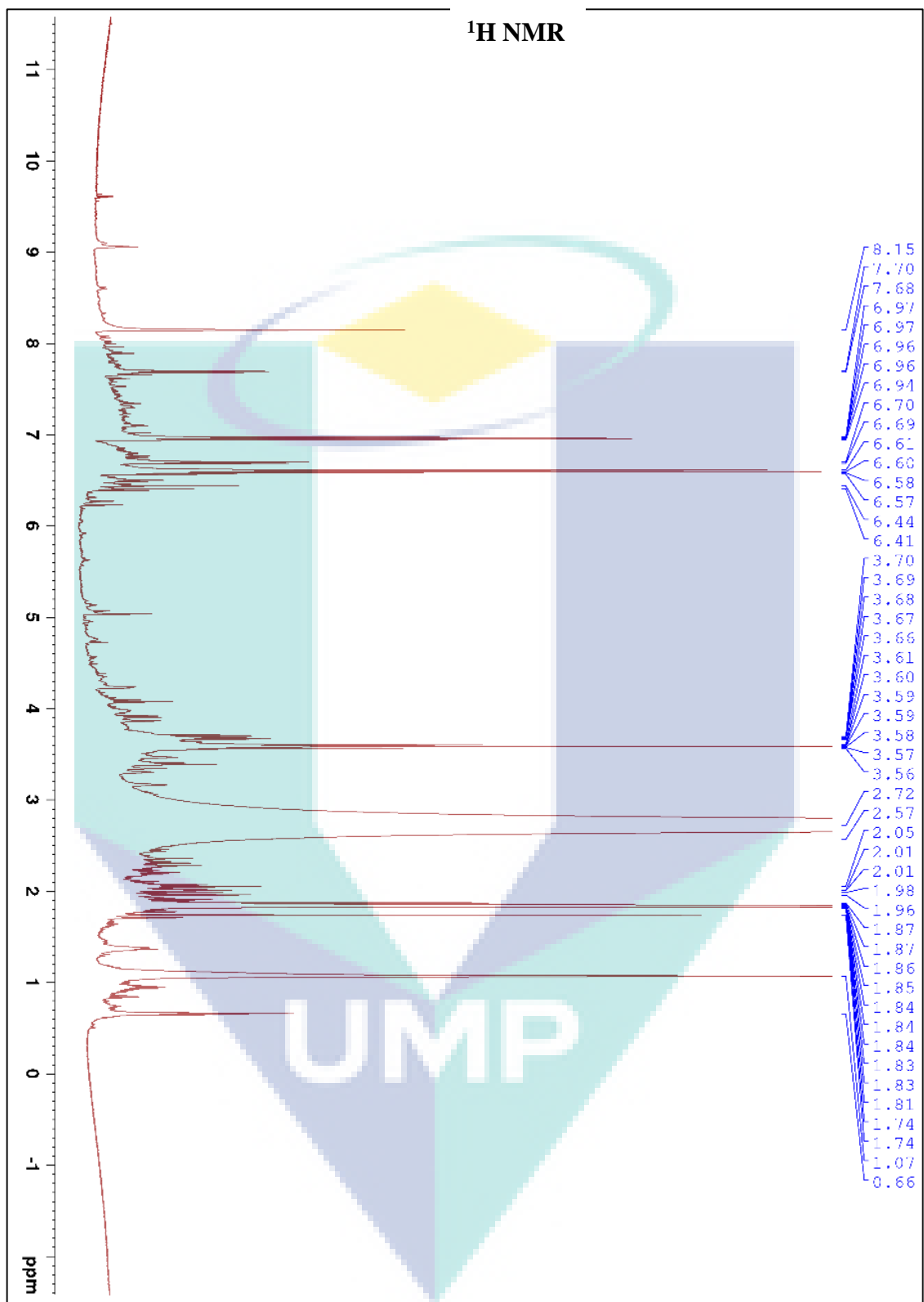
(r) Final sensitivity result curves produced that was shown in the Aspen Plus software screen. The simulated results based on the parameter of temperature ($500 - 1200^\circ\text{C}$) and pressure (1-45 bar) are shown in the following Figures (R1-R6).

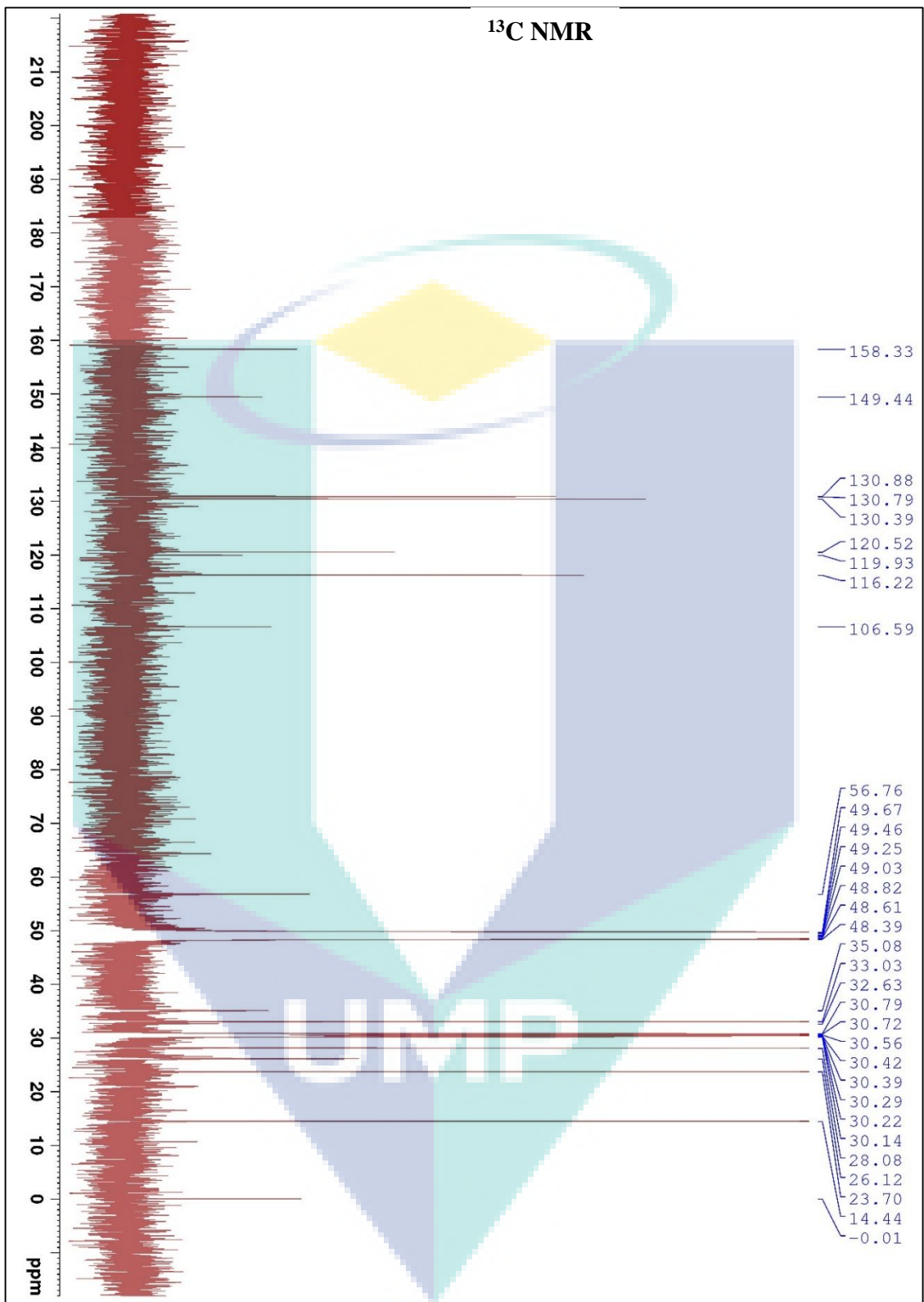


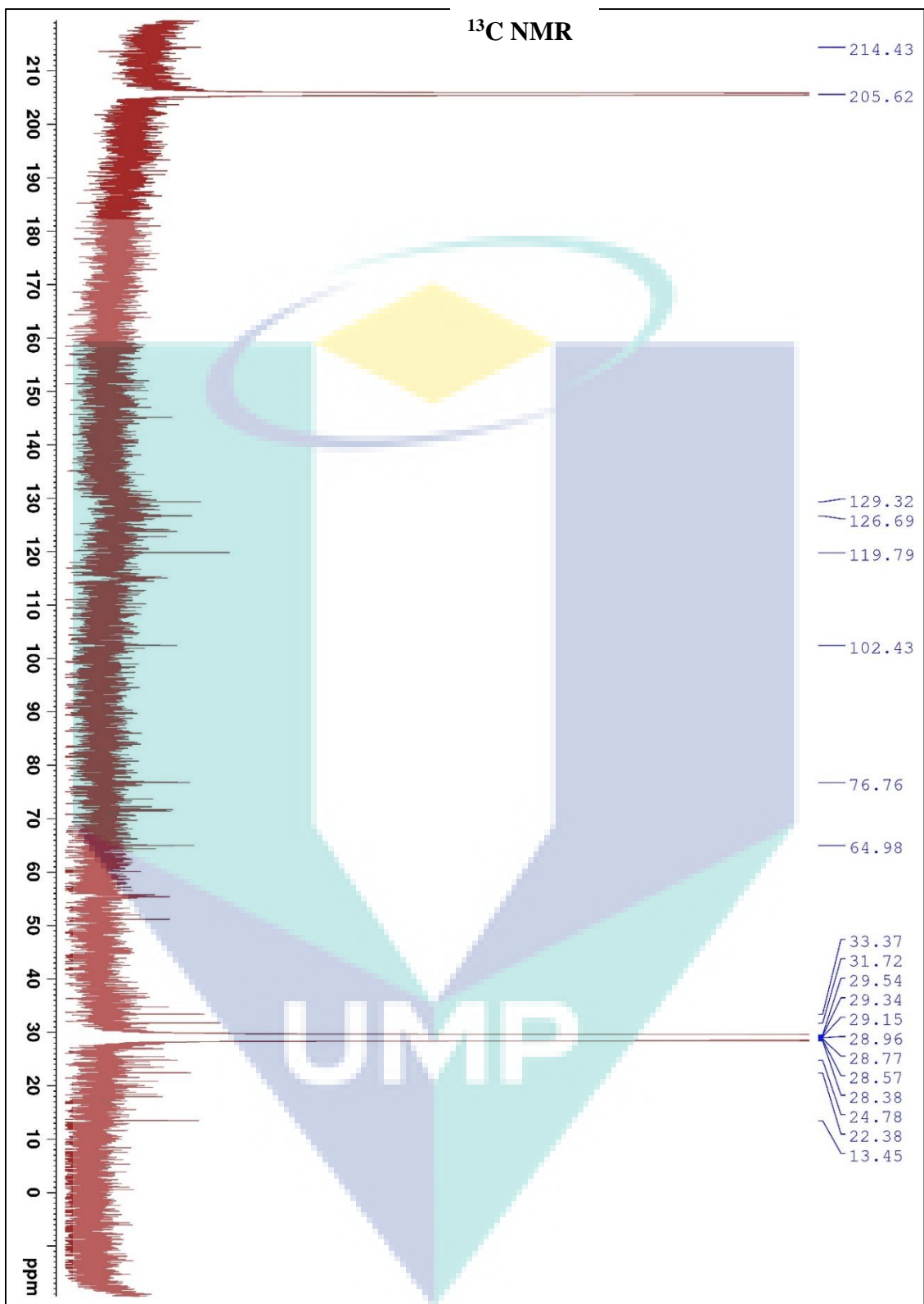
APPENDIX C
NMR (¹H AND ¹³C) FOR CO-PRODUCT TAR

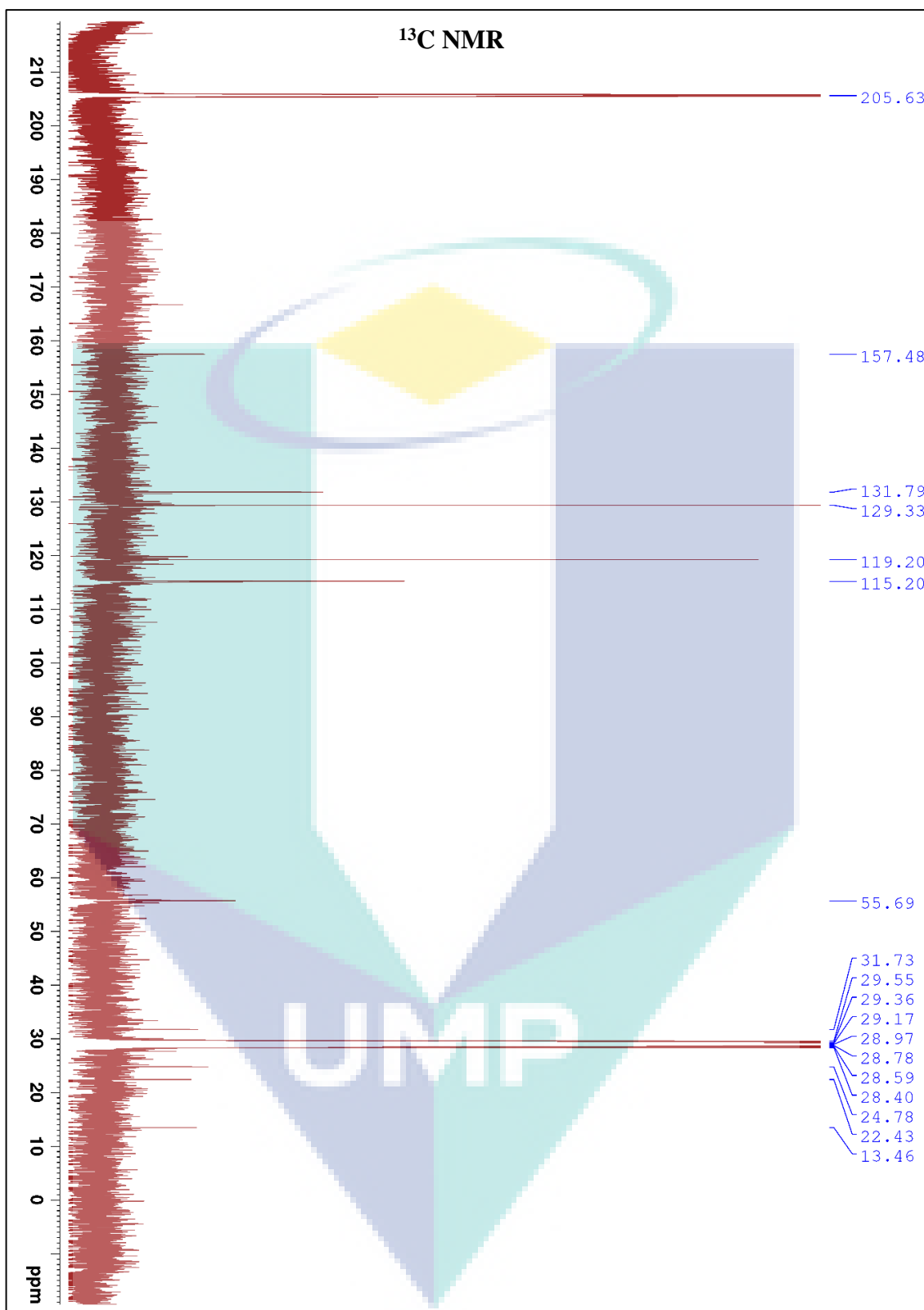




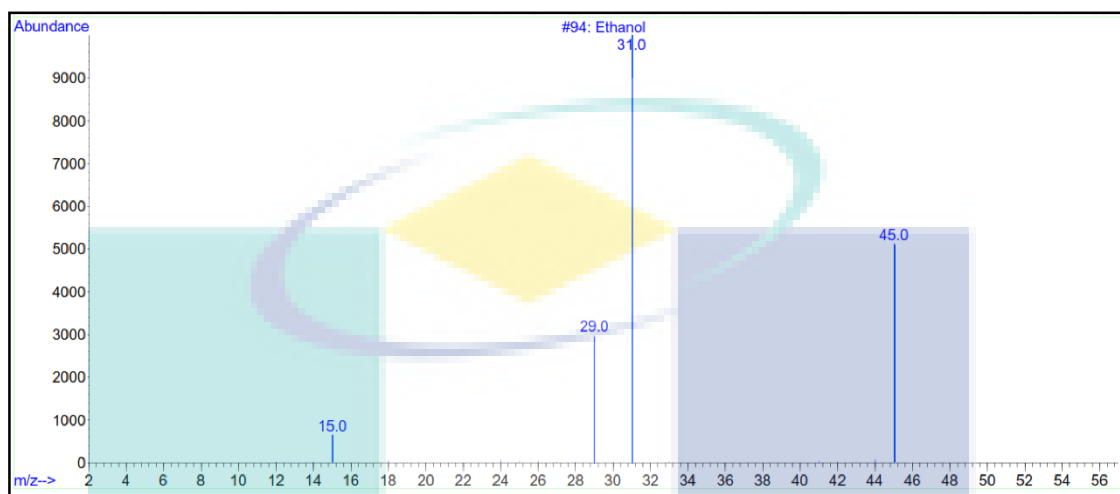








APPENDIX D
GC-MS FRACTION OF ETHANOL (STANDARD MS FRACTION (15:29:31:45)
FOR ETHANOL (99.99%).



APPENDIX E
SYNGAS COMPOSITION BEFORE AND AFTER FERMENTATION

